IL
NUOVO CIMENTO
ORGANO DELLA SOCIETÀ ITALIANA DI FISICA
SOTTO GLI AUSPICI DEL CONSIGLIO NAZIONALE DELLE RICERCHE

VOL. IV, N. 5 *Serie decima* 1° Novembre 1956

Approximations For Linear Betatron Oscillations.

F. T. ADLER and D. BARONCINI

Carnegie Institute of Technology - Department of Physics

(ricevuto il 17 Maggio 1956)

Summary. — Approximation methods for calculating the characteristic exponent of extended Hill equations are derived and applied to the computation of linear betatron oscillations.

1. – Introduction.

A general method of solving Hill's equation and for obtaining approximate values for the wavelength of linear as well as non-linear betatron oscillations [1] has been developed by K. R. SYMON [2]. To obtain the characteristic exponent ν of Hill's equation, i.e. the betatron wavelength, the exact solution is replaced by a « smoothed » solution representing the overall features of the betatron oscillations. The approximate values of the betatron wave length are obtained by matching the smooth solution with the exact solution at three points. This method is particularly useful if the period of the betatron oscillations is large compared with the period τ of the magnetic field of the accelerator.

An alternative derivation of the smooth approximation has been given by L. C. TENG [3], in which the smoothed solution is represented by a sinusoidal curve.

(1) M. S. LIVINGSTONE: *High Energy Accelerators* (New York, 1954).

(2) K. R. SYMON: *Midwestern Universities Research Association Reports, MURA-KRS-* 1, 2, 4.

(3) L. C. TENG: *Argonne National Laboratory*, ANL 5517.

In this report the results of the smooth approximation for linear betatron oscillations are deduced directly from general properties of the extended Hill equation without the assumption of the smooth approximation.

Three different approximations for $\cos \nu\tau$ are discussed, viz., a Taylor expansion, successive approximations in powers of the magnetic field flutter, and an iteration solution to integral equation of Volterra type.

Results for $\cos \nu\tau$ are given in Eq. (33) for the successive approximation method and in Eq. (47) for the integral equation method.

Numerical results for $\cos \nu\tau$ obtained by the successive approximation method for a sample case are shown in Fig. 1 and 2 and compared with those obtained from the smooth approximation and with the exact values calculated by L. J. LASLETT [4]. Figs. 1 and 2 indicate that Eq. (33) gives reliable results for small flutter even near the stability limit.

Approximate solutions for Floquet functions can also be obtained from the successive approximation method solutions given in Eq. (26) and (31).

The integral equation method may possibly be useful for non-linear stability problems. In principle, this method allows to estimate the magnitude of error in $\cos \nu\tau$ because a simple exponential series can be substituted for the Neumann series solution.

The Taylor expansion is apparently least useful for calculations. It allows though to check explicitly the general properties of the solutions of Hill's equation which are derived in the last section of this report.

After this work was completed we became aware through a discussion with Dr. WALKINSHAW of the AERE at Harwell that related work is in progress in that group.

2. – Stability Conditions.

The linear betatron oscillations are described by an extended Hill equation

$$\frac{\mathrm{d}^2 y}{\mathrm{d}t^2} = f(t) y(t) , \tag{1}$$

where

$$f(t + \tau) = f(t) \tag{2}$$

and the τ is the period of the magnetic field in the accelerator. In this section

[4] L. H. LASLETT, J. N. SNYDER and D. HUTCHINSON: *MURA Report.*

we shall express the stability condition for the betatron oscillations in terms of a fundamental solution of Eq. (1).

According to Floquet's theorem [5], Eq. (1) has particular solutions of the form

$$F(t) = \exp[i\nu t]\varphi(t), \tag{3}$$

with

$$\varphi(t + \tau) = \varphi(t),$$

so that

$$F(t + \tau) = kF(t), \tag{4}$$

where $k = \exp[i\nu\tau]$ is a constant, ν being a complex number.

The condition for stability of the motion described by the solutions of Eq. (1) is

$$|k| \leq 1, \tag{5}$$

i.e., that the characteristic exponent ν is real.

As a consequence of Floquet's theorem, the general solution of Eq. (1) can be written in the form

$$y(t) = \varphi_1(t)\cos\nu t + \varphi_2(t)\sin\nu t, \tag{6}$$

where

$$\varphi_\varkappa(t + \tau) = \varphi_\varkappa(t); \qquad \varkappa = 1, 2. \tag{7}$$

Alternately, any solution of Eq. (1) can also be written in the form

$$y(t) = y(0)G_1(t) + y'(0)G_2(t), \tag{8}$$

where $G_1(t)$ and $G_2(t)$ are the pairs of fundamental solutions of Eq. (1) for which

$$\begin{cases} G_1(0) = 1, & G_2(0) = 0, \\ G_1'(0) = 0, & G_2'(0) = 1. \end{cases} \tag{9}$$

As a solution of Eq. (1), the fundamental solution $G_1(t)$ can be expressed

---

[5] E. WHITTAKER and G. WATSON: *A Course of Modern Analysis* Cambridge (England), New York, (1944), p. 413.

in the form

$$G_1(t) = \varphi_1(t) \cos \nu t + \varphi_2(t) \sin \nu t , \tag{10}$$

with

$$\varphi_1(0) = \varphi_1(\tau) = 1 \quad \text{and} \quad \varphi_1'(0) + \nu \varphi_2(0) = 0 . \tag{11}$$

Since $\varphi_2(t)$ is periodic, we have

$$G_1(\pm \tau) = \cos \nu\tau \pm \varphi_2(0) \sin \nu\tau$$

and therefore (*)

$$\cos \nu\tau = \tfrac{1}{2}[G_1(\tau) + G_1(-\tau)] . \tag{12}$$

The condition for stability (ν real) is now expressed as

$$\cos \nu\tau = \tfrac{1}{2}[G_1(\tau) + G_1(-\tau)] \leqslant 1 . \tag{13}$$

Equation (13) specifies exactly the characteristic exponent ν or the betatron wavelength in terms of the particular solution $G_1(t)$. In Sects. **3** to **5**, we shall indicate approximation methods for evaluating $G_1(\pm \tau)$. More general properties of $G_1(\tau)$ will be derived in Sect. **6**. These properties are useful in simplifying the calculation of higher order approximations for ν.

3. – Taylor Expansion for $G_1(t)$.

An approximate expression for $\cos \nu\tau$ can be obtained by expanding $f(t)$ and $G_1(t)$ in Taylor series around the origin

$$f(t) = \sum_{k=0}^{\infty} f^{(k)}(0) \frac{t^k}{k!} , \tag{14}$$

$$G(t) = \sum_{m=0}^{\infty} g_m \frac{t^m}{m!} . \tag{15}$$

Introducing these expansions into Eq. (1) one obtains the recurrent relations

$$g_{n+2} = \sum_{j=0}^{n} g_j f^{n-j}(0) \binom{n}{j} . \tag{16}$$

(*) In the older mathematical literature this relation is referred to as Korteweg's theorem.

The first coefficients g_k are given in Table I. From Table I, it is evident that, at $t = \pm\tau$, each single term in the Taylor expansion for $G_1(t)$ is a polynomial in τ^2.

TABLE I.

$g = 1$	$g_5 = 4\frac{k_1}{\tau} f(0) + \frac{k_3}{\tau^3}$
$g_1 = 0$	$g_6 = f(0)^3 + 7\frac{k_2}{\tau^2} f(0) + 4\frac{k_1^2}{\tau^2} + \frac{k_4}{\tau^4}$
$g_2 = f(0)$	. . . . .
$g_3 = \frac{k_1}{\tau}$	$f^{(j)}(0) = \sum_i{}' f_i \left(\frac{2\pi i l}{\tau}\right)^j \equiv \frac{k_j}{\tau^j}$,
$g_4 = f(0)^2 + \frac{k_2}{\tau^2}$	$g_{n+2} = \sum_{j=0}^{n} \binom{n}{j} g_i \frac{k_{n-i}}{\tau^{n-j}}$.

From Eqs. (12) and (15) we obtain an approximate expression for $\cos \nu\tau$:

$$\frac{G_1(\tau) + G_1(-\tau)}{2} = \sum_{m=0} \frac{\tau^{2m}}{(2m)!} g_{2m} \cong \tag{17}$$

$$= \cos \sqrt{-f(0)}\tau + \tau^2 \left[\frac{k_2}{4!} + \frac{k_4}{6!} + \frac{k_6}{8!} + \ldots\right] + \ldots .$$

4. – Successive Approximations for $\cos \tau\nu$.

The Taylor expansion approximation for $\cos \nu\tau$ is not suitable for many computations. A useful approximation formula for $\cos \nu\tau$ can be obtained by successive approximations. We write $f(t)$ in the form

$$f(t) = -\lambda^2 + h\tilde{f}(t) \tag{18}$$

where

$$-\lambda^2 = f_0 = \bar{f} \tag{19}$$

and (*)

$$h\tilde{f}(t) = h \sum_k{}' f_k \exp[2\pi i k t/\tau] = h \sum_k{}' \left[a_k \cos 2\pi k \frac{t}{\tau} + b_k \sin 2\pi k \frac{t}{\tau}\right]. \tag{20}$$

(*) h is meant to be the magnitude of the largest Fourier coefficient. In many problems it corresponds directly to the magnetic field flutter, so that $h < 1$. e.g., for the spiral ridge cyclotron $h < \frac{1}{4}$.

We now obtain $\cos \nu\tau$ as a power series in h. This particular expansion will be useful only if $h < 1$.

Espanding the solution $G_1(t)$ of Eq. (1) in powers of h, we put

$$G_1(t) = \cos \lambda t + \sum_{n=1}^{\infty} h^n \Phi_n(t;\, \lambda,\, a_k,\, b_k)\,. \tag{21}$$

By comparing powers of h, we obtain from Eqs. (1) and (18) the differential equations

$$\Phi_1'' + \lambda^2 \Phi_1 = \tilde{f}(t) \cos \lambda t \tag{22}$$

$$\Phi_n'' + \lambda^2 \Phi_n = \tilde{f}(t) \Phi_{n-1}\,; \qquad n > 1. \tag{23}$$

The initial conditions, $G_1(0) = 1$, $G_1'(0) = 0$ impose on the Φ_n the initial conditions

$$\Phi_n(0) = \Phi_n'(0) = 0\,; \qquad n \geqslant 1. \tag{24}$$

From Eq. (22) we obtain

$$\Phi_1(t) = A_1 \cos \lambda t + B_1 \sin \lambda t - \tfrac{1}{2} \sum_k{}' f_k(\varphi_k \exp[i\alpha_k t] + \varphi_{-k} \exp[i\beta_k t]), \tag{25}$$

where we use the abbreviations:

$$\alpha_k = \frac{2\pi}{\tau} k + \lambda, \qquad \beta_k = \frac{2\pi}{\tau} k - \lambda\,, \tag{26}$$

$$\varphi_k = \frac{1}{\alpha_k^2 - \lambda^2}\,, \qquad \varphi_{-k} = \frac{1}{\beta_k^2 - \lambda^2}\,. \tag{27}$$

From the initial conditions we have

$$A_1 = \tfrac{1}{2} \sum_k{}' f_k[\varphi_k + \varphi_{-k}] \tag{28}$$

$$B_1 = \frac{i}{2} \sum_k{}' f_k \left[\varphi_k - \varphi_{-k} + \frac{2\pi k}{\tau\lambda} (\varphi_k + \varphi_{-k})\right]. \tag{29}$$

Furthermore

$$\Phi_1(\tau) + \Phi_1(-\tau) = A_1 \cos \lambda\tau - \cos \lambda\tau \tfrac{1}{2} \sum_k{}' f_k[\varphi_k + \varphi_{-k}] = 0, \tag{30}$$

so that Φ_1 will not contribute to $\cos \nu\tau$.

For the second approximation we obtain

$$\Phi_2(t) = A_2 \cos \lambda t + B_2 \sin \lambda t -$$

$$- (A_1 + B_1) \tfrac{1}{2} \sum_k{}' f_k \varphi_k \exp[i\alpha_k t] - (A_1 - B_1) \tfrac{1}{2} \sum_k{}' f_k \varphi_{-k} \exp[i\beta_k t] -$$

$$- \tfrac{1}{2} \sum_k{}' \sum_{s \neq -k}{}' f_k f_s [\varphi_k \varphi_{s+k} \exp[i\alpha_{k+s} t] + \varphi_{-k} \varphi_{-k-s} \exp[i\beta_{k+s} t]] -$$

$$- \frac{t}{4i\lambda} \sum_k{}' f_k f_{-k} [\varphi_k \exp[i\lambda t] - \varphi_{-k} \exp[-i\lambda t]] , \tag{31}$$

where A_2 and B_2 are again obtained from Eq. (23).

From Eq. (31) we obtain

$$\Phi_2(\tau) + \Phi_2(-\tau) = -\frac{2\tau}{4\lambda} \sin \lambda\tau \sum_k{}' f_k f_{-k} [\varphi_k + \varphi_{-k}] , \tag{32}$$

and therefore (*)

$$\cos \nu\tau = \cos \lambda\tau - \frac{\tau^4 h^2}{(4\pi)^2} \frac{\sin \lambda\tau}{\lambda\tau} \sum_k \frac{a_k^2 + b_k^2}{k^2 - (\tau\lambda/\pi)^2} . \tag{33}$$

For $|\lambda\tau| \ll 1$, Eq. (33) reduces to

$$\cos \nu\tau = \cos \lambda\tau - \frac{\tau^4 h^2}{(4\pi)^2} \sum_k \frac{a_k^2 + b_k^2}{k^2} . \tag{34}$$

If $f(t)$ is an odd function of t, Eq. (33) reduces to

$$\cos \nu\tau = 1 - \frac{\tau^4 h^2}{(4\pi)^2} \sum_k \frac{b_k^2}{k^2} . \tag{35}$$

For example, for the alternating gradient synchrotron, where

$$f(t) = n: \qquad 0 < t \leq \frac{\tau}{2}; \qquad f(t) = -n: \qquad -\frac{\tau}{2} \leq t < 0 ,$$

(*) If $\tau\lambda/\pi = k_1$ (integer). Eq. (33) reduces to

$$\cos \nu\tau = (-)^{k_1} \left\{ 1 + \frac{\tau^4 h^2}{(4\pi)^2} \frac{a_{k_1}^2 + b_{k_1}^2}{2\pi k_1^2} \right\} + \dots .$$

we obtain

$$\cos \nu\tau = 1 - \frac{\tau^4}{4.4!}\, n^2 + O(n^4)\,, \tag{36}$$

which reproduces to the same order of approximation the exact result obtained by COURANT and SNYDER (6).

Higher approximations will be discussed in Sect. 6.

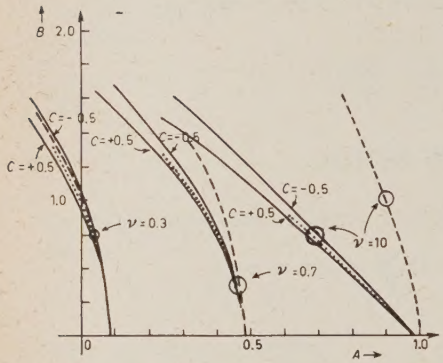

Fig. 1. – Comparison of Fourier coefficients for specified ν. Differential equation used for comparison: $d^2y/dt^2 + +(A+B\cos 2t+\cos 4t)y=0$. —— Digital Computer results of L. J. Laslett. – – – Symon approximation $B= = B(\nu, A, C)$ from $\nu^2=A+B^2/8+C^2/32$; $C=\pm\frac{1}{2}$. . . . . Successive approximation result $B = B(\nu, A, C)$ from

$$\cos \pi\nu = \cos \pi\sqrt{A} - \frac{\pi^2 \sin \pi\sqrt{A}}{16\ \pi\sqrt{A}} \cdot \left(\frac{B^2}{1-A} + \frac{C^2}{4-A}\right); \qquad C=\pm\tfrac{1}{2}\,.$$

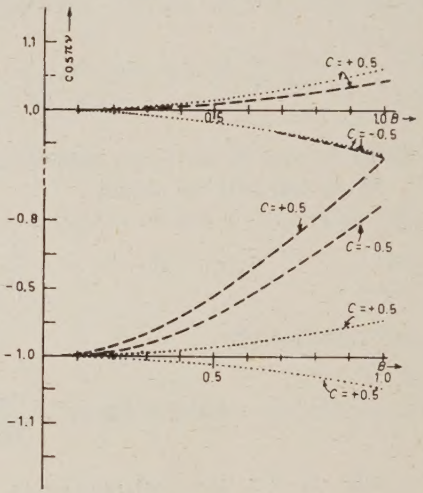

Fig. 2. – Comparison of $\cos \pi\nu$ at Stability limits $\nu=0$ and $\nu=1$. —— Digital Computer results (Identical with B axis) (A is chosen for specified B and $C=\pm\frac{1}{2}$ so that $\nu=0, 1$). – – – Symon approximation . . . . . Successive approximation for the same values of A, B and C as above.

5. – Equation of Motion as an Integral Equation.

From Eq. (1) we obtain immediately

$$y(t) = y(0) + y'(0)t + \int_0^t dt' \int_0^{t'} dt'' f(t'')y(t'')\,. \tag{37}$$

(6) E. C. COURANT and H. SNYDER: *Theory of the A. G. Synchrotron*, Brookhaven National Laboratory, Upton, L. I. (New York).

We note that

$$\int_0^t \mathrm{d}t' \int_0^{t'} \mathrm{d}t'' f(t'')y(t'') = \int_0^t (t - t')f(t')y(t')\,\mathrm{d}t' , \tag{38}$$

so that Eq. (37) can be written as an integral equation of the Volterra type

$$y(t) = a(t) + \int_0^t K(t, t')y(t')\,\mathrm{d}t' , \tag{39}$$

where

$$K(t, t') = (t - t')f(t') \tag{40}$$

and

$$a(t) = y(0) + y'(0)t . \tag{41}$$

Equation (39) can be solved formally by iteration:

$$y(t) = a(t) + \int_0^t k(t, t')a(t')\,\mathrm{d}t' + \int_0^t k(t, t')\,\mathrm{d}t' \int_0^{t'} k(t', t'')a(t'')\,\mathrm{d}t'' + \dots , \tag{42}$$

or in symbolic form

$$y(t) = \{1 + K + K^2 + \dots\}a(t) = \frac{1}{1 - K}\,a(t) , \tag{43}$$

where

$$Ka(t) = \int_0^t k(t, t')a(t')\,\mathrm{d}t' .$$

For $G_1(t)$, the initial conditions require a $a(0) = 1$, and we obtain from Eq. (42)

$$\cos \nu\tau = \tfrac{1}{2}[G_1(\tau) + G_1(-\tau)] = 1 + \int_0^\tau (\tau - t)\,\tfrac{1}{2}[f(t) + f(-t)]\,\mathrm{d}t + \tag{44}$$

$$+ \frac{1}{2}\int_0^\tau (\tau - t)\left\{f(t)\int_0^t (t - t')f(t')\,\mathrm{d}t' + f(-t)\int_0^t (t - t')f(-t')\,\mathrm{d}t'\right\}\mathrm{d}t .$$

With the abbreviations

$$\left\{\begin{aligned} f(t) &= -\lambda^2 + h[C(t) + S(t)] \\ C(t) &= \sum_{k=1} a_k \cos 2\pi k \frac{t}{\tau}, \\ S(t) &= \sum_{k=1} b_k \sin 2\pi k \frac{t}{\tau}. \end{aligned}\right. \tag{45}$$

Equation (44) becomes

$$\cos \nu\tau = 1 - \frac{\tau^2\lambda^2}{2} + \tag{46}$$

$$+ \int_0^\tau (\tau - t)\,\mathrm{d}t \int_0^t (t - t')[\lambda^4 + h^2 C(t)C(t') + h^2 S(t)S(t') - \lambda^2 h C(t) - \lambda^2 h C(t')]\,\mathrm{d}t' .$$

Confining ourselves to the second iteration we obtain

$$\cos \nu\tau = 1 - \frac{\tau^2\lambda^2}{2} + \frac{\tau^4\lambda^4}{4!} - \frac{\tau^4 h^2}{16\pi^2} \sum_k \frac{a_k^2 + b_k^2}{k^2}. \tag{47}$$

This result is clearly in agreement with the result of the successive approximation method given in Eq. (33), provided we introduce then the assumption $\lambda\tau \ll 1$, as shown in Eq. (34). Equation (47) also agrees exactly with the results of the Taylor expansion. The comparison of these three methods shows that for h not too large the successive approximation method will give the best results. If, however, $\lambda \sim h$, the integral equation will in any given iteration yeld terms of the same order of magnitude. These results can be easily compared with the result obtained by D. S. FALK [7]. Expanding $\cos \nu\tau$ and keeping only terms up to τ^2 we find, as Falk did, by a first order perturbation calculation:

$$\nu^2 \approx \lambda^2 + \frac{h^2}{2} \sum_{k=1} \frac{a_k^2 + b_k^2}{N^2 k^2}, \tag{48}$$

where $N = 2\pi/\tau$.

This integral equation formulation is, of course, not limited to the linear differential equations of the Hill type, and it may be useful in studying nonlinear problems.

[7] D. S. FALK: *Approximations for Frequency of Oscillations about the Equilibrium Orbit in a Thomas Type Cyclotron*, Oak Ridge National Laboratory, Oak Ridge, Tenn.

6. – Properties of $G_1(t)$.

General properties of $G_1(t)$ can be deduced directly from the character of the Hill equation basing the argument on the approximation methods discussed before.

As a first property, we shall prove that for the fundamental solutions $G_1(t)$ and $G_2(t)$

$$G_1(\tau) = G_2'(-\tau)\,, \tag{49}$$

$$G_2(-\tau) = -G_2(\tau)\,. \tag{50}$$

For this purpose we can combine Eq. (8) and the corresponding expression for $y'(t)$ in the matrix equation

$$\begin{pmatrix} y(t) \\ y'(t) \end{pmatrix} = \begin{pmatrix} G_1(t) & G_2(t) \\ G_1'(t) & G_2'(t) \end{pmatrix} \begin{pmatrix} y(0) \\ y'(0) \end{pmatrix} \qquad M(t,\,0) \begin{pmatrix} y(0) \\ y'(0) \end{pmatrix}. \tag{51}$$

The transformation $M(t)$ is unimodular because the Wronskian of $G_1(t)$ and $G_2(t)$ is unity. The property $|M(t, t_0)| = 1$ expresses the validity of Liouville's theorem for the motion described by Eq. (1). Since

$$M(\tau, 0) \begin{pmatrix} y(0) \\ y'(0) \end{pmatrix} = \begin{pmatrix} y(\tau) \\ y'(\tau) \end{pmatrix}, \tag{52}$$

and, from the definition of $M(t, t_0)$

$$M(0, \tau) M(\tau, 0) \begin{pmatrix} y(0) \\ y'(0) \end{pmatrix} = \begin{pmatrix} y(0) \\ y'(0) \end{pmatrix}, \tag{53}$$

we have:

$$M(0, \tau) = M^{-1}(\tau, 0)\,. \tag{54}$$

The elements $G_1(t - t_0)$, $G'(t - t_0)$, etc., of $M(t, t_0)$ depend only on the difference $t - t_0$, and therefore,

$$M(0, \tau) = M(-\tau, 0)$$

so that

$$M(-\tau, 0) = M^{-1}(\tau, 0) \tag{55}$$

and explicitly:

$$\begin{pmatrix} G_1(-\tau) & G_2(-\tau) \\ G_1'(-\tau) & G_2'(-\tau) \end{pmatrix} = \begin{pmatrix} G_2'(\tau) & -G_2(\tau) \\ -G_1'(\tau) & G_1(\tau) \end{pmatrix}. \tag{56}$$

From Eq. (56) we obtain, with the notation

$$\begin{cases} G^+(\tau) = \frac{1}{2}[G(\tau) + G(-\tau)] \\ G^-(\tau) = \frac{1}{2}[G(\tau) - G(-\tau)], \end{cases} \tag{57}$$

$$\begin{cases} G_2'^+(\tau) = G_1^+(\tau) \\ G_2'^-(\tau) = -G_1^-(\tau) \\ G_2^-(\tau) = G_1'^+(\tau) = 0. \end{cases} \tag{58}$$

Returning now to Eq. (3), we can express the particular solution $F(t)$ in terms of the fundamental solutions

$$\begin{pmatrix} G_1(t-\tau) & G_2(t-\tau) \\ G_1'(t-\tau) & G_2'(t-\tau) \end{pmatrix} \begin{pmatrix} F(0) \\ F'(0) \end{pmatrix} = k \begin{pmatrix} G_1(t) & G_2(t) \\ G_1'(t) & G_2'(t) \end{pmatrix} \begin{pmatrix} F(0) \\ F'(0) \end{pmatrix}, \tag{59}$$

and, in particular, at $t = 0$

$$\begin{pmatrix} G_1(\tau) - k & G_2(\tau) \\ G_1'(\tau) & G_2'(\tau) - k \end{pmatrix} \begin{pmatrix} F(0) \\ F'(0) \end{pmatrix} = 0. \tag{60}$$

Since there exists always a solution $F(t) \neq 0$ satisfying the requirement of Eq. (3), we have from Eq. (60), because the Wronskian is unity:

$$k^2 - k(G_1(\tau) + G_2'(\tau)) + 1 = 0. \tag{61}$$

Eliminating $G_2(\tau)$ by means of Eq. (58), the roots of Eq. (61) can be written as

$$k_{1,2} = G_1^+(\tau) \pm i\sqrt{1 - G_1^{+2}(\tau)}. \tag{62}$$

We note that the stability condition requires

$$k = \exp[i\nu\tau], \qquad \nu \text{ real},$$

so that, for stability

$$|G_1^+(\tau)| < 1. \tag{63}$$

Furthermore, we see that

$$\frac{1}{2}(k_1 + k_2) = \cos \nu\tau = \tfrac{1}{2}[G_1(\tau) + G_2'(\tau)] = G_1^+(\tau) \,. \tag{64}$$

Equation (63) shows that $G_1^+(\tau) = 1$, considered as a function of the Fourier coefficients of the function $f(t)$, determines directly the stability limits.

Furthermore it can be shown that $G_1^+(\tau)$ contains only quadratic and bilinear combinations of the Fourier coefficients b_k of the sine-terms in $f(t)$. To show this, it is convenient to rewrite $f(t)$ in the form

$$f(t) = -\lambda^2 + h_+ C(t) + h_- S(t) \,, \tag{65}$$

where $C(t)$ and $S(t)$ are respectively even and odd functions of t. In this notation Eq. (1) becomes

$$G_1''(t;\, h_+, h_-) = [-\lambda^2 + h_+ C(t) + h_- S(t)] G_1(t;\, h_+, h_-) \tag{66}$$

where we have written

$$G_1(t) = G_1(t;\, h_+, h_-)$$

to indicate explicitly the role of the even and odd parts of $f(t)$.

Applying the transformation $t \to -t$ to Eq. (66) we obtain

$$G_1''(-t;\, h_+, h_-) = [-\lambda^2 + h_+ C(t) - h_- S(t)] G_1(-t;\, h_+, h_-) \,. \tag{67}$$

On the other hand

$$G_1''(-t;\, h_+, -h_-) = [-\lambda^2 + h_+ C - h_- S] G_1(-t;\, h_+, -h_-) \,. \tag{68}$$

By comparison with Eq. (66) we find

$$G_1(-t;\, h_+, -h_-) = G_1(t;\, h_+, h_-) \,. \tag{69}$$

From Eq. (69) therefore we obtain

$$\begin{aligned} \cos \nu\tau &= G_1(\tau;\, h_+, h_-) + G_1(-\tau;\, h_+, h_-) = \\ &= G_1(-\tau;\, h_+, -h_-) + G_1(\tau;\, h_+, -h_-) \,. \end{aligned} \tag{70}$$

This result indicates that the sine-coeffcients of the function $f(t)$ contribute to $\cos \nu\tau$ only in even combinations, i.e. they will appear only as even powers and bilinear combinations.

This result, which is verified for the second power in h by Eq. (33), is useful in the calculation of higher order approximations.

Indicating with P a given power of h, we can note that, when P is even, there will be only even combinations of the h_+ and h_- coefficients, as it is verified for $P = 2$. When P is odd, only the cosine-coefficients h_+ will appear in odd powers.

A more detailed consideration of the way the different Fourier coefficients occur in $\cos \nu\tau$ can also be made, writing

$$f(t) = \cdots + \lambda^2 + h^+ C_+ + h^- C_- + h^+ S_+ + h^- S_- \cdots$$

where C_+ and S_- contain only even harmonics and C_- and S_+ contain only odd harmonics.

With this notation the contributions to $\cos \nu\tau$ of order h^P can be written as

$$(h_+^+)^i (h_+^-)^j (h_-^+)^k (h^-)^l \tag{71}$$

with $k + l =$ even and $i + j + k + l = P$. Shifting the origin to $\tau/2$ one has to the same order h^P the terms

$$(h_+^+)^i (-h_+^-)^j (h_-^+)^k (-h_-^-)^l . \tag{72}$$

Since the value of $\cos \nu\tau$ is independent on the choise of the origin, the two terms in Eq. (71) and (72) have to be equal, and therefore $j + l$ even. One verifies in this way that $P = 1$ does not give any contribution, while for $P = 2$ there are terms in h_+^{+2}, h^{-2}, h_-^{+2} and h^{+2}, as obtained by the successive approximation method. For $P = 3$ we expect terms of the form (*)

$$h_+^{+3}, \quad h_+^+ h_+^{-2}, \quad h_+^+ h_-^{+2}, \quad h_+^+ h_-^{-2}, \quad h_-^- h_+^+ h_-^-,$$

while for $P = 4$ contributions of the type

$$h_+^{+4}, \quad h_+^{+2} h^{+2}, \quad h_+^{+2} h_-^{+2}, \quad h_+^{+2} h_-^{-2}, \quad h_-^{-4}, \quad h_+^+ h_+^- h_-^+ h_+^+, \quad \ldots, \quad \text{etc.}$$

appear. The successive approximation method gives for the third order:

$$\frac{\Phi_3(\tau) + \Phi_3(-\tau)}{2} = -\frac{1}{32} \frac{\tau^6}{\pi^4} \frac{\sin \lambda\tau}{\lambda\tau} \sum_{k,j \neq k}' \frac{f_j f_{-k} f_{k-j}}{(k^2 - (\lambda^2\tau^2/\pi^2))(j^2 - (\lambda^2\tau^2/\pi^2))} \left[1 + \frac{\lambda^2\tau^2}{\pi^2 kj}\right]. \tag{73}$$

(*) We are very indebted to Dr. N. VOGT-NIELSEN for a valuable discussion on this point.

The right hand side of Eq. (73) vanishes identically if $f_k = -f_{-k}$, i.e. if $f(t)$ contains only sine-terms.

For the case of two frequencies, $2\pi/\tau$ and $4\pi/\tau$ only, we have for Eq. (73)

$$\frac{\Phi_3(\tau) + \Phi_3(-\tau)}{2} = \frac{3}{64}\frac{\tau^6}{\pi^4}\frac{\sin\lambda\tau}{\lambda\tau}\frac{a_2a_1^2 - a_2b_1^2 - 2a_1b_1b_2}{(1-\lambda^2\tau^2/\pi^2)(4-\lambda^2\tau^2/\pi^2)}. \tag{74}$$

In particular, for the case considered by L. J. LASLETT [4], ($b_1 = b_2 = 0$) the expression for $\cos\nu\tau$ to the third approximation is

$$\cos\nu\tau \cong \cos\lambda\tau - \frac{h^2}{16}\frac{\tau^4}{\pi^2}\frac{\sin\lambda\tau}{\lambda\tau}\left[\frac{a_1^2}{(1-\lambda^2\tau^2/\pi^2)} + \frac{a_2^2}{(4-\lambda^2\tau^2/\pi^2)}\right] + \frac{3h^3}{64}\frac{\tau^6}{\pi^4}\frac{\sin\lambda\tau}{\lambda\tau}\frac{a_1^2a_2}{(1-\lambda^2\tau^2/\pi^2)(4-\lambda^2\tau^2/\pi^2)}. \tag{75}$$

This result is in agreement with the general pattern of the $\cos\nu\tau$-curves obtained by L. J. LASLETT. Fig. 1 presents a comparison for a sample case of Laslett's curves with our second-order approximation. A survey-calculation indicates that our third-order correction separates the values for $B(\nu, A, C)$ for positive and negative values of C exactly as predicted by the digital computer calculations.

The fourth-order iteration gives

$$\frac{\Phi_4(\tau) + \Phi_4(-\tau)}{2} = \frac{\tau}{\lambda}\sin\lambda\tau[A_1 + A_2 + A_3] - \tau^2\cos\lambda\tau\, I_3. \tag{76}$$

The general espressions for A_1 A_2 and A_3 are given in Table II.

TABLE II.

$$A_1 = \frac{1}{8}\sum_j{}' \frac{f_j f_{-j}}{2\gamma_j}\sum_k{}' \frac{f_k f_{-k}}{8\gamma_k^2}\left(\frac{\lambda^2\tau^2}{\pi^2k^2} - 3\right) - \frac{1}{16}\sum_{\substack{k,j,l\\ k\neq j\\ l\neq j}}{}' \frac{f_{-k}f_l f_{k-j}f_{j-l}}{8\gamma_k\gamma_j\gamma_l}\left[1 + \frac{\lambda^2\tau^2}{\pi^2}\left(\frac{1}{k\cdot j} + \frac{1}{k\cdot l} + \frac{1}{j\cdot l}\right)\right]$$

$$A_2 = -\frac{1}{32}\sum_{\substack{k,l\\ k\neq l}}{}' \frac{f_{-k}f_l f_{k-j}}{4\gamma_k\gamma_j}\left(\frac{1}{k} + \frac{1}{l}\right)\sum_j{}' \frac{jf_j}{\gamma_j}$$

$$I_3 = \frac{1}{16\lambda^2}\left(\sum_k{}' \frac{jf_j}{2\gamma_k}\right)^2; \qquad \gamma_k = \frac{\pi^2k^2}{\tau^2} - \lambda^2$$

We state the result here for the special case of two cosine-components only:

$$(77)\quad \frac{\Phi_1(\tau)+\Phi_4(-\tau)}{2} = \frac{1}{16.64}\frac{\tau^8}{\pi^6}\frac{\sin\lambda\tau}{\lambda\tau}\left\{a_1^4\,\frac{8+15(\lambda\tau/\pi)^4-35(\lambda\tau/\pi)^2}{(\lambda\tau/\pi)^2(1-(\lambda^2\tau^2/\pi^2))^3(4-(\lambda^2\tau^2/\pi^2))}+\right.$$

$$a_2^4\,\frac{128+15(\lambda\tau/\pi)^4-140(\lambda\tau/\pi)^2}{(\lambda\tau/\pi)^2(4-(\lambda^2\tau^2/\pi^2))^3(16-(\lambda^2\tau^2/\pi^2))}$$

$$\left.a_1^2a_2^2\,\frac{72-618(\lambda\tau/\pi)^2+449(\lambda\tau/\pi)^4-58(\lambda\tau/\pi)^6}{(\lambda\tau/\pi)^2(1-(\lambda^2\tau^2/\pi^2))^2(4-(\lambda^2\tau^2/\pi^2))^2(9-(\lambda^2\tau^2/\pi^2))}\right\}$$

$$\frac{1}{16.32}\frac{\tau^6}{\lambda^4}\frac{\cos\lambda\tau}{\lambda^2}\left(\frac{a_1^2}{1-(\lambda^2\tau^2/\pi^2)}+\frac{a_2^2}{4-(\tau^2\lambda^2/\pi^2)}\right)^2.$$

If $f(t)$ contains a single cosine-component only, our results identically reproduce the expansion of the corresponding Mathieu function ([8]).

The case in which the function $f(t)$ has the form of a perturbation expansion, i.e. when the coefficients of the k-th harmonic are of the order h^k, is treated by HILL ([9]). In this case one expects that the odd powers of the b_k will occur in the expression for $\cos\nu\tau$, as it can be seen by the successive approximation method. For example, the second approximation introduces into the expression for $\cos\nu\tau$ a term linear in b_2.

* * *

We are very indebted to Dr. DE VOGALAERE of Notre Dame University for useful comments on this case.

([8]) J. MEIXNER and F. W. SCHAEFKE: *Mathieusche Funktionen* (Berlin, 1954).
([9]) *Acta Mathematica*, **8** (1886).

RIASSUNTO

Nel presente lavoro si discutono tre metodi di approssimazione per dedurre l'esponente caratteristico dell'equazione generalizzata di Hill. I risultati sono dedotti dalle proprietà generali dell'equazione stessa e vengono applicati al problema particolare delle « linear-betatron-oscillations » in una macchina acceleratrice.

IL NUOVO CIMENTO Vol. IV, N. 5 1° Novembre 1956

One-Time Formulation of the Relativistic Two-Body Problem. Separation of Angular Variables (*).

W. Królikowski

Institute of Physics of the Polish Academy of Sciences - Warsaw

J. Rzewuski

Institute of Physics of the Polish Academy of Sciences - Wrocław

(ricevuto il 22 Maggio 1956)

Summary. — The separation of angular variables in the relativistic one-time equation for the two-fermion problem in Quantum Electrodynamics is carried out for the case of one-quantum interaction. The momentum representation is used. A system of sixteen integral equations with respect to one variable is obtained. This system reduces to four equations in the case $j=0$ and to eight equations for $j\neq 0$.

1. – Introduction.

In the first paper of this series (1) the relativistic many-time equation for the two-fermion problem in qantum electrodynamics was transformed into the (equivalent) one-time equation possessing the form of a Schrödinger equation. The operator playing in this equation the rôle of the potential is in ge-

(*) A full account of the calculations is submitted to the *Acta Physica Polonica*.

(1) W. Królikowski and J. Rzewuski: *Nuovo Cimento*, **2**, 203 (1955); *Bull. Acad. Pol. Sci. Cl. III*, **3**, 353 (1955).

neral a complex quantity. The imaginary part of this potential is due to the instability of two-fermion states and determines the life-time of these states. Using in the kernels of the original many-time equations the functions S^{ret} (as in GÜNTHER's paper [2]) we obtain the single-particle theory of fermions; using instead the functions $(i/2)S_F$ (as in BETHE-SALPETER's paper [3]) we get the symmetrical hole theory.

The one-time equations of the many-body problem in quantum field theory were discussed further [1] from a more general point of view. The resulting equations describe bare particles. If, however, the renormalization procedure may be performed [5], they become the equations of physical particles. In the considerations of paper [1] that initial condition was used which corresponds to the single particle version of the theory of fermions. Using the condition of Feynman's type one gets the symmetrical hole version.

The next step should be the solution of the equations and comparison with experiment. In the present paper we solve the angular part of the two-fermion problem and use the solution for the separation of angular variables. The resulting set of integral equations in one variable is subject to further investigations.

In virtue of [1] (cf. in particular Sect. 4 of paper [1]) we have the following equation for the two-fermion problem in quantum electrodynamics when considering one-quantum interaction only:

$$(1.1)\qquad [W - H_1(-i\hbar\partial_1) - H_2(-i\hbar\partial_2)]\Phi(\boldsymbol{x}_1, \boldsymbol{x}_2) = \\ = \int V(\boldsymbol{x}_1, \boldsymbol{x}_2; \boldsymbol{x}_1', \boldsymbol{x}_2')\,\Phi(\boldsymbol{x}_1', \boldsymbol{x}_2')\,\mathrm{d}\boldsymbol{x}_1'\,\mathrm{d}\boldsymbol{x}_2'.$$

where

$$(1.2)\qquad \begin{cases} H_i(\boldsymbol{p}) = \gamma_4^{(i)}(ic\boldsymbol{\gamma}^{(i)}\boldsymbol{p} + m_i c^2) = c\boldsymbol{\alpha}^{(i)}\boldsymbol{p} + \beta^{(i)} m_i c^2\,, & i = 1, 2 \\ (\gamma_\mu) = (-i\beta\boldsymbol{\alpha}, \beta)\,, \end{cases}$$

$$(1.3)\qquad V(\boldsymbol{x}_1, \boldsymbol{x}_2; \boldsymbol{x}_1', \boldsymbol{x}_2') \quad \lambda\hbar c[\gamma_4^{(1)} A_0^{(1)}(\boldsymbol{x}_1, \boldsymbol{x}_2; \boldsymbol{x}_1', \boldsymbol{x}_2') \quad \gamma_4^{(2)} A_0^{(2)}(\boldsymbol{x}_1, \boldsymbol{x}_2; \boldsymbol{x}_1', \boldsymbol{x}_2')]\gamma_4^{(1)}\gamma_4^{(2)}$$

and $W = \bar{E} - i\Gamma$.

---

[2] M. GÜNTHER: *Phys. Rev.*, **88**, 1411 (1952); **94**, 1347 (1954).

[3] E. E. SALPETER and H. A. BETHE: *Phys. Rev.*, **84**, 1232 (1951); J. SCHWINGER: *Proc. Nat. Acad. Sci. U.S.*, **37**, 452, 455 (1951).

[4] W. KRÓLIKOWSKI and J. RZEWUSKI: *Nuovo Cimento*, **3**, 260 (1956); *Bull. Acad. Pol. Sci. Cl. III*, **4**, 19 (1956).

[5] P. T. MATTHEWS and ABDUS SALAM: *Phys. Rev.*, **94**, 185 (1954); K. A. JOHNSON: *Phys. Rev.*, **101**, 448 (1956).

Using the kernels of the many-time equations in Günther's form we get

$$(1.4)\qquad V(\boldsymbol{x}_1, \boldsymbol{x}_2; \boldsymbol{x}_1', \boldsymbol{x}_2') =$$

$$= \pm e^2 \left[\int \mathrm{d}x_1'' \gamma_4^{(2)} S_1^{\mathrm{ret}}(x_1 - x_1'') \gamma_\mu^{(1)} \gamma_\mu^{(2)} D_\pm(x_1'' - x_2) S_1(x_1'' - x_1') S_2(x_2 - x_2') - \right.$$

$$\left. - \int \mathrm{d}x_2'' \gamma_4^{(1)} S_2^{\mathrm{ret}}(x_2 - x_2'') \gamma_\mu^{(1)} \gamma_\mu^{(2)} D_\pm(x_1 - x_2'') S_1(x_1 - x_1') S_2(x_2'' - x_2') \right] \gamma_\mu^{(1)} \gamma_\mu^{(2)} ,$$

where the upper sign corresponds to opposite signs of charges the lower to equal signs. Considering these kernels in Bethe-Salpeter's form we obtain the formula (1.4) in which S_i^{ret} and replaced by iS_{+i}. The functions $D_- = \frac{1}{2} D_F$ and $S_{+i} = \frac{1}{2} S_{Fi}$ are the Feynman solutions of the equations

$$\Box D_\pm(x) = i\delta(x) \qquad \text{and} \qquad (\hat{c} + \varkappa_i) S_{+i}(x) = -i\delta(x) ,$$

and

$$S_i^{\mathrm{ret}}(x) = \theta^+(t) S_i(x) , \qquad \theta^+(t) = \begin{cases} 0 & \text{for } t < 0 \\ 1 & \text{for } t > 0 \end{cases}$$

is the retarded solution of the equation

$$(\hat{c} + \varkappa_i) S_i^{\mathrm{ret}}(x) = \delta(x) .$$

Making use of the formula

$$(1.5)\qquad S_i(x) = \exp\left[-\frac{i}{\hbar} H_i(-i\hbar\hat{c})t \right] i\delta(\boldsymbol{x}) \gamma_4^{(i)} ,$$

we may rewrite (1.4) in the form

$$(1.6)\qquad V(\boldsymbol{x}_1, \boldsymbol{x}_2; \boldsymbol{x}_1', \boldsymbol{x}_2') = V(\boldsymbol{x}_1, \boldsymbol{x}_2) \delta(\boldsymbol{x}_1 - \boldsymbol{x}_1') \delta(\boldsymbol{x}_2 - \boldsymbol{x}_2') ,$$

where

$$(1.7)\qquad V(\boldsymbol{x}_1, \boldsymbol{x}_2) =$$

$$= \mp ie^2 c \int_{-\infty}^{0} \mathrm{d}t \left\{ \exp\left[\frac{i}{\hbar} H_1(-i\hbar\partial_1)t \right] \Gamma D_+(\boldsymbol{x}_1 - \boldsymbol{x}_2, ct) \exp\left[-\frac{i}{\hbar} H_1(-i\hbar\partial_1)t \right] - \right.$$

$$\left. + \exp\left[\frac{i}{\hbar} H_2(-i\hbar\partial_2)t \right] \Gamma D_+(\boldsymbol{x}_1 - \boldsymbol{x}_2, ct) \exp\left[-\frac{i}{\hbar} H_2(-i\hbar\hat{c}_2)t \right] \right\}$$

and

$$(1.8)\qquad \Gamma = \gamma_4^{(1)} \gamma_4^{(2)} \gamma_\mu^{(1)} \gamma_\mu^{(2)} = 1 - \boldsymbol{\alpha}^{(1)} \boldsymbol{\alpha}^{(2)} .$$

Note that $V(\boldsymbol{x}_1, \boldsymbol{x}_2)$ is a differential operator operating on $\delta(\boldsymbol{x}_1 - \boldsymbol{x}_1') \delta(\boldsymbol{x}_2 - \boldsymbol{x}_2')$.

The I of equation (1.8) must not be confused with the imaginary part of W.

Considering the kernels in Bethe-Salpeter's form and using the formula

$$S_{ci}(x) = \Lambda_{\pm}^{(i)}(-i\hbar\partial)\varepsilon(t)\,\frac{1}{i}S_i(x)\,, \qquad \varepsilon(t) = \begin{cases} -1 & \text{for } t>0 \\ 1 & \text{for } t<0\,, \end{cases}$$

$$\Lambda_{\pm}^{(i)}(-i\hbar\partial) = \frac{H_i(-i\hbar\partial) \pm H_i(-i\hbar\partial)}{2\,H_i(-i\hbar\partial)} \qquad \begin{cases} + & \text{for } t>0 \\ - & \text{for } t<0\,, \end{cases}$$

we get (1.6) with

$$(1.7') \qquad V(\boldsymbol{x}_1, \boldsymbol{x}_2) =$$

$$= ie^2c\left\{\Lambda_{+}^{(1)}(-i\hbar\partial_1)\int_{-\infty}^{0} dt\,\exp\left[\frac{i}{\hbar}H_1(-i\hbar\partial_1)t\right] ID_{+}(\boldsymbol{x}_1-\boldsymbol{x}_2, ct)\,\exp\left[-\frac{i}{\hbar}H_1(-i\hbar\partial_1)t\right]\right.$$

$$\Lambda^{(1)}(-i\hbar\partial_1)\int_{0}^{\infty} dt\,\exp\left[\frac{i}{\hbar}H_1(-i\hbar\partial_1)t\right] ID_{-}(\boldsymbol{x}_1-\boldsymbol{x}_2, ct)\,\exp\left[-\frac{i}{\hbar}H_1(-i\hbar\partial_1)t\right] -$$

$$\Lambda^{(2)}(-i\hbar\partial_2)\int_{-\infty}^{0} dt\,\exp\left[\frac{i}{\hbar}H_2(-i\hbar\partial_2)t\right] ID_{-}(\boldsymbol{x}_1-\boldsymbol{x}_2, ct)\,\exp\left[-\frac{i}{\hbar}H_2(-i\hbar\partial_2)t\right]$$

$$\left.\Lambda^{(2)}(-i\hbar\partial_2)\int_{0}^{+\infty} dt\,\exp\left[\frac{i}{\hbar}H_2(-i\hbar\partial_2)t\right] ID_{+}(\boldsymbol{x}_1-\boldsymbol{x}_2, ct)\,\exp\left[-\frac{i}{\hbar}H_2(-i\hbar\partial_2)t\right]\right\}.$$

instead of (1.7).

2. – Transition to the Momentum Representation.

We transform now equation (1.1) to the momentum representation and obtain an equation of the form

$$(2.1) \qquad [W - H_1(\boldsymbol{p}_1) - H_2(\boldsymbol{p}_2)]\,\Phi(\boldsymbol{p}_1, \boldsymbol{p}_2) = \int\int V(\boldsymbol{p}_1, \boldsymbol{p}_2; \boldsymbol{p}_1', \boldsymbol{p}_2')\,\Phi(\boldsymbol{p}_1', \boldsymbol{p}_2')\,d\boldsymbol{p}_1'\,d\boldsymbol{p}_2'\,.$$

where

$$(2.2) \qquad \begin{cases} \Phi(\boldsymbol{p}_1, \boldsymbol{p}_2) = \int\int \langle \boldsymbol{p}_1, \boldsymbol{p}_2 | \boldsymbol{x}_1, \boldsymbol{x}_2\rangle\,\Phi(\boldsymbol{x}_1, \boldsymbol{x}_2)\,d\boldsymbol{x}_1\,d\boldsymbol{x}_2 \\ V(\boldsymbol{p}_1, \boldsymbol{p}_2; \boldsymbol{p}_1', \boldsymbol{p}_2') = \int\int \langle \boldsymbol{p}_1, \boldsymbol{p}_2 | \boldsymbol{x}_1, \boldsymbol{x}_2\rangle V(\boldsymbol{x}_1, \boldsymbol{x}_2)\langle \boldsymbol{x}_1, \boldsymbol{x}_2 | \boldsymbol{p}_1', \boldsymbol{p}_2'\rangle\,d\boldsymbol{x}_1\,d\boldsymbol{x}_2\,. \end{cases}$$

Here we have

$$(2.3)\qquad \left\{\begin{array}{l} |\boldsymbol{x}_1, \boldsymbol{x}_2\ \boldsymbol{p}_1, \boldsymbol{p}_2\rangle = (2\pi\hbar)^{-3}\, u_1(\boldsymbol{p}_1)\, u_2(\boldsymbol{p}_2)\exp\left[\frac{i}{\hbar}\,\boldsymbol{p}_1\boldsymbol{x}_1\right]\exp\left[\frac{i}{\hbar}\,\boldsymbol{p}_2\boldsymbol{x}_2\right] \\ (H_i(\boldsymbol{p})\, u_i(\boldsymbol{p}) = E_i(\boldsymbol{p})\, u_i(\boldsymbol{p}), \qquad E_i(\boldsymbol{p}) = \pm\, c\sqrt{\boldsymbol{p}^2 + (m_i c)^2}\,, \\ \qquad\qquad u_i^*(\boldsymbol{p})\, u_i(\boldsymbol{p}) = 1)\,. \end{array}\right.$$

Thus, thanks to (1.7) and (2.3), and using the formulae

$$D_\perp(x) = \frac{1}{2}\,\frac{1}{(2\pi)^3}\int \delta_+(k^2)\exp[ikx]\,\mathrm{d}k\,,$$

$$\delta_\pm(\omega) = \frac{1}{\pi}\int_0^\infty \mathrm{d}t\exp[\mp i\omega t] = \delta(\omega) \pm P\,\frac{1}{i\pi\omega}\,,$$

we get in Günther's case

$$(2.4)\qquad V(\boldsymbol{p}_1, \boldsymbol{p}_2; \boldsymbol{p}_1', \boldsymbol{p}_2') = -\frac{ie^2}{4\pi}\, u_1^*(\boldsymbol{p}_1)\, u_2^*(\boldsymbol{p}_2)\, \Gamma u_1'(\boldsymbol{p}_1')\, u_2'(\boldsymbol{p}_2')\delta(\boldsymbol{p}_1 + \boldsymbol{p}_2 - \boldsymbol{p}_1' - \boldsymbol{p}_2')\cdot$$

$$\cdot\,\frac{1}{4\pi\hbar}\int_{-\infty}^{+\infty}\mathrm{d}\omega\left\{\delta_+\left[(\boldsymbol{p}_1 - \boldsymbol{p}_1')^2 - \frac{\hbar^2}{c^2}\,\omega^2\right]\delta_+[\omega_1(\boldsymbol{p}_1) - \omega_1(\boldsymbol{p}_1') - \omega] + \right.$$

$$\left. + \delta_+\left[(\boldsymbol{p}_2 - \boldsymbol{p}_2')^2 - \frac{\hbar^2}{c^2}\,\omega^2\right]\delta_+[\omega_2(\boldsymbol{p}_2) - \omega_2(\boldsymbol{p}_2') - \omega]\right\},$$

where $E_i(\boldsymbol{p}) = \hbar\omega_i(\boldsymbol{p}) = \pm\, c\sqrt{\boldsymbol{p}^2 + (m_i c)^2}$.

Going over to the centre of mass system ($\boldsymbol{p}_1 = -\boldsymbol{p}_2 = \boldsymbol{p}$) and neglecting the imaginary part of V (*) we obtain

$$(2.5)\qquad [E - H_1(\boldsymbol{p}) - H_2(-\boldsymbol{p})]\,\Phi(\boldsymbol{p}) = \int V(\boldsymbol{p}, \boldsymbol{p}')\,\Phi(\boldsymbol{p}')\,\mathrm{d}\boldsymbol{p}'$$

where

$$(2.6)\qquad V(\boldsymbol{p}, \boldsymbol{p}') = +\frac{e^2}{4\pi}\, u_1^*(\boldsymbol{p})\, u_2^*(-\boldsymbol{p})\,\Gamma u_1'(\boldsymbol{p}')\, u_2'(-\boldsymbol{p}')\cdot$$

$$\cdot\,\frac{1}{(2\pi)^2\hbar}\cdot\frac{\alpha}{|\boldsymbol{p} - \boldsymbol{p}'|}\left[\frac{1}{|\boldsymbol{p} - \boldsymbol{p}'| + (1/c)(E_1 - E_1')} + \frac{1}{\boldsymbol{p}\quad \boldsymbol{p}' \quad - (1/c)(E_2 \quad E_2')}\right].$$

Here we denote $E_i = E_i(\boldsymbol{p})$, $E_i' = E_i(\boldsymbol{p}')$.

(*) The separation of angular variables may be carried out in exactly the same way when the full, complex expression for V is used (cf. Sect. 6).

We note that equation (2.5) in the position representation takes the form

$$[E - H_1(-i\hbar\partial) - H_2(+i\hbar\partial)]\Phi(\boldsymbol{x}) = \int V(\boldsymbol{x}, \boldsymbol{x}')\,\Phi(\boldsymbol{x}')\,\mathrm{d}\boldsymbol{x}' , \tag{2.7}$$

where

$$\begin{cases} \Phi(\boldsymbol{x}) = \int \langle \boldsymbol{x}|\boldsymbol{p}\rangle\,\mathrm{d}\boldsymbol{p}\,\Phi(\boldsymbol{p}) \\ V(\boldsymbol{x}, \boldsymbol{x}') = \iint \langle \boldsymbol{x}|\boldsymbol{p}\rangle\,\mathrm{d}\boldsymbol{p}\,V(\boldsymbol{p}, \boldsymbol{p}')\,\mathrm{d}\boldsymbol{p}'\langle \boldsymbol{p}'|\boldsymbol{x}'\rangle . \end{cases} \tag{2.8}$$

Here we have

$$\langle \boldsymbol{x}|\boldsymbol{p}\rangle = (2\pi\hbar)^{-\frac{3}{2}}\,u_1(\boldsymbol{p})\,u_2(-\boldsymbol{p})\exp\left[\frac{i}{\hbar}\boldsymbol{p}\boldsymbol{x}\right] . \tag{2.9}$$

The kernel (2.8) has in the static approximation (we put in (2.6) $E_i - E_i' = 0$) the well known form

$$V(\boldsymbol{x}, \boldsymbol{x}') = \mp\frac{e^2}{4\pi}\,\frac{\Gamma}{r_{\boldsymbol{x}}}\,\delta(\boldsymbol{x} - \boldsymbol{x}') . \tag{2.10}$$

Equation (2.7) is then the Breit equation with electromagnetic instantaneous interaction.

Similar calculations as in Günther's case (1.7) we may perform in the case of Bethe-Salpeter (1.7′). We obtain equation (2.5) with

$$V(\boldsymbol{p}, \boldsymbol{p}') = \mp\frac{e^2}{4\pi}\,u_1^*(\boldsymbol{p})\,u_2^*(-\boldsymbol{p})\,\Gamma u_1'(\boldsymbol{p}')\,u_2'(-\boldsymbol{p}')\cdot\frac{1}{(2\pi)^2\hbar}\cdot\frac{1}{\boldsymbol{p} - \boldsymbol{p}'}\cdot$$
$$\cdot\left[\frac{\frac{E_1}{|E_1|}}{|\boldsymbol{p} - \boldsymbol{p}'| + \frac{1}{c}\,\frac{E_1}{|E_1|}\,(E_1 - E_1')} + \frac{\frac{E_2}{|E_2|}}{|\boldsymbol{p} - \boldsymbol{p}'| + \frac{1}{c}\,\frac{E_2}{|E_2|}\,(E_2 - E_2')}\right] . \tag{2.6′}$$

instead of (2.6). The formula (2.6′) takes in the static approximation in the position representation the well known form

$$V(\boldsymbol{x}, \boldsymbol{x}') =$$
$$= \mp\frac{e^2}{4\pi}[\Lambda_+^{(1)}(-i\hbar\partial)\,\Lambda_+^{(2)}(i\hbar\partial) - \Lambda_-^{(1)}(-i\hbar\partial)\,\Lambda_-^{(2)}(i\hbar\partial)]\,\frac{\Gamma}{r_{\boldsymbol{x}}}\,\delta(\boldsymbol{x} - \boldsymbol{x}') . \tag{2.10′}$$

The wave function $\Phi(\boldsymbol{p})$ in equation (2.5) is labelled by the unit spinors u_1

and u_2: $\Phi(\boldsymbol{p}) = (\Phi_{u_1 u_2}(\boldsymbol{p}))$. Now we go over to the new wave function $\Phi(\boldsymbol{p}) = (\Phi_{\alpha_1 \alpha_2}(\boldsymbol{p}))$, which is labelled by the spinor indices α_1 and α_2, similar to $\Phi(\boldsymbol{p}) = (\Phi_{\alpha_1 \alpha_2}(\boldsymbol{x}))$. Performing the transformation

$$\Phi_{\alpha_1 \alpha_2}(\boldsymbol{p}) = \sum_{u_1 u_2} u^{(1)}_{\alpha_1}(\boldsymbol{p}) u^{(2)}_{\alpha_2}(-\boldsymbol{p}) \Phi_{u_1 u_2}(\boldsymbol{p})$$

and using the formula

$$(2.11) \qquad \sum_{\text{spin}} u^{(i)}_{\alpha}(\boldsymbol{p}) u^{(i)}_{\beta}(\boldsymbol{p}) = \Lambda^{(i)}_{\pm \alpha, \beta}(\boldsymbol{p}), \qquad \text{where} \qquad \Lambda^{(i)}_{\pm}(\boldsymbol{p}) = \frac{\pm E_i(\boldsymbol{p}) + H_i(\boldsymbol{p})}{2 |E_i(\boldsymbol{p})|},$$

we get from (2.5) an equation of the form

$$(2.12) \qquad (\varepsilon - h_1 - h_2) \Phi(\boldsymbol{p}) =$$

$$= \mp \frac{\alpha}{2\pi^2} \int \frac{1}{8} \sum_{\text{sign}} \{(h_1 + \varepsilon_1) \Gamma(h'_1 + \varepsilon'_1) M(\varepsilon_1, \varepsilon'_1) + (h_2 + \varepsilon_2) \Gamma(h'_2 + \varepsilon'_2) M(\varepsilon_2, \varepsilon'_2)\} \Phi(\boldsymbol{p}') \, \mathrm{d}\boldsymbol{p}',$$

where $\varepsilon = E/c$, $e_i = E_i/c$, $h_1 = (1/c) H_1(\boldsymbol{p})$, $h_2 = (1/c) H_2(-\boldsymbol{p})$,

$$(2.13) \qquad \begin{cases} h'_1 = \dfrac{1}{c} H_1(\boldsymbol{p}'), \qquad h'_2 = \dfrac{1}{c} H_2(-\boldsymbol{p}'), \\ \sum\limits_{\text{sign}} f(E, E') = f(E, E') + f(-E, E') + f(E, -E') + f(-E, -E') \end{cases}$$

and

$$(2.14) \qquad M(\varepsilon, \varepsilon') = \begin{cases} [|\boldsymbol{p} - \boldsymbol{p}'| \varepsilon \varepsilon' \{|\boldsymbol{p} - \boldsymbol{p}'| + \varepsilon - \varepsilon'\}]^{-1} & \text{in Günther's case} \\ \dfrac{\varepsilon}{|\varepsilon|} \left[|\boldsymbol{p} - \boldsymbol{p}'| \varepsilon \varepsilon' \left\{ |\boldsymbol{p} - \boldsymbol{p}'| + \dfrac{\varepsilon}{|\varepsilon|} (\varepsilon - \varepsilon') \right\} \right]^{-1} & \text{in the case of Bethe-Salpeter.} \end{cases}$$

3. – Solution of the Angular Problem.

As a first step towards the solution of equation (2.12) we shall try to separate the angular variables. This is certainly possible due to the invariance of our dynamical system with respect to rotations in threedimensional space. This invariance secures the conservation of the total angular momentum

$$(3.1) \qquad \begin{cases} J_i = -i\hbar M_i, \qquad M_i = m_i + s_i \\ m_i = p_j \dfrac{\partial}{\partial p_k} - p_k \dfrac{\partial}{\partial p_j}, \qquad s_i = \dfrac{1}{2} [\gamma^{(1)}_j \gamma^{(1)}_k + \gamma^{(2)}_j \gamma^{(2)}_k] \end{cases}$$

$$(i = 1, 2, 3; \ i, j, k = \text{cyclic permutation of } 1, 2, 3)$$

of the system and, consequently, its commutability with the integral operator of equation (2.12). We may, therefore, consider a system of three commuting

observables (there are three degrees of freedom left after separation of the center of mass variables) consisting of the integral operator of equation (2.12) and of the differential operators

$$J_3 \quad \text{and} \quad J_i^2 = J_1^2 + J_2^2 + J_3^2 . \tag{3.2}$$

The full system of equations consists now of (2.12) and of the two equations

$$J_3 \Phi(\boldsymbol{p}) = \hbar m \Phi(\boldsymbol{p}) , \tag{3.3}$$

$$J_i^2 \Phi(\boldsymbol{p}) = \hbar^2 j(j+1) \Phi(\boldsymbol{p}) . \tag{3.4}$$

We easily verify the commutability of the operators (3.2)

$$[J_i^2, J_3] = 0 \tag{3.5}$$

and the commutability of J_i (and, therefore also of J_i^2) with the integral operator of equation (2.12)

$$\left\{ \begin{array}{l} [M_i, h_1] = [M_i, h_2] = 0 , \quad i = 1, 2, 3 \\ M_i \int \mathrm{d}\boldsymbol{p}'(h_k + \varepsilon_k) I'(h_k' + \varepsilon_k') M(\varepsilon_k, \varepsilon_k') \Phi(\boldsymbol{p}') = \\ = \int \mathrm{d}\boldsymbol{p}'(h_k + \varepsilon_k) I'(h_k' + \varepsilon_k') M(\varepsilon_k, \varepsilon_k') \cdot M_i' \Phi(\boldsymbol{p}') , \\ \qquad\qquad (i = 1, 2, 3; \ k = 1, 2). \end{array} \right. \tag{3.6}$$

Equation (2.12) is inconvenient for direct treatment insofar as it contains angular variables as well under the integral sign as outside the integral by the intermediary of the operators h_1 and h_2. We shall remove this dependence from h_1 and h_2 by means of a unitary transformation

$$\overline{\Phi} = u\Phi , \qquad \overline{F} = uFu^{-1} , \tag{3.7}$$

where F is an arbitrary operator and u is the unitary operator

$$u = \exp[s_2 \vartheta] \exp[s_3 \varphi] \quad (*) , \tag{3.8}$$

ϑ and φ being the angular coordinates of the vector $\boldsymbol{p}$ in an arbitrary polar coordinate system.

(*) Transformations of this type were used e.g. by SOMMERFELD in the case of the Hydrogen atom (A. SOMMERFELD: *Atombau und Spektrallinien*, II. Band, 4. Kapitel and Zusatz 15) and by M. GÜNTHER (unpublished) in his treatment of the relativistic two-body problem. We are very much indebted to Dr. GÜNTHER for showing us his manuscript prior to publication and for valuable discussions.

The set of equations (2.12) and (3.3–4) is transformed by the transformation (3.7–8) into

$$(3.9)\qquad (\varepsilon - \bar{h}_1 - \bar{h}_2)\bar{\Phi}(\boldsymbol{p}) = -\frac{\alpha}{2\pi^2}\int \frac{1}{8}\sum_{\text{sign}} \{(\bar{h}_1 + \varepsilon_1) u\Gamma u'^{-1}(\bar{h}'_1 + \varepsilon'_1)\, M(\varepsilon_1, \varepsilon'_1) - (\bar{h}_2 + \varepsilon_2)\, u\Gamma u'^{-1}(\bar{h}'_2 + \varepsilon'_2)\, M(\varepsilon_2, \varepsilon'_2)\}\, \bar{\Phi}(\boldsymbol{p}')\, \mathrm{d}\boldsymbol{p}'$$

$$(3.10)\qquad \bar{J}_3\bar{\Phi}(\boldsymbol{p}) = \hbar m\bar{\Phi}(\boldsymbol{p})\,,$$

$$(3.11)\qquad \bar{J}_i^2\bar{\Phi}(\boldsymbol{p}) = \hbar^2 j(j+1)\bar{\Phi}(\boldsymbol{p})\,,$$

where

$$(3.12)\qquad \begin{cases} \bar{h}_1 = \gamma_4^{(1)}(ip\gamma_3^{(1)} + m_1 c) \\ \bar{h}_2 = \gamma_4^{(2)}(-ip\gamma_3^{(2)} + m_2 c) \end{cases}$$

do not depend on the angular variables and

$$(3.13)\qquad \begin{cases} \bar{M}_3 = -\dfrac{\partial}{\partial\varphi} \\ \bar{M}_i^2 = \dfrac{1}{\sin\vartheta}\dfrac{\partial}{\partial\vartheta}\left(\sin\vartheta\dfrac{\partial}{\partial\vartheta}\right) + \dfrac{1}{\sin^2\vartheta}\left(\dfrac{\partial^2}{\partial\varphi^2} - 2s_3\cos\vartheta\dfrac{\partial}{\partial\varphi} + s_3^2\right). \end{cases}$$

Equation (3.10) takes, on account of (3.13) and (3.1), the form

$$(3.14)\qquad \frac{\partial\bar{\Phi}}{\partial\varphi} = im\bar{\Phi}\,,$$

and possesses solutions of the form

$$(3.15)\qquad \bar{\Phi}(\varphi, \vartheta, p) = \exp[im\varphi]\chi(\vartheta, p)\,.$$

The boundary conditions $\bar{\Phi}(\varphi, \vartheta, p) \quad \bar{\Phi}(\varphi - 2\pi, \vartheta, p)$ are satisfied if m is an integer ($m = 0, \pm 1, \pm 2, \ldots$).

Introducing (3.15) into (3.11) we get, on account of (3.13),

$$(3.16)\qquad \left[\frac{1}{\sin\vartheta}\frac{\partial}{\partial\vartheta}\left(\sin\vartheta\frac{\partial}{\partial\vartheta}\right) + \frac{1}{\sin^2\vartheta}(-m^2 - 2ims_3\cos\vartheta + s_3^2)\right]\chi(\vartheta, p) = -j(j+1)\,\chi(\vartheta, p)\,.$$

Let us first solve equation (3.16) for $m = 0$. It takes in this case, if we

write out s_3^2 explicitly, the form

$$(3.17)\quad \left[\frac{1}{\sin\vartheta}\frac{\partial}{\partial\vartheta}\left(\sin\vartheta\frac{\partial}{\partial\vartheta}\right) - \frac{\{\frac{1}{2}[1-\gamma_1^{(1)}\gamma_2^{(1)}\gamma_1^{(2)}\gamma_2^{(2)}]\}^2}{\sin^2\vartheta}\right]\chi(\vartheta,p) = -j(j+1)\,\chi(\vartheta,p)\,.$$

Equation (3.17) possesses the form of the differential equation of spherical harmonics with the upper index $-s_3^2 = \frac{1}{2}[1 - \gamma_1^{(1)}\gamma_2^{(1)}\gamma_1^{(2)}\gamma_2^{(2)}]$ and with the lower index j

$$(3.18)\qquad Z_j^0(\cos\vartheta) = P_j^{-s_3^2}(\cos\vartheta)\,.$$

The meaning of (3.18) becomes immediately clear if one considers that the two mutually orthogonal operators

$$\tfrac{1}{2}[1-\gamma_1^{(1)}\gamma_2^{(1)}\gamma_1^{(2)}\gamma_2^{(2)}] \qquad \text{and} \qquad \tfrac{1}{2}[1+\gamma_1^{(1)}\gamma_2^{(1)}\gamma_1^{(2)}\gamma_2^{(2)}]$$

are indepotent and possess, therefore, the eingenvalues 0 and 1.

We may thus write instead of (3.18)

$$(3.19)\quad Z_j^0(\cos\vartheta) = \frac{1}{2}[1+\gamma_1^{(1)}\gamma_2^{(1)}\gamma_1^{(2)}\gamma_2^{(2)}]P_j^0(\cos\vartheta) + \frac{1}{2}[1-\gamma_1^{(1)}\gamma_2^{(1)}\gamma_1^{(2)}\gamma_2^{(2)}]P_j^1(\cos\vartheta) =$$

$$= \left\{\frac{1}{2}[1+\gamma_1^{(1)}\gamma_2^{(1)}\gamma_1^{(2)}\gamma_2^{(2)}] + \frac{1}{\sqrt{j(j+1)}}\frac{1}{2}[1-\gamma_1^{(1)}\gamma_2^{(1)}\gamma_1^{(2)}\gamma_2^{(2)}]\frac{\partial}{\partial\vartheta}\right\}P_j^0(\cos\vartheta)\,.$$

We use throughout this paper spherical harmonics normalized to unity

$$(3.20)\qquad \int_0^\pi P_j^m P_k^m \sin\vartheta\,\mathrm{d}\vartheta = \delta_{jk}\,.$$

Due to the rotational invariance of our equations in threedimensional space, the equations for the radial component cannot depend on the value of the quantum number m and, therefore, we may use already the eigenfunctions Z_j^0 of equation (3.17) for the separation of the variable ϑ. Nevertheless it may be of some interest to know also the eigensolutions of the general equation (3.16) with m an arbitrary integer. These eigensolutions were derived by M. GÜNTHER (cf. footnote on page 000) from Z_j^0 as generating function by a change of the pole of the polar coordinate system. The result is

$$(3.21)\quad Z_j^m(\cos\vartheta) =$$

$$= \left\{\frac{1}{2}[1+\gamma_1^{(1)}\gamma_2^{(1)}\gamma_1^{(2)}\gamma_2^{(2)}] + \frac{1}{\sqrt{j(j+1)}}\frac{1}{2}[1-\gamma_1^{(1)}\gamma_2^{(1)}\gamma_1^{(2)}\gamma_2^{(2)}]\left(\frac{\partial}{\partial\vartheta} - i\gamma_1^{(1)}\gamma_2^{(1)}\frac{m}{\sin\vartheta}\right)\right\}P_j^m(\cos\vartheta)$$

For $m = 0$ we get herefrom the function (3.19).

It may be verified directly that the Z_j^m are eigensolutions of equation (3.16). For this purpose it is convenient to write the second order differential operator occuring in (3.16) as the square of a first order differential operator

$$\frac{1}{\sin\vartheta}\frac{\partial}{\partial\vartheta}\left(\sin\vartheta\frac{\partial}{\partial\vartheta}\right)+\frac{1}{\sin^2\vartheta}(-m^2-2ims_3\cos\vartheta+s_3^2)=K^2\,, \tag{3.22}$$

where

$$K=\gamma_2^{(1)}\left(\frac{\partial}{\partial\vartheta}+i\gamma_1^{(1)}\gamma_2^{(1)}\frac{m}{\sin\vartheta}-s_3^2\operatorname{ctg}\vartheta\right). \tag{3.23}$$

Now we verify easily that Z_j^m is an eigenfunction of K:

$$KZ_j^m=-\sqrt{j(j+1)}\,Z_j^m\gamma_2^{(1)}\gamma_1^{(2)}\gamma_2^{(2)} \tag{3.24}$$

and, therefore,

$$K^2Z_j^m=-j(j+1)Z_j^m\,. \tag{3.25}$$

4. – Separation of the Angular Variables.

Having thus obtained the solutions of the angular problem (3.10–11) we may now proceed to the separation of the angular variables from the integral equation (3.9). As already stated on page 968, the result of the separation cannot depend on m and, therefore, we may use for our purposes the functions $Z_j^0(\cos\vartheta)$. We write the solutions in the form

$$\bar{\Phi}(\boldsymbol{p})=Z_j^0(\cos\vartheta)f(p)\,, \tag{4.1}$$

introduce this into the integral equation (3.9), multiply on the left with $Z_j^0(\cos\vartheta)$ and integrate over the solid angle ($\mathrm{d}\omega=\sin\vartheta\,\mathrm{d}\vartheta\,\mathrm{d}\varphi$). Due to the commutability of Z_j^0 with $\bar{h}_1$ and $\bar{h}_2$ we may write the result in the form

$$\begin{aligned}(\varepsilon-\bar{h}_1-\bar{h}_2)f(p)=\mp\frac{\alpha}{4\pi^3}\int_0^\infty\frac{1}{8}\sum_{\text{sign}}\{&(\bar{h}_1+\varepsilon_1)\Gamma K_j(\varepsilon_1,\varepsilon_1')(\bar{h}_1'+\varepsilon_1')+\\&+(\bar{h}_2+\varepsilon_2)\Gamma K_j(\varepsilon_2,\varepsilon_2')(\bar{h}_2'+\varepsilon_2')\}\,f(p')p'^2\,\mathrm{d}p'\end{aligned} \tag{4.2}$$

with

$$K_j(\varepsilon,\varepsilon')=\int\mathrm{d}\omega\int\mathrm{d}\omega'\,Z_j^0 u M(\varepsilon,\varepsilon')\,u'^{-1}Z_j^{0'}\,. \tag{4.3}$$

In this set of equations the angular variables no longer occur. It deter-

mines the energy eigenvalues and eigenfunctions of the relativistic two-body problem in the desired approximation (one-quantum interaction).

The fact that for $j = 0$ the projection operator $\frac{1}{2}[1 + \gamma_1^{(1)}\gamma_2^{(1)}\gamma_1^{(2)}\gamma_2^{(2)}]$ occurs as factor in the solution $f(p)(Z_0^0 - \frac{1}{2}[1 - \gamma_1^{(1)}\gamma_2^{(1)}\gamma_1^{(2)}\gamma_2^{(2)}]P_0^0)$ shows that the lowest state of the total angular momentum may be realised only in such a way that the orbital momentum as well as the total spin are zero ($\frac{1}{2}[\gamma_1^{(1)}\gamma_2^{(1)} - \gamma_1^{(2)}\gamma_2^{(2)}]f(p) = 0$) i.e. the particles posses opposite spins.

For further treatment of equation (4.2) we need, first of all, the explicit form of $K_j(\varepsilon, \varepsilon')$. To calculate (4.3) we note first that $M(\varepsilon, \varepsilon')$ depends on the angular variables through the intermediary of

$$\boldsymbol{p} - \boldsymbol{p}' = \sqrt{p^2 + p'^2 - 2pp' \cos\theta} \tag{4.4}$$

(cf. (2.14)), where $\cos\theta = \cos\vartheta \cos\vartheta' + \sin\vartheta \sin\vartheta' \cos(\varphi - \varphi')$ is the angle between $\boldsymbol{p}$ and $\boldsymbol{p}'$. We may expand, therefore, $M(\varepsilon, \varepsilon')$ in a series of Legendre's polynomials

$$\begin{cases} M(\varepsilon, \varepsilon') = \sum_{k=0}^{\infty} M_k(\varepsilon, \varepsilon') P_k(\cos\theta) \\ M_k(\varepsilon, \varepsilon') = \int_0^{\pi} M(\varepsilon, \varepsilon') P_k(\cos\theta) \sin\theta \, \mathrm{d}\theta \,. \end{cases} \tag{4.5}$$

Introducing (4.5) into (4.3) and using the summation theorem of spherical harmonics

$$P_k(\cos\theta) = \frac{1}{\sqrt{k + \frac{1}{2}}} \sum_{m=-k}^{m=+k} P_k^m(\cos\vartheta) P_k^m(\cos\vartheta') \exp[im(\varphi - \varphi')] \tag{4.6}$$

($P_k^{-m} = (-1)^m P_k^m$), we may write

$$K_j(\varepsilon, \varepsilon') = \sum_{k=0}^{\infty} \frac{M_k(\varepsilon, \varepsilon')}{\sqrt{k + \frac{1}{2}}} \sum_{m=-k}^{m=+k} \int \mathrm{d}\omega \int \mathrm{d}\omega' \, Z_j^0 U P_k^m \exp[im(\varphi - \varphi')] P_k^{m\prime} U^{\prime -1} Z_j^{0\prime} \,. \tag{4.7}$$

Integration over the angles φ and φ' yields

$$\int_0^{2\pi} \mathrm{d}\varphi \int_0^{2\pi} \mathrm{d}\varphi' \exp[im(\varphi - \varphi')] \exp s_3(\varphi - \varphi') = (2\pi)^2 \left\{ \frac{1}{2}[1 + \gamma_1^{(1)}\gamma_2^{(1)}\gamma_1^{(2)}\gamma_2^{(2)}] \delta_{m,0} - \right. \tag{4.8}$$

$$\left. - \frac{1}{2}[1 - \gamma_1^{(1)}\gamma_2^{(1)}\gamma_1^{(2)}\gamma_2^{(2)}] \frac{1}{2} (\delta_{m,-1} + \delta_{m,-1}) + \frac{1}{2}[\gamma_1^{(1)}\gamma_2^{(1)} + \gamma_1^{(2)}\gamma_2^{(2)}] \frac{1}{2i} (\delta_{m,-1} - \delta_{m,-1}) \right\} .$$

By virtue of (4.8) and (3.19) we may write (4.7) in the form

$$K_j(\varepsilon,\varepsilon') = \tag{4.9}$$

$$= (2\pi)^2 \sum_{k=0}^{\infty} \frac{M_k(\varepsilon,\varepsilon')}{\sqrt{k+\frac{1}{2}}} \cdot \int_0^{\pi} \sin\vartheta\,\mathrm{d}\vartheta \int_0^{\pi} \sin\vartheta'\,\mathrm{d}\vartheta'\, Z_j^0 \exp[s_2\vartheta] Z_k^0 \cdot Z_k^{0'} \exp[-s_2\vartheta'] Z_j^0 .$$

The remaining integrals may be evaluated with help of the well known recurrent formulae for spherical harmonics. After a rather lengthy but straightforward calculation we get finally

$$\frac{K_j(\varepsilon,\varepsilon')}{(2\pi)^2} = \frac{1}{2}[1+\gamma_3^{(1)}\gamma_1^{(1)}\gamma_3^{(2)}\gamma_1^{(2)}]\frac{M_j(\varepsilon,\varepsilon')}{\sqrt{j+\frac{1}{2}}} + \tag{4.10}$$

$$+\frac{1}{2}[1-\gamma_3^{(1)}\gamma_1^{(1)}\gamma_3^{(2)}\gamma_1^{(2)}]\left\{\frac{1}{2}\left[1+\frac{\gamma_1^{(1)}\gamma_2^{(1)}\gamma_1^{(2)}\gamma_2^{(2)}}{2j+1}(1-\gamma_3^{(1)}\gamma_1^{(1)}2\sqrt{j(j+1)})\right]\frac{M_{j+1}(\varepsilon,\varepsilon')}{\sqrt{j+\frac{3}{2}}} + \right.$$

$$\left. -\frac{1}{2}\left[1-\frac{\gamma_1^{(1)}\gamma_2^{(1)}\gamma_1^{(2)}\gamma_2^{(2)}}{2j+1}(1-\gamma_3^{(1)}\gamma_1^{(1)}2\sqrt{j(j+1)})\right]\frac{M_{j-1}(\varepsilon,\varepsilon')}{\sqrt{j-\frac{1}{2}}}\right\} .$$

The functions $M_j(\varepsilon,\varepsilon')$ occurring in (4.10) are given by the formulae (4.5) and (2.14). The integrals may in principle be evaluated by elementary integrations but we did not succeed in finding the general formula for arbitrary j. We shall write out these integrals explicitly using Günther's form of interaction (cf. (2.14)) and evaluate them for the two simplest cases: $j=0$ and $j=1$.

$$M_k(\varepsilon,\varepsilon') = -\frac{1}{\varepsilon\varepsilon'}\int_{\pi}^{0} \frac{P_k(\cos\theta)\sin\theta\,\mathrm{d}\theta}{p^2+p'^2-2pp'\cos\theta+(\varepsilon-\varepsilon')\sqrt{(p^2+p'^2-2pp'\cos\theta}} . \tag{4.11}$$

$$\left\{\begin{aligned} M_0(\varepsilon,\varepsilon') &= \sqrt{\frac{1}{2}}\cdot\frac{1}{\varepsilon\varepsilon'}\cdot\frac{1}{pp'}\ln\left|\frac{p+p'+\varepsilon-\varepsilon'}{p-p'+\varepsilon-\varepsilon'}\right| \\ M_1(\varepsilon,\varepsilon') &= \sqrt{\frac{3}{2}}\cdot\frac{1}{\varepsilon\varepsilon'}\cdot\frac{1}{pp'}\cdot \\ &\cdot\left[-1+\frac{\varepsilon-\varepsilon'}{p}+\frac{p^2+p'^2-(\varepsilon-\varepsilon')^2}{2pp'}\ln\left|\frac{p+p'+\varepsilon-\varepsilon'}{p-p'+\varepsilon-\varepsilon'}\right|\right] . \end{aligned}\right. \tag{4.12}$$

5. – Reduction of the System.

The integral equation (4.2) represents a system of sixteen equations for the sixteen components of the spinor $f(p)$ (cf. the definition of $\Phi_{\alpha_1\alpha_2}(\boldsymbol{p})$ on page 965). This system may be reduced for $j=1$ to eight equations for

eight unknown functions and for $j = 0$ to four equations with four unknown functions. This is due to the fact that for $j \neq 1$ the spinors $\gamma_2^{(1)}$ and $\gamma_2^{(2)}$ occur only through the intermediary of their product $\gamma_2^{(1)}\gamma_2^{(2)}$ (cf. (4.2) and (4.10)). For $j = 0$ the terms in (4.10) containing $\gamma_3^{(1)}\gamma_1^{(1)}$ vanish and the resulting equations contain another pair of spinors occurring only in form of their product namely $\gamma_1^{(1)}$ and $\gamma_1^{(2)}$.

The commutation relations between the γ-matrices of equation (4.2) may be satisfied if we represent these matrices as Cartesian products of the second rank Pauli matrices

$$\text{(5.1)} \qquad \begin{cases} 1\,, \quad \sigma_1''\,, \quad \sigma_2''\,, \quad \sigma_3''\,; \\ \sigma_i^p\sigma_k'' + \sigma_k^p\sigma_i'' = 2\delta_{ik}\,; \qquad \sigma_i^p\sigma_k'' = i\sigma_j''\,, \end{cases}$$

corresponding to three different twodimensional spinor spaces. To distinguish between these spaces we denote the corresponding Pauli matrices (5.1) by σ_i, ϱ_i and Σ_i respectively.

We put

$$\text{(5.2)} \qquad \begin{cases} \gamma_1^{(1)} = \sigma_3\varrho_1 = \sigma_3^p \times \sigma_1^p \times 1 = (\sigma_{3\alpha\beta}^p\, \sigma_{1\gamma\delta}^p\, \delta_{\varepsilon\eta}) \\ \gamma_3^{(1)} = \sigma_2\varrho_1 = \sigma_2^p \times \sigma_1^p \times 1 = (\sigma_{2\alpha\beta}^p\, \sigma_{1\gamma\delta}^p\, \delta_{\varepsilon\eta}) \\ \gamma_4^{(1)} = \sigma_1\varrho_1 = \sigma_1^p \times \sigma_1^p \times 1 = (\sigma_{1\alpha\beta}^p\, \sigma_{1\gamma\delta}^p\, \delta_{\varepsilon\eta}) \\ \gamma_1^{(2)} = \varrho_1\Sigma_3 = 1 \times \sigma_1^p \times \sigma_3^p = (\delta_{\alpha\beta}\, \sigma_{1\gamma\delta}^p\, \sigma_{3\varepsilon\eta}^p) \\ \gamma_3^{(2)} = \varrho_1\Sigma_2 = 1 \times \sigma_1^p \times \sigma_2^p = (\delta_{\alpha\beta}\, \sigma_{1\gamma\delta}^p\, \sigma_{2\varepsilon\eta}^p) \\ \gamma_4^{(2)} = \varrho_1\Sigma_1 = 1 \times \sigma_1^p \times \sigma_1^p = (\delta_{\alpha\beta}\, \sigma_{1\gamma\delta}^p\, \sigma_{1\varepsilon\eta}^p) \\ \gamma_2^{(1)}\gamma_2^{(2)} = \varrho_2 = 1 \times \sigma_2^p \times 1 = (\delta_{\alpha\beta}\, \sigma_{2\gamma\delta}^p\, \delta_{\varepsilon\eta})\,. \end{cases}$$

The function $f(p)$ appears now as a spinor possessing three indices β, δ, η corresponding to the three twodimensional spinor spaces. Each of these indices takes on the values 1 and 2. Equations (4.2) represent, therefore, a set of eight equations for the eight components $f_{\beta\delta\eta}(p)$ ($\beta, \delta, \eta = 1, 2$) of the spinor $f(p)$.

In the case $j = 0$ two twodimensional spinor spaces suffice. Putting

$$\text{(5.3)} \qquad \begin{cases} \gamma_3^{(1)} = \sigma_2 \quad \sigma_2'' \times 1 = (\sigma_{2\alpha\beta}^p\, \delta_{\gamma\delta}) \\ \gamma_4^{(1)} = \sigma_1 = \sigma_1^p \times 1 = (\sigma_{1\alpha\beta}^p\, \delta_{\gamma\delta}) \\ \gamma_3^{(2)} = \Sigma_2 = 1 \times \delta_2^p = (\delta_{\alpha\beta}\, \sigma_{2\gamma\delta}^p) \\ \gamma_4^{(2)} = \Sigma_1 = 1 \times \sigma_1^p = (\delta_{\alpha\beta}\, \sigma_{1\gamma\delta}^p) \\ \gamma_1^{(1)}\gamma_1^{(2)} = \gamma_2^{(1)}\gamma_2^{(2)} = \sigma_3\Sigma_3 = \sigma \times_3^p \sigma_3^p = (\sigma_{3\alpha\beta}^p\, \sigma_{3\gamma\delta}^p)\,, \end{cases}$$

we get a system of four equations for the four components $f_{\beta\delta}(p)$ $(\beta, \delta = 1, 2)$ of the spinor $f(p)$.

6. – Discussion.

We did not succeed, so far, in solving equation (4.2) exactly. This seems to be very difficult if at all possible. However, equation (4.2) offers already certain advantages as compared with the original equation (1.1) or (2.12). Due to the fact that it is an integral equation with one independent variable only, one has better possibilities of applying here variational numerical methods than with respect to the original equations in three independent variables. In general, the fact that one obtains equations with one independent variable seems to be the main advantage of the one-time formulation over the many-time formulation of Bethe-Salpeter and Günther which even after separation of the angular variables (cf. GÜNTHER's paper, footnote page 966) remain equations with two independent variables.

Another advantage seems to be the possibility of applying stationary perturbation methods. E.g. in the case of equation (4.2) we may use as the unperturbed equation the static approximation of (4.2) (cf. (2.10)). Putting in K_j $\varepsilon - \varepsilon' = 0$ we get

$$(\varepsilon - \bar{h}_1 - \bar{h}_2) f(p) = + \frac{\alpha\Gamma}{4\pi^3} \int_0^\infty K_j^{\text{static}}(p, p') f(p') p'^2 \, \mathrm{d}p' , \tag{6.1}$$

with $K_j^{\text{static}}(p, p')$ given by formula (4.10) where for M_j one has to take expression (4.11) multiplied by $\varepsilon\varepsilon'$ and with $\varepsilon - \varepsilon' = 0$.

$$M_k^{\text{static}}(p, p') = \int_0^\infty \frac{P_k(\cos\theta) \sin\theta \, \mathrm{d}\theta}{p^2 + p'^2 - 2pp' \cos\theta} . \tag{6.2}$$

If it is possible to find exact eigensolutions and eigenvalues of (6.1) one may perform the conventional perturbation calculation to find the corrections to the eigenvalues and eigenfunctions caused by retardation and in this way to estimate the goodness of the static approximation (6.1). We hope to come back to this question elsewhere.

The angular part of the two-body problem is independent of the order of approximation in the coupling constant α. The functions Z_j^0 or Z_j^m separate, therefore, the angular variables in the two-fermion problem up to any desired order in α and of course also in the exact equation of this problem. They also separate the angular variables if the imaginary part of the kernel V is taken into account. We have then only to replace the functions

$[\boldsymbol{p}-\boldsymbol{p}'\cdot\varepsilon-\varepsilon']^{-1}$ or $[\boldsymbol{p}\quad\boldsymbol{p}'-(\varepsilon/\varepsilon\ (\varepsilon\quad\varepsilon')]^{-1}$ of formulae (2.14) by $\pi i\delta_{+}[|\boldsymbol{p}-\boldsymbol{p}'|+\varepsilon-\varepsilon']$ or $\pi i\delta_{+}[|\boldsymbol{p}-\boldsymbol{p}'|+(\varepsilon/|\varepsilon'|)(\varepsilon-\varepsilon')]$ respectively. The calculations of Sects. 3-5 may be carried out in exactly the same way as for real V. The only effect of the imaginary part of V is to change the form of $M_k(\varepsilon,\varepsilon')$. E.g. in Günther's case one obtains instead of (4.11) the expression

$$M_k(\varepsilon,\varepsilon') = -\frac{\pi i}{\varepsilon\varepsilon'}\int_0^{\pi}\frac{P_k(\cos\theta)\sin\theta\,\mathrm{d}\theta}{\sqrt{p^2+p'^2-2pp'\cos\theta}}\,\delta_{+}(\sqrt{p^2+p'^2-2pp'\cos\theta}+\varepsilon\quad\varepsilon')\,. \tag{6.3}$$

Finally it may be noted that the functions Z_j^0 and Z_j^m separate also the angular variables in the problem of two fermions interacting by means of a meson-field. In this case the characteristic expression $p^2+p'^2-2pp'\cos\theta$ of equation (4.11) has to be replaced by $p^2+p'^2+M^2c^2-2pp'\cos\theta$ where M is the mass of the meson.

RIASSUNTO (*)

Si esegue la separazione delle variabili angolari nell'equazione relativistica monotemporale del problema dei due fermioni nell'elettrodinamica quantistica per il caso dell'interazione di un quanto. Si usa la rappresentazione nello spazio dei momenti ottenendo un sistema di sedici equazioni integrali rispetto a una variabile. Tale sistema si riduce a quattro equazioni nel caso $j=0$ e a otto equazioni per $j\neq 0$.

(*) *Traduzione a cura della Redazione.*

IL NUOVO CIMENTO Vol. IV, N. 5 1° Novembre 1956

Analytical Solution of the Covariant Meson Nucleon Integral Equation.

I. E. McCarthy

Cavendish Laboratory - Cambridge, England

(ricevuto il 23 Giugno 1956)

Summary. — The covariant integral equation for meson scattering in the $T = \frac{3}{2}$ state is investigated by the Fredholm method. Assuming that the zeros of the Fredholm denominator give resonances in the scattering cross-sections, the known resonance is accounted for using $G^2/4\pi = 14.1$. The experimental cross-sections are fitted reasonably well when radiative corrections are accounted for by a numerical factor in the low energy approximation, and discrepancies are accounted for qualitatively.

1. – Introduction.

Many attempts have been made to explain the interactions of pions with nucleons by means of a one-parameter covariant field theory. Since pions are pseudoscalar, their coupling to the nucleons must be pseudoscalar or pseudovector. Theories with pseudovector coupling are at present considered unrenormalizable, so the only possible theory is pseudoscalar meson theory with pseudoscalar coupling.

It has long been recognised that the interactions cannot be described by a power series in the coupling constant $G^2/4\pi = g^2$, which is accurately determined to be about 14 from photomeson production using the result of Kroll and Ruderman [1] that in the limit of zero photon energy, the photoproduction of pions is described exactly by the Born approximation. This simplification does not occur in the case of pion scattering in which the Born approximation [2]

---

[1] N. M. Kroll and M. A. Ruderman: *Phys. Rev.*, **93**, 233 (1954).

[2] M. Peshkin: *Phys. Rev.*, **81**, 425 (1951).

gives a coupling constant about ten times too small, and has no success in describing the cross-sections. It is thought that the smallness of the experimental cross-sections in comparison with the Born approximation is due to radiative corrections which depress terms involving nucleon pair production ([3]). This phenomenon is noticed in π^0 decay and antiproton production.

A more satisfactory description than by perturbation theory may be attainable with a Tamm-Dancoff type of approximation in which successive approximations consist in omitting terms from the interaction which contain more than a fixed number of mesons at any time. The covariant equation in the two meson approximation has been discussed by LEVY, KROLL, FUBINI and GREEN ([4-7]) and is of the following form,

$$q_r(k) = F_r(k) - G^2 \int K_{rs}(k, l) q_s(l) \, \mathrm{d}^4 l \, . \tag{1}$$

Iteration of this equation would destroy any advantage gained by using the Tamm-Dancoff approach, because we would again have a power series in g^2.

DYSON *et al.* ([8]) and KALOS and DALITZ ([9]) have solved the relativistic Tamm-Dancoff equation numerically and find good agreement with experiment for $g^2 = 15.5$ without allowing for the suppression of nucleon pair production terms.

The equation (1) is formally of the Fredholm type. The Fredholm solution would be particularly interesting because it is known a priori to be absolutely convergent. KALOS and DALITZ ([9]) have remarked that their equation does not satisfy the Fredholm condition because the kernel has a pole at infinity.

MCCARTHY and GREEN ([10]) have shown how to renormalize the equation in such a way that the Fredholm condition is satisfied. The renormalization procedure is equivalent to the usual one in which the kernel $K(p^2; k, l)$ is replaced by $K(p^2; k, l) - K(m^2; k, l)$.

Very satisfactory results for pion scattering have recently been obtained in a cut-off theory by LOW and CHEW ([11]). They have shown that an effective

---

([3]) K. A. BRUECKNER, M. GELL MANN and M. L. GOLDBERGER: *Phys. Rev.*, **90**, 476 (1953).

([4]) M. M. LEVY: *Phys. Rev.*, **94**, 460 (1954).

([5]) N. KROLL: *Proceedings of the Fourth Annual Rochester Conference on High Energy Nuclear Physics*, 156 (1954).

([6]) S. FUBINI: *Nuovo Cimento*, **10**, 851 (1953).

([7]) H. S. GREEN: *Phys. Rev.*, **95**, 548 (1954).

([8]) F. J. DYSON, M. ROSS, E. E. SALPETER, S. S. SCHWEBER, M. K. SANDARESAN, N. M. VISSCHER and H. A. BETHE: *Phys. Rev.*, **95**, 1644 (1954).

([9]) M. H. KALOS and R. H. DALITZ: *Phys. Rev.*, **100**, 1515 (1955).

([10]) I. E. MCCARTHY and H. S. GREEN: *Proc. Phys. Soc.* (*London*), A **67**, 719 (1954).

([11]) G. F. CHEW and F. E. LOW: *Phys. Rev.*, **101**, 1570 (1956).

range theory can be used, and the value $g^2 = 14$ is predicted. Dispersion relations [12] also seem to give good results in predicting the resonance at 195 MeV which is observed experimentally in the p-wave scattering. These theories are independent of the model, and it will be as well to interpret the results of the present one-parameter theory in the light of the information gained from these considerations.

It is the purpose of this paper to apply the methods described by McCARTHY and GREEN [10] for obtaining a discrete spectrum of eigenvalues from the homogeneous equation for bound states, and a general formal solution of the inhomogeneous equation, to the calculation of bound states or resonances and scattering cross-sections for $T = \frac{3}{2}$.

The Fredholm solution of (1) is

$$\varphi_r(k) = F_r(k) + \int \frac{D_{rs}(\lambda; k, l)}{D(\lambda)} F_s(l)\, \mathrm{d}^4 l\,, \tag{2}$$

where

$$\begin{cases} \lambda = G^2 \\ D_{rs}(\lambda; k, l) = \lambda K_{rs}(k, l) - \lambda^2 \{u_1 K_{rs}(k, l) - K^{(2)}_{rs}(k, l)\} + \dots\,, \\ D(\lambda) = 1 - \lambda u_1 + \tfrac{1}{2}\lambda^2 (u_1^2 - u_2) - \dots \end{cases} \tag{3}$$

$K^{(n)}_{rs}(k, l)$ is the n-th iterated kernel defined by

$$\begin{cases} K^{(1)}_{rs}(k, l) = K_{rs}(k, l) \\ K^{(n)}_{rs}(k, l) = \int K_{rq}(k, j) K^{(n-1)}_{qs}(j, l)\, \mathrm{d}^4 j \\ u_n = \int \mathrm{spur}\, K^{(n)}_{rr}(k, k)\, \mathrm{d}^4 k \end{cases} \tag{4}$$

$$(2\pi)^4 i K_{rs}(k, l) = \{S(p - k) \Gamma_5(p - k, p - k - l) S(p - k - l) \cdot \Gamma_5(p - k - l, p - l)\}_{rs} D(l)\,, \tag{5}$$

where

$$p = \gamma^\mu p_\mu\,, \tag{6}$$

p_μ is the resultant energy-momentum 4-vector of the system, k_μ, l_μ are the energy-momentum 4-vectors of the final and intermediate mesons respectively,

---

[12] H. L. ANDERSON, W. G. DAVIDSON, M. GLICKSMAN and U. E. KRUSE: *Phys. Rev.*, **100**, 279 (1955).

$S(p)$, $D(k)$ are the propagation functions of nucleons and mesons of 4-momenta p_μ, k_μ, and $\Gamma_5(p, q)$ is the operator for a vertex between fermion lines of 4-momenta, p_μ, q_μ.

The bound states and resonances are given by the homogeneous equation corresponding to (1) in which $F_r(k) = 0$. Hence, a finite solution is possible only for

$$D(\lambda) = 0 . \tag{7}$$

This equation gives us the eigenvalues of p^2 for resonance as functions of λ.

The real part of p^2 is proportional to the position of the resonance or the mass of the corresponding excited state of the pion-nucleon system, the imaginary part gives the resonance width and is inversely proportional to the lifetime of the bound state.

Although it is known that $D(\lambda)$ is convergent, it is important in practice to know the rapidity of convergence because calculations of u_n for $n \geqslant 3$ are impracticable. Hence the whole series will have to be approximated using the first few terms. For the sake of simplicity it is preferred to calculate the zeros of $\exp[\alpha\lambda]D(\lambda)$ and $\exp[\alpha\lambda - \beta\lambda^2]D(\lambda)$ in the first and second order cases respectively where α and β are chosen so as to make the coefficients of λ^2 and λ^3 respectively vanish. Higher powers of λ are omitted. This method gives

$$\begin{cases} u_1\lambda - 1 . \\ \\ u_2\lambda^2 - 1 . \end{cases} \tag{8}$$

as successive approximations to (7).

There is no a priori reason why this method should give quicker convergence than by omitting powers of λ in a straightforward way, but it enables us to plot g^2 against p^2 more easily.

Whether these equations give a good approximation to (7) is not known for the relativistic problem, but in non-relativistic cases remarkably accurate results have been achieved in the first order for nucleon-nucleon scattering by JOST and PAIS ([13]), for meson-nucleon scattering by GAMMEL ([14]), and for the second order deuteron problem by MCCARTHY and GREEN ([10]). It was considered that these results were good enough to justify the performing of the present calculation in covariant theory to order λ^2.

Radiative corrections to the nucleon propagator and the vertex operator have been accounted for in the approximation of small meson momenta by

([13]) R. JOST and A. PAIS: *Phys. Rev.*, **82**, 840 (1951).
([14]) J. L. GAMMEL: *Phys. Rev.*, **95**, 209 (1954).

a constant numerical factor f. It has not been found possible to obtain an independent estimate of f. It is shown that f appears in the numerator of the scattering amplitude but not in the denominator, the essential difference being that the terms in the denominator are represented only by closed Feynman diagrams, while those of the numerator are all found in the perturbation solution.

Hence, in this approximation it is possible to estimate the value of the coupling constant independently of radiative corrections and pair suppression. The value corresponding to a resonance at 195 MeV is $g^2 = 14.1$. The value of g^2 is very insensitive to the position of the resonance.

The results of the scattering theory are given in the form of a calculation of f^{-1} by comparing the results of the theory with experimental results for differential and total cross-sections. The calculations are made at a part of the curve that is far enough from the peak not to be greatly affected by the fact that in the present approximation (in which the kernel is symmetric), the eigenvalues are real, and the peak infinitely high.

The reality of the eigenvalues also means that, in the present approximation, the lifetime of a bound state would be infinite. Higher approximations contributing asymmetric terms to the kernel would of course give a finite lifetime but there is no means of estimating the order of magnitude in order to predict, whether bound states should be observable.

It is found that $f^{-1} = 8.3$, predicting a pair suppression factor of about 100.

In addition to the two meson approximation, modified for small momenta by the factor f, powers of the meson-nucleon mass ratio higher than the second have been neglected in order to make calculation of the integrals possible.

2. – The Integral Equation.

In writing down an explicit expression for $K(k, l)$, radiative corrections to the nucleon propagator S and the vertex operator Γ_5 must be taken into account. The renormalized propagation function S may be written

$$S(p) = f(p)(p - m)^{-1} . \tag{9}$$

The renormalization is defined so that for an external nucleon for which $p^2 = m^2$,

$$f(p) = f(m) = 1 . \tag{10}$$

For the vertex operator

$$\Gamma_5(p, q) = \gamma_5 g(-p, q) . \tag{11}$$

According to the usual renormalization procedure, we have, when $p^2 = q^2 = m^2$,

$$g(m, m) = 1 . \tag{12}$$

The explicit exression for $K(k, l)$ is as follows

$$K(k, l) = \frac{f(p-k)}{p-k-m}\gamma_5 g(-p+k,\ p-k-l)\cdot \cdot\frac{f(p-k-l)}{p-k-l-m}\gamma_5 g(-p+k+l,\ p-1)\,D(l) , \tag{13}$$

where the numerical factor $(2\pi)^4 i$ has been omitted for convenience. For small nucleon and meson momenta, we may write

$$K(k, l) = \frac{f(m)}{p-k-m} g(m, -m)\frac{f(-m)}{p-k-l+m} g(-m, m)\,D(l) = = \frac{1}{p-k-m}\frac{1}{p-k-l+m} D(l)\cdot f , \tag{14}$$

where

$$f = f(-m)g(m, -m)g(-m, m) . \tag{15}$$

The radiative factor f does not reduce to 1 on account of the known values $f(m) = 1$ and $g(m, m) = 1$. In this respect the amplitude for meson scattering differs radically from that for photo-meson production.

In the Fredholm denominator $D(\lambda)$, we are dealing with closed diagrams in which there are no external momenta but the effective contribution to the integrals still comes from near the poles of the integrand, where the nucleon and meson momenta are small. One is therefore justified in replacing $f(p)$ and $g(-p, q)$ by $f(\pm m)$ and $g(\pm m, \pm m)$; also, since $f(-m)$ is small [3] compared with $f(m)$, the major contribution to the integrals will be obtained by choosing the value $f(m)$. In this case therefore we assume that the result found by KROLL and RUDERMAN [1] for photo-meson production holds: that is to say radiative corrections cancel.

The value of $f(-m)$ can be estimated from the work of BRUECKNER, GELL-MANN and GOLDBERGER [3] who used a perturbation argument. This method is so inaccurate that nothing can be said except that $f(-m)$ is small compared with 1.

The Fredholm denominator as it stands, contains solutions for two different spin states, and two different energy states. Consideration of simplified covariant equations has shown that this is accounted for by a factor $\frac{1}{4}$ on the left hand side of the equation (8).

3. – Scattering Cross Sections.

The matrix element for the calculations of scattering cross-sections given by the Fredholm theory is

$$M_F = D(\lambda; k, l)/D(\lambda) . \tag{16}$$

Since the solutions corresponding to opposite spins for the incident and scattered particles contribute equal factors to $D(\lambda)$, we may write

$$D(\lambda) = \{C(\lambda)\}^2 . \tag{17}$$

It is well known that

$$D(\lambda; k, l) = P(\lambda; k, l) D(\lambda) ,$$

where $P(\lambda; k, l)$ is the Liouville-Neumann solution. A simple factor $C(\lambda)$ can therefore be cancelled from the numerator and denominator. For the purpose of this discussion the scattering matrix element

$$M = C(\lambda; k, l)/C(\lambda) \tag{18}$$

will be used, where

$$C(\lambda) C(\lambda; k, l) = D(\lambda; k, l) . \tag{19}$$

To the second order in λ,

$$M = \frac{\lambda K_1 + \lambda^2(K_2 - \frac{1}{2}u_1 K_1)}{1 - \frac{1}{2}u_1\lambda - \frac{1}{4}(u_2 - \frac{1}{2}u_1^2)\lambda^2} , \tag{20}$$

where

$$K_n = K^{(n)}(k,l) . \tag{21}$$

It is well known from the general theory of scattering ([15]) that the cross-sections σ are given by

$$\mathrm{d}\sigma = \sin\theta \, \mathrm{d}\theta \, \mathrm{d}\varphi (2\pi)^{-2} w^2 V^2 |M|^2 , \tag{22}$$

where

$$|M|^2 = \mathrm{spur}\{M(p_1 + m) M(p_2 + m)\} . \tag{23}$$

([15]) N. F. MOTT and H. S. W. MASSEY: *Theory of Atomic Collisions* (Oxford, 1953).

$p_{1\mu}$ and $p_{2\mu}$ are the initial and final nucleon momenta and $(p_1-m)\,2m$ and $(p_2-m)/2m$ are the positive energy projection operators for initial and final states. V is the volume under consideration and w and E are the meson and nucleon energies in the centre of mass system respectively.

Let

$$K_{ij} = \text{spur}\{K_i(p_1+m)K_j(p_2+m)\}. \tag{24}$$

Then

$$|M|^2 = \{C(\lambda)\}^{-2}\{\lambda^2 K_{11} + \lambda^3(K_{12}+K_{21}-u_1K_{11}) + \\ + \lambda^4[K_{22} - \tfrac{1}{2}u_1(K_{12}+K_{21}) + \tfrac{1}{4}u_1^2K_{11}]\}. \tag{25}$$

Defining α_4, α_6, α_8 in the appropriate way

$$|M|^2 = \{C(\lambda)\}^{-2}\{\lambda^2\alpha_4 + \lambda^3\alpha_6 + \lambda^4\alpha_8\}, \tag{26}$$

where

$$C(\lambda) = 1 - \tfrac{1}{2}u_1\lambda - \tfrac{1}{4}(u_2 - \tfrac{1}{2}u_1^2)\lambda^2. \tag{27}$$

Denote the total cross-sections in units of λ corresponding to α_4, α_6 and $4\alpha_8$ respectively by σ_1, σ_6, σ_8 and the corresponding differential cross-sections by σ_4', σ_6', σ_8'.

For the purpose of comparison with experimental data, it is convenient to calculate the differential cross-section in the centre of mass system.

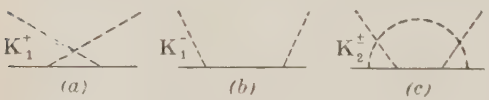

Fig. 1.

In the Born approximation, two types of diagram must be taken into account (Fig. 1).

It is evident from charge conservation that (*a*) applies to π^+, p, and (*b*) to π^-, p scattering. Calculations of the π^-, p cross-sections σ^- are evidently easier, because they do not involve charge exchange. The second Born approximation diagram (*c*) represents both σ^+ and σ^- scattering.

Peshkin [2] gives the exact formula for the Born approximation,

$$\sigma_4^{+\prime} = \frac{1}{32\pi^2}\,\frac{1}{(w+E)^2}\,\frac{2w^2E^2 - \mu^2k^2 + k^2(2wE+\mu^2)\cos\theta}{(2wE - \mu^2 + 2k^2\cos\theta)^2}. \tag{28}$$

CORINALDESI and FIELD [16] have calculated the differential and total cross-sections to 4-th and 6-th orders in g. Their results are calculated non-relativistically using the approximations

$$\frac{|p|^2}{m^2} \ll 1 \qquad \text{and} \qquad w < 3\mu ,$$

where $p^2 = (w + E)^2$.

These approximations are consistent with the case we are studying, but the results have certain defects which are important in this work. Their results are

$$\sigma_4^+ = \frac{\pi}{m^2} \frac{(1 + (w/m))}{(4\pi)^2} \tag{29}$$

$$\sigma_6 = -\frac{3}{4m^2} \frac{(2+(3w/m))}{(4\pi)^3} \tag{30}$$

$$\sigma_4^{+\prime} = \frac{1}{(4\pi)^2 4m^2} \left(1 + \frac{w}{m} - \frac{p^2}{mw} \cos\theta\right) \tag{31}$$

$$\sigma_6' = -\frac{3}{16\pi m^2} \frac{1}{(4\pi)^3} \left(2 + 3\frac{w}{m} - \frac{p^2}{mw} \cos\theta\right) . \tag{32}$$

$\sigma_4^{-\prime}$ is obviously a bad approximation for low values of θ, because there is a zero at about $\theta = 30°$ below which $\sigma_4^{+\prime}$ is negative. This zero is spurious because $\sigma_4^{-\prime}$ is necessarily a positive definite quantity. A similar defect may be assumed to exist in (32).

It is found that the first order Fredholm theory of scattering, in which the numerator is the Born approximation, does not fit the data, because the angular distribution, whichis not altered in shape by the denominator, has the wrong shape.

The second order matrix element requires a knowledge of K_{22} which has not been evaluated in any approximation up to the present time. It will be shown in the appendix that, if the ratios of all meson momenta to the nucleon mass are neglected,

$$K_{22} = (K_{12} + K_{21})^2 / 4K_{11} . \tag{33}$$

Hence, it is easily verified that

$$\alpha_8 = \alpha_6^2 / 4\alpha_4 . \tag{34}$$

[16] E. CORINALDESI and G. FIELD: *Phil. Mag.*, **41**, 364 (1950).

Using (22) (26), (34) and the fact, explained above, that K_n must be multiplied in the numerator by f^n to allow for radiative corrections, the differential cross-section will be

$$\sigma' = \lambda^2 f^2 \frac{\sigma_4'}{C^2}\left\{1 - \frac{1}{2}u_1\lambda + \frac{1}{2}\frac{\sigma_6'}{\sigma_4'}f\right\}^2 . \tag{35}$$

There is some doubt perhaps that the « renormalization » factor f representing radiative corrections is the same in the fourth order term as in the second order term, but, since the fourth order term is in any case the dominant contribution to σ', the error introduced in assuming the same value of f in the two contexts could not be large.

4. – Calculation of u_1 and u_2.

It is convenient to separate u_1 into simpler integrals.

$$\begin{cases} u_1 = \int \text{spur } K(k, k)\, \mathrm{d}^4k \\ \quad = \int\left\{\dfrac{1}{KK'} + \dfrac{4}{KM} - \dfrac{p^2 - m^2}{KK'M}\right\} \mathrm{d}^4k . \end{cases} \tag{36}$$

where

$$K = k^2 - \mu^2 , \qquad K' = (k - p)^2 - m^2 , \qquad M = (2k - p)^2 - m^2 .$$

The details of the calculations of the terms of (36) and similar terms of u_2 will not be reproduced here, but will be supplied privately by the author to interested persons.

Using Feynman's procedure ([17]) we find

$$\int \frac{\mathrm{d}^4k}{KK'} = \int_{m^2}^{\pm\infty} \mathrm{d}(m^2) \int_0^1 \mathrm{d}u \, \frac{\pi^2 i v}{a(b^2p^2 - Ba^2)^3} , \tag{37}$$

where $u + v = 1$

$$a = u + v - 1$$

$$b = -v$$

$$B = u\mu^2 + v(p^2 - m^2) .$$

([17]) R. P. FEYNMAN: *Phys. Rev.*, **76**, 769 (1949).

The integral (37), as it stands, is logarithmically divergent. The renormalization procedure consists in subtracting off the corresponding expression with m^2 substituted for p^2. Carrying out this procedure, and integrating over m^2, we have

$$\int \frac{\mathrm{d}^4k}{KK'} = -i\pi^2 \int_0^1 \mathrm{d}v \ln\left\{\frac{v^2p^2 - v(p^2 - m^2 + \mu^2) + \mu^2}{v^2m^2 - v\mu^2 + \mu^2}\right\}. \tag{38}$$

This integration has basically the same characteristics as the others in the computation of u_1 and u_2 and, being the simplest, will be shown in more detail as an illustration of the procedures used throughout the calculation.

If μ^2/m^2 is neglected in (38), the calculation will be simplified considerably. However, if μ^2 is neglected entirely, the decay threshold for the bound state will be given by $p^2 = m^2$, where it should be $p^2 = (m + \mu^2)$.

The second integral of (36), which is the same as (38) with $2k$ substituted for k, and hence 2μ for μ, is the only exception in these calculations. It is a pathological case corresponding to the emission of two successive undistinguishable mesons of momentum k, and cannot occur in the 4-th order calculation.

(38) can be calculated exactly without neglecting μ^2, but the other integrals cannot. We will calculate (38) both with and without μ^2 in order to provide an analogy for a correction for μ^2 up to the first order in μ^2/m^2.

From the theory of radioactive decay, p^2 must be complex for $p^2 > (m+\mu)^2$. Hence u_n is complex.

For $p^2 < (m+\mu)^2$, p^2 is real, and hence u_n is real. We want our results to satisfy this condition, although it must be remembered that, in our approximation, the eigenvalue of p^2 is real. Hence, overall, u_n must be real, although its terms, which could appear in a calculation with an asymmetric kernel must satisfy the condition, in general.

Neglecting μ^2,

$$\int \frac{\mathrm{d}^4k}{KK'} = i\pi^2 \frac{m^2}{p^2}\left(1 - \frac{p^2}{m^2}\right)\ln\left(1 - \frac{p^2}{m^2}\right). \tag{39}$$

Put

$$x = p^2/m^2, \quad y = \mu^2/m^2. \tag{40}$$

$$\int \frac{\mathrm{d}^4k}{KK'} = i\pi^2 \int_0^1 \mathrm{d}v \ln\left\{\frac{x(v-a)(v-b)}{(v-c)(v-d)}\right\}, \tag{41}$$

where

$$(42)\qquad \begin{cases} a = \dfrac{1}{2x}(x+y-1+\alpha) \\ b = \dfrac{1}{2x}(x+y-1-\alpha) \\ c = \dfrac{1}{2}(y+\beta) \\ d = \dfrac{1}{2}(y-\beta) \end{cases}$$

and

$$(43)\qquad \begin{cases} \alpha = \{(x+y-1)^2 - 4xy\}^{\frac{1}{2}} \\ \quad = \dfrac{1}{m^2}[p^2-(m+\mu)^2]^{\frac{1}{2}}[p^2-(m-\mu)^2]^{\frac{1}{2}} \end{cases}$$

$$(44)\qquad \begin{cases} \beta = \{y^2 - 4y\}^{\frac{1}{2}} \\ \quad = \dfrac{\mu^2}{m^2}\{(\mu+2m)(\mu-2m)\}^{\frac{1}{2}}. \end{cases}$$

α is real for $p^2 > (m+\mu)^2$, imaginary for $p^2 < (m+\mu)^2$, zero for $p^2 = (m+\mu)^2$. β is imaginary.

It can be verified that when α is imaginary, (38) is real. Hence our condition is satisfied.

The object of the correction for μ^2 is to find a method of inserting μ into the expression obtained by neglecting μ in such a way as to have an expression correct to order μ^2/m^2.

The denominator of the logarithm in (41) leads to an expression which vanishes as $\mu \to 0$. We will only be interested in

$$(45)\qquad \int_0^1 \ln\{x(v-a)(v-b)\}\,dv =$$

$$-\frac{1}{2}\frac{x+y-1-\alpha}{x}\ln y + \frac{1}{2}\frac{\alpha}{x}\left\{\ln\left[\frac{y(x+y-1+\alpha)}{x+y-1-\alpha}\right] + \ln\left[\frac{x-y+1-\alpha}{x-y+1+\alpha}\right]\right\} + i\pi\alpha/x.$$

From (43)

$$(46)\qquad \alpha = (x-1) - \frac{x+1}{x-1}y + 0(y^2).$$

Hence, as $y \to 0$, (45) becomes $((x-1)/x)\ln(1-x)$ as it should from (39). Neglecting y^2, but not $y\ln y$ in (45), we have

$$(47)\quad \frac{1}{x-1}\,y\ln y - \frac{1}{2x}\left\{x-1 \quad y\left(\frac{x+1}{x-1}\right)\right\}\left\{\ln\left[(x-1)^2 \quad y\right] - \ln\left[\frac{x+y-1}{x-y-1}\right]\right\}.$$

Expanding (47) in powers of y where possible, it may be seen that, in neglecting y, we neglect from the real part

$$(48)\qquad \frac{1}{x-1}\,y\ln y \;-\frac{y}{x}\,\frac{x+1}{x-1}\ln(x-1) + 0(y^2)\,.$$

The imaginary part is $i\pi\alpha/x$ instead of $i\pi(x-1)/x$. It is just the expressions containing $\ln(1-x)$ which affect the reality condition for the u_n, and they are the only ones which depend on μ in this manner. Hence, the addition of (48) to every term of the form (49) should correct the term up to order μ^2/m^2. All terms in the calculations of u_1 and u_2 are treated in this manner except the one mentioned above.

We know that, in our approximation, u_1 is real. Hence we will omit the imaginary parts of our approximate calculations, believing that they would cancel in an exact calculation.

Applying the above procedures in the cases of the other integrals, we find

$$(49)\qquad u_1 = \frac{-\pi^2}{(2\pi)^4}\left\{\varphi\left[\frac{3}{2}\ln(x-1) - \frac{3}{2}\ln 2 + \frac{1}{2}\varphi^{-\frac{1}{2}}(8-9\varphi)^{\frac{1}{2}}\cos^{-1}\left\{\frac{5\varphi-4}{\varphi(1-\varphi)}\right\}\right] + \right.$$
$$\left. + \frac{9}{2}\,\frac{1}{x-1}\,y\ln y + \frac{8y}{x-1}\ln 2 - \frac{9}{2}\,\frac{y}{x}\,\frac{x+1}{x-1}\ln(x-1)\right\},$$

where

$$\varphi = 1 \;-1/x\,.$$

u_2 can be reduced to a sum of simpler integrals, putting $\mu = 0$

$$(50)\qquad u_2 = \iint \mathrm{spur}\, K(k,l)\,K(l,k)\,\mathrm{d}^4k\,\mathrm{d}^4l =$$
$$= 2\iint \mathrm{d}^4k\,\mathrm{d}^4l\left\{-\frac{p^2 \;-m^2}{KLK'L'M} - \frac{2}{KK'M^2} + \frac{2}{KK'LM} + \frac{1}{K'L'M^2} + \frac{1}{KLM^2}\right\},$$

where

$$K = k^2\,, \qquad K' = (k-p)^2 - m^2\,, \qquad M = (k+l-p)^2 - m^2\,.$$

Putting

$$0 = \frac{m^2 \;-p^2}{p^2}\,,$$

it is found that the first term can only be calculated in powers of θ. This is the largest term, and we must go as far as the term in θ^2. Similarly the last term is calculated to order θ^2.

The evaluation of the integrals in (50) is much more complicated than for u_1, but not essentially different in principle. The result is

$$(51) \qquad u_2 = 8c^2 \left\{ 5.038\left(1-\frac{1}{x}\right) + \left(1-\frac{\pi^2}{12}\right)(1-x) - 0.0059(1-x)^2 - \right.$$

$$3\left(1-\frac{1}{x}\right)\ln(x-1) + \ln x \ln(x-1) - \frac{1}{2}(\ln x)^2 - 2\left(1-\frac{1}{x}\right)\ln x + Rl\left(\frac{1}{x}\right)$$

$$-\frac{3y}{x-1}\ln y + \frac{3y}{x-1}\,\frac{x+1}{x}\ln(x-1) - \left(1-\frac{1}{x}\right)^2\left[\ln\left(1-\frac{1}{x}\right) - 2 + \right.$$

$$\left. \left. - Rl\left(\frac{x}{x-1}\right) \right\} \{\ln(x-1)\}^2 + \ln(x-1)\ln x - \frac{\pi^2}{6} - \frac{1}{4}\xi(2)\right]\right\},$$

where

$$c = 1/32\pi^2,$$

$\xi(x)$ is the Riemann ξ function, and $Rl(x)$ is the function

$$Rl(x) = \int_1^x \frac{\ln x}{x-1}\,\mathrm{d}x$$

tabulated by POWELL [18].

5. – Numerical Results.

The values of u_1 and u_2 corresponding to relevant values of the kinetic energy of the meson in the laboratory system and corresponding values of x are shown in Table I. To make the numbers easy to write, we have tabu-

TABLE I. – *u_1' and u_2' corrected for the meson mass.*

K.E.	x	u_1'	u_2'
89	1.51	0.6482	3.5367
140	1.62	0.5916	3.3964
169	1.68	0.5500	3.2760
212	1.78	0.4815	3.0728
256	1.87	0.4063	2.8380

[18] E. O. POWELL: *Phil. Mag.*, (7), **34**, 600 (1943).

lated u_1' and u_2' where

$$16\pi^2 u_1' = u_1 \qquad \text{and} \qquad 128\pi^4 u_2' = u_2 \,. \tag{52}$$

In Fig. 2, the value of u_2' neglecting the meson mass is plotted, and it can be seen that the meson mass correction, where it is valid, raises the value of u_2' slightly. As u_2' is renormalized so that it is zero for $p^2 = m^2$, we assume that the corrected value remains slightly greater than the uncorrected value for $p^2 > m^2$. The curves for u_1 and u_2 have a negative slope within the expected 10% error in the range including the 195 MeV resonance. Hence, one more resonance is predicted at a lower energy. Although the position of the resonance is not predicted at all accurately, it appears from the extrapolation of the corrected u_2 curve that it is in the region of the threshold for decay of the bound state. It could be consistent with the resonance at the threshold predicted by dispersion theory. It has no physical counterpart so far as is known.

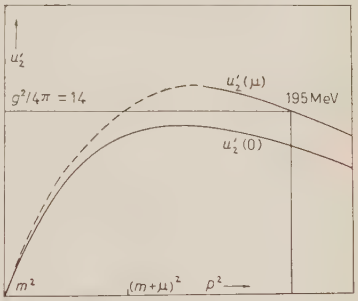

Fig. 2.

The 195 MeV resonance corresponds, in this approximation to a value

$$g^2 = 14.1 \,.$$

In the calculations of scattering cross-sections we will use the results of FERMI *et al.* [19]. For convenience, the straightforward method of putting the denominator of the matrix element M equal to zero will be used at the peak. Choosing λ so that $C(\lambda) = 0$ for 195 MeV, we find

$$g^2 = 12.50 \,.$$

Using the equations (31) and (32) for $\sigma_4^{+\prime}$ and σ_6', and equation (35) for the differential cross-section, we give in Table II the values of f^{-1} corresponding to the experimental values of $\sigma^{+\prime}$ given by FERMI *et al.*

The error in the Corinaldesi and Field approximation to σ_6' would account for the inconsistency in the angular distribution. Besides the spurious zero, their value depends too sensitively on θ. For $\cos\theta = 0$, it appears that the value of f^{-1} obtained is too large.

We may expect the distribution of the differential cross-section at 90° in the laboratory system to give a truer indication of the consistency of the

TABLE II. – *Values of f^{-1} obtained by calculating the differential cross-section, using $g^2 = 12.5$.*

K.E. (MeV)	$\sigma^{+\prime}$ (Lab. system)		
	45°	90°	135°
115	30	8.29	11.3
125	—	8.35	
140	—	8.76	

theory with experiment. Since at 90° in the laboratory system $\cos\theta \neq 0$, it will be slightly too large.

The values of f^{-1} increase slightly with energy, which is to be expected because the theoretical peak is infinite. The total cross-section is obtained by integrating (35),

$$\sigma = \lambda^2 f^2 \{(1 - \tfrac{1}{2}u_1)^2\sigma_4 + \lambda f(1 - \tfrac{1}{2}u_1)\sigma_6 + \tfrac{1}{4}\lambda^2 f^2 \sigma_8\}/C^2 , \tag{53}$$

where

$$\sigma_8 = 2\pi \int_0^\pi \mathrm{d}\theta \, \sin\theta \sigma_6^{\prime 2}/\sigma_4' . \tag{54}$$

In calculating the integral, the formulae (31) and (32) were used for $\sigma_4^{i\prime}$ and σ_6'. The evaluation of the integral is straightforward, and will not be reproduced.

Comparison with the Fermi data gives for the total cross-section at 115 MeV

$$f^{-1} = 8.24 .$$

Hence, the scattering theory gives roughly constant values of f^{-1} and all discrepancies can be accounted for qualitatively.

To summarize the physical predictions of the theory, it predicts firstly a coupling constant of roughly the same magnitude as the dispersion theory, numerical Tamm-Dancoff solution, and photomeson production theory. The advantage over the numerical solution of the Tamm-Dancoff equation by Kalos and Dalitz is that radiative corrections arising from nucleon pair production terms are roughly accounted for in the prediction. The predicted factor for pair suppression is roughly 100. As the theory is so sensitive to the value of the coupling constant the magnitude of this really depends roughly only on the order of magnitude of the whole theory, so an accurate prediction of g^2 is not in itself strong evidence for the correctness of the theory in detail.

It must be remembered that dispersion theory, which takes no account of the detail of the interaction, also predicts the correct value for g^2. However, it may be taken as evidence for the rapid convergence of the Fredholm solution, in a covariant problem, and, on that account, is interesting from the point of view of method. The theory predicts a second resonance in the $T=\frac{3}{2}$ scattering at an energy near the threshold for decay of the bound state. There appears to be nothing in present experimental results to indicate that this represents something physical. No inconsistency is encountered in the prediction of cross-sections although the calculation is not accurate enough to provide a good indication of consistency. The lifetimes of the bound states corresponding to the resonances are not predicted, so we have no estimate of whether they should be observable in practice.

* * *

The author would like to thank Professor H. S. GREEN for constant help and encouragement throughout the course of this work, and Dr. J. HAMILTON for helpful discussions. He is indebted to the University of Adelaide for a grant under which most of the work was completed, and to the Royal Dutch Shell Group for a further grant.

APPENDIX

To obtain an approximation for K_{22} in terms of K_{11} and $K_{12}+K_{21}$ as defined in equation (24), consider the four well-known projection operators $\varepsilon_j(p)$, $j=1,\ldots,4$ which, acting on a Dirac matrix representing the propagation of an external fermion ($p^2=m^2$), leave a fermion in one of the four possible energy-spin states, $++$, $+-$, $-+$ and $--$ respectively.

In evaluating M^2 we use the positive energy projection operator $(\varepsilon_1-\varepsilon_2)$ because spinless mesons cannot alter the nucleon spin state.

$$\begin{aligned} K_{ij} &= \text{spur}\,\{(\varepsilon_1+\varepsilon_2)K_i(\varepsilon_1+\varepsilon_2)K_j\} \\ &= \text{spur}\,\{\varepsilon_1K_i\varepsilon_1K_j+\varepsilon_1K_i\varepsilon_2K_j+\varepsilon_2K_i\varepsilon_1K_j+\varepsilon_2K_i\varepsilon_2K_j\}\,. \end{aligned}$$

Now ε_j commutes with p but not with the meson momenta, so if we neglect the ratio of meson momenta to the nucleon mass we can commute the projection operators with the amplitudes. Using the well known properties of the ε_j, we have

$$\begin{aligned} K_{ij} &= \text{spur}\,\{\varepsilon_1K_i\varepsilon_1\varepsilon_1K_j\varepsilon_1+K_i\varepsilon_1\varepsilon_2K_j+K_i\varepsilon_2\varepsilon_1K_j+\varepsilon_2K_i\varepsilon_2\varepsilon_2K_j\varepsilon_2\} \\ &= (K_i)_{11}(K_j)_{11}+(K_i)_{22}(K_j)_{22}\,. \end{aligned}$$

In the above representation, these matrix elements represent states of equal positive energy and opposite spin, so the amplitudes represented by them are identical.

Hence

$$K_{ij} = 2(K_i)_{11}(K_j)_{11}$$

and

$$K_{22} = (K_{12} + K_{21})^2/4K_{11} \,. \tag{33}$$

RIASSUNTO (*)

Col metodo di Fredholm si studia l'equazione integrale covariante dello scattering mesonico nello stato $T = \frac{3}{2}$. Assumendo che gli zeri del denominatore di Fredholm diano risonanze nelle sezioni d'urto di scattering, si ottiene la risonanza nota per $f^2/4\pi = 14.1$. Le sezioni d'urto sperimentali si riproducono con sufficiente esattezza per mezzo di un fattore numerico nell'approssimazione di bassa energia, mentre delle deviazioni si dà ragione qualitativamente.

(*) *Traduzione a cura della Redazione.*

IL NUOVO CIMENTO Vol. IV, N. 5 1º Novembre 1956

Dinamic Determination of Viscosity.

A. Carrelli and A. De Vito
Istituto di Fisica dell'Università - Napoli

(ricevuto il 5 Luglio 1956)

Summary. — A method is described that gives the measurement of the coefficient of internal friction in fluids, in such conditions that the velocity of the various layers and the velocity gradient are not constant in time. The experimental results show that the fluids having a complex molecular structure exhibit in such dinamical conditions of measurement values of the coefficient of internal friction which differ from the ones obtained in the conditions in which the velocities and the velocity gradient are constant.

The coefficient of internal friction of fluids can usually be determined by methods in which the speed and its gradient are static (constant in respect of time).

But when the fluid consists of molecules of a complex geometric shape, as for instance, when the molecule has the form of a very much elongated ellipsoid or a spiral shape, etc., one is led to imagine that if the speed varies with time from layer to layer, it is possible that such dynamic conditions can produce a viscosity coefficient different from the one obtained under conditions of a stationary movement.

In our research an experimental method has been achieved by which definite conditions of the problem can be determined. The following device has been applied. Two coaxial cylinders (Fig. 1) determine the width s of a cylindric gear; the outer cylinder is interchangeable and thus provides the possibility of modification of the width s. The inner cylinder is governed alternatively by a moment of constant value, and with a frequency equal to 50 Hz, obtained by a current directed in a $DABC$ circuit, formed by an U-shaped small brass bar 2 mm wide, placed between the poles of a permanent magnet. In the

centre of the stretch A-B was fixed a cylinder measuring 1.1 cm in diametre, and 16.8 cm in length. This cylinder was then introduced into the coaxial cylinder containing the fluid whose coefficient of internal friction was to be measured.

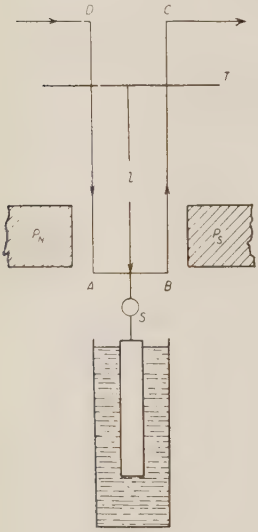

Fig. 1.

At the passage of the current, the stretch formed by the $ABCD$ brass bar (fixed above points C and D) is thus subjected to forces which cause to the cylinder torsional oscillations, of a frequency equal to that of the current. The length of A-D and B-V had been adjusted in such a way as to permit resonance to the U-shaped wire.

By means of a light beam reflected by a small mirror s, placed at the centre of A-B, were obtained the amplitude of the vibrations on a screen, as well as the angle at which the mirror itself was rotating as a result of the current passing through the stretch $DABC$ in the magnetic field.

As a result of the alternative *sine wave* movement of the inner cylinder a wave viscosity is generated in the fluid. The various cylindrical layers, in which the distribution of the fluid takes place, are thus put under the influence of forces which impart them a speed u equal to $\omega_0 r$.

Since the angles at which the inner cylinder is rotating are small, the cylindrical surfaces can be assumed as flat, and the reactions of the viscous medium can be compared with those of laminar motion.

On the basis of this supposition, an equation of the viscous wave can be deduced. The speed u of the viscous wave complies with the following relation:

$$\frac{\partial^2 u}{\partial y^2} = i\,\frac{\omega_0 \varrho}{\eta}\,u\,. \qquad \varrho = \text{density},\ \eta = \text{viscosity}. \tag{1}$$

By finding the integral of this formula, and bearing in mind the conditions at its extremes ($u = 0$ at $y = s$; $u = a$ at $y = 0$) the following results are obtained:

$$u = a\,\frac{\operatorname{sh}\{(1+i)\sqrt{\omega_0 \varrho/\eta}(s-y)\}}{\operatorname{sh}\{(1+i)\sqrt{\omega_0 \varrho/\eta}\,s\}}\,\exp[i(\omega_0 t + \varepsilon)]\,. \tag{2}$$

On the basis of (2) the following formula is obtained for the retarding force

F, in relation to the area unit on the oscillating surface:

$$F = -\eta\left[\frac{\partial u}{\partial y}\right]_{y=0} = -\eta(1+i)\sqrt{\frac{\omega_0\varrho}{2\eta}}\operatorname{ctgh}\left\{(1+i)\sqrt{\frac{\omega_0\varrho}{2\eta}}\,s\right\} a\exp[i(\omega_0 t - \varepsilon)]$$

$$= \eta(1+i)\sqrt{\frac{\omega_0\varrho}{2\eta}}\operatorname{ctgh}\left\{(1+i)\sqrt{\frac{\omega_0\varrho}{2\eta}}\,s\right\} u_{y=0}$$

$$= k u_{y=0} = kr\frac{d\alpha}{dt}.$$

Once this has been established, the equation of the cylinder motion can be written in the following manner: the angle at which the cylinder rotates is indicated by α, the self-pulsation of the bifilar suspension by ω, the moment of inertia of the oscillating system by I, while the retarding force F, which is proportional to the speed, can be calculated as equal $F' = ckr(d\alpha/dt)$. If $M\sin\omega_0 t$ is the moment due to the mechanical actions of the bifilar suspension, the following result is obtained:

$$I\frac{d^2\alpha}{dt^2} + ck\frac{d\alpha}{dt} + \omega^2\alpha = M\sin\omega_0 t. \tag{4}$$

From this the value of the amplitude α_0 of the oscillations performed by the cylinder can be deduced:

$$\alpha_0 = \frac{M_0 I}{\sqrt{(\omega_0^2 - \omega^2)^2 + (c^2k^2/I)\omega_0^2}}.$$

At resonance of the following:

$$\alpha_0 = \frac{M_0}{ck\omega_0^2} = \frac{c'}{k} = c'\left|\eta\frac{(1+i)}{\sqrt{2}}\sqrt{\frac{\omega_0\varrho}{\eta}}\right|^{-1}\operatorname{tgh}\left\{\frac{(1+i)}{\sqrt{2}}\sqrt{\frac{\omega_0\varrho}{\eta}}\,s\right\}.$$

The modulus of α_0 thus gives us the value of the amplitude α_0 under the conditions of resonance:

$$\alpha = \frac{c^*}{\sqrt{\varrho\eta}}\operatorname{tgh}\left\{\sqrt{\frac{\omega_0\varrho}{\eta}}\,s\right\}. \tag{5}$$

In this formula the various constants which are not essential to the problem have been integrated in the c^*.

The formula (5) makes it possible to state that the maximum elongation α_0, if the applied external moment is always the same, is proportional according

to an instrumental constant, to the expression.

$$\frac{1}{\sqrt{\varrho\eta}}\,\mathrm{tgh}\left\{\sqrt{\frac{\omega_0\varrho}{\eta}}\,s\right\} = \frac{1}{\sqrt{\varrho\eta}}\,\mathrm{tgh}\,\beta\,.$$

In the first place, an experimental check of formula (5) was carried out, for which fluids were used whose values of $\sqrt{\varrho\eta}$ comprehend a field which ranges from 1 to 4 (C.G.S.).

The following fluids were used for this test: glycerine, glycerine and water, some mineral oils, paraffin solutions in benzol, nylon solutions in formic acid, and vaseline solutions in benzol.

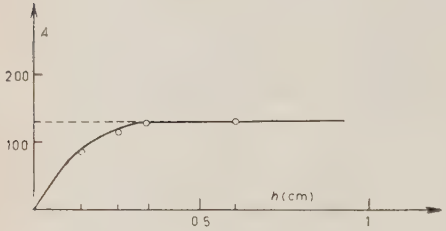

Fig. 2.

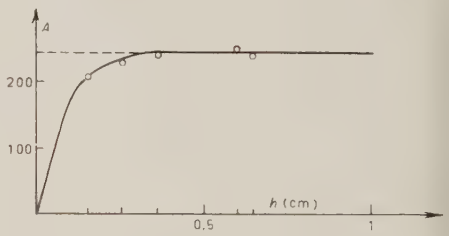

Fig. 3.

The numerical data for $\mathrm{tgh}\,\beta$ given below refer to different values of s, for the glycerine, and with this values is obtained the curve reproduced in Fig. 2. The asymptotic amplitude has been obtained assuming the maximal experimental amplitude.

s in cm	$\sqrt{\frac{\omega_0\varrho}{\eta}}$	$s\sqrt{\frac{\omega_0\varrho}{\eta}} = \beta$	$\mathrm{tgh}\,\beta$	Theoretical amplitude corresponding to the experimental maximum
0.1	—	0.625	0.555	74
0.2	—	1.250	0.850	111
0.3	6.25	1.875	0.950	125
0.4	—	2.500	0.990	129
0.5	—	3.125	0.999	130

Similar results have been obtained with mineral oils (Fig. 3) with solutions of glycerine in water (Fig. 4), paraffin in benzol (Fig. 5). Also for these solutions the values of the experimental amplitude are in sufficient agreement with those of (4) after substitution to a' of the maximum experimental value.

One would be quite justified in deducing that in fact the viscosity wave behaves in the same manner with all the liquids which have been used for the test, as well as with those consisting of a very complex molecular group. For all the tested fluids, except for the vaseline and benzol solutions, the

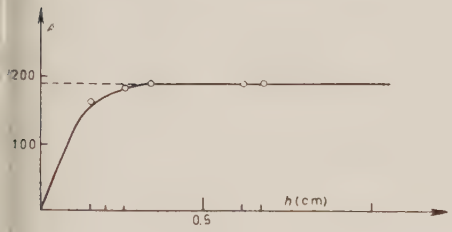

Fig. 4.

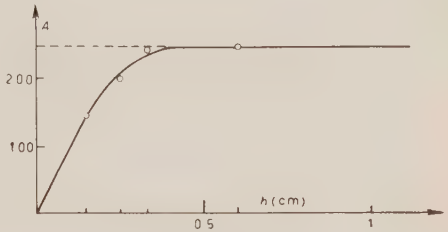

Fig. 5.

determination of the coefficient of internal friction was carried out with Ostwald's viscosity-meters with 0.6 mm diameter capillaries. The values of η coincide, in fact, allowing for experimental errors, with those obtained by a method of viscosity measurement by which one measures the linearly falling speed of a lead sphere placed in the fluid. In the diagram of Fig. 6 are shown the values of η for glycerine at 15 °C, obtained by the above method in dependence of the diameter of the sphere. As it is well known, with this method the influence of the wall of the fluid container decreases in indirect proportion with the distance between the internal wall of the container and the lead sphere, that is, the smaller the diameter d of the container, the smaller will be the influence of the wall. The value of η, therefore, decreases in proportion with the decrease of d, and can be distributed along a curve (which results to be a straight line), whose intersection with the axis of the abscissa provides, through extrapolation, a value of about 10.0 poise, which is in perfect agreement with the value of 10.12 obtained for the same glycerine at the same temperature, by means of Ostwald's viscosity-meters with sufficiently small capillaries. In order to measure the viscosity of the vaseline and benzol solutions Seare's viscosity meter was used based on the rotation of an outer cylinder containing the liquid.

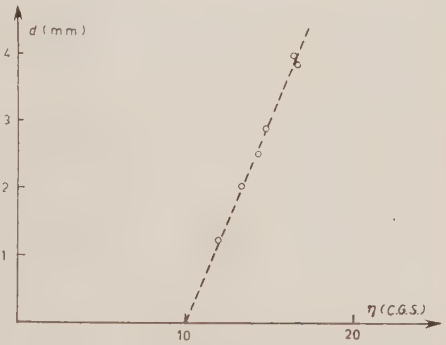

Fig. 6.

This rotation causes a rotation at a definite angle α of the inner cylinder, suspended on a torsion wire. The coefficient of internal friction η, by indicating with G, r_0, l the torsion modulus, the radius and the length of the wire, by h

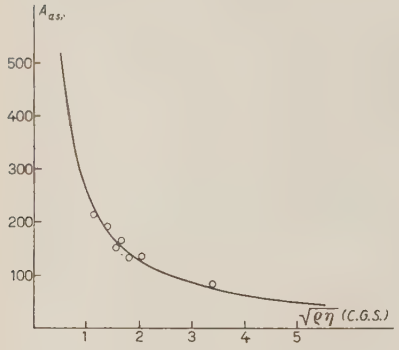

Fig. 7.

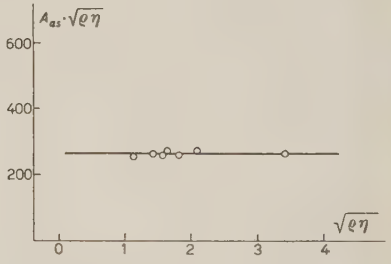

Fig. 8.

the length of stretch of the inner cylinder immersed in the fluid, by R_0 the radius of the outer cylinder, by R_i the radius of the inner cylinder, and by ω_0 the constant angular speed of the outer cylinder, can thus be calculated by the following formula:

$$\eta = \frac{Gr_0^4(R_0^2 - R_i^2)}{8hl\omega_0 R_0^2 R_i^2}\,\alpha\,.$$

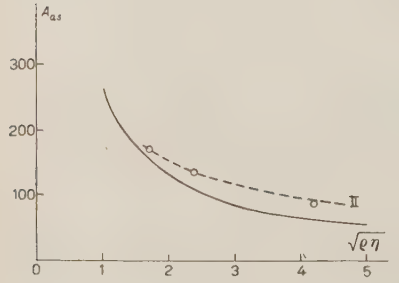

Fig. 9.

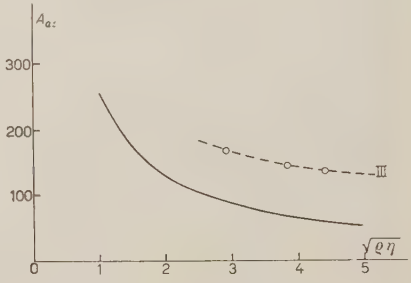

Fig. 10.

By means of the above described device, the value of $\eta = 2.4 \pm 0.21$ poise has been found for vaseline oil, which is in perfect agreement with the value 2.3 ± 0.1 poise, obtained by the Ostwald viscosity-meter at the same temperature. From the above theoretical considerations and experimental results,

we have seen that the amplitude of torsional oscillation of a cylinder immersed in another coaxial cylinder containing the fluid whose coefficient of internal friction under dynamic conditions is the object of research (with the same ϱ, η, and ω_0), is proportional to the difference between the radia of the coaxial cylinders. For the values of s exceeding 0.5 cm (for the liquids and the frequency used) tgh $\sqrt{\omega_0 \varrho/\eta}\, s$ has the value 1. By reproducing then the values of the asymptotic value α_0 as a function of $\sqrt{\varrho\eta}$ for the various fluids, an equilateral hyperbola should be obtained, corresponding to following equation:

$$\alpha_0 \sqrt{\varrho\eta} = k \,. \tag{6}$$

By using as ascissa the value of $\sqrt{\varrho\eta}$ and as ordinates the experimental asymptotic amplitude α_0 (obtained by using such cylinder as to insure a good width s of the cylindrical layer), the results shown by Fig. 7 have been obtained for fluids such as glycerine, vaseline oil, mineral oils and glycerine and water solutions. These fluids are thus in accordance, allowing for experimental errors, with the value resulting from (6).

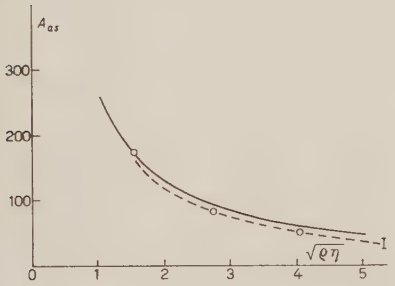

Fig. 11.

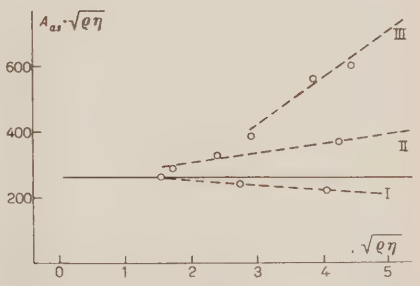

Fig. 12.

In order to carry out a better check of equation (6) the products $\alpha_0 \sqrt{\varrho\eta}$ as function of $\sqrt{\varrho\eta}$ have been reproduced in Fig. 8, so that it may be verified whether in fact these points are to be found on a straight line.

We have then considered solutions of substances of a particular molecular shape in benzol and formic acid. We think, for example, in these terms of para in benzol; para has, as is well known, macromolecules in a broken line. Now, when measuring these solutions, it has been found that the points relative to the amplitude α_0 are not to be found, at the variation of $\sqrt{\varrho\eta}$ as a hyperbola (Fig. 9).

The same behaviour occurs, only in a more acute form, for solutions of vaseline and benzol (Fig. 10). Irregularities in the opposite sense have been noted with nylon and formic acid solutions (Fig. 11). We have reproduced

in Fig. 12 the products $\alpha_0\sqrt{\varrho\eta}$, concerning all these anomalous solutions; it is clearly shown by the figure how such anomalies are in opposite sense for nylon solutions.

In order to show the variation of the viscosity of these molecules by the torsional method, we obtained, by using the curves of Figs. 9, 10, 11 from the value of maximum amplitude, the value of $\sqrt{\varrho\eta}$ (and consequently of η) if the points were falling on the curve. The Fig. 13 shows the values obtained with the aid of Ostwald's viscosity-meter. If there were no variety, the points would fall on a straight line at an inclination of 45°, while actuallly the variation is quite evident.

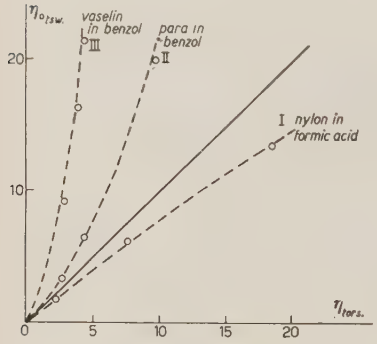

Fig. 13.

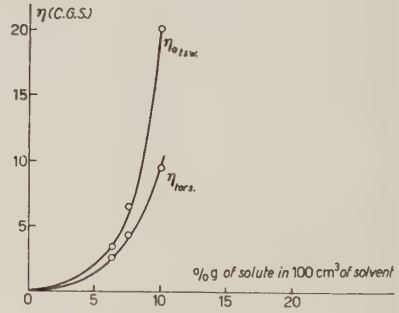

Fig. 14.

In the case of para in benzol, one can see that, with increasing concentration the difference between the values of η obtained by the dynamic (torsional) method and the classical Ostwald's viscosimeter (Fig. 14) also increases.

RIASSUNTO

In questo lavoro viene esposto un metodo che effettua la misura del coefficiente di attrito interno dei fluidi in condizioni tali che la velocità nei vari strati ed il suo gradiente non sono costanti nel tempo. I risultati sperimentali ottenuti mostrano che i fluidi a struttura molecolare complessa hanno, in tali condizioni dinamiche di misura, valori del coefficiente di attrito interno diversi da quelli ottenuti con determinazioni nelle quali la velocità ed il suo gradiente sono costanti.

IL NUOVO CIMENTO Vol. IV, N. 5 1° Novembre 1956

Scattering in Field Theory (*).

H. Ekstein

Argonne National Laboratory - Lemont, Illinois

(ricevuto il 12 Luglio 1956)

Summary. — A precise statement of the scattering problem, general enough to include composite particles in field theory, is proposed: the four Heisenberg operators P_μ which represent the total energy-momentum vector, can be expressed asymptotically ($t \to \pm\infty$) as integrals of mutually commuting operators $A_\tau^{(\pm)\dagger}(\boldsymbol{k}) k_{\tau\mu} A_\tau^{(\pm)}(\boldsymbol{k})$ which represent the four-momenta of the incident and outgoing particles, both elementary and composite. For a theory given in terms of bare-particle creation operators $a_\tau^\dagger$, the problem consists in finding the asymptotic operators $A^{(\pm)}$ as functions of the a_τ and $a_\tau^\dagger$. A system of linear equations for this purpose is derived. Alternatively, the S-matrix can be obtained by solving a bi-linear equation, the inhomogeneous term of which consists essentially of products of one-particle state vectors.

1. – Introduction.

All conventional formulations of the scattering problem are based on the division of the Hamiltonian or Lagrangian into an unperturbed and an interaction part. In the simplest non relativistic case, this division is firmly grounded on the distinction between kinetic and potential energy, and in more complicated non relativistic cases, a generalization of this method is still possible.

In field theory, the total Hamiltonian operator H is usually divided into two terms, H_0 and H_1, the first of which is bilinear in the field operators, while the second is of higher degree. In the older literature, H_0 was the energy of the uncoupled fields [1], while, more recently, certain renormalization terms

(*) Work performed under the auspices of the U.S. Atomic Energy Commission.

(1) G. Wentzel: *Quantum Theory of Fields* (New York, 1949).

have been added ([2,3]), without, however, changing the bilinear character of H_0. The eigenfunctions of H_0, either with mechanical or observable masses, represent (by definition) bare particles which have no direct physical significance. It is well understood that observable quantities should be expressed in terms of states describing real particles, but these are not readily available. Where no composite particles exist, as in electrodynamics, the accepted method to avoid this difficulty in scattering theory is the introduction of a fictitious adiabatic switching-on of the interaction between the uncoupled fields, the mathematical expression of which is the appearance of a convergence factor $\exp[-\varepsilon\,|t|]$ in the equations of motion or the S-matrix ([4]). While this artifice has not been rigorously justified, it is intuitively reasonable and evidently successful in weak-coupling calculations of higher order.

In presence of composite particles, there seems to be no way to generalize this method, and it becomes necessary to give a statement of the scattering problem without recourse to the bare particles. Without regard to difficulties in solving the problem, we shall first discuss its statement, i.e., the connection between the observed probabilities (cross-sections) and the mathematical formalism.

In non relativistic particle theory, the scattering problem is usually stated in connection with the time-independent solutions of the Schrödinger equation ([5,6]). Solutions of a partial differential equation with well-defined asymptotic form are connected to the scattering cross-sections in a simple manner. In field theory, configuration space becomes useless, and the connection between observations and solutions of the time-independent Schrödinger equation becomes obscure. For instance, in the simplest case of meson scattering by a static nucleon, the expectation value of the current operator at large distances is essentially the differential cross-section. But if, in addition to mesons, deuterons are scattered, it is not clear how the scattered mesons can be separated from those belonging to the deuteron.

It is necessary to return to prime principles: probability amplitudes must be identified with projections of the state vector on eigenvectors of operators which represent the measurement. The asymptotic limits of these probabilities are essentially the differential cross-sections. What are the operators which represent the measurements in scattering? It appears that field theory

([2]) F. J. Dyson: *Phys. Rev.*, **75**, 486 (1949).

([3]) S. Gupta: *Proc. Phys. Soc.* (*London*), A **64**, 426 (1951).

([4]) F. J. Dyson: *Advanced Quantum Mechanics*, Lecture Notes, (Cornell University 1951).

([5]) E. P. Wigner and L. Eisenbud: *Phys. Rev.*, **72**, 29 (1947).

([6]) N. F. Mott and H. S. W. Massey: *The Theory of Atomic Collisions* (Oxford, 1949).

does not provide an answer to this question, and that an additional physical principle is necessary.

The primary physical interpretation of field theory (1) gives information on energy-momentum densities, angular momentum densities etc., i.e. field quantities, but not particle properties. The additional interpretation in terms of particles is then carried out for non interacting fields only, and the customary method amounts to accepting this particle interpretation also for interacting fields, with the addition of an adiabatic switch-on. For composite particles, no such device is practicable, and the need for an additional interpretative principle arises.

The principle formulated in this paper may be stated in simple language as follows: particles are those entities which asymptotically (in the distant past and future) remain stable, i.e. conserve their four-momenta and internal variables.

The operators describing the observed particles are defined for the distant past and future only. No unambiguous definition of real particles during the period of interaction is given and, for our purpose, none is necessary.

For the purpose of the basic statement, no use is made of the splitting of the Hamiltonian or Lagrangian into free and interacting parts. It is well known that the bare particles described by one part of the Hamiltonian have no observable significance. Therefore, it is only logical that a basic statement should not contain any reference to these bare particles, much as their introduction may be mathematically useful. It is found possible to give a complete statement of the problem without recourse to the eigenvectors of the unperturbed Hamiltonian or other basis vectors. For mathematical convenience, however, it is found preferable to use basis vectors which represent real non interacting particles. This approach is a generalization of the time-dependent theory of multichannel scattering (7) for non relativistic particles.

2. – Asymptotic Mechanics.

Systems which are not confined by an external force, disintegrate ultimately into elementary particles and composite particles which move like free particles without interaction. Using a felicitous expression of STUECKELBERG (8) we will call their theory asymptotic mechanics. A single free elementary particle is characterized by the fact that operators representing the four components of the energy-momentum vector $p_1 \dots p_4$ commute, and that their

(7) H. EKSTEIN: *Phys. Rev.*, **101**, 880 (1956). Further referred to as (EI).

(8) E. C. G. STUECKELBERG: *Helv. Phys. Acta*, **18**, 195 (1945). The present paper owes much inspiration to the basic ideas of STUECKELBERG.

eigenvalues are related by $\sum p_\mu^2 = -m^2$. A collection of N free particles can be defined by the condition that their momenta $p_{\mu 1} \cdots p_{\lambda N}$ ($\mu, \lambda = 1$ to 4) all commute. In addition, operators representing internal co-ordinates (spin and isotopic spin) also commute with all momenta and among each other. This definition is general enough to describe non interacting composite particles. In asymptotic mechanics, the condition of freedom is attained ultimately. Hence, asymptotic mechanics is characterized by the condition that the four momentum-energy Heisenberg operators $P_\mu(t)$ of the total system ultimately become sums of commuting operators $p_{\mu n}$ describing N_- initial and N_+ final particles, composite or simple:

$$\lim_{t \to \pm\infty} P_\mu(t) = \sum_{n=1}^{N_\pm} p_{\mu n}, \tag{2.1}$$

with

$$[p_{\mu n}^{(\pm)}, p_{\lambda m}^{(\pm)}] = 0\,, \tag{2.2}$$

and also

$$\sum_\mu p_{\mu n}^{(\pm)} p_{\mu n}^{(\pm)} = -m_n^2\,. \tag{2.3}$$

The equations (2.1) to (2.3) are not quite satisfactory because they do not express the fact that the existence of the various elementary and composite particles for $t \to \pm\infty$ is also a matter of probability. A more natural definition is obtained in the formalism of second quantization. Any number of free particles of a given species is characterized by

$$P_\mu = \sum_s \int A_s^\dagger(\boldsymbol{k}) k_{s\mu} A_s(\boldsymbol{k})\, \mathrm{d}\boldsymbol{k}\,, \tag{2.4}$$

where the summation is extended over spin- and charge states; the operators $A^\dagger$ and A are the usual time-independent creation and destruction operators for either Fermi or Bose particles [1]. (We deviate slightly from Wentzel's notation: an operator $A_r^\dagger(\boldsymbol{k})$ creates a particle with momentum $-\boldsymbol{k}$ and positive energy.) M species of non interacting particles r are characterized by

$$P_\mu = \sum_{r=1}^{M} \sum_s \int A_{rs}^\dagger(\boldsymbol{k}) k_{r\mu} A_{rs}(\boldsymbol{k})\, \mathrm{d}\boldsymbol{k}\,, \tag{2.5}$$

where

$$\sum_\mu k_{r\mu}^2 = -m_r^2\,. \tag{2.6}$$

Clearly,

$$[A^{\dagger}_{rs}(\boldsymbol{k})k_{r\mu}A_{rs}(\boldsymbol{k}),\ A^{\dagger}_{r's'}(\boldsymbol{k}')k'_{r'\mu'}A_{r's'}(\boldsymbol{k}')] = 0\,, \tag{2.7}$$

which is the analogue of Eq. (2.2). The condition of asymptotic mechanics for interacting particles will be the existence of operators $A_r^{(\pm)}(\boldsymbol{k})$ such that

$$\lim_{t\to\pm\infty} P_\mu(t) = \sum_r^N \int A_r^{(\pm)\dagger}(\boldsymbol{k})k_{r\mu}A_r^{(\pm)}(\boldsymbol{k})\,\mathrm{d}\boldsymbol{k}\,, \tag{2.8}$$

where r stands for the species as well as for spin and charge variables. The operators $A_r^{(\pm)}$ satisfy again the usual commutation — or anticommutation relations of Schrödinger creation and destruction operators, so that Eq. (2.7) holds for them. Every possible stable composite particle has a set of operators $A_r^{(\pm)}(k)$. Eq. (2.6) holds again, m_r being the observed rest mass of the composite particle.

The four equations (2.8) are considered as fundamental postulates in the sense that they are taken to be the formal expressions of an empirical condition which exists *sometimes*. Examples: a linear harmonic oscillator has no asymptotic mechanics. A particle interacting with a fixed, limited, attractive potential may have an asymptotic mechanics if either there is no discrete energy spectrum or if the states are restricted so that there is no admixture of discrete spectrum eigenstates. A system with a time-dependent external force may have an asymptotic mechanics, if the external force vanishes asymptotically at least in effect, i.e., where the particles are ultimately located. The latter condition means again a restriction on the states. When the forces (Hamiltonian) in the system allow an asymptotic mechanics, all operators are understood to have their domains restricted to those states which have an asymptotic mechanics.

The operators $A_r^{(\pm)}$ will be called asymptotic particle operators for the distant future (past).

The precise meaning of the limit of Heisenberg operators in Eq. (2.8) is given in Sect. **9**.

In the particular case where external forces are absent, the four operators P_μ are time-independent, and Eq. (2.8) becomes

$$P_\mu = \sum_r^N \int A_r^{(\pm)\dagger}(\boldsymbol{k})k_{r\mu}A_r^{(\pm)}(\boldsymbol{k})\,\mathrm{d}\boldsymbol{k}\,. \tag{2.9}$$

A particular theory is usually formulated by the equations of motion and commutation relations of operators φ_r which describe the bare particles or fields. From these operators, creation and destruction operators $a_r^{\dagger}$, a_r are defined in the usual way [1], and the total energy-momentum operators of

the system, P_μ, may be expressed by them. In conventional theories only three of these expressions ($\mu = 1$ to 3) are of the form of Eq. (2.4)

$$\left\{\begin{array}{ll} P_\mu = \sum_r^M \int a_r^\dagger(\boldsymbol{k}) k_{r\mu} a_r(\boldsymbol{k})\, \mathrm{d}\boldsymbol{k}\,, & (\mu = 1 \text{ to } 3) \\ P_4 = \sum_r^M \int a_r^\dagger(\boldsymbol{k}) k_{r4} a_r(\boldsymbol{k})\, \mathrm{d}\boldsymbol{k} + iH_1\,, & \end{array}\right. \tag{2.10}$$

where H_1 is the interaction Hamiltonian. The two expressions for P_μ differ not only by a term of more than second degree (H_1), but in the number of bilinear terms. M is the number of species of bare particles, while N is the number of species of stable particles, elementary or composite; evidently, $N \geq M$. For this reason alone, it is clear that there can be no unitary, and indeed, no linear transformation which takes the bare-particle operators a_r into the asymptotic particle operators $A_r^{(-)}$, although they satisfy the same commutation relations. Eq. (2.9) states that in absence of external forces two sets of operators $A_r^{(-)}$, functions of the bare-particle operators $a_r^\dagger$, a_r exist, in terms of which all four operators P_μ can be expressed as though all particles (elementary or composite) described by the $A_r^{(\pm)}$ were free.

In most situations, the only measurable quantities are the asymptotic momentum distributions. Hence, the principal problem of asymptotic mechanics is the relationship between the operators $A_r^{(+)}$ to the set $A_r^{(-)}$. The operators

$$A_r^{(-)\dagger}(\boldsymbol{k}) k_{r\mu} A_r^{(\pm)}(\boldsymbol{k})\,,$$

together with operators describing internal variables (spin, isotopic spin) have each a system of simultaneous eigenstates $\psi_n^{(\pm)}$, where the label n stands for all eigenvalues of the commuting operators $A_r^{(\pm)\dagger}(\boldsymbol{k}) k_{r\mu} A_r^{(\pm)}(\boldsymbol{k})$ and the «internal» operators. Both systems of state vectors are, incidentally, eigenstates of the four operators $\lim_{t\to\pm\infty} P_\mu(t)$.

(It is awkward to label states associated with the distant future and with operators $A_r^{(+)}$ by a minus superscript, but we do so because they will be identified, in the simplest case, with the usual incoming-wave solutions which are traditionally labeled by minus signs).

From here on, we assume that P_4 does not depend on time explicitly. One is interested in the «transition» from the state in the distant past to that in the distant future. If, in the distant past, a set of eigenvalues of the operators $A_r^{(-)\dagger}(\boldsymbol{k}) k_{r\mu} A_r^{(-)}(\boldsymbol{k})$ corresponding to the label i has been observed, then the probability of observing, in the distant future, a set of eigenvalues of the operators $A_r^{(+)\dagger}(\boldsymbol{k}) k_{r\mu} A_r^{(+)}(\boldsymbol{k})$, symbolized by the label f, is

$$W_{fi} = (\psi_f^{(+)}, \psi_i^{(-)})^2\,. \tag{2.11}$$

We define the S-matrix by

$$S_{fi} = (\psi_f^{(-)}, \psi_i^{(+)}) , \tag{2.12}$$

and we shall show that this definition is in agreement with the usual one in those problems which are well understood. In the general case of field theory with composite particles, however, the definition of the observable scattered particles itself is in question. We shall then consider Eqs. (2.8) or (2.9) and (2.12) as the fundamental statement of the problem: the operators $A_r^{(\pm)}(k)$ will *define* real particles, composite and elementary.

Eq. (2.12) is the only form of the S-matrix for the simplest one-channel case [9] which survives in the general theory, although the definition of the states $\psi_n^{(\pm)}$ is altogether different from that used in the simplest case.

The states $\psi_n^{(\pm)}$ have been defined by their properties. Their formal construction, i.e., the statement of the equations which they satisfy for a given theory, will be the major task of the following sections.

We note that the present concept of transition probability is quite different from that usually employed. We do not consider transitions between states of an unperturbed Hamiltonian under the influence of an interaction: rather both states $\psi_n^{(\pm)}$ are eigenstates of the total Hamiltonian, so that their probabilities are constants. The « transition » is here caused only by the fact that observations in the distant past are described by one set of eigenstates of the Hamiltonian ($\psi_n^{(+)}$) and those in the distant future by another set ($\psi_n^{(-)}$).

From the definition of the operators $A_r^{(\pm)}(\boldsymbol{k})$, one can construct Heisenberg operators $A_r^{(\pm)}(\boldsymbol{k}t)$ as usual by the relation $i\dot{A} = [A, H]$. Since the operator $P_4 = iH$ is time-independent, one obtains, by using the commutation relations [1]

$$i\dot{A}_r^{(\pm)}(\boldsymbol{k}t) - E_r A_r^{(\pm)}(\boldsymbol{k}t) = 0 . \tag{2.13}$$

The $\psi_n^{(-)}$ are labelled by the momenta and internal co-ordinates of the particles (simple and composite) which are observed asymptotically. By their definition, they can be built up by creation operators $A^{(-)\dagger}$ from a lowest eigenstate Ψ_0, the vacuum. A state

$$A_r^{(\pm)\dagger}(\boldsymbol{k})\Psi_0 = \psi_{r\boldsymbol{k}}^{(\pm)} \tag{2.14}$$

represents a single particle of species r with momentum $\boldsymbol{k}$. A state

$$A_r^{(\pm)\dagger}(\boldsymbol{k})A_{r'}^{(\pm)\dagger}(\boldsymbol{k}')\Psi_0 = \psi_{r\boldsymbol{k},r'\boldsymbol{k}'}^{(\mp)} \tag{2.15}$$

---

[9] M. GELL-MANN and M. L. GOLDBERGER: *Phys. Rev.*, **91**, 398 (1953).

describes the collision of two particles, with in- or outgoing scattered waves, etc. Since all states $\psi_n^{(-)}$ are orthonormal by their definition, it follows that the states which belong to different entrance channels (e.g. two deuterons on the one hand, and one proton and one triton on the other) must be orthogonal. This consequence of the postulate is not obvious, but it is in agreement with the situation in non relativistic multi-channel scattering ([7]).

It is not possible in the general case, to identify the asymptotic particle operators or their linear combinations with in- and out-fields in the sense of YANG and FELDMAN ([10]), HAAG ([11]) and LEHMANN, SYMANZIK and ZIMMERMANN ([12]), i.e. with asymptotic forms of the bare-particle operators. This can be anticipated by remembering that the number of bare particles is smaller than the number of all stable particles, elementary and composite. We return to this question in Sect. **15**.

Since in field theory the distinction between elementary and composite physical particles becomes blurred, we shall drop this distinction in language ([11]). One-particle solutions comprise all those eigenstates of the Hamiltonian which describe stable elementary and composite particles; e.g., in nuclear theory, π-mesons, nucleons and anti-nucleons, deuterons and all stable nuclei. The formal definition of these states is as follows: in specifying a state vector, eigenvalues of the three total momentum operators P_1 to P_3 can be used as quantum numbers. In absence of external forces, these operators commute with P_4; hence eigenfunctions of $H = -iP_4$ can be written as $\prod_{i=1}^{3} \delta(P_i' - P_{0i})\psi$. One-particle eigenstates are distinguished by the fact that $(\psi, \psi) < \infty$, i.e., the significant parts of the state vectors are normalizable in the strict sense of the word. A group theoretical definition of one-particle states is given by HAAG ([11]).

3. – Direct Construction of the S-Matrix.

In order to relate the asymptotic particle operators $A^{(\pm)}$ to the bare-particle operators a_r, we expand the former into a sum of products of the latter:

$$A^{(\pm)\dagger} = \sum f(NN')C(N)D(N') \,, \tag{3.1}$$

where $C(N)$ is a product of N bare creation operators, and $D(N')$ a similar product of destruction operators, each in some fixed order ([13]).

([10]) C. N. YANG and D. FELDMAN: *Phys. Rev.*, **79**, 972 (1950).

([11]) R. HAAG: *Kgl. Danske Videnskab. Selskab, Nat.-Phys. Medd.*, **29**, No. 12 (1955).

([12]) H. LEHMANN, K. SYMANZIK and W. ZIMMERMANN: *Nuovo Cimento*, **1**, 205 (1955).

([13]) A similar, but 4-dimensional representation has been studied by K. NISHIJIMA: *Prog. Theor. Phys.*, **10**, 549 (1953).

It is convenient to order the states in the product $C(N)$ in the reverse direction to that chosen for $D(N')$, e.g.

$$C(N)\,D(N') = a_8^\dagger a_7^\dagger a_6^\dagger a_1 a_2 a_3 ,$$

because we have then the simple relation

$$(C(N)\,D(N'))^\dagger = C(N')\,D(N) , \tag{3.2}$$

while, without this convention, a minus-sign may appear on account of a commutation of Fermion creation operators.

We assume that the expansion (3.1) is unique; that is, we assume that no product $C(N)\,D(N')$ is equivalent to a linear combination of other such products with respect to all states in Hilbert space, although for any given state such an equivalent combination exists.

From Eq. (2.13), we obtain for the Schrödinger operators $A^{(\pm)\dagger}$

$$[H, A_r^{(\pm)\dagger}(\boldsymbol{k})] - E_r(\boldsymbol{k}) A_r^{(\pm)\dagger}(\boldsymbol{k}) = 0 . \tag{3.3}$$

The commutator $[H_0, C(N)\,D(N')]$ is just the difference between the energies of the bare particles described by $C(N)$ and those described by $D(N')$.

In order to use the expansion (3.1), the commutator $[H_1, C(N)\,D(N')]$ must be re-expressed in terms of N-ordered products. Since the Hamiltonian is given in terms of bare-particle operators, this expansion can be done explicitly:

$$[H_1, C(N)\,D(N')] = \sum d_{NN',MM'}\, C(M)\,D(M') . \tag{3.4}$$

We obtain from Eqs. (3.1), (3.3) and (3.4):

$$(E_M - E_{M'} - E) f(MM') + \sum d_{NN',MM'} f(NN') = 0 . \tag{3.5}$$

This equation has, as usual, two types of solutions which describe in- and outgoing waves, respectively, and hence are associated with the operators $A^{(\pm)}$, respectively. However, it is clear that not all solutions of Eq. (3.5) will lead to operators $A^\dagger$ in conjunction with Eq. (3.1). For instance, a product $A_p^\dagger A_{p'}^\dagger$ will also satisfy Eq. (3.3). Hence, the solutions f must be restricted by the requirement that the operators $\sum f(NN')\,C(N)\,D(N')$ satisfy the simple commutation relations of the operators A:

$$[A_r(\boldsymbol{k}), A_s^\dagger(\boldsymbol{k}')]_\pm = \delta_{rs}\delta(\boldsymbol{k} - \boldsymbol{k}') . \tag{3.6}$$

Insertion of Eq. (3.1) leads to a set of equations which the desired solutions

f_k must satisfy:

$$\sum_{NN'MM'} f_k^*(NN') f_{k'}(MM') h(N'NMM'KK') = \delta_K \delta_{\bar{K}} \delta(k - k') , \tag{3.7}$$

where h is defined by

$$[C(N') D(N), C(M) D(M')]_+ = \sum_{KK'} h(N'NMM'KK') C(K) D(K') . \tag{3.8}$$

These relations take the place of boundary conditions which are usually imposed to specify the desired solutions. Eq. (3.7) provides also the normalization of the coefficients f.

In order to form the S-matrix according to Eq. (2.12), (2.14) and Eq. (3.1), we need also the scalar products

$$g(NN') = (C(N) D(N') \Psi_0, \Psi_0) . \tag{3.9}$$

From the identity

$$(C(N) D(N') \Psi_0, H\Psi_0) = (HC(N) D(N') \Psi_0, \Psi_0) = 0 , \tag{3.10}$$

one obtains as before [14]

$$E_{N'} g(NN') + \sum d^*_{NN'MM'} g(MM') = 0 . \tag{3.11}$$

In the conventional theory, one assumes the existence of a bare vacuum Φ_0 such that $D\Phi_0 = 0$. We replace this by the weaker assumption that any expression $D\Psi_0$ is normalizable. If follows that g must be bounded. This provides a strong restriction on the desired solution of Eq. (3.11), since the quantity $E_N - E_{N'}$ may vanish:

$$\sum d^*_{NN'MM'} g(MM') = 0 . \qquad (E_N = E_{N'}). \tag{3.12}$$

Hence, the S-matrix can be constructed from the solutions of the linear equations (3.5) and (3.11) with the « boundary conditions » (3.7) and (3.12), respectively. It is remarkable that a complete system of time-independent equations can be given without the questionable assumption of the existence of a bare vacuum [11] nor of any specific representation of the operators a_r and $a_r^\dagger$. The natural assumption

$$\| \prod_{r,k} a_r(k) \Psi_0 \| < \infty$$

is sufficient to state the problem explicitly.

---

[14] The same equation, with different boundary conditions and different physical interpretation, has been used by F. J. Dyson: *Phys. Rev.*, **91**, 1543 (1953).

Instead of pursuing the direct approach, we turn to another, probably more useful method which uses basis vectors Φ_n to represent the physical but non interacting particles.

4. – Basis Vectors.

The conventional treatment of scattering problems is based on a system of basis vectors which describe in some sense free particles and which are not eigenstates of the four operators P_μ. In the past, these vectors were chosen to be eigenstates of an unperturbed Hamiltonian H_0; more recently, non orthogonal basis vectors have been used ([7,15]) which are not eigenstates of any linear operator. The usefulness of these basis vectors consists in their ability to generate the states $\psi_n^{(\pm)}$ by the operation

$$\int c(n)\psi_n^{(\mp)}\,\mathrm{d}n = \lim_{t\to\pm\infty}\int c(n)\exp[i(H-E_n)t]\Phi_n\,\mathrm{d}n\,, \tag{4.1}$$

(where $c(n)$ is a normalizable c-number function), which we write symbolically

$$\psi_n^{(\mp)} = \lim_{t\to\pm\infty}\exp[i(H-E_n)t]\Phi_n\,. \tag{4.2}$$

In the simplest (one-channel) case, the basis vectors Φ_n are simultaneous eigenstates of the momentum operators P_1 to P_3. In the non-relativistic multi-channel case, they are symmetrized or antisymmetrized products of plane waves in the center of mass co-ordinates and of bound-state eigenfunctions of the colliding composite particles. We will be concerned with the appropriate choice for field theory.

Of course, the choice cannot be arbitrary; we must require *a*) that the limit in Eq. (4.1) actually exists ([16]), *b*) that the limits $\psi_n^{(\mp)}$ are simultaneous eigenstates of the four operators P_μ, with eigenvalues equal to the sum of the four-momenta of the incident particles, and *c*) that the two sets, $\psi_n^{(\mp)}$ should be orthonormal. Then it is well known from the theory of non interacting fields that these sets are indeed simultaneous eigenstates of the operators

$$A_r^{(\pm)\dagger}(\boldsymbol{k})k_{r\mu}A_r^{(\mp)}(\boldsymbol{k})\,,$$

which is the original definition.

([15]) G. C. Wick: *Rev. Mod. Phys.*, **27**, 339 (1955).

([16]) In many papers, non-existing limits are replaced by substitute limits defined ad hoc, which are presumed to describe a slow switching-off of an interaction. Since we are concerned primarily with composite particles, this artifice is not permissible. A deuteron would simply disintegrate if the interaction were switched off.

The requirement *a*) can be rephrased more conveniently by requiring the existence of two time-independent functions $c_{\pm}(n)$ such that

$$\lim_{t \to -\infty} \left| \left(i \frac{\partial}{\partial t} - H \right) \int \exp\left[- iE_n t \right] c_{\pm}(n) \Phi_n \, \mathrm{d}n \right| = 0 \,. \tag{4.3}$$

Eq. (4.3) can be considered as an expression of the asymptotic equivalence of the Φ_n with the energy eigenfunctions $\psi_n^{(-)}$, since Eq. (4.3) would be valid without the limit if this substitution were made. (Naturally, eigenfunctions of H which would satisfy Eq. (4.3) trivially, are useless since they do not give two different sets through Eq. (4.2).)

5. – Field Theory without Vacuum Polarization 1.

We consider a theory in which the Bose field is treated relativistically but the Fermi particles non-relativistically. It is customary, in this case, to describe the Fermi particles by Schrödinger wave functions. We prefer to describe them by non-relativistic second quantization, for uniformity of the notation. Then, the Hamiltonian commutes with the number of Fermi- but not of Bose-particles.

In the non relativistic case ([7]), the choice of the appropriate basis functions Φ_n was suggested by their behavior in configuration space. In field theory, a more formal definition of the basis vectors is necessary, without reliance on configuration space.

We will try to construct the basis vectors Φ_n for field theory by analogy with particle mechanics, and verify that they meet the requirements. For this purpose, we first paraphrase the definition of the Φ_n's in (EI) into the language of second quantization.

The one-particle solutions from which the Φ_n's were constructed, are bound-state solutions of a Schrödinger equation truncated by omission of all terms involving some elementary particles, actually present. In the language of second quantization, one of these one-particle solutions is an actual solution of the Schrödinger equation, characterized by a number of elementary particles smaller than that appearing in the Φ_n, i.e., only those elementary particles which belong to the composite particle under consideration. The basis functions Φ_n were defined as symmetrized or anti-symmetrized products of these one-particle solutions. In the language of second quantization, this construction may be described more simply. Any state may be constructed by letting linear combinations of products of bare-particle creation operators $a_j^{\dagger}(\boldsymbol{k})$ (Bose and Fermi particles) act on the lowest energy eigenstate of the Hamiltonian (the vacuum state Ψ_0). If $\boldsymbol{c}_{sk}$ designates that combination of

creation operators $a_r^\dagger(\boldsymbol{k})$ which creates an eigenstate of the Hamiltonian describing a single composite particle with total momentum $\boldsymbol{k}$, i.e.,

$$\psi_{s\boldsymbol{k}} = \boldsymbol{c}_{s\boldsymbol{k}}\Psi_0 , \tag{511}$$

then the symmetrized or antisymmetrized products Φ may be written

$$\Phi_{s\boldsymbol{k},s'\boldsymbol{k}'\ldots} = C\boldsymbol{c}_{s\boldsymbol{k}}\boldsymbol{c}_{s'\boldsymbol{k}'}\ldots\Psi_0 , \tag{5.2}$$

where C is a normalization constant.

It is easy to see that an interchange of the two operators in Eq. (5.2) will produce a (+) or (−) factor, the latter if $s = s'$ and the number of elementary Fermi-particles contained in s is odd. This is a paraphrasing of the well-known statement that composite particles behave rigorously like Fermi- or Bose-particles when they do not interact ([17]). Hence,

$$\boldsymbol{c}_{s\boldsymbol{k}}\boldsymbol{c}_{s'\boldsymbol{k}'} = \pm\,\boldsymbol{c}_{s'\boldsymbol{k}'}\boldsymbol{c}_{s\boldsymbol{k}} , \tag{5.3}$$

the upper sign being valid for two different particles or two identical Bose-particles, the lower sign for two identical Fermi-particles. If s and s' are different, the sign in Eq. (5.3) is $(-1)^{n_1 n_2}$ where n_1 and n_2 are the numbers of elementary Fermi-particles which are contained in the composite particles s_1 and s_2, respectively.

This definition of the basis vectors will be adopted for field theory without vacuum polarization. The only difference is that the number of Bose-particles is no longer sharp, so that the operators $\boldsymbol{c}$ consist of sums of products of creation operators such that not all terms of the sum have the same number of factors. Since the only creation operators which do not commute, describe Fermi particles which do have well-defined numbers, Eq. (5.3) is still valid. The set of basis functions Φ_n has the vacuum state Ψ_0 and the one-particle states $\psi_{s\boldsymbol{k}}$ in common with a system of eigenstates of H, but the two- and many-particle states Φ_n are not eigenfunctions of H. As in (EI) we associate energies E_n to each basis vector Φ_n; they are sums of the energies of the particles which are represented by Φ_n, for instance, the energy $E_{s\boldsymbol{k},s'\boldsymbol{k}'}$ is $E_{s\boldsymbol{k}}+E_{s'\boldsymbol{k}'}$, the sum of the eigenvalues of H belonging to $\psi_{s\boldsymbol{k}}$ and $\psi_{s'\boldsymbol{k}'}$.

We will show now that this set Φ_n satisfies the requirement (4.3) i.e., that there exist linear combinations

$$\int \exp[\quad iE_n t]c_\pm(n)\Phi_n\,\mathrm{d}n ,$$

([17]) P. Ehrenfest and J. R. Oppenheimer: *Phys. Rev.*, **37**, 333 (1931).

which are, for the distant future (past) solutions of the time-dependent Schrödinger equation. Consider first a wave packet constructed from one-particle states ψ_{sk} which represent a particle moving in the positive x-direction.

$$\Psi_{s1}(t) = \int \exp[-iE_s(\boldsymbol{k})t] v_{s1}(\boldsymbol{k}) \psi_{s\boldsymbol{k}} \, \mathrm{d}\boldsymbol{k} \,, \tag{5.4}$$

such that v_{s1} vanishes for all directions with $k_x < 0$. Clearly, $\Psi_{s1}(t)$ is a solution of the Schrödinger equation for all times.

We will write, for brevity,

$$\Psi_{s1}(t) = \boldsymbol{c}_{s1}(t)\Psi_0 \,, \tag{5.5}$$

as a generalization of Eq. (5.1). Then,

$$i\dot{\boldsymbol{c}}_{s1}(t)\Psi_0 = H\boldsymbol{c}_{s1}\Psi_0 \,. \tag{5.6}$$

We now assume that the clouds of bare particles which represent real particles are of limited range. More precisely, we assume that the state vector which represents a localized real particle

$$\Psi_s(0) = \int \psi_{s\boldsymbol{k}} \, \mathrm{d}\boldsymbol{k} \,,$$

when analyzed in terms of bare particle creation operators $a_s^\dagger(\boldsymbol{x})$ (the Fourier transforms of $a_s^\dagger(\boldsymbol{k})$) has no operators $a_s^\dagger(\boldsymbol{x})$ if $|\boldsymbol{x}$ is larger than some finite cloud radius, or at least that the coefficients of such operators decrease exponentially with $|\boldsymbol{x}$. However, in electrodynamics, the photon cloud about an electron is extended, so that particles of zero mass should be excluded from this point on; they can probably be considered as a limiting case.

It follows that the creation operators of bare particles $a_s^\dagger(\boldsymbol{x})$ which are implied in $\boldsymbol{c}_{s1}(t)$, commute with creation and destruction operators of Bose fields at $\boldsymbol{x}'$ (in a region distant from the instantaneous position) and anticommute with field operators of the (s-th) Fermi field at $\boldsymbol{x}'$. Therefore, as the packet moves in the positive x-direction, $\boldsymbol{c}_{s1}(t)$ commutes asymptotically ($t \to \infty$) with products of field operators with arguments $x < 0$, in which Fermi creation and destruction operators occur bilinearly. But the Hamiltonian density $\mathscr{H}(\boldsymbol{x})$ has always this property, for obvious reasons of conservation. If we subdivide the total Hamiltonian into two parts, containing field operators with $x < 0$ and $x > 0$, respectively,

$$H = H_1 + H_2 = \int_{x>0} \mathscr{H} \, \mathrm{d}\boldsymbol{x} + \int_{x<0} \mathscr{H} \, \mathrm{d}\boldsymbol{x} \,, \tag{5.7}$$

then

$$\lim_{t\to\infty}[\boldsymbol{c}_{s1}(t), H_2] = 0\,. \tag{5.8}$$

Similarly, we can construct a wave packet which propagates only in the negative x-direction

$$\Psi_{s'2}(t) = \int \exp[-iE_{s'}(\boldsymbol{k})t] v_{s'2}(\boldsymbol{k}) \psi_{s'\boldsymbol{k}}\,\mathrm{d}\boldsymbol{k}\,, \tag{5.4a}$$

where $v_{s'2}$ vanishes for $k_x > 0$. We have also

$$i\dot{\boldsymbol{c}}_{s'2}(t)\Psi_0 = H\boldsymbol{c}_{s'2}\Psi_0\,, \tag{5.6a}$$

and

$$\lim_{t\to\infty}[\boldsymbol{c}_{s'2}, H_1] = 0\,. \tag{5.8a}$$

The wave packet of basis functions Φ_n is now constructed by «multiplying» the packets (5.4) and (5.4a), i.e.,

$$\int c(n)\exp[-iE_n t]\Phi_n\,\mathrm{d}n = \iint \mathrm{d}\boldsymbol{k}\,\mathrm{d}\boldsymbol{k}'\, v_{s1}(\boldsymbol{k})\, v_{s'2}(\boldsymbol{k}')\boldsymbol{c}_{s\boldsymbol{k}}\boldsymbol{c}_{s'\boldsymbol{k}'} \cdot \exp[-i\{E_s(\boldsymbol{k}) + E_{s'}(\boldsymbol{k}')\}t]\Psi_0 = \boldsymbol{c}_{s1}(t)\boldsymbol{c}_{s'2}(t)\Psi_0\,, \tag{5.9}$$

and we wish to prove that it asymptotically satisfies the Schrödinger equation:

$$\lim_{t\to\infty}\left|\left(i\frac{\partial}{\partial t} - H\right)\boldsymbol{c}_{s1}(t)\boldsymbol{c}_{s'2}(t)\Psi_0\right| = 0\,. \tag{5.10}$$

By Eqs. (5.7), (5.8), (5.8a), (5.3), (5.6), (5.6a), we have, omitting the argument t:

$$\begin{aligned}
&\lim_{t\to\infty}\left|\left(H_1 + H_2 - i\frac{\partial}{\partial t}\right)\boldsymbol{c}_{s1}\boldsymbol{c}_{s'2}\Psi_0\right| - \\
&= \lim_{t\to\infty}\left|\pm\boldsymbol{c}_{s'2}H_1\boldsymbol{c}_{s1} + \boldsymbol{c}_{s1}H_2\boldsymbol{c}_{s'2} - i\frac{\partial}{\partial t}(\boldsymbol{c}_{s1}\boldsymbol{c}_{s'2})\right|\Psi_0 = \\
&= \lim_{t\to\infty}\left|\pm\boldsymbol{c}_{s'2}H\boldsymbol{c}_{s1} + \boldsymbol{c}_{s1}H\boldsymbol{c}_{s'2} + \boldsymbol{c}_{s'2}H_2\boldsymbol{c}_{s1} - \boldsymbol{c}_{s1}H_1\boldsymbol{c}_{s'2} - i\frac{\partial}{\partial t}(\boldsymbol{c}_{s1}, \boldsymbol{c}_{s'2})\right|\Psi_0 = \\
&= \lim_{t\to\infty}\left|i(\dot{\boldsymbol{c}}_{s1}\boldsymbol{c}_{s'2} + \boldsymbol{c}_{s1}\dot{\boldsymbol{c}}_{s'2})\Psi_0 - \boldsymbol{c}_{s1}\boldsymbol{c}_{s'2}(H_1 + H_2)\Psi_0 - i\frac{\partial}{\partial t}(\boldsymbol{c}_{s1}\boldsymbol{c}_{s'2})\Psi_0\right| = 0\,.
\end{aligned} \tag{5.11}$$

The last step follows from the fact that the energy of the vacuum state Ψ_0 is zero. The choice of signs in Eq. (5.11) depends on the sign in Eq. (5.3).

The generalization to several particles is obvious and will not be given explicitly. It has been shown that the limit in Eq. (4.3) exists with the present choice of Φ_n. The first part of the requirement *b*), that the vectors $\psi_n^{(\pm)}$ should be eigenvectors of the operator P_4, is essentially implied in the foregoing, but it can be shown explicitly as in Eqs. (29) to (32) of (EI). We show next that the states $\psi_n^{(\pm)}$ are also eigenstates of the three momentum operators P_1 to P_3. Since, in absence of external field, these operators commute with the Hamiltonian, Eq. (4.2) indicates that it is sufficient to prove that the Φ_n are eigenstates of P_1 to P_3.

A state described by

$$\prod_{ki} a^\dagger(\boldsymbol{k}_i)\Psi_0$$

is evidently an eigenfunction of the three momentum operators with eigenvalue $\boldsymbol{P} = \sum \boldsymbol{k}_i$. Since ψ_{sk} in Eq. (5.1) is an eigenstate of the momentum, the operator $\boldsymbol{c}_{sk}$ must consist of integrals of products of creation operators with a factor $\delta(\sum \boldsymbol{k}_i - \boldsymbol{k})$. If several operators $\boldsymbol{c}$ are multiplied in accordance with Eq. (4.2), it is always possible to extract from every term of the product a factor $\delta(\sum \boldsymbol{k}_i - \boldsymbol{k} - \boldsymbol{k}')$. Hence $\Phi_{sk,s'k'}$ as defined by Eq. (5.2) is an eigenstate of the momentum operator $\boldsymbol{P}$ with eigenvalue $\boldsymbol{k}+\boldsymbol{k}'$, and the same argument evidently holds for a product of any number of operators $\boldsymbol{c}$. Requirement *b*) has now been satisfied.

We show now that the basis vectors satisfy the requirement *c*).

While the basis vectors are not orthogonal, they can be normalized (in the improper sense) so that

$$(\Phi_n, \Phi_m) = \delta(n - m) + g(nm)\,, \tag{5.12}$$

where $g(nm)$ is well-behaved in the following sense: if the set of labels implied in m is divided into parameters of degeneracy α_m and the energy E_m, then the integral

$$\bar{g}(E_m) = \int c(m)\, g(nm)\, \mathrm{d}\alpha_m\,, \tag{5.13}$$

(where $c(m)$ is square-integrable), is an absolutely integrable function of the energy E_m. This assertion can be proved by inspection of the scalar products (Φ_n, Φ_m). Consider as an example, the two basis vectors representing one (physical) nucleon and one or two mesons, respectively. They are

$$\begin{cases} \Phi_{kp} = a_k^\dagger \psi_p\,, \\ \Phi_{k'k''p'} = 2^{-\frac{1}{2}} a_{k'}^\dagger a_{k''}^\dagger \psi_{p'}\,, \end{cases} \tag{5.14}$$

where ψ_p is a one-particle eigenstate of H, and $a_k^\dagger$ are meson-creation operators. Then

$$2^{\frac{1}{2}}(\Phi_{k_p}, \Phi_{k'k''p'}) = (a_{k'}a_{k''}\psi_p, a_k\psi_{p'}) + \delta(k-k')(a_{k''}\psi_p, \psi_{p'}) + \\ + \delta(k-k'')(a_{k'}\psi_p, \psi_{p'}) , \tag{5.15}$$

The scalar products appearing on the right hand side of Eq. (5.15) are clearly well-behaved functions of the labels, but the delta-functions may be thought to cause trouble. However, if the function $\bar{g}$ according to Eq. (5.13) is formed, integrations with respect to k' (for the second term) or with respect to k'' (for the third term) result in well-behaved functions of

$$E_{k'k''p'} = (k'^2+\mu^2)^{\frac{1}{2}} + (k''^2+\mu^2)^{\frac{1}{2}} + (p'^2+m^2)^{\frac{1}{2}} , \tag{5.16}$$

where μ and m are the masses of mesons and nucleons, respectively. The same argument can be carried through in general.

To prove the orthonormality of the $\psi_n^{(\pm)}$, we form now, according to Eq. (4.1)

$$\left(\psi_n, \int c(m)\psi_m \,\mathrm{d}m\right) = \lim_{t\to\pm\infty} \int \left\{\exp[i(H - E_n)t]\Phi_n, \exp[i(H - E_m)t]\Phi_m\right\} c(m)\,\mathrm{d}m \tag{5.17}$$

$$= \lim_{t\to\pm\infty} \int \exp[i(E_n - E_m)t](\Phi_n, \Phi_m)c(m)\,\mathrm{d}m =$$

$$= c(n) + \lim_{t\to\pm\infty} \int \exp[i(E_n - E_m)t]g(nm)\,c(m)\,\mathrm{d}m =$$

$$= c(n) + \lim_{t\to\pm\infty} \int \exp[i(E_n - E_m)t]\bar{g}(E_m)\,\mathrm{d}E_m = c(n) ,$$

since the Fourier integral of an absolutely integrable function vanishes asymptotically.

In (EI), the orthonormality of the $\psi_c^{(+)}$ and, separately, of the $\psi_n^{(-)}$, was proved essentially in the same manner, but with the stronger assertion

$$(\Phi_n, \Phi_m) < \infty \qquad (n \neq m).$$

This assertion is incorrect in general, but the weaker statement [Eq. (5.13)] is sufficient to obtain the same result.

The preceding cumbersome proof seems to be indispensable if one wants to be reasonably certain that the limits actually exist and have physical significance. The usual formal theory of scattering amounts to choosing for Φ_n arbitrarily eigenfunctions of H_0; defining $\psi_n^{(\pm)}$ by Eq. (4.2) and the S-matrix

by Eq. (2.12) or its equivalent. If time-limits manifestly fail to exist, the usual cavalier limiting procedures lead to expressions which are useful in simple cases, but lack in generality.

By expressing the limit in Eq. (4.2) in a convenient form and inserting it into Eq. (2.12) as in (EI), the scattering problem can be formulated as a time-independent non linear integral equation as follows:

If two matrices $R^{(\pm)}$ are defined by

$$R^{(+)}(mn) = ((H - E_m)\Phi_m, \psi_n^{(+)}) , \tag{5.18}$$

$$R^{(-)}(mn) = (\psi_m^{(-)}, (H - E_n)\Phi_n) , \tag{5.19}$$

they are shown to be connected with the S-matrix by

$$S(mn) = \delta(m - n) - 2\pi i\,\delta(E_m - E_n)\,R^{(\pm)}(mn) . \tag{5.20}$$

We consider now the integral equations for the scattering amplitudes derived in (EI). Some care is required in adapting the third term in Eqs. (EI) (70) and (71) to field theory. In expanding the function $(H - E_n)$, we wrote there separately the terms which contained discrete spectrum eigenfunctions ψ_b, because an expression of the type

$$((H - E_n)\Phi_n, \psi_b)$$

cannot be identified with a matrix element R_{nb}, since ψ_b is not defined by an equation of the type (EI), Eq. (29), from which the integral equation for R was derived. The same thing is true of the one-particle states in field theory. Hence, Eqs. (71) and (70) of (EI) must be paraphrased for field theory as follows:

$$R^{(-)}(mn) = (\Phi_m, (H - E_n)\Phi_n) - \int \frac{R^{(-)}(ln)\overset{*}{R}{}^{(-)}(lm)}{E(l) - E(m) - i\varepsilon}\,dl \int \frac{(\psi_l, (H - E_m)\Phi_m)^*\,(\psi_l, (H - E_n)\Phi_n)}{E(l) - E(m)}\,dl , \tag{5.21}$$

and

$$R^{(+)}(mn) = (\Phi_m, (H - E_n)\Phi_n) \int \frac{R^{(+)}(ml)\overset{*}{R}{}^{(+)}(nl)}{E(l) - E(n) - i\varepsilon}\,dl \int \frac{((H - E_m)\Phi_m, \psi_l)((H - E_n)\Phi_n, \psi_l)^*}{E(l) - E(n)}\,dl . \tag{5.22}$$

Actually, because of momentum conservation, the momentum of the one-particle solutions ψ_l is fixed by the total momentum of Φ_n, so that the third term in Eqs. (5.21) and (5.22) is a sum over all one-particle solutions (elementary and composite particles). In nucleon-theory, virtual deuterons, etc., contribute to this term.

We discuss now the construction of the operators $\boldsymbol{c}$, which determine the basis vectors. In Sect. 3, a set of linear equations with « boundary conditions » for the construction of the operators $A^{(\pm)\dagger}$ was derived. The operators $\boldsymbol{c}$ and $A^{(\pm)\dagger}$ create the same one-particle states when acting on the vacuum

(5.1), (2.14) $$\boldsymbol{c}_k\Psi_0 = A_k^{(\pm)\dagger}\Psi_0 = \psi_k ,$$

but they differ in general. In particular,

(5.2) $$C\boldsymbol{c}_k\boldsymbol{c}_{k'}\Psi_0 = \Phi_{kk'} ,$$

which is a basis vector and not an eigenvector of the Hamiltonian, while

(2.15) $$A_k^{(\pm)\dagger}A_{k'}^{(\pm)\dagger}\Psi_0 = \psi_{kk'}^{(\mp)} ,$$

which is a scattering eigenstate of the Hamiltonian, with incident particles k and k'. The operators $\boldsymbol{c}$ are obtained from the operator $A^{(\pm)\dagger}$ by simply omitting all terms with bare particle destruction operators:

(5.23) $$\boldsymbol{c}_k = \sum_N f(N0)\, C(N) ,$$

where $f(N0)$ are the coefficients of those products $C(N)\,D(N')$ which have no destruction operators ($N' = 0$). To illustrate the difference between $A^\dagger$ and $\boldsymbol{c}$, we notice that in a theory without vacuum polarization the creation operator $\boldsymbol{c}_k$ for a meson is identical with the bare-particle operator $a_k^\dagger$, while $A^\dagger$ has many additional terms with bare-particle destruction operators to the right. These additional terms annul the vacuum state, but not other states.

6. – Field Theory with Vacuum Polarization.

In a theory with vacuum polarization, where the lowest eigenstate of the Hamiltonian Ψ_0 (the physical vacuum) is not also the lowest eigenstate of the unperturbed Hamiltonian Φ_0 (the mathematical vacuum), a difficulty appears. The reasoning of Sect. 5 was straightforward, because all states could be constructed by the action of only bare-particle *creation* operators on the vacuum. If it is assumed that, in the general case, the one-particle states

can also be constructed by creation operators $a_r^\dagger$ alone, acting on the real vacuum, all conclusions of Sect. **5** are valid in general. We shall discuss this assumption or possible substitutes for it.

The operators $\boldsymbol{c}$ differ from the operators $A^\dagger$, for instance, as follows:

$$\boldsymbol{c}_k = A_k^\dagger(1 + h_1\{A\}) + h_2\{A\}\,, \tag{6.1}$$

where h_1 and h_2 are some functions of all destruction operators A.

What selects the particular operators $\boldsymbol{c}$ which we need? An essential element of the proof of Eq. (4.3) was the statement that the operators $\boldsymbol{c}(\boldsymbol{x})$, the Fourier transforms of $\boldsymbol{c}_k$, should be expressible in terms of a bare-particle operator cloud of limited range, because the essential Eq. (5.7) was based on this property. Since, as it is well known, the rate of asymptotic decrease of a function in x-space is determined by its singularities in k-space (for instance, a function with all derivatives existing has an exponentially decreasing Fourier transform) this requirement means that the coefficients $c(NN')$ in

$$\boldsymbol{c} = \sum c(NN')\,C(N)\,D(N') \tag{6.2}$$

must be a smooth function of all momentum variables, contrary to the coefficients $f(NN')$. Our hypothesis amounts to assuming that the coefficients $C(NN')$ are obtained from the solution $f(NN')$ of Eq. (3.5) by setting

$$c(N0) = f(N0)\,, \qquad c(NN') = 0 \qquad (N' \neq 0). \tag{6.3}$$

It is not implausible that this choice could be justified.

On the other hand, assume that the above assumption is not rigorously correct. Then, we can consider

$$\psi_k \approx \sum f_k(N0)\,C(N)\Psi_0$$

as an approximation. In another paper ([18]), arguments were given for the conjecture that the S-matrix is largely insensitive toward the substitution of approximations for the rigorous one-particle state vectors, i.e. that the S-matrix as calculated from a class of approximate basis vectors is rigorously correct. This conjecture of insensitivity can therefore be considered as an alternative to the assumption expressed by Eq. (6.3). From a pragmatic point of view, this question is rather unimportant, since the equations for the coefficients f can only be solved approximately. For these reasons, the extension of the results of Sect. **5** to the general case seems justified.

([18]) H. EKSTEIN and K. TANAKA: to be published in *Phys. Rev.*

Finally, we illustrate the calculating scheme which results from the present discussion, by the example of the meson-deuteron scattering. In order to construct the inhomogeneous part of the integral equations (5.21) or (5.22), we need basis vectors which represent « products » of plane waves of the following particles: meson and deuteron, neutron and proton, and possibly several mesons with either group of particles. Approximations to the creation operators $A^\dagger$ for physical mesons or nucleons can be obtained either by iteration of Eq. (3.5), the leading term being $b^\dagger$ or $a^\dagger$, or by the analog of the Tamm-Dancoff method, i.e., by dropping all coefficients f which describe more than N bare particles. The normalization is given by Eq. (3.7).

As an approximation for the creation operator $\boldsymbol{c}_{\text{Deuteron}}$, we can take a linear combination of a product of bare neutron and proton creation operators, the coefficient being one of the usual approximations to the deuteron wave function. For those basis vectors which describe two « elementary » (not bare) particles, the first creation operator $\boldsymbol{c}$ will be approximated simply by the corresponding bare-particle creation operator.

If the conjectured insensitivity of Eqs. (5.21) or (5.22) holds ([17]), then the integral equation written with this approximate inhomogeneous term should still give the rigorously correct result, if solved exactly.

The problems arising from the renormalization of Eqs. (5.21), (5.22) and methods of solution will not be discussed here.

7. – Real-Particle Operators.

The following sections are mainly intended to show that the proposed principle leads to the usual results in those cases which are well understood.

In order to calculate the S-matrix, it is evidently desirable to find operators $A_r(\boldsymbol{kt})$ with known equations of motion and commutators which become asymptotically identical with $A_r^{(\pm)\dagger}(\boldsymbol{kt})$, i.e.,

$$\lim_{t\to\pm\infty} [A_r(\boldsymbol{kt}) - A_r^{(\pm)}(\boldsymbol{kt})] = 0 \,. \tag{7.1}$$

Such operators A_r may be called real-particle operators since they merge asymptotically with both asymptotic particle operators $A_r^{(\pm)}$. In the simplest case, it will be shown that the operators $A_r(\boldsymbol{kt})$ can be chosen to be just the Heisenberg destruction operators of bare particles, and their equations of motion are those which are given at the outset.

If the equations of motion of these real-particle operators are known and if they are solved in the form

$$A_r^{(+)} = A_r^{(+)}(A_r^{(-)}) \,,$$

then the S-matrix can be found by determining the canonical transformation between the operators $A_r^{(+)}$ and $A_r^{(-)}$, i.e., by solving the equation

$$A_r^{(+)}(\boldsymbol{k}) = S_Y^{-1} A_r^{(-)}(\boldsymbol{k}) S_Y \,, \tag{7.2}$$

where S_Y is the scattering operator of YANG and FELDMAN ([10,19]). Since the states $\psi_n^{(\pm)}$ are orthonormal simultaneous eigenstates of $A_r^{(\pm)}(k) k_{r\mu} A_r^{(\pm)}(k)$, it is clear that

$$\psi_n^{(+)} = S_Y \psi_n^{(-)} \,, \tag{7.3}$$

and hence, from Eq. (2.12)

$$S_{fi} = (\psi_f^{(+)}, S_Y \psi_i^{(+)}) \,. \tag{7.4}$$

For the case of a single particle, the formalism of second quantization is unnecessarily cumbersome, and we shall maintain the asymptotic conditions in the form of Eqs. (2.1) to (2.3) (without summation). The subsequent statements are then simplified: the functions $\psi_n^{(\mp)}$ are simultaneous eigenfunctions of the operators $p_\mu^{(\pm)}$; a set of operators which merges asymptotically with $p_\mu^{(\pm)}$ will be called π_μ and its property is defined by

$$\lim_{t \to \pm \infty} \pi_\mu(t) = p_\mu^{(\pm)} \,, \tag{7.5}$$

instead of Eq. (7.1). If $p_\mu^{(+)}$ is known as a function of $p_\mu^{(-)}$, the scattering operator of Yang and Feldman is given by

$$p_\mu^{(+)} = S_Y^{-1} p_\mu^{(-)} S_Y \,. \tag{7.6}$$

We shall discuss several cases of asymptotic mechanics in ascending order of complexity and show that the present statement of the problem agrees with previous formulations in the simpler cases.

8. – Classical, Non Relativistic Particle.

We consider the scattering of a single particle by a constant potential V. The equations of motion

$$m\ddot{\boldsymbol{x}} = -\nabla V \tag{8.1}$$

([19]) To be distinguished from the more usual scattering operator S which is connected to the «observable» S_{fi} by $S_{fi} = (\Phi_f, S\Phi_i)$, where $\Phi_{i,f}$ are eigenstates of an «unperturbed» Hamiltonian. This usual S-operator does not exist in general, while S_Y always exists, see Sect. **11**.

can be written in integral form:

$$\boldsymbol{x}(t) = \boldsymbol{x}_0 + (t - t_0)\dot{\boldsymbol{x}}_0 - \int_{t_0}^{t} (t - t')(1/m)\nabla V(\boldsymbol{x}(t'))\,\mathrm{d}t' \,. \tag{8.1}$$

If the potential and the initial conditions are suitably restricted,

$$\lim_{|t|\to\infty} V(\boldsymbol{x}(t)) = \lim_{|t|\to\infty} \nabla V(\boldsymbol{x}(t)) = 0 \,, \tag{8.3}$$

we have the asymptotic forms with(constant vectors $\boldsymbol{x}_\pm$)

$$\lim_{t\to\pm\infty} [\boldsymbol{x}(t) - \boldsymbol{x}_\pm - t\dot{\boldsymbol{x}}(\pm\infty)] = 0 \,, \tag{8.4}$$

and this is the condition of asymptotic mechanics. Eq. (8.2) can then be written

$$\boldsymbol{x}(t) = \boldsymbol{x}_{\text{in}}(t) - \int_{-\infty}^{t} (t - t')(1/m)\nabla V(\boldsymbol{x}(t'))\,\mathrm{d}t' \,, \tag{8.5}$$

and

$$\boldsymbol{x}_{\text{out}}(t) = \boldsymbol{x}_{\text{in}}(t) - (t/m)\int_{-\infty}^{\infty} \nabla V(\boldsymbol{x}(t'))\,\mathrm{d}t' + \int_{-\infty}^{\infty} (t'/m)\nabla V(\boldsymbol{x}(t'))\,\mathrm{d}t' \,, \tag{8.6}$$

where $\boldsymbol{x}_{\text{in}}$ and $\boldsymbol{x}_{\text{out}}$ are defined for all times t in accordance with Eq. (8.4):

$$\underset{\text{in}}{\boldsymbol{x}_{\text{out}}}(t) = \boldsymbol{x}_\pm + t\dot{\boldsymbol{x}}(\pm\infty) \,. \tag{8.7}$$

Hence, the limit of the solution of Eq. (8.5) for $t \to +\infty$ provides $\boldsymbol{x}_{\text{out}}$ as a function of $\boldsymbol{x}_{\text{in}}$. Both of these functions satisfy the equations of free motion

$$\underset{\text{out}}{\ddot{\boldsymbol{x}}_{\text{in}}}(t) = 0 \,, \tag{8.8}$$

and the energy E can be written:

$$E = (m/2)[\dot{\boldsymbol{x}}(\pm\infty)]^2 \,, \tag{8.9}$$

or, if E is considered as a function of $\boldsymbol{x}$ and $\dot{\boldsymbol{x}}$,

$$\lim_{t\to\pm\infty} E(\boldsymbol{x}, \dot{\boldsymbol{x}}) = (m/2)\dot{\boldsymbol{x}}^2 \,. \tag{8.10}$$

9. – Wave-Mechanics, Non Relativistic Single Particle.

We consider the previous problem in wave-mechanics. Eqs. (8.1) and (8.2) are the equations of motion in differential and integral form; the dynamical variables are now Heisenberg operators.

In scattering processes, the Schrödinger wave function $\Psi(t)$ is, after a sufficiently long time, completely outside the range of a potential of limited range, i.e. ([20]),

$$\lim_{|t|\to\infty} (\Phi_n, V(0)\Psi(t)) = 0 , \tag{9.1}$$

and

$$\lim_{|t|\to\infty} (\Phi_n, \nabla V(0)\Psi(t)) = 0 , \tag{9.2}$$

where $V(0)$ and $\nabla V(0)$ are Schrödinger operators, and Φ_n is a bounded function, not necessarily normalizable, such as an eigenfunction of the momentum operators. Instead of Eqs. (9.1) and (9.2) we will write for brevity

$$\lim_{|t|\to\infty} V\Psi(t) = \lim_{|t|\to\infty} \nabla V\Psi(t) = 0 , \tag{9.3}$$

with the understanding that this equation may be used formally to form scalar products such as

$$\lim_{|t|\to\infty} (\Phi_n, V\Psi(t)) = 0 , \tag{9.4}$$

where $\Psi(t)$ is a solution of the Schrödinger equation, suitably restricted. We emphasize this symbolic meaning of our limit equations because the equation

$$\lim_{|t|\to\infty} \Psi(t) = 0 \tag{9.5}$$

is also correct for every point x, and for the same class of functions, but it does, of course not follow that

$$\lim_{|t|\to\infty} (\Phi_n, \Psi(t)) = 0 .$$

To avoid confusion, we will never use the limit $t \to \pm\infty$ in the sense of Eq. (9.5), and the Eq. (9.4) is implied in all equations which involve time-limits.

([20]) H. EKSTEIN: *Phys. Rev.*, **94**, 1063 (1954) and (EI).

Eq. (9.3) can also be written

$$\lim_{|t|\to\infty} V(t)\Psi(0) = \lim_{|t|\to\infty} \nabla V(t)\Psi(0) = 0\,, \tag{9.6}$$

where $V(t)$ and $\nabla V(t)$ are Heisenberg operators. The restrictions on $\Psi(0)$ necessary for the validity of Eq. (9.1) have been discussed previously ([20]): $\Psi(0)$ must be normalizable and contain no admixture of eigenstates of the discrete energy spectrum. Then only is the mechanics asymptotic.

In the following, it will be assumed that all operators act only on functions restricted in this sense, so that we write Eq. (9.4) simply

$$\lim_{|t|\to\infty} V(t) = \lim_{|t|\to\infty} \nabla V(t) = 0\,. \tag{9.7}$$

Under these conditions, Eqs. (8.4) to (8.8) of the classical theory may be considered as correct operator equations, following from Eqs. (8.1) to (8.3).

We have for all times t

$$H = (1/2m)\boldsymbol{p}^2(t) + V(t)\,, \tag{9.8}$$

but asymptotically

$$\lim_{t\to\pm\infty} [H(\boldsymbol{p}, \boldsymbol{q}) - (1/2m)\boldsymbol{p}^2(t)] = 0\,, \tag{9.9}$$

or, since H is time-independent, for all times

$$H = (1/2m)[\boldsymbol{p}(\infty)]^2 = (1/2m)[\boldsymbol{p}(-\infty)]^2\,, \tag{9.10}$$

in agreement with the classical equations (8.9) and 8.(10). The asymptotic commutability of the four momentum-energy operators, in accordance with Eq. (2.2) is an obvious consequence of Eq. (9.10). Hence, the Heisenberg operators $\pi_\mu(t)$ defined by Eq. (7.5), which merge asymptotically with $p_\mu^{(\pm)}$, may be chosen to be equal to the operators $\boldsymbol{p}(t)$, $iH(t)$, as was to be expected. Of course, an infinite number of other operators $\pi_\mu(t)$ exists.

Since both $\boldsymbol{x}_{\text{in}}(t)$ and $\boldsymbol{x}_{\text{out}}(t)$ satisfy the equations of free motion (8.8), and since their commutators with their time derivatives are the same, they can differ only by a unitary time-independent transformation which will presently be identified with S_F:

$$\boldsymbol{x}_{\text{out}}(t) = S_F^{-1}\boldsymbol{x}_{\text{in}}S_F\,, \tag{9.11}$$

and, since, by Eq. (8.7)

$$\dot{\boldsymbol{x}}_{\substack{\text{out}\\\text{in}}} = \dot{\boldsymbol{x}}(\pm\infty)\,, \tag{9.12}$$

it follows that

$$\boldsymbol{p}(\infty) = S_r^{-1}\boldsymbol{p}(-\infty)S_r\,, \tag{9.13}$$

in agreement with Eq. (7.6). In order to interpret the operator S_r in terms of the Schrödinger formalism, consider, for simplicity, that $V(t)\Psi(0)$ vanishes beyond a long time $\pm T$. At the time $t = T$, we have

$$\Psi(T) = \exp[-iHT]\Psi(0)\,, \tag{9.14}$$

and for $t > T$,

$$\Psi(t) = \exp[-iW(t-T)]\exp[-iHT]\Psi(0)\,, \tag{9.15}$$

where W is the operator of the kinetic energy. Since at all times

$$\Psi(t) = \exp[-iHT]\Psi(0)\,, \tag{9.16}$$

we may write, dropping the unnecessary additional restriction,

$$\lim_{t\to\pm\infty}\left(\exp[-iHt] - \exp[-iWt]\lim_{\tau\to\pm\infty}\exp[iW\tau]\exp[-iH\tau]\right) = 0\,. \tag{9.17}$$

We define length-preserving operators [21]

$$\lim_{\tau\to\pm\infty}\exp[iH\tau]\exp[-iW\tau] = \Omega_{\mp}\,, \tag{9.18}$$

and we can write for the asymptotic form of $\boldsymbol{x}(t)$

$$\boldsymbol{x}(t) = \exp[iHt]\boldsymbol{x}(0)\exp[-iHt] \to \Omega_{\mp}\boldsymbol{x}^{(0)}(t)\Omega_{\mp}^{\dagger}\,,$$

or, more precisely,

$$\lim_{t\to\pm\infty}[\boldsymbol{x}(t) - \Omega_{\mp}\boldsymbol{x}^{0}(t)\Omega_{\mp}^{\dagger}] = 0\,, \tag{9.19}$$

[21] This operator is more often considered to be not-length-preserving. (See reference [9], contrary to reference [20]). The difference is in the definition and not in the substance. One can consider $\Omega_{\mp}^{\dagger}$ as that operator which carries the interaction state vector $\Phi(0)$ into $\Phi(\pm\infty)$, as in reference [20]. Then, Ω exists only if $\Phi(\pm\infty)$ exists; the domain and range (i.e. the Hilbert space of state vectors) must be restricted, and Ω is length-preserving. On the other hand, one can define a sequence of operators $U_\varepsilon(t)$ which carry $\Phi(0)$ into $\Phi(t)$ *in the limit* $\varepsilon=0$, but defined so that $U_\varepsilon(\infty)$ exists without restrictions on the domain, as in reference [9]. Then, $\Omega_{\pm}$ is defined as $\lim_{\varepsilon\to 0} U_\varepsilon(\infty)$, and it may exist without restriction, but it is then in general not length-preserving. In the present context, the existence of actual limits rather than of substitute limits is a defining criterion, and this is why we have chosen the first definition.

where

$$\boldsymbol{x}^0(t) = \exp[iWt]\boldsymbol{x}(0)\exp[-iWt] \tag{9.20}$$

is the operator $\boldsymbol{x}(t)$ in interaction representation. Evidently, $\boldsymbol{x}^0(t)$ satisfies the equations of free motion

$$i\dot{\boldsymbol{x}}^0(t) = [\boldsymbol{x}^0(t), W], \tag{9.21}$$

or

$$m\ddot{\boldsymbol{x}}^0 = 0, \tag{9.22}$$

i.e., the same equations as $\boldsymbol{x}_{\substack{\text{in}\\\text{out}}}(t)$. Since $\boldsymbol{x}_{\substack{\text{in}\\\text{out}}}$ are, by definition, those solutions of Eq. (9.22) which tend asymptotically toward $\boldsymbol{x}(t)$, we have identified:

$$\boldsymbol{x}_{\substack{\text{out}\\\text{in}}}(t) = \Omega_{\mp}\boldsymbol{x}^0(t)\Omega_{\mp}^{\dagger}, \tag{9.23}$$

and by eliminating $\boldsymbol{x}^0(t)$ from these two equations,

$$\boldsymbol{x}_{\text{out}}(t) = \Omega_{-}\Omega_{+}^{\dagger}\boldsymbol{x}_{\text{in}}(t)\Omega_{+}\Omega_{-}^{\dagger}, \tag{9.24}$$

so that the scattering operator S_F is identified:

$$S_F = \Omega_{+}\Omega_{-}^{\dagger}. \tag{9.25}$$

From Eq. (9.24) ,one obtains by differentiation

$$\boldsymbol{p}(\pm\infty) = \Omega_{\mp}\boldsymbol{p}(0)\Omega_{\mp}^{\dagger}. \tag{9.26}$$

If Φ_n is a set of simultaneous eigenfunctions of $p_j(0)$ ($j = 1$ to 3), then by Eq. (9.26),

$$\psi_n^{(\pm)} = \Omega_{\pm}\Phi_n \tag{9.27}$$

is a set of simultaneous eigenfunctions of $p_j(\pm\infty)$. Hence, the S-matrix is

$$S_{fi} = (\psi_f^{(+)}, \Omega_{+}\Omega_{-}^{\dagger}\psi_i^{(+)}) = (\Phi_f, \Omega_{-}^{\dagger}\Omega_i\Phi_i) = (\Phi_f, S\Phi_i), \tag{9.28}$$

where

$$S = \Omega_{-}^{\dagger}\Omega_{+}, \tag{9.29}$$

in agreement with GELL-MANN and GOLDBERGER [9]. Thus, it has been shown that the principle stated in Sect. 2 leads to the usual statement of the scat-

tering problem. The functions $\psi_n^{(\pm)}$ are, in previous papers, defined by

$$\psi_n^{(\pm)} = \Omega_\pm \Phi_n = \lim_{t \to \mp\infty} \exp[iHt] \exp[-iWt] \Phi_n , \tag{9.30}$$

or by [9]

$$\psi_n^{(\pm)} = \Phi_n - (H - E_n \mp i\varepsilon)^{-1} V \Phi_n , \tag{9.31}$$

which follows from Eq. (9.30), or by asymptotic boundary conditions (out- and ingoing waves) imposed upon the time-independent Schrödinger equation in co-ordinate representation. Neither of these definitions is sufficiently general to include field theory; the first two, because the division of the Hamiltonian into an unperturbed operator H_0 and a proper scattering potential V which satisfies Eq. (9.7), becomes impossible; the third, because the concept of configuration space becomes useless in field theory. The definition of $\psi_n^{(\mp)}$ as simultaneous eigenfunctions of the operators $A_r^{(\pm)\dagger}(\boldsymbol{k}) k_\mu A_r^{(\pm)}(\boldsymbol{k})$ which are the analogues of $p_\mu^{(\pm)}$ for many particles, is general.

For the purpose of comparison with Eq. (7.5) where only Heisenberg operators appear, it is important to notice that both $\underset{\text{out}}{\boldsymbol{x}_{\text{in}}}(t)$ and $\underset{\text{out}}{\boldsymbol{p}_{\text{in}}}$ are rigorous Heisenberg operators at all times t, i.e., they satisfy the equation of motion

$$i \dot{\underset{\text{out}}{\boldsymbol{x}_{\text{in}}}}(t) = [\underset{\text{out}}{\boldsymbol{x}_{\text{in}}}, H] , \tag{9.32}$$

while $\boldsymbol{x}^0(t)$, the interaction operator, does not. For $\underset{\text{in}}{\boldsymbol{x}_{\text{in}}}(t)$, this can be seen most easily from Eq. (8.5). Since the second term on the right hand side is a particular solution of the equations of motion, it satisfies naturally the Heisenberg equations $i\dot{A} = [A, H]$, and since $\boldsymbol{x}(t)$ does so by definition, it is clear that their difference $\underset{\text{in}}{\boldsymbol{x}_{\text{in}}}(t)$ does also. The proof for $\underset{\text{out}}{\boldsymbol{x}_{\text{out}}}(t)$ is analogous. Hence, there exist two sets of 6 operators, $\underset{\text{out}}{\boldsymbol{x}_{\text{in}}}(t)$, $\underset{\text{out}}{\boldsymbol{p}_{\text{in}}}$ in terms of which the scattering problem has precisely the aspect of a free particle problem:

$$\ddot{\underset{\text{in}}{\boldsymbol{x}_{\text{out}}}} = 0 , \qquad \underset{\text{in}}{\boldsymbol{p}_{\text{out}}} = \text{const} .$$

with the usual simple commutation relations. The only difference is that $\underset{\text{in}}{\boldsymbol{p}_{\text{out}}}$ are not the momentum operators for finite times.

The results of this section apply, of course, to the scattering of two free particles in the center of mass system. Furthermore, they can be generalized to describe any number of different particles which are initially and finally infinitely distant from each other; this is the case considered by BELINFANTE and MØLLER [22].

[22] F. J. BELINFANTE and C. MØLLER: *Danske Videnskab. Selskab*, **28**, No. 6 (1954).

10. Many Particles, Scattered by an External Potential.

We discuss next a trivial generalization of Sect. 9 where many particles are scattered by the potential V, but where they do not interact. The purpose is only to introduce the formalism of second quantization in the simplest case where many complications do not yet arise.

We use throughout as variables the creation and destruction Heisenberg operators $a^\dagger(\boldsymbol{k}t)$, $a(\boldsymbol{k}t)$ in momentum representation. Of course, these operators do not have the simple relationship to the positive and negative frequency parts of the field operators as the corresponding operators in interaction representation ([23]). While this choice destroys the manifest covariance of the equations in the relativistic case, it allows a uniform notation for Fermi- and Bose-particles, while the more usual field operators require different Green's functions. Furthermore, the use of k-space avoids the necessity of a more stringent definition of convergence than Eq. (9.4) which would be inevitable if we used x-space ([12]).

The Hamiltonian is

$$H = H_0 + H_1 = \int a^\dagger(\boldsymbol{k}) E(\boldsymbol{k}) a(\boldsymbol{k}) \, \mathrm{d}\boldsymbol{k} + \int a^\dagger(\boldsymbol{k}) V(\boldsymbol{k} \quad \boldsymbol{k}') a(\boldsymbol{k}') \, \mathrm{d}\boldsymbol{k} \, \mathrm{d}\boldsymbol{k}' , \tag{10.1}$$

where $a^\dagger$, a are the usual creation and destruction operators for either Bose of Fermi particles.

Under the same conditions as in Sect. 9,

$$\lim_{|t| \to \infty} H_1(t) = 0 . \tag{10.2}$$

The equations of motion are

$$i\dot{a}(\boldsymbol{k}t) - E(\boldsymbol{k}) a(\boldsymbol{k}t) = \int V(\boldsymbol{k} - \boldsymbol{k}') a(\boldsymbol{k}'t) \, \mathrm{d}\boldsymbol{k}' , \tag{10.3}$$

where V is now a c-number. Since the right-hand side vanishes asymptotically, Eq. (10.3) can be written as an integral equation

$$a(\boldsymbol{k}t) = a_{\mathrm{in}}(\boldsymbol{k}t) - i \int_{-\infty}^{t} \int \exp[-iE(\boldsymbol{k})(t - t')] V(\boldsymbol{k} - \boldsymbol{k}') a(\boldsymbol{k}'t') \, \mathrm{d}t' \, \mathrm{d}\boldsymbol{k}' , \tag{10.4}$$

where a_{in} is that solution of the homogeneous equation which becomes asymptotically ($t \to -\infty$) equal to a. For large positive values of t,

$$a_{\mathrm{out}}(\boldsymbol{k}t) = a_{\mathrm{in}}(\boldsymbol{k}t) - i \int_{-\infty}^{\infty} \int \exp[-iE(\boldsymbol{k})(t - t')] V(\boldsymbol{k} - \boldsymbol{k}') a(\boldsymbol{k}'t') \, \mathrm{d}t' \, \mathrm{d}\boldsymbol{k}' . \tag{10.5}$$

([23]) E.g., E. Freese: *Zeits. f. Naturf.*, **8a**, 776 (1953).

Eqs. (10.4) and (10.5) are the equations of Yang and Feldman for the simplest case ([10]).

The operator a in the interaction representation is

$$a^0(t) = \exp[iH_0t]a(0)\exp[-iH_0t]\,. \tag{10.6}$$

By the same reasoning as in Sect. 9, we conclude

$$\lim_{t\to\pm\infty}[a(t) - \Omega_{\mp}a^0(t)\Omega_{\mp}^{\dagger}] = 0\,, \tag{10.7}$$

where Ω is defined by Eq. (9.18), with W replaced by H_0. The homogeneous equation corresponding to Eq. (10.3)

$$i\dot{a}_{\substack{\text{in}\\\text{out}}} - Ea_{\substack{\text{in}\\\text{out}}} = 0\,, \tag{10.8}$$

of which $a_{\substack{\text{in}\\\text{out}}}$ are solutions, is linear, so that its solutions must be related by a time-independent unitary transformation. Since $a^0(t)$ is such a solution, we have identified, in agreement with previous results ([23,24]):

$$a_{\substack{\text{in}\\\text{out}}}(t) = \Omega_{\pm}a^0(t)\Omega_{\pm}^{\dagger}\,. \tag{10.9}$$

Since $a_{\substack{\text{in}\\\text{out}}}$ are solutions of the linear Eq. (10.8), they are both of the form

$$a_{\substack{\text{in}\\\text{out}}}(\boldsymbol{k}t) = a_{\substack{\text{in}\\\text{out}}}(\boldsymbol{k}0)\exp[-iE(\boldsymbol{k})t]\,, \tag{10.10}$$

so that the products $a^{\dagger}_{\substack{\text{in}\\\text{out}}}(\boldsymbol{k}t)a_{\substack{\text{in}\\\text{out}}}(\boldsymbol{k}t)$ are time-independent. Since at all times the total momentum $\boldsymbol{P}$ is ([1])

$$\boldsymbol{P} = \int a^{\dagger}(\boldsymbol{k}t)\boldsymbol{k}a(\boldsymbol{k}t)\,\mathrm{d}\boldsymbol{k}\,, \tag{10.11}$$

and since, by Eqs. (10.7) and (10.9), the operator $a(\boldsymbol{k}t)$ is asymptotically equal to $a_{\substack{\text{in}\\\text{out}}}(\boldsymbol{k}t)$, it follows that

$$\lim_{t\to\pm\infty}\boldsymbol{P}(t) = \int a^{\dagger}_{\substack{\text{out}\\\text{in}}}(\boldsymbol{k}t)\boldsymbol{k}\,a^{\dagger}_{\substack{\text{out}\\\text{in}}}(\boldsymbol{k}t)\,\mathrm{d}\boldsymbol{k}\,. \tag{10.12}$$

For the same reason, and in view of Eq. (10.2),

$$\lim_{t\to\pm\infty}H = \int a^{\dagger}_{\substack{\text{out}\\\text{in}}}(\boldsymbol{k}t)E(\boldsymbol{k})\,a^{\dagger}_{\substack{\text{out}\\\text{in}}}(\boldsymbol{k}t)\,\mathrm{d}\boldsymbol{k}\,. \tag{10.13}$$

([24]) H. Kita: *Prog. Theor. Phys.*, **10**, 231 (1953).

Naturally, the limit in Eq. (10.13) may be omitted, since the Hamiltonian is time-independent in the present case. Since both for Fermi and Bose statistics $a^\dagger(\boldsymbol{k})a(\boldsymbol{k})$ commutes with the same product at all points $\boldsymbol{k}'$, the same is true for the $a^\dagger_{\substack{\text{in}\\\text{out}}}(\boldsymbol{k}t)a_{\substack{\text{in}\\\text{out}}}(\boldsymbol{k}t)$ which are obtained from the former by unitary transformation. Hence, the integrands in Eqs. (10.12) and (10.13) commute with each other, and the condition of asymptotic freedom (Eq. (2.2)) is satisfied if we set

$$A^{(\pm)}(\boldsymbol{k}) = a_{\substack{\text{out}\\\text{in}}}(\boldsymbol{k}0)\,. \tag{10.14}$$

Consider a set of basis functions Φ_n which are simultaneous eigenfunctions of all operators $a^\dagger(\boldsymbol{k}0)\boldsymbol{k}a(\boldsymbol{k}0)$; they are the usual eigenfunctions of H_0 in occupation number representation. From Eqs. (10.9) and (10.14), we have

$$A^{(\mp)\dagger}(\boldsymbol{k})k_\nu A^{(\mp)}(\boldsymbol{k}) = \Omega_\pm a^\dagger(\boldsymbol{k}0)k_\nu a(\boldsymbol{k}0)\Omega^\dagger_\pm\,. \tag{10.15}$$

Hence, a system of simultaneous eigenfunctions of all operators defined by Eq. (10.15) is constructed by

$$\psi_n^{(\pm)} = \Omega_\pm \Phi_n\,, \tag{10.16}$$

and the S-matrix is again

$$S_{nm} = (\psi_n^{(-)}, \psi_m^{(+)}) = (\Phi_n, \Omega^\dagger_- \Omega_+ \Phi_m)\,, \tag{10.17}$$

as in Sect. 9. Hence, the principle stated in Sect. 2 leads again to the known formulation of the scattering problem. We note again that $a_{\substack{\text{in}\\\text{out}}}(t)$ are Heisenberg operators ([21]) which satisfy the same simple equations of motion and commutation relations as the interaction operators $a^0(t)$; only the momentum is not expressed through them in a simple way for finite times.

11. Nonrelativistic Particles with Multi-Channel Scattering.

We consider M kinds of elementary particles which interact through potentials of limited range. The Hamiltonian is ([25])

$$H = H_0 + H_1\,, \tag{11.1}$$

where

$$H_0 = \sum_r^M \int a_r^\dagger(\boldsymbol{k})\,E_r(\boldsymbol{k})\,a_r(\boldsymbol{k})\,\mathrm{d}\boldsymbol{k}\,, \tag{11.2}$$

([25]) H. A. KRAMERS: *Die Grundlagen der Quantentheorie* (Leipzig, 1938).

and

$$H_{\mathrm{I}} = \frac{1}{2} \sum_{r,r'=1}^{M} \int a_r^{\dagger}(\boldsymbol{k}) a_{r'}^{\dagger}(\boldsymbol{k}) V_{rr'}(\boldsymbol{k}\boldsymbol{k}') a_r(\boldsymbol{k}') a_{r'}(\boldsymbol{k}') \, \mathrm{d}\boldsymbol{k} \, \mathrm{d}\boldsymbol{k}' + \ldots \,. \tag{11.3}$$

The omitted terms may contain expressions of degree higher than 4 in the destruction and creation operators, which describe many-body forces of limited range. The operators $a_r^{\dagger}(k)$, $a_r(k)$ satisfy the usual commutation or anti-commutation relations.

We consider only systems without external force. In this case, the restriction on the class of state vectors must be modified by excluding admixtures of eigenstates of the Hamiltonian belonging to the discrete energy spectrum *in the center of mass system*. Then, the mechanics is asymptotic, and the results obtained in (EI) are valid.

In presence of composite particles, the interaction $H_{\mathrm{I}}(t)$ never ceases to be effective; it does not vanish asymptotically. Similarly, the non linear terms in the equations of motion do not vanish asymptotically. Hence, the Heisenberg operators $a_r(\boldsymbol{k}t)$ do not have simple asymptotic forms, and bilinear forms $a_r^{\dagger}(\boldsymbol{k}t) a_r(\boldsymbol{k}t)$ have no asymptotic limits. Any attempt to introduce substitute limits (e.g., Abel's limit) into the equations of motion would remove the composite particles and thereby defeat the purpose ([26]). We shall show, nevertheless, that two sets of operators $A_r^{(\pm)}(\boldsymbol{k})$ can be found, in terms of which the energy-momentum vector P_μ is expressed by Eq. (2.9) and which satisfy the usual commutation or anticommutation relations

$$[A_r^{(\pm)}(\boldsymbol{k}), A_{r'}^{(\pm)\dagger}(\boldsymbol{k}')]_{\pm} = \delta(\boldsymbol{k} - \boldsymbol{k}') \delta_{rr'} \,, \tag{11.4}$$

where the $\pm$ sign applies to Fermi-particles with $r = r'$. The number N of operators $A_r^{(\pm)}$ is the number of all possible stable composite and elementary particles so that $N > M$. Since there exists no simple relationship between $A_r^{(\pm)}$ and the elementary particle operators a_r, we shall define a set of operators by their action on a complete set of state vectors, and show that they have all the properties required of the $A_r^{(\pm)}$.

In (EI), two sets of eigenfunctions of H, $\psi_n^{(\pm)}$, were defined which describe scattering of any number of elementary or composite particles, with outgoing or incoming waves respectively. In configuration space, these functions are asymptotically equal to the corresponding basis functions Φ_n which are sym-

([26]) Note the difference between states belonging to the discrete energy spectrum in the center of mass system (bound states) and the existence of stable composite particles among the incident or scattered particles. KITA ([21]) has discussed the possibility of taking the former into account, even if Abel's limit is used in the equations of motion.

metrized or anti-symmetrized products of fundamental solutions; these, in turn, are eigenfunctions of «truncated Hamiltonians» which describe an elementary or composite particle with a definite total momentum. The basis functions Φ_n describe physical, but not interacting particles (elementary or composite). They are, of course, not eigenfunctions of H. The basis functions Φ_n form a redundant (i.e., linearly non-independent) and non-orthogonal set. Nevertheless, it was shown in (EI) that the eigenfunctions $\psi_n^{(\pm)}$ which have a one-to-one correspondence to the Φ_n, form each an orthogonal set. If the physical one-particle states themselves are included in the sets $\psi_n^{(+)}$, they may be presumed to be complete sets. A function $\psi_n^{(\pm)}$ is labeled by the species and momentum of the particles (elementary or composite) in the entrance channel, i.e., the subscript n stands for $(\boldsymbol{k}_1 r_1, \boldsymbol{k}_2 r_2, \ldots)$ where the number of particles, elementary and composite, is unrestricted, and the number of different labels r_i may be less than, but cannot exceed N. We can then define time-independent creation and destruction operators $A_r^{(\pm)\dagger}(\boldsymbol{k})$ of the usual kind which, when acting on the vacuum, create the states $\psi_{\boldsymbol{k}r}^{(\mp)}$. Clearly, the functions $\psi_n^{(\mp)}$ are simultaneous eigenfunctions of all operators $A_r^{(-)\dagger}(\boldsymbol{k}) k_{r\mu} A_r^{(\mp)}(\boldsymbol{k})$. Since the functions $\psi_n^{(\pm)}$ are, by definition, eigenfunctions of the total Hamiltonian with eigenvalues $E_{r1}(\boldsymbol{k}_1)+E_{r2}(\boldsymbol{k}_2)+\ldots$, the fourth equation (2.9) ($\mu = 4$) is clearly satisfied by the present choice of operators.

It will now be shown that the basis functions Φ_n are eigenfunctions of the total momentum operators $\boldsymbol{P}$ ($\mu = 1, 2, 3$). Consider first a basis vector $\Phi_{\boldsymbol{k}_1 r_1, \boldsymbol{k}_2 r_2}$ which describes two composite particles r_1 and r_2 with momenta $\boldsymbol{k}_1$ and $\boldsymbol{k}_2$. In a representation in which the momenta $\boldsymbol{p}_i$ of the elementary particles are diagonal, Φ_n is of the form

$$(11.5) \qquad \Phi_{\boldsymbol{k}_1 r_1, \boldsymbol{k}_2 r_2} = \delta\Big(\sum_1^{n_1} \boldsymbol{p}_i - \boldsymbol{k}_1\Big)\varphi_1(\boldsymbol{p}_1 \ldots \boldsymbol{p}_{n_1}) \cdot \delta\Big(\sum_{n_1+1} \boldsymbol{p}_i - \boldsymbol{k}_2\Big)\varphi_2(\boldsymbol{p}_{n_1+1} \ldots \boldsymbol{p}_{n_2}),$$

if all elementary particles 1 to n_2 are distinguishable. The operator $\boldsymbol{P} = \sum_1^{n_2} \boldsymbol{p}_i$ multiplies Φ_n by $(\boldsymbol{k}_1 + \boldsymbol{k}_2)$, and it is clear that Φ_n is an eigenfunction of $\boldsymbol{P}_j$ with eigenvalue $(\boldsymbol{k}_{1j} + \boldsymbol{k}_{2j})$ ($j = 1, 2, 3$). If some of the elementary particles are identical, Φ_n is a sum of terms of the form (11.5), but it is still an eigenfunction of $\boldsymbol{P}$, and the same is evidently true for any number of particles described by Φ_n.

The connection between the basis vectors Φ_n and the $\psi_n^{(\pm)}$ is given by Eq. (4.1). Since in absence of external forces, $\boldsymbol{P}$ commutes with H, $\psi_n^{(\mp)}$ is also an eigenfunction of $\boldsymbol{P}$ with the same eigenvalues $\sum \boldsymbol{k}_i$. Hence, the first three equations (2.9) are also satisfied by the present choice for the operator $A_r^{(-)}$.

Hence, the scattering problem is reduced to the determination of the functions $\psi_n^{(\pm)}$ from which, by Eq. (2.12), the S-matrix can be obtained. Since it was shown in (EI) that these functions are the scattering states of the usual

time-independent theory, the present statement of the scattering problem is again equivalent to the usual formulation.

Is it possible to find real-particle Heisenberg operators $A_r(\boldsymbol{kt})$ which merge asymptotically with $A_r^{(\pm)}(\boldsymbol{kt})$ in accordance with Eq. (7.1), as in the simpler cases? Certainly, the operators A_r cannot be identified with the a_r which describe the elementary particles; most obviously, because the number of operators $A_r^{(\pm)}$ is N, while that of the a_r is only M. This difference also makes it obvious that there can be no canonical transformation, and, indeed, no linear transformation, which carries the a_r's into the $A_r^{(\pm)}$'s. However, one could define creation-and-destruction operators which act in the usual manner on the labels of the basis functions Φ_n, as the operators $A^{(\pm)}$ act on the labels of the functions $\psi_n^{(\pm)}$. But since the Φ_n are non-orthogonal and not linearly independent, the commutation relations would be awkward; this is clearly a consequence of the fact that the Φ_n describe composite particles with a finite extension.

While, as was shown in (EI), no linear operator S exists in the general case, there exists undoubtedly a unitary transformation S_r which carries the operator $A_r^{(-)}$ into the operator $A_r^{(+)}$, since both sets satisfy the same linear equations of motion, the same simple commutation relations and both act on the same vacuum state Ψ_0. This is in agreement with the previous statement to the effect that Yang and Feldman's scattering operator S_r exists where S does not.

12. – Bose-Field with Constant c-Number Sources.

This case is physically well understood ([27,28]). Since the sources have no degree of freedom, they are not influenced by an incident wave, and there is no scattering; the scattering operator should be the unit operator. However, the conventional definition of the S-operator does not give this simple result, unless it is supplemented by an adiabatic switching-on and-off of the sources ([28]).

It should be noted that this case is different from those previously considered. In the older literature, the artificial adiabatic process was used in the description of the simplest scattering problem only because the initial state was taken to be non normalizable. FRIEDRICHS ([29]) noticed that this artifice was unnecessary if wave packets were used correctly, and this view

([27]) R. J. GLAUBER: *Phys. Rev.*, **84**, 395 (1951).

([28]) K. O. FRIEDRICHS: *Mathematical Aspects of the Quantum Theory of Fields* (New York, 1953), particularly pp. 100, 110.

([29]) K. O. FRIEDRICHS: *Comm. on Pure and Appl. Math.*, **1**, 361 (1948).

was supported recently by HACK and MOSES ([30]). In the present case, on the contrary, the S-operator as usually defined, does not exist, and the use of the artificial substitute limit is indispensable ([28]).

The new definition of the S-operator proposed here leads directly to the obvious result, without any substitute limit.

The equation of motion for the Bose field operator φ is

$$(\Box - \mu^2)\varphi = -j\,, \tag{12.1}$$

where j is a real, constant c-number function of limited range. If destruction operators $a(\boldsymbol{k})$ are defined as usual ([1]), then the corresponding Heisenberg operators $a(\boldsymbol{k}t)$ satisfy the equations of motion

$$i\dot{a} - \omega a = -(2\omega)^{-\frac{1}{2}} j^*(\boldsymbol{k})\,, \tag{12.2}$$

where $j(\boldsymbol{k})$ is the Fourier transform of $j(\boldsymbol{x})$ and $\omega = (k^2 + \mu^2)^{\frac{1}{2}}$.

The four energy-momentum operators are ([1])

$$P_j(t) = \int a^\dagger(\boldsymbol{k}t)\, k_j\, a(\boldsymbol{k}t)\, \mathrm{d}\boldsymbol{k}\,, \qquad (j = 1, 2, 3)$$

$$-P_0 = \int a^\dagger(\boldsymbol{k})\,\omega(\boldsymbol{k})\, a(\boldsymbol{k})\, \mathrm{d}\boldsymbol{k} - \int [2\omega]^{-\frac{1}{2}} [a^\dagger(\boldsymbol{k}) + a(\boldsymbol{k})] j(\boldsymbol{k})\, \mathrm{d}\boldsymbol{k}\,. \tag{12.3}$$

If we define operators b by

$$b(\boldsymbol{k}) = a(\boldsymbol{k}) - [2\omega]^{-\frac{1}{2}} j^*(\boldsymbol{k})\,, \tag{12.4}$$

then the equations of motion are

$$i\dot{b} - \omega b = 0\,, \tag{12.5}$$

while the commutation relations are unchanged:

$$[b(\boldsymbol{k}t),\, b^\dagger(\boldsymbol{k}'t)] = \delta(\boldsymbol{k} - \boldsymbol{k}')\,. \tag{12.6}$$

The solution of Eq. (7.5) is

$$b(t) = \exp[-i\omega t] b(0)\,, \tag{12.7}$$

and the operators P_μ in terms of b become

$$-P_0 = \int b^\dagger(\boldsymbol{k}t)\,\omega\, b(\boldsymbol{k}t)\, \mathrm{d}\boldsymbol{k}\,, \tag{12.8}$$

([30]) M. N. HACK: *Phys. Rev.* **96**, 196 (1954), H. E. MOSES: *Nuovo Cimento*, **1**, 104 (1955).

$$(12.9)\quad P_j(t) = \int b^{\dagger}(\boldsymbol{k}t)k_j b(\boldsymbol{k}t)\,\mathrm{d}\boldsymbol{k} + \int \exp[-i\omega t]k_j b^{\dagger}(\boldsymbol{k}0)[2\omega]^{-\frac{3}{2}}j^*(\boldsymbol{k})\,\mathrm{d}\boldsymbol{k} + \int \exp[i\omega t]k_j b(\boldsymbol{k}0)[2\omega]^{-\frac{3}{2}}j(\boldsymbol{k})\,\mathrm{d}\boldsymbol{k} + \int [2\omega]^{-3}j^*(\boldsymbol{k})k_j j(\boldsymbol{k})\,\mathrm{d}\boldsymbol{k}\,. \qquad (j = 1 \text{ to } 3).$$

We can choose the representation in which the operators b, $b^{\dagger}$ are the matrices which usually represent a, $a^{\dagger}$. Then it can be shown by using the asymptotic vanishing of Fourier integrals, ([28]), that the second and third integrals in Eq. (12.9) tend to zero for $|t| \to \infty$. The fourth integral vanishes because $j^*(\boldsymbol{k}) = j(-\boldsymbol{k})$ for the Fourier transform of the real function $j(\boldsymbol{x})$, and because the integrand is therefore an odd function. Hence, we have

$$(12.10)\quad \lim_{|t|\to\infty} P_j = \int b^{\dagger}(\boldsymbol{k}t)k_j b(\boldsymbol{k}t)\,\mathrm{d}\boldsymbol{k}\,.$$

Hence, the operators b satisfy all the requirements imposed on the operators $A^{(\pm)}$. Furthermore, since b_{in} is evidently equal to b_{out} by Eq. (7.7), the operator S_r exists and is just the unit operator.

Thus, the new statement of the scattering problem leads here to the physically correct result without artificial limiting process, which, in the conventional formulation, is indispensable even if one uses wave packets correctly.

13. – Field Theory without Composite Particles.

When no composite particles exist, the number of asymptotic particle operators $A_r^{(\pm)}$ is the same as that of the bare particle operators a_r, in terms of which the problem is initially stated. In this particular case, a linear transformation between the bare-particle operators a_r and the asymptotic particle operators $A_r^{(\pm)}$ is at least not excluded at the outset, and one may expect that a simple relationship exists between the a_r and a physically meaningful real particle operator A_r which merges asymptotically with $A_r^{(\pm)}$ in the sense of Eq. (7.1). We say a meaningful operator, since there are infinitely many operator functions (not Heisenberg operators) which satisfy this equation. This is the formal expression of the physical circumstance that « real particles » in field theory have no precise definition; the only precise definition can be given when the real particles do not interact; the real particles are then defined by the operators $A_r^{(\pm)}$, but any operator A which asymptotically merges with $A_r^{(\pm)}$ may be considered as a correct description of real particles.

The Heisenberg operators a_r in terms of which a theory is initially formulated, satisfy equations of motion of the type

$$i\dot{a}_r(\boldsymbol{k}t) - E_r^{(0)}(\boldsymbol{k})a_r(\boldsymbol{k}t) = N_r(\boldsymbol{k}t)\,, \tag{13.1}$$

where

$$(E_r^{(0)}(\boldsymbol{k}))^2 = m_r^{(0)2} + k^2\,, \tag{13.2}$$

with the mechanical masses $m_r^{(0)}$, as distinguished from the observed masses m_r which, in our scheme, define the energies E_r in the equations of motion of the $A^{(\pm)}$, according to Eq. (2.13). In Eq. (13.2), N_r is a non linear function of the operators a_s. In order to construct operators A_r one begins by adding linear terms on both sides of Eq. (13.2) so as to make the left-hand side of this equation equal to that of Eq. (2.13). The equations of motion appear then in the renormalized form

$$i\dot{a}_r(\boldsymbol{k}t) - E_r(\boldsymbol{k})a_r(\boldsymbol{k}t) = N_r'(\boldsymbol{k}t)\,. \tag{13.3}$$

The expression N_r' now contains also linear terms with unknown coefficients, since the relationship between the observed and the unrenormalized constants is not known at the outset.

As a next step, one writes Eq. (13.3) in integral form,

$$a_r(\boldsymbol{k}t) = a_r^0 + \frac{1}{i}\int_{t_0}^{t} \exp[-iE_r(\boldsymbol{k})(t-t')]\,N_r'(\boldsymbol{k}t')\,\mathrm{d}t'\,, \tag{13.4}$$

where a_r^0 is a solution of the homogeneous equation. If the integration limit could be extended to $-\infty$, then a_r^0 could be identified with $A_r^{(-)}$ as in Sect. **10**. However, the integrand in Eq. (13.4) does not vanish asymptotically ([31]), so that another step is necessary: as a substitute for the non-existent limit $t_0 \to -\infty$ of the integral, one uses Abel's limit, thereby defining a new operator a_r':

$$a_r'(\boldsymbol{k}t) = a_{r\,\mathrm{in}}'(\boldsymbol{k}t) + \left(\frac{1}{i}\right)\lim_{\varepsilon\to 0}\int_{-\infty}^{t} \exp[\varepsilon t']\exp[-iE_r(\boldsymbol{k})(t-t')]\,N_r'(\boldsymbol{k}t')\,\mathrm{d}t'\,. \tag{13.5}$$

If renormalization constants can be so chosen that Eq. (13.5) has solutions, then the asymptotic forms $a_{r\,\mathrm{out,\,in}}'$ which satisfy

$$\lim_{t\to\pm\infty}[a_r'(\boldsymbol{k}t) - a_{r\,\substack{\mathrm{out}\\ \mathrm{in}}}(\boldsymbol{k}t)] = 0 \tag{13.6}$$

may be identified with $A_r^{(\pm)}(kt)$ as in Sect. **10**. The question of the existence of such renormalization constants has been investigated most thoroughly in

([31]) G. KÄLLÉN: *Physica*, **19**, 850 (1953).

perturbation theory. YANG and FELDMAN ([10]) have shown that the solution of Eq. (10.5) by iteration leads to Dyson's expansion of the S-matrix ([32]) and the non-perturbation approach has been investigated for electrodynamics by KÄLLÉN ([31]). It is well known that, while the existence of finite renormalization constants is doubtful, the use of infinite constants leads to practically satisfactory results for one class of theories which are called renormalizable.

We have shown that the present statement of the scattering problem leads to the usual result, in the usual conditional sense. The necessity for both renormalization and the use of the adiabatic switching-on stems directly from prime principles rather than from divergent integrals if one wants to construct an operator A_r by analogy to the simplest case.

It is true that only mass-and not charge renormalization appears as logically indispensable, regardless of divergences. This is presumably due to a too narrow formulation of the principle of asymptotic mechanics. In fact, free particles are also recognizable by a constant and mutually independent charge, so that an asymptotic condition for the charge operator, similar to Eq. (2.8) should be added.

From the present viewpoint, there is nothing surprising in the fact that only some theories are renormalizable, since the technique of constructing A_r in analogy to Sect. **10** is not the only conceivable one. Certainly, the impossibility of using it in a given case does not exclude the existence of the operators $A_r^{(\pm)}$ and of the S-matrix.

While we have avoided the use of artificial limiting processes in other sections, we have used it here. It may be remarked that there are three different uses of substitute limits such as Abel's limit:

1) The observable is defined as a limit of a definite quantity. *a*) The limit is shown to exist, but for reasons of mathematical convenience it is expressed as a result of some particular limiting process. This is unobjectionable. *b*) The limit does not exist, and is replaced by a substitute. This constitutes an infringement on the physical basis of the theory, and is unsatisfactory.

2) The physical postulates do not define the observable as a limit of a definite quantity. The substitute limit of a function which is not required to have a limit by physical postulates, may be identified with the observable if it, (the limit) satisfies other requirements. This is the present case.

([32]) F. J. DYSON: *Phys. Rev.*, **75**, 486 (1949).

14. – Field Theory without Vacuum Polarization 2.

In absence of vacuum polarization, an eigenstate of H which represents a single meson, may be written

$$\psi_{\boldsymbol{k}} = a^{\dagger}(\boldsymbol{k})\Psi_0 \,, \tag{14.1}$$

where $a^{\dagger}$ is the creation operator of a bare meson. Consequently, the operators $\boldsymbol{c}_{s\boldsymbol{k}}$ of Eq. (5.2) which refer to mesons, are all equal to the corresponding bare meson creation operators. A basis vector Φ which describes a nucleon with momentum $\boldsymbol{p}$ and mesons with momenta $\boldsymbol{k}_1 \,..\, \boldsymbol{k}_n$ may be written as

$$\Phi_{\boldsymbol{k}_1 \ldots \boldsymbol{k}_n, \boldsymbol{p}} = n^{-\frac{1}{2}} a^{\dagger}(\boldsymbol{k}_1) \ldots a^{\dagger}(\boldsymbol{k}_n)\psi_p \,, \tag{14.2}$$

where $\psi_{\boldsymbol{p}}$ is an eigenstate with one nucleon of momentum $\boldsymbol{p}$. The scattering amplitude for a (one meson, one nucleon) into another (one meson, one nucleon) state may be written by Eqs. (5.18) and (5.19).

$$R^{(+)}(\boldsymbol{p}'\boldsymbol{k}', \boldsymbol{p}\boldsymbol{k}) = \left((H - E_{p'} - E_{k'})a^{\dagger}_{\boldsymbol{k}'}\psi_{\boldsymbol{p}'}, \psi^{(+)}_{\boldsymbol{p}\boldsymbol{k}}\right) , \tag{14.3}$$

$$R^{(-)}(\boldsymbol{p}'\boldsymbol{k}', \boldsymbol{p}\boldsymbol{k}) = \left(\psi^{(-)}_{\boldsymbol{p}'\boldsymbol{k}'}, (H - E_{\boldsymbol{p}} - E_{\boldsymbol{k}})a^{\dagger}(\boldsymbol{k})\psi_{\boldsymbol{p}}\right) . \tag{14.4}$$

For the simplest case, where the nucleon is fixed, two unconventional definitions of the scattering amplitude have been proposed in recent literature [33,31] and we will first show that they agree with Eqs. (14.3) and (14.4) respectively.

If isobars are excluded, the energy of the nucleon alone, E_p, is constant and may be set equal to zero. If, in addition, the interaction Hamiltonian is linear in the meson operators a and $a^{\dagger}$, we have

$$[H - E(\boldsymbol{k})]a^{\dagger}(\boldsymbol{k})\psi_{0i} = a^{\dagger}(\boldsymbol{k})H\psi_{0i} + \left\{[H, a^{\dagger}(\boldsymbol{k})] - E(\boldsymbol{k})a^{\dagger}(\boldsymbol{k})\right\}\psi_{0i} = V(\boldsymbol{k})\psi_{0i} \,, \tag{14.5}$$

where ψ_{0i} is one of the degenerate states of the nucleon, and V an operator with respect to spin and isotopic spin, but not creating or destroying mesons. Hence, the scattering amplitudes (14.3) and (14.4) become

$$R^{(+)}(\boldsymbol{k}'_i, \boldsymbol{k}_j) = \left(V(\boldsymbol{k}')\psi_{0i}, \psi^{(+)}_{\boldsymbol{k}j}\right) , \tag{14.6}$$

$$R^{(-)}(\boldsymbol{k}'_i, \boldsymbol{k}_j) = \left(\psi^{(-)}_{\boldsymbol{k}'i}, V(\boldsymbol{k})\psi_{0j}\right) . \tag{14.7}$$

[33] R. J. Riddell and B. D. Fried: *Phys. Rev.*, **94**, 1736 (1954).
[34] G. C. Wick: *Rev. Mod. Phys.*, **27**, 339 (1955).

The subscripts i and j stand here for spin and charge of nucleons and mesons. Eqs. (33) and (34) are the scattering amplitudes of Riddell and Fried, and of Wick, respectively. Clearly, an infinite number of expressions for the scattering amplitude can be given which differ only off the energy shell.

We want to show that Eq. (5.21) implies Low's equation for nucleon-meson scattering ([35]).

The Heisenberg operators $a(\boldsymbol{k}t)$ which are obtained in the usual manner from the Schrödinger meson-destruction operators $a(\boldsymbol{k})$ satisfy equations of motion

$$i\dot{a}(\boldsymbol{k}t) - E(\boldsymbol{k})a(\boldsymbol{k}t) = [a(\boldsymbol{k}t), H_{\mathrm{I}}] \equiv N(\boldsymbol{k}t)\,, \tag{14.8}$$

where H_{I} is the interaction Hamiltonian. If H_{I} is linear in the meson field operators, N contains no meson field operators, and hence commutes with a_r and $a_r^\dagger$, taken at the same time. This makes it possible to express the first term on the right-hand side of Eq. (5.21) in terms of the matrix element $R^{(-)}(nm)$. Consider an element which refers to an initial nucleon with momentum etc., p and a meson described by k, and a final state (p', k'). Then, by Eq. (14.2)

$$\begin{aligned}(\Phi_m, (H - E_n)\Phi_n) &= (a^\dagger(\boldsymbol{k}')\psi_{p'}, (H - E_k - E_p)a^\dagger(k)\psi_p) = \\ &= (a^\dagger(k')\psi_{p'}, N^\dagger(k)\psi_p) = (N(\boldsymbol{k})\psi_{p'}, a(k')\psi_p)\,.\end{aligned} \tag{14.9}$$

The second step follows from commuting H with $a^\dagger(k)$ and using Eq. (14.8) with the time $t = 0$. The third step follows from the commutability of N and $N^\dagger$ with the creation operator $a^\dagger$. On the other hand, one obtains by commuting H with $a(k')$:

$$Ha(k')\psi_p = a(k')\psi H_p + [H, a(k)]\psi_p = [(E_p - E_{k'})a(k') - N(k')]\psi_p\,, \tag{14.10}$$

or

$$a(k')\psi_p = -(H - E_p + E_{k'})^{-1}N(k')\psi_{p'}\,. \tag{14.11}$$

If this expression is inserted into Eq. (14.9) and $N(k')\psi_p$ is expanded in terms of the complete set $\psi_n^{(-)}$, one obtains

$$\begin{aligned}(\Phi_m, (H - E_n)\Phi_n) &= \\ &= -\int (E_l - E_p + E_{k'})^{-1}(N(k)\psi_{p'}, \psi_l^{(-)})(\psi_l^{(-)}, N(k')\psi_p)\,\mathrm{d}l - \\ &-\int (E_l - E_p + E_{l'})^{-1}(N(k)\psi_{l'}, \psi_l)(\psi_l, N(k')\psi_p)\,\mathrm{d}l\,,\end{aligned} \tag{14.12}$$

([35]) F. E. Low: *Phys. Rev.*, **97**, 1392 (1955).

where the second term is again the contribution of one-particle states ψ_l, and actually a sum over spin and isotopic spin states with fixed momentum.

The factors in the integrand of the first term can be identified as matrix elements $R^{(-)}$ as follows: according to the reasoning which leads to Eq. (14.9), Eq. (14.4) can be written

$$R^{(-)}(m, pk) = (\psi_m^{(-)}, N^+(\boldsymbol{k})\psi_p) \,. \tag{14.13}$$

Hence, the first term of Eq. (5.21) can be written as an integral bilinear in the $R^{(-)}$, plus an integral which has the same form as the third term of Eq. (5.21). The identification with Low's equation is then only a matter of algebra. (We have omitted the « contact term » for the sake of brevity.)

From the present viewpoint, the replacement of the inhomogeneous term by an integral containing the unknown itself seems surprising, since the purpose of the integral equation is to obtain the scattering amplitudes $R^{(\ )}$ in terms of the matrix elements $(\Phi_m, (H - E)\Phi_n)$ which contain the physical data of the problem. The question arises, naturally, whether this substitution has not reduced the integral equation to a partly tautological statement. This question is discussed in a paper by CASTILLEJO, DALITZ and DYSON ([36]).

It is surprising that the integral equation (5.21) leads precisely to Low's equation, *if vacuum polarization is omitted*, since Low's equation was obtained from Dyson's S-matrix without approximation. On the other hand, it is shown in Sect. **8** that the present formulation is also equivalent to Dyson's, in absence of composite particles. It would seem, then, that different approximate forms for the Φ_n's lead *exactly* to the same result, i.e., that the S-matrix is largely insensitive toward substitution of approximate basis functions for the correct ones. This question is discussed in a paper by K. TANAKA and the author ([15]).

15. – Real-Particles Operators for the Multi-Channel Case.

Our asymptotic particle operators $A^{(-)}$ are identical with the in- and out-fields of YANG and FELDMAN ([10]) only in the single-channel case. It is clear that there can be no unitary transformation between the a_r and $A_r^{(\pm)}$ in general, if the number N of species of stable particles (including, by our definition, composite particles) is larger than the number M of species of bare particles defined by the bare-particle operators a_r.

Nevertheless, one can ask if there exist real-particle operators A_r which merge in the distant future (past) with asymptotic particle operators $A_r^{(+)}(A_r^{(-)})$. As in the non relativistic case, one could define such operators as being des-

([36]) L. CASTILLEJO, R. H. DALITZ and F. J. DYSON: *Phys. Rev.*, **101**, 453 (1956).

truction operators with respect to the labels of the basis states Φ_n. The commutation relations of these operators would not be of the usual simple kind, since the basis vectors Φ_n are non-orthogonal and redundant. Contrary to the non relativistic case, not even the commutators for those operators which create physical elementary particles can be simple, since all physical particles in field theory have finite extent.

From this viewpoint, we can give a tentative answer to the question investigated by HAAG ([11]). HAAG defines quantities essentially equivalent to our $A_r^{(\pm)}$ which describe asymptotically observable particles. He then asks whether Lorentz-invariant equations of motion and commutation relations for operators A_r exist such that Eq. (7.1) is satisfied and that these operators are « causal », in the sense that the commutators of the field operators corresponding to the operator A_r vanish for space-time points which are on a space-like surface. It appears that in general, if Lorentz-invariant and causal equations are given for a set of operators a_r, they do not satisfy Eq. (7.1), which does, however, not prevent the existence and, indeed explicit determination of operators $A^{(\pm)}$. While we cannot exclude the possible existence of « causal » operators A_r in the general case, the most obvious choice for them (destruction operators with respect to the basis vectors Φ_n) assigns « acausal » commutation relations to them. It seems that the stringent requirements investigated by HAAG cannot be satisfied by field theories, but also that this is not necessary to obtain physical results.

* * *

The author wishes to express his gratitude for helpful discussions to Drs. F. COESTER, M. L. GOLDBERGER, M. HACK, and K. TANAKA, to Prof. K. MENGER for a discussion of asymptotic observables in classical physics, and to Dr. H. KITA for an interesting correspondence.

RIASSUNTO (*)

Si propone una precisa enunciazione del problema dello scattering, abbastanza generale per comprendere nella teoria dei campi le particelle composte: i quattro operatori di Heisenberg P_μ che rappresentano il vettore energia-momento totale possono essere espressi asintoticamente ($t \to \pm \infty$) come integrali di operatori che mutuamente commutano $A_r^{(\pm)\dagger}(\boldsymbol{k}) k_{r\mu} A_r^{(\pm)}(\boldsymbol{k})$ che rappresentano i quadrimomenti delle particelle incidenti ed uscenti, sia elementari che composte. Per una teoria esposta in termini di operatori $a_r^\dagger$ di particelle nude, il problema consiste nel trovare gli operatori $A^{(\pm)}$ asintotici in funzione delle a_r e $a_r^\dagger$. A tale scopo si deriva un sistema di equazioni lineari. In alternativa si può ottenere la matrice S risolvendo un'equazione bilineare il cui termine inomogeneo è formato essenzialmente da prodotti di vettori di uno stato singolo.

(*) *Traduzione a cura della Redazione.*

IL NUOVO CIMENTO Vol. IV, N. 5 1° Novembre 1956

Remarks on the Analysis of τ-Meson Experiments.

N. Brene, K. H. Hansen, J. E. Hooper and M. Scharff

Institute for Theoretical Physics, University of Copenhagen - Copenhagen, Denmark

(ricevuto il 27 Luglio 1956)

Summary. — The results from the analysis of 75 stopped τ-meson decays, found in a stack of emulsions exposed to the Berkeley Bevatron, are discussed. Special attention is paid to the effects of the finite dimensions of the stack, and a brief analysis of the problem is given. The experimental results are compared with those from other laboratories, and the authors conclude that there is no good evidence that the spectrum of the π-mesons from τ-decay is in accord with either of those which have been predicted for the two lowest spin-parity combinations: 0^- and 1^+.

1. – Introduction.

The recent evidence that the masses and lifetimes of all the K-mesons are the same within experimental errors ([1-4]) suggests that all the various modes of decay observed belong to the same particle. Apparently conflicting with this evidence is that from studies of the decay of the τ-meson. The τ-meson is of particular interest because, decaying as it does into three charged particles, the number of measurable quantities associated with the decay is unusually large, and it has been shown that the distributions of the various decay parameters can give information on the spin and parity of the decaying meson. Much of the previously published evidence on the shape of the measured distributions has been in favour of a spin and parity of the τ-meson of 0^-;

([1]) H. H. Heckman, F. M. Smith and W. H. Barkas: *Nuovo Cimento*, **3**, 85 (1956).
([2]) S. Fuug, A. Pevsner, D. Ritson and N. Mohler: *Phys. Rev.*, **101**, 493 (1956).
([3]) G. Harris, J. Orear and S. Taylor: *Phys. Rev.*, **100**, 932 (1955).
([4]) L. M. Alvarez, F. S. Crawford, M. L. Good and M. L. Stevenson: *Phys. Rev.*, **101**, 503 (1956).

the spin and parity of the χ-meson which decays into two π-mesons cannot be the same. As there exist, at present, no direct measurements of the spin of any of the K-mesons, the evidence on the spin and parity of the τ-meson can thus provide valuable information on the question of the number of different heavy mesons.

In this paper, we consider only the decay of the positive τ-meson into three charged π-mesons. The kinematics of the decay is usually described in terms of the quantities ([5-7]):

$$\boldsymbol{P} = \frac{1}{\sqrt{3}}(\boldsymbol{p}_1 + \boldsymbol{p}_2 + \boldsymbol{p}_3)\,,$$

$$\boldsymbol{q} = \frac{1}{\sqrt{2}}(\boldsymbol{p}_2 - \boldsymbol{p}_1)\,,$$

$$\boldsymbol{p} = \sqrt{\frac{2}{3}}(\boldsymbol{p}_3 - \tfrac{1}{2}(\boldsymbol{p}_1 + \boldsymbol{p}_2))\,,$$

where $\boldsymbol{p}_1$ and $\boldsymbol{p}_2$ are the momenta of the two positive π-mesons and $\boldsymbol{p}_3$ is the momentum of the negative π. In the centre of mass system (which in most cases is identical with the laboratory system, because the τ comes to rest before decaying) $\boldsymbol{P} = 0$ and, therefore, $\boldsymbol{p} = \sqrt{\frac{3}{2}}\boldsymbol{p}_3$. $\boldsymbol{p}$ and $\boldsymbol{q}$ are related by the conservation of energy, which in the non-relativistic approximation is expressed by $Q = (p^2 + q^2)/2m_\pi$ (Q is the total kinetic energy released in the c.m.s.).

The momentum triangle is completely determined by the independent variables p and the angle ϑ between $\boldsymbol{p}$ and $\boldsymbol{q}$. Using these variables, DALITZ and FABRI ([5-7]) have calculated, for various spin-parity combinations of the τ-meson, the relative transition probabilities, W, from the τ-state to different 3π states (p, ϑ). Their results are summarized in Table I for the 5 combinations for which W is unique to the lowest order of angular momentum.

TABLE I.

Spin	Parity	Probability W
0	—	1
1	+	p^2
1	—	$p^4q^4 \sin^2\vartheta \cos^2\vartheta$
2	+	$p^4q^2 \sin^2\vartheta$
3	—	$p^4q^4 \sin^2\vartheta(5+3\cos^2\vartheta)$

([5]) R. H. DALITZ: *Phil. Mag.*, **44**, 1068 (1953).
([6]) R. H. DALITZ: *Phys. Rev.*, **94**, 1046 (1954).
([7]) E. FABRI: *Nuovo Cimento*, **11**, 479 (1954).

It is seen that in all these cases W is a product of a function of p and a function of ϑ. In the calculations no account is taken of interactions (Coulomb and π-π) in the final state, and they are based upon rather special assumptions about the decay mechanism.

The configuration of the decay may, as has been suggested by DALITZ [5], be very conveniently represented as a point in an equilateral triangle of height equal to the Q-value of the decay. The distances from the point to each of the three sides are equal to the three π-energies, that from the base being conventionally chosen as that of the π^--meson. In the non-relativistic approximation, conservation of momentum restricts the points which represent possible decay configurations to the inside of the inscribed circle. If relativistic effects are taken into account, the area within which the points fall is further slightly restricted, as shown in Fig. 1. It should be noted that the centre of the populated region is, however, still $Q/3$ from the base, and that this quantity is not equal to $E_{\max}/2$, where $E_{\max}$ is the maximum energy which one of the π-mesons can obtain. In such a diagram each point corresponds to one, and only one decay configuration (p, ϑ).

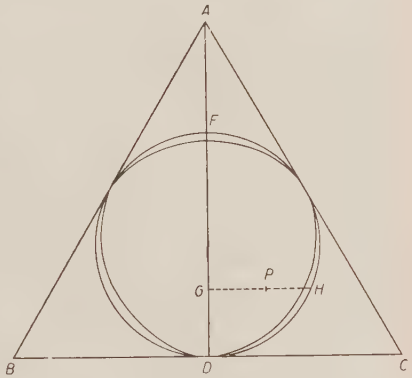

Fig. 1. – The Dalitz triangle.

In the Dalitz diagram, the quantity $\cos\vartheta$ corresponding to a point P is given by the ratio PG/GH, where G and H are the intersections of a line through P parallel to the base of the triangle with the altitude AD, and the circumference of the inscribed circle, respectively. All decay configurations which share a common value of ϑ lie on an ellipse with DF as its major axis. Decays with $\vartheta = \pi/2$ lie along DF, and those with $\vartheta = 0$ lie on the circumference of the circle. The area element in the Dalitz diagram is proportional to the phase space element; thus, a distribution of points on the diagram of density W gives a direct representation of the expected distribution of decays in phase space. For comparison with experiment we want the energy spectrum of the π^-. It is obtained by integrating the density in strips parallel to the base, while the ϑ distribution is obtained by integrating along the ellipses of constant ϑ. These relations are not strictly true in a relativistic treatment.

The energy spectra of the π^--meson obtained on the five spin parity assumptions in Table I are shown in Fig. 2 ($\varepsilon = E_{\pi^-}/\frac{2}{3}Q$) and the corresponding distributions in ϑ in Fig. 3. It may be seen that it should not be difficult on the basis of the distribution in ϑ to distinguish experimentally between $(0^-, 1^+)$

and the three other cases which differ considerably from isotropy. In fact, all the experimental results are consistent with an isotropic distribution in ϑ, thus favouring the spin-parity combinations 0^- or 1^+. To distinguish between these two possibilities one may utilize the fact that the corresponding energy spectra of the π^--meson are not at all similar. From an experimental point of view, the most easily recognized difference is that, while the spectrum from the decay of a 0^- τ-meson is expected to be symmetric about the energy $Q/3$, that from the 1^+ is skew to higher energies. While a detailed comparison of the experimental data with the various predicted spectra can only be useful when very large statistics are available, it should not be difficult to determine whether or not, within certain limits, depending on the statistics, the spectrum is symmetric. However, there seems to be considerable disagreement between the experimental results which have been published up to the present. While some of the data appear to be fully consistent with a symmetric spectrum, there exist data of almost equal weight which are consistent neither with a symmetric spectrum nor with a spectrum which is as asymmetric as that predicted by DALITZ for the 1^+ decay. A more detailed analysis of the data published up to the time of writing is included in Sect. **4**.

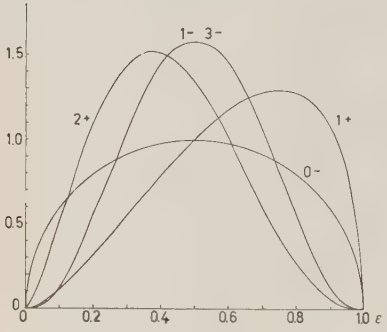

Fig. 2. – The theoretically predicted energy spectra of the negative secondary: ($\varepsilon = E_{\pi^-}/\frac{2}{3}Q$).

The explanation of the discrepancy between the various data could possibly be due to some sort of bias in the selection of the events upon which the experimental distributions are based. A bias arising in the scanning would be expected to be small, for in most stacks the grain density of all the τ-meson secondaries at the point of decay is sufficiently high to allow them to be recognized without difficulty, especially when one takes into consideration the fact that, if two of them are rather thin, the third will be so much the greyer. Geometric bias, on the other hand, which is that due to the restricted dimensions of the sensitive volume of emulsion within which

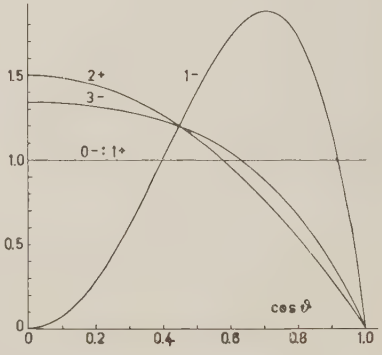

Fig. 3. – The theoretically predicted distribution in ϑ.

the τ-meson decays occur, can be shown to produce very considerable effects. As it is not possible to compare directly the published results from different laboratories unless they are bias-free, or at least biassed to the same extent, in the next section we examine in some detail the problem of geometric bias, and the related problem of selecting an unbiassed sample by the use of a suitable set of criteria which do not restrict the statistics too gravely.

2. – Geometric Bias.

It is well known that in emulsion stacks of limited size the observed distributions of parameters such as E_{π^-} and ϑ can be influenced by geometric bias ([6]). The reason for this is that a determination of either of these parameters requires that charge be assigned to each of the secondaries, and this in turn can only be done when the secondary in question is brought to rest in the emulsion, so that it is possible to examine its end point for decay or interaction. If the dimensions of the emulsion stack are limited in certain directions, only certain decay configurations can always be identified, for the others will be such that two or three of the secondaries may escape from the stack.

The effect can be simply illustrated by considering a very idealised experiment in which all the decays take place at the centre of a spherical block of emulsion. Disregarding the effects due to scattering and range straggling, all of the secondaries whose energy does not exceed a certain critical value will stop in the emulsion, while all of the secondaries whose energy exceeds this value will escape. If we further know that all the τ-mesons are positive (e.g. we have plates exposed to a magnetically analysed beam), then the charges of all the secondaries are determined if the π^--meson is stopped (class $+-$) or, more generally, at least two secondaries are stopped (class $++-$, $+-$, $++$).

Assuming a radius for the spherical emulsion block of ≈ 8 mm, the bias resulting from the selection of a sample of events from each of the two classes defined above is illustrated in Fig. 4*a* and *b*. All the decay configurations which are included in the samples lie within the hatched areas. It is now possible to define a bias function $P\ (E_{\pi^-}, \vartheta)$ such that it represents the probability that a decay, whose co-ordinates in the Dalitz diagram are (E_{π^-}, ϑ), can be analysed. This function is extremely simple for decays at the centre of a spherical block of emulsion, for at every point in the diagram its value is either 1 or 0. The expected experimental distributions, taking bias into account, may be obtained by multiplying the theoretically predicted densities at every point (Table I) by the appropriate value of the bias function before carrying out the integrations. In the idealized experiment under discussion, we may obtain some idea of the effect by considering the effect on the spectrum of a (0) τ-meson, for which the unbiassed theoretical density is uniform over

the whole Dalitz circle. The biassed distribution is then identical with the bias function, and it is immediately seen from Fig. 4*a* and *b* that the observed distributions will depend strongly on the class of τ-decays chosen for examination. If, for example, we choose to use only decays of class (–), then there

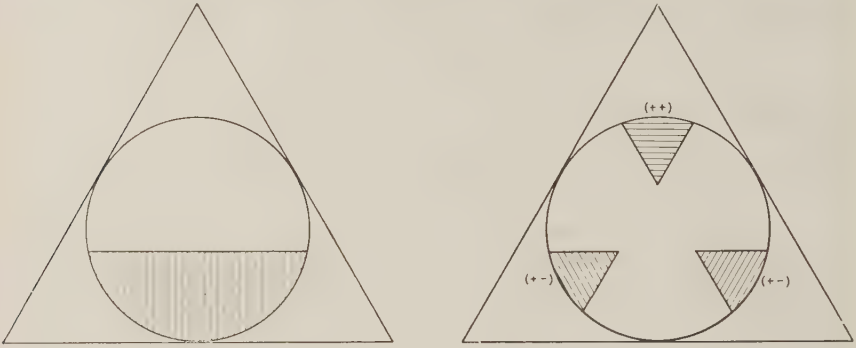

Fig. 4. – Bias diagrams for class (—), (*a*), and class (++—, +—, -++), (*b*), in a spherical block of emulsion. Critical energy equal to 20 MeV.

will be included in our data no decays in which the energy of the π^--meson exceeds the critical energy for the stack, whereas, choosing events of class (++—, ++, +—), we include in our data both high energy and low energy π^--mesons, the latter being twice as frequent as the former. As the radius of the stack is increased the general features of the bias will remain the same, but its absolute magnitude will diminish, until it vanishes completely when the shaded areas fill the Dalitz circle. This occurs at a radius of 23 mm for events in the class (++—, ++, +—) and at a radius of 36 mm for events in the class (—).

Although the above simple considerations have no direct bearing on the effects produced by bias in real emulsion stacks, they display very clearly some fundamental differences between the two classes of events. For both classes the geometric bias tends to shift the spectrum of the π^--mesons towards lower energies, but the effect is much more considerable if the events are chosen from class ( ). Further, the minimum size of a stack, from which a bias-free sample is obtained, is much larger if one uses events from class (—).

Some idea of the influence of the geometry of the experiment on the ϑ distributions may also be obtained from the above simple bias diagrams, but the quantitative effects are not quite so easy to see. It is worth mentioning, however, that the distribution obtained from class ( ) events is completely bias-free if the unbiassed distribution in E_{π^-} and ϑ is independent. Even if we consider the class (++—, ++, +—), the bias on the ϑ distribution is only

moderate, in the sense that the bias factor is finite for all values of ϑ, although the critical energy may be very low. This may be seen at once from the fact that all the ellipses of constant ϑ pass through some of the shaded area. More severe bias on the ϑ distribution will result from choosing only events in the subclass $(++-)$ which, from a « naive » point of view, might be considered to be unbiassed. The bias function is plotted in Fig. 5 for a critical energy of 30 MeV. It can be seen that, if the critical energy is smaller than 38 MeV, no values of ϑ close to 0 will be found.

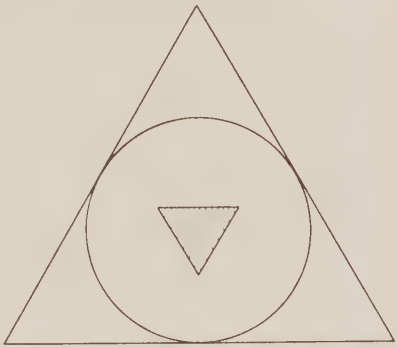

Fig. 5. – Bias diagram for class $(++-)$ in a spherical block of emulsion. Critical energy equal to 30 MeV.

The problem of geometric bias in the stacks of emulsions actually used is somewhat more intricate than that sketched for the idealized stack above. For simplicity, we shall restrict the analysis to those events whose projected distances from all the natural edges of the plates are more than 36 mm, so that the secondary particles can only escape from the stack through the top and bottom plates. Although this restriction may reduce considerably the number of useful events in small stacks exposed to cosmic radiation, it is of much less consequence in machine exposed plates, because the beam of particles is usually directed in such a way that the condition is fulfilled for practically all the τ-mesons stopping in the stack.

Before discussing the effects of bias we shall determine certain criteria which will enable us to extract from a given sample of τ-meson decay events a bias-free sub-group. For this purpose, we neglect the effect of multiple scattering, so that the trajectories of the secondary meson may be considered to be rectilnear. In this approximation a secondary will be stopped if its track does not cross one of the two lines l_1 and l_2 defined by the intersections of the decay plane with the top and bottom surface of the stack. The useful portion of any decay plane is a strip which is completely determined by the distances d_1 and d_2 of the decay point from the lines l_1 and l_2. Any particular event may now be considered to be bias-free if, and only if, d_1 and d_2 are so large that the event may be analysed irrespective of the decay configuration. In other words, every point within the Dalitz circle must correspond to an event which could be analysed if it decayed at this particular point in the decay plane. A basic assumption for the validity of this scheme is that there is no correlation between the configuration of the decay and the orientation of the decay plane in the laboratory system.

If, as a suitable condition, we choose that d_1 and d_2 are both greater than 36 mm, so that all the secondaries are certainly stopped in the stack, we find that in stacks of small or medium size the bias-free sample so obtained is only a very small proportion of the total number of events. However, to determine the charge of all three secondaries it is sufficient to stop two of them. We may thus ask, for which sets of d_1, d_2 is this condition secured for the whole of the Dalitz circle? For a given value of d_1 we calculate the smallest value of d_2 such that, for all decay configurations, at least two secondaries will be stopped. The results of such calculations, using the range energy relations of Fay, Gottstein and Haynes, are shown in Fig. 6, in which the allowed and forbidden regions are plotted in the d_1, d_2 plane. Each decay observed corresponds to a point on the diagram, and it will belong to the bias-free sample if it falls outside the shaded region. For simplicity, the limiting contour is represented by sections of straight lines, which may be shown to be a sufficiently good approximation.

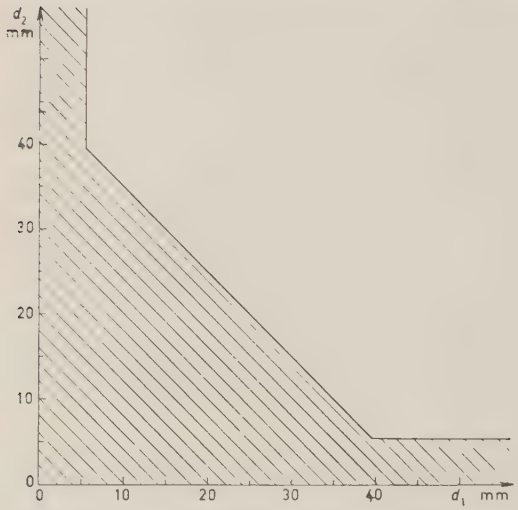

Fig. 6. All events lying outside the shaded area are classified as unbiassed. d_1 and d_2 are the distances in the decay plane from the point of decay to the surfaces of the stack.

A slightly more detailed analysis of the problem shows that this simple method of selecting events does not provide the largest bias-free subgroup, and that it is possible to increase considerably the number of accepted events by reinterpreting the quantities d_1 and d_2. We assume that any given decay configuration (i.e. a certain momentum triangle) is orientated at random in the decay plane. We can then introduce no bias by selecting those decay events which have some specified orientation in the decay plane, or, in particular, by distinguishing between that side towards which two of the secondaries are emitted, and that to which only one is emitted. Calling the corresponding distances d_2 and d_1, respectively, the indices now indicating the number of secondaries with a component of velocity in the corresponding directions, we obtain a new selection diagram which is shown in Fig. 7. As before, the decay events falling in the unshaded region are considered to

be bias-free. The diagram shows the trivial result that, if d_2 is sufficiently large ($d_2 > 22.5$ mm), two secondaries must always be stopped, even though d_1 should be zero. It should, however, be remembered that only half of the events with any given decay plane are selected, the remaining portion being such that two secondaries are directed out wards through the surface of the stack.

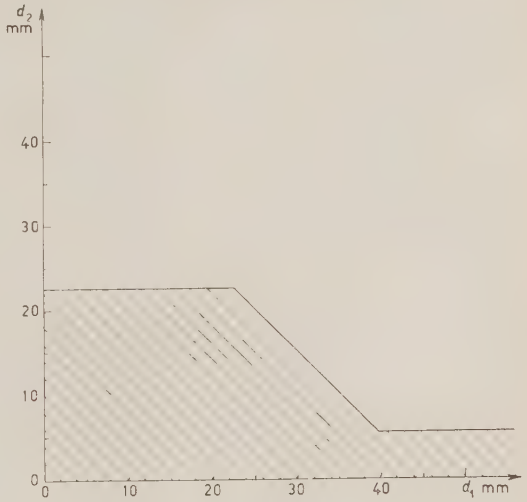

Fig. 7. – All events lying outside the shaded area are classified as unbiassed. d_1 and d_2 are defined as in Fig. 6, but here the index on d refers to the number of secondaries emitted towards the surface in question.

Using the criterion we have developed above, and assuming that the normals to the decay planes are isotropically distributed in space, it is of interest to ask what proportion of the total number of events found may be selected as unbiassed. We have calculated this fraction as a function of x, the thickness of the stack above the decay point, and y, the thickness of the stack below the decay point. The full lines in Fig. 8 are the curves of equal unbiassed fraction in the x, y plane, whereas each of the broken lines represents the locus of all possible decay points (x, y) occurring in a stack of given total thickness, indicated by the total number of 600 μm thick plates in the stack. The τ-decays observed in an actual experiment

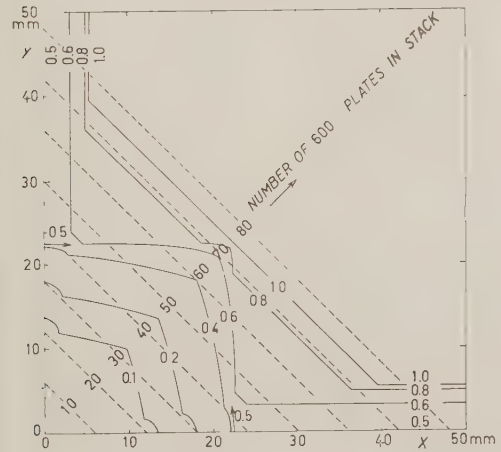

Fig. 8. – Lines of equal unbiassed fraction as a function of the distances x and y of the point of decay from the stack surfaces (full lines). Each of the broken lines is the locus of decay points in a stack of some given thickness.

must fall on a section of one of the dashed lines, and it may be seen from the diagram that the plates near the top and bottom of a small stack will provide the greatest proportion of bias-free events. Again, the relative number of useful events increases very rapidly with increasing stack size; this is perhaps better illustrated in Fig. 9, in which are plotted curves showing the proportion of the bias-free events as a function of the thickness of the stack. Two of the curves, (*a*) and (*b*), refer to the centre and edge plates of the stack respectively, while the third curve (*c*) gives the mean for a uniform distribution of decays throughout the stack.

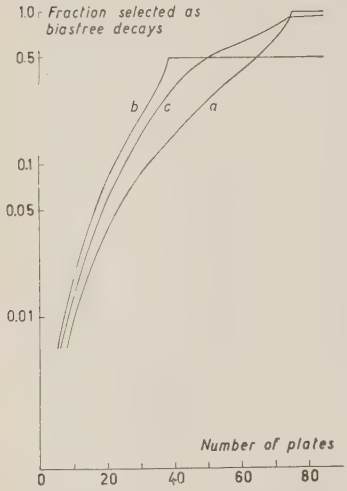

Fig. 9. – The fraction of the decays found, selected as unbiassed, as a function of stack thickness. Curve (*a*) represents events in the centre plate; (*b*) events in the outer plates; (*c*) the mean for a uniform distribution of events throughout the stack.

Using Fig. 9 it is easy to determine which is the most profitable part of a stack to scan for τ-meson decay events, and a bias-free sample may then be selected from those found by plotting the appropriate data on Fig. 7. We suggest that such an analysis should always be carried out in experiments in which it is not obvious that all events may be considered to be completely free from bias. The resulting lists of bias-free events can then be collected at some later date in order to make the maximum possible use of the available statistics in the determination of the details of the various energy and angular distributions.

At present, however, when it is not yet certainly known whether the $E_{\pi\pi}$-spectrum is or is not symmetric, it is desirable to make use of all available information, and we shall therefore attempt to estimate the errors which arise from the neglect of the effects of geometrical bias on the samples which are in fact observed. An investigation of this sort has already been carried out by BHOWMIK *et al.* [8] for that class of decay events in which the negative secondary is stopped. With this method of selection, the bias function must decrease with increasing energy of the π^--meson, but it depends in no other way on the co-ordinates of the decay configuration in the Dalitz diagram. From this the authors conclude that the resulting distribution in ϑ is unbiassed, but it should be noted that this conclusion is only correct if there is no correlation between the distributions of ϑ and $E_{\pi\pi}$. This condition is fulfilled in the simple Dalitz theory for the lowest spin values, as the appropriate matrix element is a single product of a function of $E_{\pi\pi}$ and a function of ϑ.

A more refined theory, which might include several partial waves as well as take account of Coulomb and π-π interaction, would not be expected to retain the simple product form of the matrix element.

Bias tends to move the maximum of the E_{π^-}-spectrum from events of class (—) towards lower energy, and BHOWMIK *et al.* [8] have shown how this effect may be corrected. However, as this correction to the shape of the spectrum is very large, we prefer to consider that class of events in which at least two secondaries are stopped (+ + —, + +, + —). It is immediately clear from the above discussion of the bias effects in a spherical block of emulsion that this latter class of events will be subject to much smaller distortion than the former. In fact, when there are more than ≈ 40 plates in the stack under discussion the effects are so small that they may be neglected so long as it is only the crude shape of the spectrum which is of interest.

To demonstrate the order of magnitude of the effects to be expected from bias on the E_{π^-} spectra we have calculated the observed spectra resulting from the effect of bias on those predicted by the simple Dalitz theory. As the calculations themselves are rather tedious they have only been made for a few characteristic examples of stack geometry. The procedure was as follows. At a given depth in the stack the inclination of the decay plane determines the two bordering lines l_1 and l_2. A point in the Dalitz diagram was then chosen, and the corresponding decay configuration was rotated in the decay plane, the angular intervals within which at most one of the secondaries crossed the bordering lines being measured graphically. Calling the sum of these angular intervals φ, the ratio $\varphi/2\pi$ is the probability that the decay configuration in question has at least two secondaries stopped. By measuring φ for a number of different inclinations of the decay plane, and assuming that the normal to the decay plane is randomly orientated in space, one may find by integration the value of the bias function

$$P = \frac{1}{2\pi}\int_0^{\pi/2} \varphi(u)\cdot \sin u \, \mathrm{d}u \, ,$$

where u is the angle between the normal of the decay plane and the normal to the surface of the plates. Such calculations were carried out for a number of points within the Dalitz semi-circle and from these were plotted level diagrams representing the bias function $P(E_{\pi^-}, \vartheta)$. Fig. 10 shows the results obtained for a stack of twenty plates. Diagrams (*a*) and (*b*) refer to decay in the centre

---

(8) B. B. BHOWMIK, D. EVANS, I. J. VAN HEERDEN, and D. J. PROWSE: *Nuovo Cimento*, **3**, 574 (1956).

plate and at one of the surfaces respectively. Application of these weighting factors to the theoretically predicted decay distributions allows the biassed

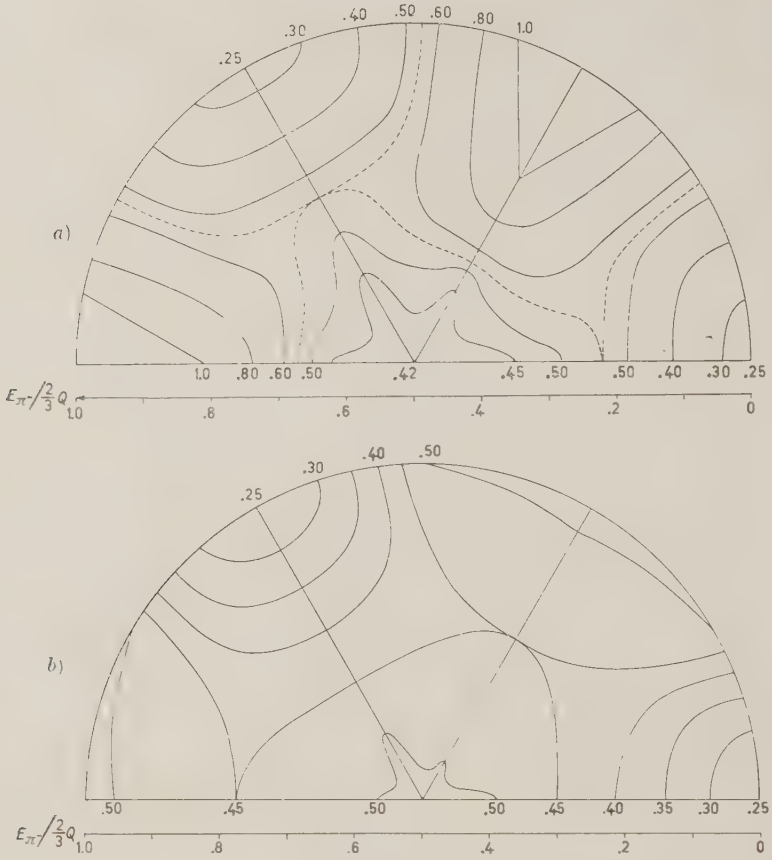

Fig. 10. – Bias contours in the Dalitz diagram for decays of class (+ + —, + —, + +) in the middle, (*a*), and close to the surface, (*b*), of a stack of 20 600 μm emulsions.

E_{π^-} spectra and θ distributions to be calculated. Results for some of the E_{π^-} spectra are shown in Fig. 11, (*a*), (*b*) and (*c*) corresponding to various assumed properties of the τ-meson. On each diagram the unbiassed spectrum is plotted (full line) as well as the biassed spectrum arising from events decaying in the middle of the stack (dashed curve) and that from events close to the surface of the stack (dash-dot curve). All the curves are normalized to the same total area.

From the diagram it may be seen that the effect of the bias is always to increase the area under the lower energy half of the spectrum. The shift is thus in the same direction as for events chosen from class (—), but it is not so strongly marked. The spectrum for 0⁻-events shows clearly how the bias tends to produce a peak at low energy, and a smaller one near E_{max}; this behaviour is that which the above treatment of the simple spherical stack has led us to expect (see Fig. 4). It is also worth mentioning that, because the un-

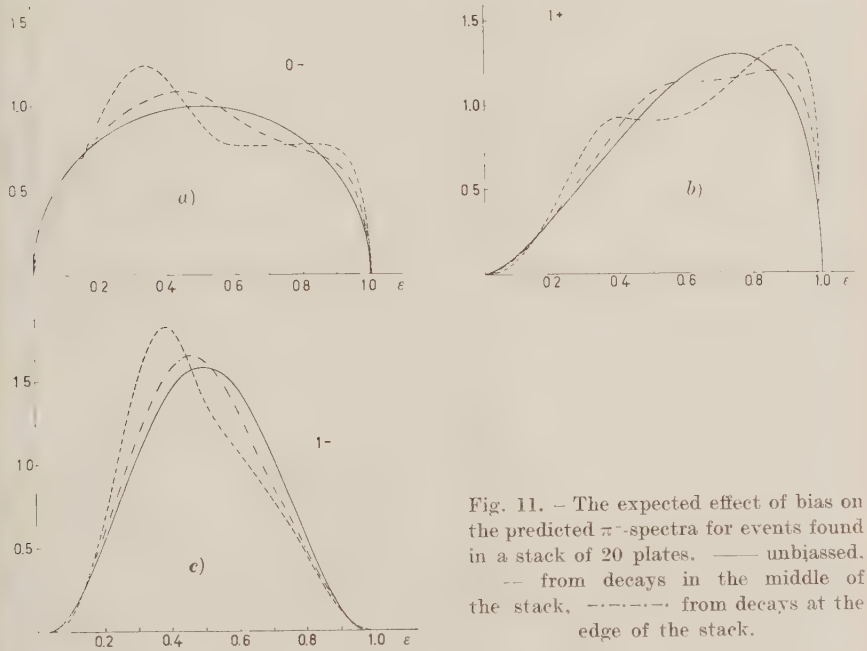

Fig. 11. – The expected effect of bias on the predicted π^--spectra for events found in a stack of 20 plates. —— unbiassed. -- from decays in the middle of the stack. -·-·-·- from decays at the edge of the stack.

biassed 0⁻-spectrum corresponds to a uniform distribution in the Dalitz circle, any geometric bias on the classes (++—, ++, + —) and (+ + —) must leave the centre of gravity of the spectrum at $E = \frac{1}{3}Q$. This follows simply from the fact that the bias function must be invariant to reflections in the symmetry axes of the Dalitz triangle, and the result also holds strictly for a relativistic treatment.

The biassed spectra shown in Fig. 11 give an idea of the order of magnitude of the effects which are to be expected. If the stack consists of only a few plates, the bias will be very much stronger and lead to results which resemble those found for a spherical stack of small radius. On the other hand, the bias effect in stacks of more than 20 plates rapidly decreases as the thickness in-

creases, so that in a stack of 40 plates the decay events taking place in the surface plates are unbiassed (with $P = 0.50$ over the complete Dalitz circle), though there is still a small effect on decays occurring near the middle of the stack.

The effect of bias on the ϑ distributions is very much smaller than that on the energy spectra. While the latter in a stack of twenty plates results in changes of about 30-50%, the former are subject to errors of at most 5%, which are not of practical importance at present. We shall therefore not discuss the matter further.

The investigation of bias discussed above is intended only as a guide to the order of magnitude of the effects to be expected, and for this reason we have throughout used the conveniently tabulated range-energy curves of Fay, Gottstein and Haynes, although they are known to give ranges which are too large for high energy π-mesons. We have, in addition, completely neglected the effect of scattering. When this is taken into account, there is no meaning in saying that the selected events are completely bias-free, for there is a finite probability that the secondaries deviate sufficiently from the decay plane to allow them to leave the stack, even though the event was classified as bias-free. An estimate of the importance of this effect may be obtained from a consideration of the root mean square of the distance, d, of the stopping point of a π-meson from its original line of motion. $\sqrt{\langle d^2 \rangle}$ is a function of the range and may be calculated from the formulae given by ROSSI and GREISEN [9]. Using for the range energy relation a simple power law, and integrating the diffusion equation for variable energy, one finds

$$\sqrt{\langle d^2 \rangle} \approx 0.145 R^{0.95} ,$$

where R is the range expressed in mm. Thus the standard limit for deviations from the original line is approximately a cone of half angle 7°; a π-meson will stop within this cone with a probability of $\frac{2}{3}$. The effective direction of the secondary tracks is thus rather well defined, so that scattering will only affect the comparatively rare decay planes which lie very close to that of the emulsion strips. We may thus safely neglect the effect of scattering.

Another possible source of error in the above treatment is the assumption that the probability of a decay configuration occurring is independent of the orientation of the decay plane in the laboratory system. This condition might be violated if the τ-meson beam were partially or completely polarized. However, no evidence for polarization of the stopped τ-mesons has ever been found, and even if it existed to some small degree, it would appear most

---

[9] B. ROSSI and K. GREISEN: *Rev. Mod. Phys.*, **13**, 240 (1941).

directly in the orientation of the decay plane, and only in the second order affect the decay configuration. Thus, while it might alter to some extent the calculated bias curves, it would have a very much smaller effect on the selection of bias-free events.

Finally, it should be emphasized that we have only dealt with the geometric bias. Any possible scanning bias is very much more difficult to evaluate. In this respect, there should, however, be considerable advantages in the use of machine exposed plates in which the density of K-events in the scanned regions is very high compared with the background of star-like events. It is therefore rather difficult to imagine that τ-meson decays can be overlooked or misinterpreted in the conditions usually met with in track or end-point scanning for K-mesons. If, however, some configurations are sometimes lost in scanning, it is possible to say that the loss will be a function of the velocities and angles of the secondaries, and that it will therefore have the same symmetry properties in the Dalitz diagram as the geometric bias function. Thus, one may conclude, for the classes $(+\,+\,-,\ +\ -,\ +\,+)$ and $(+\,+\,-)$, that any significant deviation of the mean energy $\langle E_{\pi^-} \rangle$ from $Q/3$ can only mean that the density of decay probabilities within the Dalitz circle is non-uniform, and can be due to neither geometric nor scanning bias.

3. – Experimental Results.

In this laboratory, 75 examples of τ-meson decay have been found in 15 plates (26-40) of the « K_1 » stack, which was exposed to the magnetically analyzed K^--beam of the Berkeley Bevatron during the summer of 1955. The majority of these events were found in the course of an area scan for the decays of stopped K-mesons, in the appropriate region of the plates, but the 18 events in the « *b* » half of the stack were found by track scanning. In addition, 17 events, in plates 26-30*a*, were found by a special scan for τ-meson events.

During the course of the work we had in our possession plates 1-40, but, due to damage, plates 1 and 2 were not suitable for following through. In addition, we were able to borrow plates 41-45*a* from the group at Saclay; thus the effective number of emulsion thicknesses available was 43 for the 57 events in the « *a* » half of the stack, and 38 for the 18 events in the « *b* » half.

Of the events found, 11 had only one secondary track which stopped in the stack, and 34 were such that only one secondary escaped. All three of the secondaries from a further 30 events were stopped. Events in which only one of the secondaries is stopped are not considered further in the following analysis. Of the remaining 64 events 3 have been eliminated because there were indications of a lack of momentum balance or coplanarity, and one be-

cause it decayed in the surface of an emulsion layer and could not be sufficiently well analyzed. The remaining 60 events, together with the relevant experimental data, are listed in Table II.

The following measurements were made on each event.

1) the ranges of all the secondaries stopped in the stack;
2) angles between the secondaries at the point of decay;
3) angles between the decay plane and the normal to the emulsion surface.

The method of measurement of the angles was such that the direction of each track was measured to within about 2°, the main source of error being in the measurement of the dip. A check on the general accuracy of the experimental data was provided by calculating, for those events in which only two secondaries were stopped, the energy of the escaping track, from the measured angles. The Q-values so obtained were found to have a mean standard deviation of 1.78 MeV, which is in good agreement with that expected from the errors of measurement. The mean Q-value from these events, (74.8 ± 0.3) MeV, is in good agreement with that obtained from events in which all three secondaries were stopped, using the measured ranges only: $Q = (74.9 \pm 0.2)$ MeV. The range-energy curve of BARONI *et al.* [10] was used. All the emulsions were assumed to be exactly 600 μm thick at the time of exposure, and the shrinkage factor was assumed to be two, no attempt being made to calibrate this, or stopping power, more accurately.

The energy used for those secondaries which escaped from the stack was calculated from the Q-value obtained from the events in which all the secondaries were stopped, and the measured ranges of the two secondaries which were stopped. It is this value which is quoted in Table II, and not that obtained from momentum balance. Similarly, in dividing the spectrum into suitable portions for the histogram, and in determining its mid-point, we have used the experimental value of Q, the mid-point then lying at $Q/3$.

Fig. 12 shows the observed spec-

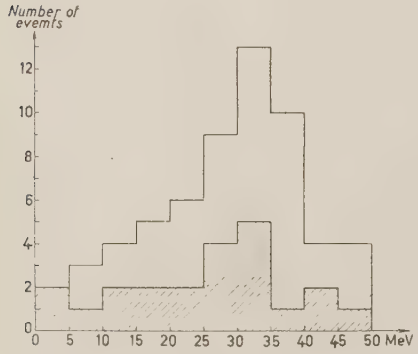

Fig. 12. – The π^--spectrum from the 60 events listed in Table II. The bias-free events are shown shaded.

[10] G. BARONI, C. CASTAGNOLI, G. CORTINI, C. FRANZINETTI and A. MANFREDINI: *CERN. BS9* (1954).

TABLE II.

Event	Plate No.	Ranges (mm)	Signs	Energies MeV	Angles	cos ϑ (×)	Measured non-co-planarity (degrees)	u°	Un-biassed
1	35*a*	12.36	—	26.7	112.8	0.248	0.2	36	no
		13.23	+	27.7	112.2				
		6.36	+	17.9	134.8				
2	34*a*	18.39	—	33.7	100.8	0.174	1.0	14	yes
		10.65	+	24.3	124.1				
		6.12	+	17.5	135.1				
3	34*a*	14.34	—	29.0	114.1	0.355	1.6	74	no
		15.23	+	30.0	107.2				
		5.04	+	15.65	138.7				
4	34*a*	17.45	—	32.6	102.8	0.129	6.4	21	yes
		10.12	+	23.7	122.3				
		6.86	+	18.7	134.7				
5	33*a*	7.27	—	19.4	164.2	1.000	1.1	22	yes
		32.86	+	48.0	24.4				
		1.67	+	8.34	171.5				
6	33*a*	18.20	—	33.4	104.0	0.719	3.2	28	yes
		18.32	+	33.6	100.0				
		0.99	+	6.16	156.1				
7	33*a*	16.95	—	32.0	109.4	0.550	0.9	56	no
		18.04	+	33.2	104.6				
		2.67	+	10.9	146.3				
8	33*a*	11.60	—	25.5	131.1	0.767	0.6	58	no
		24.18	+	39.9	73.9				
		1.75	+	8.58	155.1				
9	33*a*	19.33	—	34.7	94.7	0.088	0.9	27	yes
		8.92	+	21.9	131.1				
		6.68	+	18.5	134.8				
10	32*a*	11.39	—	25.2	130.5	0.705	6.1	19	yes
		23.61	+	39.1	77.8				
		2.41	+	10.3	151.4				
11	32*a*	22.26	—	38.0	85.5	0.179	0.6	84	no
		8.93	+	21.9	136.3				
		4.97	+	15.5	138.2				

(×) Calculated as $\cos\vartheta = \dfrac{|p_2^2 - p_1^2|}{p_3\sqrt{2(p_1^2+p_2^2) - p_3^2}}$.

TABLE II (*continued*).

Event	Plate No.	Ranges (mm)	Signs	Energies MeV	Angles	cos ϑ (×)	Measured non-co-planarity (degrees)	u^0	Un-biassed
12	31*a*	17.17	—	32.2	115.7	0.850	1.8	62	no
		23.08	+	38.8	80.0				
		0.51	+	4.22	164.2				
13	31*a*	0.12	—	1.87	168.5	0.346	2.9	12	yes
		23.65	+	39.1	78.8				
		19.01	+	34.3	113.1				
14	31*a*	19.38	—	34.8	100.4	0.690	1.3	31	yes
		18.95	+	34.3	107.9				
		1.25	+	7.07	151.4				
15	31*a*	21.35	—	37.0	90.4	0.835	2.8	67	no
		19.34	+	34.8	108.9				
		0.36	+	3.48	160.8				
16	38*a*	5.65	—	16.7	140.2	0.690	2.2	51	no
		25.60	+	41.1	73.9				
		4.91	+	15.5	146.1				
17	31*a*	18.14	—	33.4	112.2	0.190	6.5	69	no
		10.86	+	24.8	119.5				
		5.91	+	17.3	128.1				
18	31*a*	20.44	—	35.9	92.7	0.520	1.0	25	yes
		14.87	+	29.8	115.3				
		2.25	+	9.9	151.9				
19*	30*a*	16.64	—	31.8	101.1	0.466	1.6	62	no
		15.15	+	30.0	112.8				
		3.10	+	11.8	146.3				
20*	30*a*	5.95	—	17.2	137.9	0.550	2.1	39	no
		23.67	+	39.2	82.7				
		6.61	+	18.4	139.4				
21*	30*a*	13.55	—	28.0	116.2	0.360	7.0	29	yes
		16.29	+	31.3	105.5				
		5.49	+	16.5	137.9				
22*	28*a*	25.40	—	41.0	77.1	0.746	4.2	23	yes
		14.65	+	30.0	123.12				
		0.71	+	5.1	159.9				

TABLE II (*continued*).

Event	Plate No.	Ranges (mm)	Signs	Energies MeV	Angles	cos ϑ (×)	Measured non-co-planarity (degrees)	u°	Un-biassed
23*	26*a*	3.31	—	12.3	143.8	0.473	1.6	70	no
		23.85	+	39.4	84.4				
		10.04	+	23.4	131.8				
24*	26*a*	16.24	—	31.3	104.4	0.154	2.4	63	no
		10.95	+	24.9	124.7				
		6.81	+	18.6	130.8				
25	32*b*	30.68	—	46.0	34.3	0.112	2.0	6	yes
		4.72	+	15.0	161.4				
		3.70	+	13.1	163.7				
26	31*b*	31.91	—	47.1	12.4	0.236	0.8	65	no
		4.55	+	14.8	171.4				
		3.24	+	12.2	175.7				
27	29*b*	11.86	—	25.9	130.5	0.614	1.4	27	yes
		21.50	+	37.0	85.5				
		3.11	+	11.9	143.8				
28	27*b*	3.39	—	12.5	158.0	0.863	0.6	20	yes
		30.37	+	45.8	45.6				
		5.48	+	16.5	156.1				
29	30*b*	27.27	—	43.0	63.9	0.631	1.5	88	no
		12.10	+	26.2	131.7				
		1.28	+	7.16	164.4				
30*	28*a*	10.37[a,c]		24.0	128.8	0.600	2.0	55	no
				< 25.2					
		19.53	+	35.0	82.7				
		2.88[d,f]		> 11.4	148.4				
31	38*a*	7.61	—	19.9	145.2	0.718	0.1	69	yes
		3.77	+	13.3	149.1				
		—	(+)	41.7	69.7				
32	38*a*	10.36	—	23.9	125.7	0.049	2.5	42	yes
		12.28	+	26.4	116.7				
		—	(+)	24.6	117.2				
33	38*a*	20.19	—	35.7	98.0	0.558	1.5	62	no
		1.93	+	9.05	148.8				
		—	(+)	30.1	113.4				

TABLE II (*continued*).

Event	Plate No.	Ranges (mm)	Signs	Energies MeV	Angles	cos ϑ (×)	Measured non-co-planarity (degrees)	u^0	Un-biassed
34	38*a*	—[i]	(−)	45.9	45,2	0.103	0.1	40	no
		3.88	+	13.5	159.9				
		4.90	+	15.5	155.1				
35	38*a*	10.26	—	23.7	118.0	0.091	1.5	56	no
		10.28	+	23.7	125.3				
		—	(+)	27.5	116.9				
36	38*a*	—	(−)	40.1	72.9	0.442	1.6	50	yes
		2.35	+	10.1	154.2				
		10.96	+	24.7	133.1				
37	38*a*	19.42	—	34.8	101.7	0.560	1.5	72	no
		2.00	+	9.25	150.8				
		—	(+)	30.8	108.1				
38	36*a*	1.80	—	8.70	162.4	0.728	0.1	31	no
		9.27	+	22.3	147.3				
		—	(+)	43.9	50.4				
39	36*a*	—	(−)	25.7	120.1	0.314	0.3	89	no
		16.04	+	31.0	111.1				
		6.50	+	18.2	130.2				
40	35*a*	0.60	—	4.63	160.6	0.236	1.6	11	yes
		17.33	+	32.5	113.3				
		—	(+)	37.8	85.8				
41	35*a*	23.61	—	39.2	72.1	0.551	0.3	88	no
		1.69	+	8.40	155.8				
		—	(+)	27.3	132.1				
42	35*a*	—	(−)	45.2	45.0	0.619	1.9	31	no
		1.56	+	8.00	162.6				
		8.79	+	21.7	152.5				
43	34*a*	—	(−)	40.9	71.0	0.396	1.1	69	no
		9.87	+	23.2	136.1				
		2.65	+	10.8	152.1				
44	32*a*	8.57	—	21.3	124.0	0.099	0.9	63	no
		14.10	+	28.7	114.2				
		—	(+)	24.9	121.9				

TABLE II (*continued*).

Event	Plate No.	Ranges (mm)	Signs	Energies MeV	Angles	cos ϑ (×)	Measured non-co-planarity (degrees)	u^0	Un-biassed
45	32*a*	3.45	—	12.6	165.5	0.935	2.1	32	yes
		4.78	+	15.2	165.5				
		—	(+)	47.1	29.2				
46	31*a*	—	(−)	39.4	85.0	0.099	3.3	65	no
		7.28	+	19.4	133.6				
		5.25	+	16.1	141.4				
47	31*a*	0.77	—	5.35	173.2	0.905	3.3	25	yes
		10.41	+	24.0	170.1				
		—(6)	(+)	45.5	15.4				
48*	29*a*	—	(—)	38.4	83.2	0.421	6.1	56	no
		2.71	+	11.0	145.4				
		11.67	+	25.5	131.2				
49*	29*a*	11.02	—	24.8	120.5	0.004	0.3	77	no
		11.28	+	25.1	117.6				
		—	(+)	25.0	122.1				
50*	29*a*	—	(—)	28.5	123.7	0.729	2.0	25	yes
		22.61	+	38.2	83.2				
		1.62	+	8.20	154.2				
51*	28*a*	—	(—)	37.1	89.3	0.569	0.5	83	no
		14.52	+	29.2	120.1				
		1.74	+	8.55	150.2				
52*	28*a*	10.10	—	23.5	124.9	0.373	1.8	28	yes
		6.47	+	18.2	133.9				
		—	(+)	33.2	101.4				
53	38*b*	—	(—)	39.6	79.9	0.870	0.5	82	no
		17.42	+	32.6	111.8				
		0.23	+	2.70	167.6				
54(§)	35*b*	24.1	—	39.6		0.984			
		0.012	+	0.47	176.8				
		—	(+)	34.8					
55	35*b*	—	(—)	33.6	101.4	0.657	4.0	39	no
		18.28	+	33.6	105.0				
		1.47	+	7.70	153.4				

TABLE II (*continued*).

Event	Plate No.	Ranges (mm)	Signs	Energies MeV	Angles	cos ϑ (×)	Measured non-co-planarity (degrees)	u^0	Unbiassed
56	34*b*	12.74	—	27.0	116.7	0.119	2.9	67	no
		8.75	+	21.6	123.10				
		—	(+)	26.3	120.3				
57	32*b*	6.06	—	17.4	155.6	0.815	1.6	62	no
		3.77	+	13.3	154.6				
		—	(+)	44.2	46.8				
58	32*b*	4.45	—	14.6	142.3	0.461	1.3	89	no
		8.97	+	21.9	135.0				
		—	(+)	38.4	82.9				
59	26*b*	—(*i*)	(—)	32.0	104.2	0.680	0.4	61	no
		19.73	+	35.1	102.2				
		1.50	+	7.80	153.8				
60	26*b*	1.11	—	6.60	156.2	0.032	1.1	77	no
		19.22	+	34.5	101.6				
		—	(+)	33.8	102.2				

(*) Found by a special scan for τ-mesons.
(*i*) Secondary interacts in flight. (*ss*) Single scatter $\approx 150°$. (*df*) Decay in flight.
(§) Previously published by N. BRENE: *Nuovo Cimento*, **3**, 1140 (1956).

trum of the π^--mesons. All the data listed in Table II are used, for, as shown in the preceding section, under our experimental conditions, the bias is expected to be small. The corresponding distribution in cos ϑ is plotted in Figure 13. The data corresponding to the 21 events in our bias-free sample, chosen according to the criteria discussed above, are shown shaded in both diagrams.

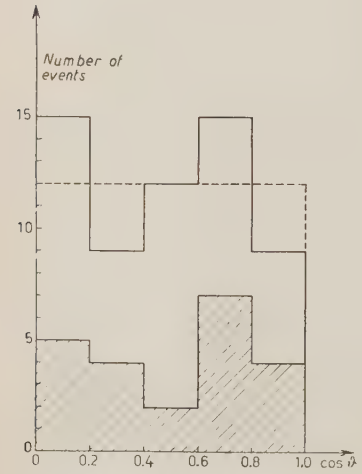

Fig. 13. – The ϑ distribution of the 60 events listed in Table II. Unbiassed events are shown shaded.

4. – Comparison with Other Experiments.

As mentioned above, the effect of geometric bias on the ϑ-distribution is small and events from class (·) are completely unbiassed, provided that the ϑ-distribution is independent of the distribution in energy. Fig. 14 shows the collected ϑ-distribution from 399 analyzed events (Berkeley [11]) 100, Göttingen [12]) 87, Bristol [8]) 61, Copenhagen 60, M.I.T. [13]) 54, Bristol [14]) 37). This distribution suggests isotropy, as do all the results from the individual experiments, and we therefore concentrate our interest on the distributions relevant to the two spin-parity combinations 1^+ and 0^-. That the other three spin-parity combinations need not be considered may be seen from the fact that a χ^2 test leads to a Pearson probability of 10^{-10} for 3^-, which lies nearest the observed distribution. The corresponding theoretical spectra of the π-mesons differ primarily in their symmetry properties. For this reason we introduce a symmetry parameter k defined by the relation $k = n/N$, where n is the number of particles in the spectrum with energy greater than $Q/3$, and N is the total number of particles. The theoretically predicted values of k are 0.50 from 0^- decay and 0.71 from 1^+ decay. These values might be slightly altered in a relativistic treatment.

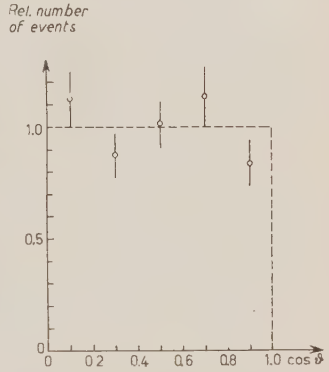

Fig. 14. The collected ϑ distributions from 5 different experiments. 399 events are included.

The values of k found in 7 different experiments are compared in Fig. 15. Results up to and including those published in the Report of the Pisa Conference (1955) are omitted because most of the events were found in small stacks and are therefore expected to be strongly biassed, (Table III). Neither are the results of Bhowmik *et al.* [8]) discussed, because these authors selected their events from class (—) in a small stack. In all 7 experiments are used data from the analysis of decays with at least two stopped π-mesons.

---

[11]) R. P. Haddock: *UCRL* - 3284.

[12]) N. N. Biswas, L. Ceccarelli-Fabbrichesi, M. Ceccarelli, K. Gottstein, N. C. Varshneya and P. Waloschek: *Nuovo Cimento*, **3**, 825 (1956).

[13]) B. P. Feld, A. C. Odian, D. M. Ritson and A. Wattenberg: *Phys. Rev.*, **100**, 1539 (1955).

[14]) B. Bhowmik, D. Evans, S. Nilsson and D. J. Prowse: K-2 *Stack Collaboration Report* (preprint).

TABLE III. – *Effect of geometric bias on the expected value of k. Values of k are given for stacks of two thicknesses on the assumption that the events are chosen from the class* $(+\,+-,\ +-,\ ++)$.

Spin and parity of τ	40 plates		20 plates	
	value of k for τ-decays near the			
	edge *	middle	edge	middle
0	0.500	0.485	0.482	0.450
1	0.712	0.694	0.689	0.676

(*) Unbiassed.

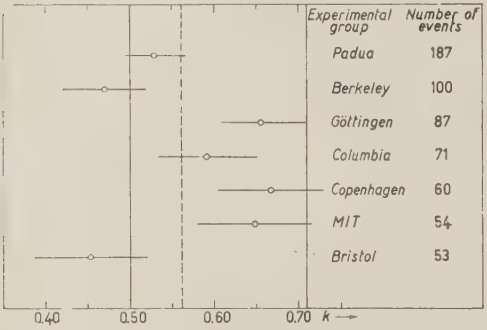

Fig. 15. – The experimental values of

$$k\left(=\frac{\text{(number of events with } E_{\pi^-} > Q/3)}{\text{total number of events}}\right)$$

obtained by a number of different laboratories. The theoretically predicted values for 0 and 1 are drawn in full lines, and the weighted mean of all the results appears as adotted line.

Assuming a binomial distribution of n, the r.m.s. deviation on k is

$$\sqrt{\langle \Delta k^2 \rangle} = \sqrt{p(1-p)}\,\frac{1}{\sqrt{N}},$$

where p is the probability that the π^--meson from a particular decay is emitted with an energy greater than $Q/3$. The value of p used in the calculation of errors drawn in the figure is 0.5, which leads to the maximum error $1/2\sqrt{N}$. However, the error is not particularly sensitive to changes in the values of p. For example, we find

$$\sqrt{\langle \Delta k^2 \rangle} = 0.45\,\frac{1}{\sqrt{N}} \qquad \text{for} \qquad p = 0.71.$$

The diagram in Fig. 15 shows that the experimental results are not self-consistent. Although, in this situation, the weighted mean has no well defined meaning, we have drawn it dashed on the figure to emphasize the degree of inconsistency; of the seven points only two lie within one standard deviation from the mean. In fact, the points appear to fall in two relatively well defined groups, one being consistent with a mean value of $k = 0.50$, and the second with a mean value of $k = 0.64$. If the true value of k is 0.50, the probability of finding a fluctuation as large as that represented by the latter group

is $\approx 10^{-4}$. It is therefore necessary to look for errors in the different experiments.

The lowest point in the $k = 0.5$ group is that from Bristol [11]. The authors themselves point out that their grain density in their plates was so low that it was impossible to carry out any experiments on K-meson secondaries, due to the danger of missing them in scanning. If some of the τ-mesons with have two fast secondaries are classified as τ' or χ decays, the resulting bias on the experimental results will be similar to that in the spherical stack discussed above. This bias leads not only to a lower value of k, but also to the absence of π -mesons of very low energy. The fact that they have only 1 π^--meson with energy less than 10 MeV out of 53 tends to confirm this suspicion. It should be remarked, however, that the authors themselves do not believe that events with two high energy secondaries are missed; they assume that there may be a tendency to lose some of those events in which the secondary energies are approximately equal. (Prowse, private communication). They stress that such an effect would not seriously affect the π -spectrum, if the distribution within the Dalitz circle is uniform, but it would cause a considerable loss of events with $\vartheta \approx \pi/2$.

The account published of the Berkeley [11] experiment does not enable one to obtain an estimate of the bias. The fact that events were taken from three different stacks suggests either that the stacks individually were small or that only a small proportion of the useful events in each stack was used. No evidence is presented to show that a selection, if made, was unbiassed.

Very little is know about the Padua [15] experiment for it has not yet been published. Our information is based on copies of the experimental data presented at the Rochester Conference 1956.

With respect to the other four experiments it is known that all events found were analyzed if possible. Moreover, there was no geometric bias on three [12,13,16] of them, while on our own it is known to be small. If a correction were made on our results it would increase the k-value by about one per cent. It is perhaps worth recalling that any small bias due to the loss of fast tracks in scanning or by interaction would tend to lower the experimental value of k.

Another test for consistency with the theoretical 0- distribution is provided by the fact that for this distribution the mean π -energy, $Q/3$, will not be altered by the effect of any bias which is symmetric in the three π-energies. This is also true in a relativistic theory. The experimental mean values of E_{π^-} and $Q/3$ from the 4 experiments at Göttingen, Columbia, M.I.T. and

---

[15] Padua Group: private communication.

[16] J. Orear, G. Harris and S. Taylor: *NEVIS* - 23.

Copenhagen are

$$E_{\pi^-} = (27.6 \pm 1.7) \text{ MeV} ; \qquad \langle Q/3 \rangle = 24.8 \text{ MeV} .$$

This is a very insensitive test for deviations from the 0 -distribution, but it is independent of any bias which might have affected the values of k. Although not statistically significant, the observed deviation gives some support to the evidence from the k-value that the distribution in the Dalitz circle is non-uniform. On the other hand the absence of a deviation would not be evidence for a uniform distribution.

Of particular interest is the behaviour of the spectrum at very low energies. In Table IV are set out the observed numbers of low energy π -mesons. The numbers expected on the assumption of 0^- and 1^+ are also included.

TABLE IV.

	Total No.	Energy observed		Expected No.	
		range	No.	0^-	1
Berkeley [11]	100	0–10 MeV	7	14.3	3.5
Bristol [14]	53	0–10 MeV	1	7.6	1.9
Padua [16]	187	0 8 MeV	19	19.5	3.9
	340		27	41.4 + 6.0	9.3 + 4.8
Göttingen [12]	87	0 8 MeV	4	9.0	1.8
Columbia [15]	71	0–10 MeV	13	10.2	2.5
M.I.T. [13]	54	0– 8 MeV	2	5.6	1.1
Copenhagen	60	0–10 MeV	5	8.6	2.1
	272		24	33.4 + 5.3	7.5 - 4.3

Here again we find evidence for a divergence from the theoretical 0^- distribution and it is worth pointing out that in this respect the two groups of experiments are consistent.

5. – Conclusions.

A consideration of the ϑ-distributions shows that the theoretical predictions for 1^-, 2^+ and 3^- can be strongly excluded, whereas that for $(0^-, 1^+)$ is in good agreement with all the experimental results.

The π -spectra, on the other hand, from the different experiments are not consistent. However, there is evidence that the degree of asymmetry of the spectrum is between that expected from theory for 0^- and 1^+. That

there is a deviation from theory is supported by evidence from the low energy end of the spectrum. In this situation it is difficult to believe that the present theoretical approach is sufficient, and as a consequence, it would not seem possible at present to determine the spin of the τ-meson from the experimental decay distribution. In particular, we would point out that it is not very promising to make a χ^2 test in order to find out to which of the theoretical spectra the observed one lies nearest.

The vital points at the present time are the experimental determination of the spectrum and the explanation of the present inconsistencies. If any success is to be had in this project it is necessary that published results should include as much information as possible on the experimental conditions.

So far we have considered only those spin-parity combinations for which the Dalitz-Fabri theory predicts the spectra uniquely; the other distributions depend upon free parameters, which implies that an eventual fit is not significant. It is in fact very difficult to exclude any particular spin-parity on the basis of the experimental distributions. MARSHAK [17], for example, has shown that a comparatively simple change in the basic assumptions of the Dalitz theory can lead to distributions for a 2^+ - τ-meson which are not very different from those observed experimentally.

* * *

Our special thanks are due to Professor POWELL who arranged the exposure and development of the plates. We are also indebted to the Bevatron Group at Berkeley who exposed the plates and to the group of Saclay for the loan of plates 41-45. We gratefully acknowledge the hospitality extended to us by Professor NIELS BOHR and the continued encouragement and interest which we have received from Professors J. K. BØGGILD and AAGE BOHR. A very considerable contribution to this work was made by our team of scanners.

[17] MARSHAK: private communication.

RIASSUNTO (*)

Si discutono i risultati dell'analisi dei decadimenti di 75 mesoni τ arrestati, trovati in un pacco di emulsioni esposte al Bevatrone di Berkeley. Si presta speciale attenzione agli effetti delle dimensioni finite del pacco e si fa una breve analisi del problema. Si confrontano i risultati sperimentali con quelli ottenuti in altri laboratori e gli autori concludono che non si hanno prove convincenti che lo spettro dei mesoni π derivanti dal decadimento dei τ sia d'accordo con alcuno di quelli previsti per le due più basse combinazioni spin-parità: 0^- e 1^+.

(*) *Traduzione a cura della Redazione.*

Actions chimiques des ultrasons sur l'eau et les solutions aqueuses.

M. Haïssinsky et A. Mangeot

Institut du Radium et Faculté de Pharmacie - Paris

(ricevuto il 27 Luglio 1956)

Resumé. — On a étudié la formation de l'eau oxygénée et l'oxydation de divers composés minéraux sous une atmosphère d'oxygène et d'argon. On introduit une unité U qui permet d'exprimer les transformations sono-chimiques en grandeurs relatives et de comparer leurs rendements sous diverses conditions. La présence de l'oxygène n'est pas indispensable aux actions oxydantes des ultra-sons ni à la formation de H_2O_2. Celle-ci est notablement influencée par la présence d'électrolytes neutres. On relève de nouvelles analogies entre les effets chimiques des ultrasons et ceux des rayons α.

1. – Introduction.

Malgré le nombre relativement déjà grand des recherches en chimie ultrasonique, cette jeune science porte encore un caractère essentiellement semi-quantitatif, sinon qualitatif. Les difficultés de mesures quantitatives et cinétiques sont sans doute dues, en premier lieu, au fait qu'on ne voit pas bien comment lier les transformations chimiques à l'acte physique qui les provoque et caractériser celui-ci par des grandeurs d'énergie et d'intensité qui soient en rapport avec les processus chimiques. Ceux-ci se produisent, en effet, en même temps et en relation directe ou indirecte avec toute une conjugaison d'actes physiques: excitation piézo-électrique, propagation sonore, compression et dilatation rythmiques du liquide de cavitation avec formation et destruction de bulles gazeuses, phénomènes de luminescence, électriques et thermiques qu'impliquent ces modifications de phases et d'interfaces, etc.

Il n'est pas alors très étonnant que non seulement le mécanisme des effets sono-chimiques reste encore très obscur, mais que parfois les auteurs ne soient pas d'accord sur des faits expérimentaux essentiels, tels que la nécessité de

l'oxygène pour la production de l'eau oxygénée, l'existence d'un effet de température pour cette réaction, la formation d'ozone dans une atmosphère d'oxygène, etc. (1). En faisant varier apparemment un seul facteur physico-chimique, par exemple la température, on risque en effet, de faire varier en même temps d'autres facteurs, comme l'intensité du champ ultrasonore ou la solubilité du gaz (2), et ceci d'une façon parfois difficilement comparable, si les conditions expérimentales ne sont pas rigoureusement identiques.

Cependant certaines analogies entre les effets ultrasonores et les actions chimiques des radiations ionisantes (3-5) ont amené divers auteurs à rapprocher les uns des autres et à considérer avec FRENKEL (6) les premiers effets comme conséquence de petites décharges électriques produites en relation avec la cavitation. D'autres théories attribuent ces effets à des élévations locales de température (7), ou à des ruptures mécaniques des molécules du liquide en relation avec la rupture ou les oscillations de résonance des bulles gazeuses (8,9). Mais il semble que tous les auteurs soient d'accord pour considérer les *actions* sur les solutés comme *indirectes*, se produisant par l'intermédiaire des fragments du solvant, d'où la nécessité de connaître en premier lieu les transformations que subit celui-ci. Etant donné les difficultés de doser des micro-quantités des produits gazeux (H_2 et O_2) qui se forment dans l'eau ultrasonnée en présence de l'atmosphère gazeuse nécessaire pour la cavitation, l'étude de ces transformations se ramène jusqu'ici au dosage de l'eau oxygénée produite sous différentes conditions. D'autre part, de même qu'en chimie des radiations, on peut obtenir indirectement des renseignements importants sur le mécanisme des réactions en examinant l'influence de la composition chimique, de la concentration, de la nature de l'atmosphère gazeuse et d'autres facteurs cinétiques sur cette production et sur les phénomènes d'oxydo-réduction en solution ultrasonnée.

C'est en partant de ces considérations que nous avons entrepris une étude systématique sur les transformations de l'eau et des solutions aqueuses soumises aux ultrasons, dont nous allons décrire ici quelques résultats préliminaires.

(1) Pour la bibliographie, voir notamment, *a*) L. BERGMANN: *Der Ultraschall* (Zürich, 1954); *b*) O. LINDSTRÖM: *Journ. Acoust. Soc. Amer.*, **27**, 654 (1953); *c*) H. SCHICK: Wisc-2-AEC- 2 (1951).

(2) A. DOGNON et Y. SIMONOT: *Journ. Chim. Phys.*, **50**, 94 (1953).

(3) P. GRABAR et R. PRUDHOMME: *Journ. Chim. Phys.*, **46**, 323 (1939).

(4) M. HAÏSSINSKY et R. PRUDHOMME: *Journ. Chim. Phys.*, **47**, 925 (1950).

(5) N. MILLER: *Trans. Far. Soc.*, **46**, 546 (1950).

(6) I. FRENKEL: *Acta Physico-chim. URSS*, **12**, 317 (1940).

(7) Par exemple, F. BOWDEN et A. YAFFÉ: *Research*, **1**, 581 (1948).

(8) A. WEISSLER et H. COOPER: cité en référ. (1b).

(9) W. WEYL et E. MARBOL: *Research*, **2**, 19 (1949); *Journ. Appl. Phys.*, **21**, 937, (1950).

2. - Dispositif et conditions expérimentales.

L'appareil utilisé est un émetteur piézo-électrique SCAM, dont le projecteur est muni d'un quartz de 3 mm et la fréquence est de 960 kHz. La puissance acoustique totale est de 75 W environ, lorsqu'on opère avec de l'eau pure. Les expériences ont été conduites soit avec de l'oxygène, soit avec de l'argon comme gaz de remplissage. Afin de saturer par le gaz voulu la solution, on soumettait celle-ci, traversée continuellement par un courant du gaz, à une ébullition prolongée, avec une réfrigération à reflux, suivie d'un rapide refroidissement. Le liquide ultrasonné, de 50 cm^3 de volume, se trouvait dans une éprouvette en pyrex, à col allongé, dont le fond était fermé par une membrane *pliofilm* (caoutchouc chloré, 3,5 mg/cm^2), perméable aux ultrasons et imperméable au gaz. Nous avons vérifié l'efficacité de cette technique et en même temps l'étanchéité de la membrane en polymérisant, sous argon par les ultrasons, l'acrylonitrile en solution aqueuse: la présence de traces d'oxygène par un mauvais dégazage ou par pénétration à travers la membrane de l'air, dont le bain du thermostat était saturé, aurait empêché ou retardé la polymérisation. Les essais ainsi effectués ont toujours montré l'absence d'air.

Les solutions se trouvaient dans un thermostat maintenu à une température voisine de 15 °C, mais dans certaines expériences, celle-ci a été fixée à des valeurs allant jusqu'à 45°. Nous avons pu ainsi nous rendre compte de l'existence d'un effet de température pour la formation de l'eau oxygénée, déjà signalé par SCHICK [1]. On s'est contenté jusqu'ici de mesurer la température du liquide ultrasonné immédiatement après l'irradiation, vu les difficultés que nous avons rencontrées dans la réalisation de mesures continues pendant l'opération. Nous cherchons actuellement à améliorer à ce point de vue notre dispositif, et dans ce qui suit nous allons négliger l'effet de la température en indiquant seulement les résultats obtenus dans un domaine très étroit de celle-ci, de 23 à 27 °C, températures généralement supérieures de 8 à 10 °C à celle du bain extérieur.

Nous reviendrons ailleurs sur les autres détails expérimentaux et sur les méthodes analytiques employées.

En l'absence d'unités énergétiques rationnelles en chimie ultrasonore, nous allons exprimer nos mesures à l'aide d'une unité relative U, définie comme *le rapport entre le nombre des molécules formées ou transformées par unité de temps et par unité de volume au nombre des molécules de* H_2O_2 *formées dans l'eau pure sous oxygène*, toutes autres conditions physiques de marche de l'appareil générateur (fréquence, puissance, température, etc.) étant identiques. Les résultats ainsi exprimés, éventuellement rapportés à l'unité de puissance, permettraient de comparer non seulement les rendements de diverses réactions chimiques réalisées avec le même appareil, mais aussi les valeurs données par divers auteurs pour un corps donné, et même l'efficacité relative de ces réactions comparée à celle des mêmes réactions provoquées par d'autres agents physiques, lumière, radiations ionisantes, etc.

Or, il se trouve que dans les conditions de marche de notre appareil, l'eau

oxygénée se forme sous l'oxygène à 25 °C avec un rendement *horaire* initial voisin de $60 \cdot 10^{16}$ molécules par cm³ (10^{-3} M/l·heure). Nous prendrons celui-ci arbitrairement comme référence; par définition donc $U = 1$ *pour un rendement de* 10^{16} *molécules ou* $2 \cdot 10^{16}$ *équivalents quelconques formés par* cm³ *et par min.* ($2 \cdot 10^{-3}$ g équiv./l·heure). Le plus souvent le rendement diminue avec l'augmentation de la durée de l'expérience et la courbe représentative du nombre des molécules en fonction du temps présente un palier. Nous parlerons alors du rendement relatif initial U_i, déterminé par la tangente à l'origine de la courbe.

Fig. 1. – Formation d'eau oxygénée sous oxygène. ● H_2O; x H_2SO_4; + H_3PO_4; △ $HClO_4$.

3. – Résultats expérimentaux.

3·1. *Formation de* H_2O_2.

a) Eau et acide sulfurique. – Conformément aux résultats de LINDSTRÖM ([1b]), nous avons trouvé sous oxygène le même rendement initial pour l'eau et l'acide sulfurique N. Dans les limites des erreurs expérimentales, celui-ci est constant pendant 1 heure environ: $U_i = 1.2$ (Fig. 1). Pour des durées plus grandes, le rendement baisse lentement. Par suite des incertitudes concernant l'effet de température, il est difficile d'affirmer que les rendements sous argon sont les mêmes que sous oxygène ou légèrement inférieurs comme la Fig. 2 le semble indiquer. Il est probable que les coefficients de température soient différents pour la production de H_2O_2 dans les deux gaz.

b) H_3PO_4. – Les rendements initiaux dans H_3PO_4 N (pH voisin de 1) sont encore sensiblement les mêmes que dans les deux milieux précédents (Fig. 1 et 2), mais on note une constance remarquable sous oxygène pendant au moins 3 h.

c) HCl *et* HNO_3. – Ces deux acides, surtout le premier, ont une action

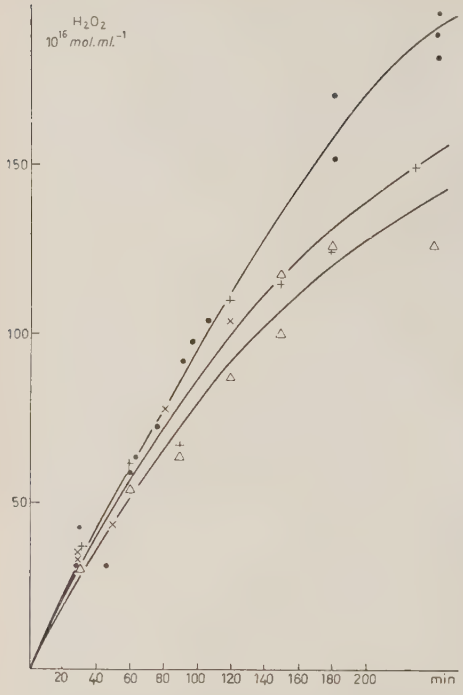

Fig. 2. – Formation d'eau oxygénée sous argon. ● H_2O; x H_2SO_4; + H_3PO_4; △ $HClO_4$.

inhibitrice sur la formation ultrasonore de H_2O_2 (Fig. 3). Dans HNO_3 N sous oxygène $U_i = 0.3$, tandis que dans une solution de HCl N, la formation est complètement annulée sous l'oxygène et atteint sous l'argon à peine $4.6 \cdot 10^{16}$ molécules/cm³ après 2 h. Les rendements après 1 h d'ultrasonation pour les autres concentrations de HCl dans H_2SO_4 N sont donnés ci-après:

Table I. – U.

HCl	Oxygène	Argon
0.2 N	0.07	0.11
0.1 »	0.2	0.12
0.05 »	0.3	0.15
0.025 »	0.4	0.18

Pour toutes les concentrations supérieures à 0.025 N les rendements diminuent rapidement avec le temps et les quantités limites de H_2O_2 formés restent très petites. Celles-ci semblent être plus faibles pour l'argon, si les concentrations de HCl sont inférieures à 0.2 M, tandis que l'inverse se vérifie pour HCl 0.2 N et N.

d) $HClO_4$ N. – Ici encore U_i n'est pas très différent de celui que nous avons mesuré pour les acides sulfurique ou phosphorique, probablement un peu plus faible. Mais on note une baisse sensible du ren-

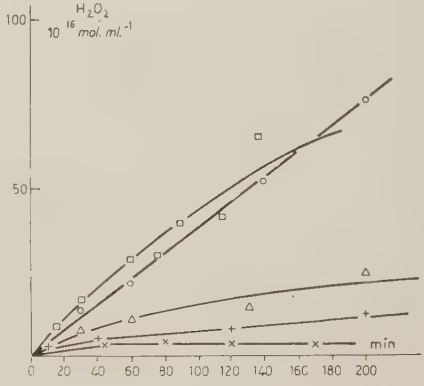

Fig. 3. – Formation d'eau oxygénée. Sous oxygène: □ NHO_3 N; ○ HCl 0.025 N; x HCl 0.2 N. Sous argon: △ HCl 0.025 N; + HCl 0.2 N.

dement avec la prolongation de l'ultrasonation, surtout sous oxygène (Fig. 1). Ceci pourrait s'expliquer par l'action inhibitrice des ions Cl^-, dont nous avons mis en évidence la formation en petites quantités, en même temps que celle de ClO_3. Des résultats analogues ont été signalés pour la décomposition radiochimique des perchlorates [10].

c) Electrolytes neutres. – L'addition de Na_2SO_4 ou de $MgSO_4$ en concentrations comprises entre 1 et 2 *M* favorise nettement la formation d'eau oxygénée dans l'eau ou dans H_2SO_4 N *sous oxygène*. Avec des concentrations plus élevées, le rendement baisse en devenant égal à celui de l'eau pure, dans le cas de $MgSO_4$, pour une concentration 2.5 *M* environ. La baisse est associée à une forte diminution de la solubilité du gaz et de la cavitation, qui se manifeste, aux concentrations très élevées, par la suppression du geyser.

Des concentrations de 0.6 à 1.5 *M* de ces sulfates, qui augmentent encore légèrement le rendement sous oxygène, font diminuer celui-ci considérablement sous argon. La baisse est surtout marquée avec les sulfates de cations polyvalents, comme le tableau suivant le montre (voir plus loin pour l'effet du sulfate ferrique):

TABLE II. – *Rendements d'eau oxygénée après ultrasonation pendant* 1 h *exprimés en* 10^{16} molécules/cm³.

Sous oxygène		Sous argon	
H_2SO_4 N, ...	72	H_2SO_4 N	58
» , Na_2SO_4 1.22 *M* .	108		
» , $MgSO_4$ 1.5 *M* .	100	H_2O, $MgSO_4$ 1.35 *M* . . .	15
» , » 1.65 *M* .	135		
» , $Al_2(SO_4)_3$ 0.11 *M*	72	H_2SO_4 N, $Al_2(SO_4)_3$ 0.11 *M*	23
» , $Th(SO_4)_2$ 0.05 *M*	25	» , $Th(SO_4)_2$ 0.05 *M*	25

Le chlorure de magnésium, comme HCl, est un inhibiteur de formation de H_2O_2.

3·2. *Oxydations.*

a) $FeSO_4$. – MILLER a observé [5] l'oxydation totale de ce sulfate en solution H_2SO_4 0.8 *M* par ultrasonation à l'air. D'après l'auteur, l'oxydation croît linéairement avec le temps (jusqu'à 10 min) et présente un effet de con-

[10] M. COTTIN: *Thèse*, Paris (1956).

centration analogue à celui qu'on rencontre souvent en chimie des radiations: rendement croissant d'abord avec la concentration du sel, puis pratiquement constant.

Nos propres expériences montrent également que l'oxydation est totale sous oxygène et sous argon et qu'elle varie linéairement avec le temps. Pour une solution 10^{-3} M dans H_2SO_4 N, nous avons mesuré dans l'oxygène un rendement de l'ordre $U \cong 3$; dans l'argon $\cong 1.5$ (Fig. 4).

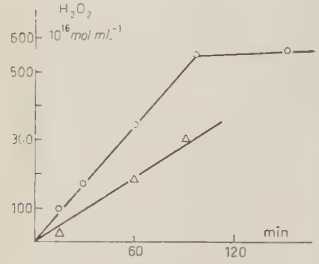

Fig. 4. – Oxydation de $FeSO_4$ 10^{-2} M (H_2SO_4 N). ○ oxygène; △ argon.

Lorsque l'oxydation est terminée, on observe la formation de H_2O_2, mais avec un rendement inférieur à celui qu'on mesure dans l'acide seul, exempt du sel. Il en est de même pour les solutions acides contenant initialement $Fe_2(SO_4)_3 \cdot 10^{-3}$ M: $U_i(O_2) = 1.1$; $U_i(A) = 0.5$. Dans les deux cas il baisse beaucoup plus rapidement avec le temps qu'en l'absence du sel (Fig. 5).

b) Arsénite. – Les solutions d'arsénite de sodium à 10^{-3} M à pH 7.5 sont complètement oxydées tant à l'air que sous argon. Les quantités oxydées croissent dans le premier cas linéairement avec le temps, $U = 0.9$. Le rendement initial semble être plus élevé sous argon, mais ce point demande encore une vérification.

c) H_3PO_3. – L'étude de ce composé nous a paru intéressante, car il n'est pratiquement pas oxydé par l'eau oxygénée. Or nous avons constaté son oxydation totale par les ultrasons. Le rendement est particulièrement élevé sous oxygène: pour une solution 10^{-2} M à pH 3.2, $U_i = 6.7$; sous argon il est au moins quatre fois plus petit. En même temps on observe dans les deux cas la formation d'eau oxygénée et, sous oxygène, d'ozone. Nous avons détecté la présence de ce dernier produit à la fois par l'odeur, par la coloration de la leuco-fluorescéine introduite dans la solution après l'ultra-sonation et par les colorations d'un papier imbibé d'une solution de KI ou de tétrabase (tétra-

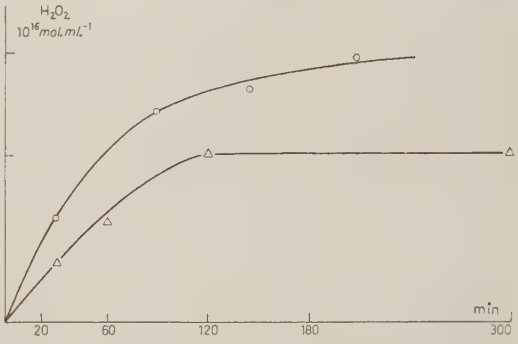

Fig. 5. – Formation d'eau oxygénée en solution de $Fe_2(SO_4)_3$ 10^{-3} M (H_2SO_4 N). ○ oxygène; △ argon.

méthyl-diamino-diphénylméthane) et suspendu dans l'atmosphère d'oxygène au dessus de la solution congélée à — 40 °C.

4. - Discussion.

Malgré le caractère quelque peu fragmentaire de nos résultats, on peut en tirer un certain nombre de conclusions significatives pour le mécanisme des réactions chimiques produites par les ultra-sons, tandis que d'autres points doivent encore être examinés avec plus de soins.

1) Nos expériences montrent définitivement que la présence d'oxygène n'est indispensable ni pour la formation de H_2O_2 ni pour les réactions d'oxydation. Les auteurs qui ont abouti à une conclusion contraire ont sans doute opéré soit avec des gaz qui ne sont pas tout à fait inertes en chimie ultrasonique (N_2, H_2) soit avec des gaz qui ne sont pas favorables à la cavitation (CO_2).

2) Les différences de rendement de production de H_2O_2 sous l'oxygène et sous l'argon ne sont pas considérables et paraissent être du même ordre de grandeur que celles qu'on doit attribuer à l'effet de température. Ce résultat est à rapprocher du comportement des rayons α, qui produisent également H_2O_2 dans les solutions acides désaérées avec un rendement qui est inférieur de 20 % seulement à celui qu'on mesure en présence d'oxygène [11]. On sait, par contre, que la présence de ce gaz est nécessaire pour la production de quantités mesurables de H_2O_2 dans les solutions irradiées par les rayons X ou γ (mais non pour les oxydations). D'autres analogies entre le comportement des ultrasons et celui des particules à ionisation dense, comme les rayons α, ont été déjà signalées précédemment [4].

3) Contrairement à la conclusion de Lindström [13], l'égalité des rendements aux pH 0 et 6 n'est pas un fait commun aux ultra-sons et aux rayons γ. La chute de rendement commence, en effet, dans ce cas déjà aux pH supérieurs à 3 [12]. Elle constitue, par contre, une autre analogie entre les ultrasons et les rayons α. Pour les premiers, Schick a même trouvé [1c] un léger accroissement du rendement en passant de H_2SO_4 0.008 à 0.0001 N, domaine de pH qui n'a pas été exploré avec les rayons α. La baisse du rendement en solution nettement alcaline se produit dans tous les cas.

4) L'oxydation totale de l'arsénite (donc l'absence de réduction de l'arséniate) par les ultrasons représente encore une autre analogie avec les rayons α,

[11] M. Anta: *Thèse*, Paris (1955).

[12] P. Bonet-Maury et M. Lefort: *Journ. Chim. Phys.*, **47**, 179 (1950); A. Koulkès: travail en cours.

qui oxydent aussi totalement ce composé, tandis qu'avec les rayons γ on obtient un état stationnaire, caractérisé par un rapport constant arsénite-arséniate qui dépend du pH, mais est indépendent de la concentration initiale en arsénite et arséniate ([13]).

5) L'oxydation des phosphites est une nouvelle preuve du mécanisme radicalaire, puisqu'ils ne réagissent pas chimiquement avec l'eau oxygénée. Il n'est cependant pas encore clair si les rendement très élevés observés en présence d'oxygène doivent être attribués à une composé en chaîne, comme dans l'oxydation par les rayonnements ionisants ([10]), ou si c'est l'ozone qui intervient ici.

6) Un mécanisme radicalaire, la formation notamment du radical libre OH, permet de comprendre l'action inhibitrice des ions Cl^- et NO_3^- sur la formation de H_2O_2 à l'aide des réactions admises en chimie des radiations et en photochimie :

$$OH + Cl^- = OH^- + Cl$$

$$H_2O_2 + Cl = HO_2 + HCl$$

$$OH + NO_3^- = HO_2 + NO_2^-$$

$$HO_2 + OH = H_2O + O_2$$

$$NO_2^- + H_2O_2 = NO_3^- + H_2O \quad \text{(en solution acide).}$$

L'acide nitreux pourrait se former aussi par décomposition directe de l'acide nitrique et réagir ensuite avec OH :

$$NO_2^- + OH = NO_2 + OH^-$$

$$NO_2 + H_2O_2 = H_2O + NO + O_2$$

7) Le rapport entre les rendements d'oxydation de $FeSO_4$ en présence et en absence d'oxygène est de l'ordre de 2, approximativement égal à celui qu'on connaît pour cette réaction en chimie des radiations.

8) L'effet considérable qu'exercent les électrolytes neutres et apparemment inertes sur la formation de H_2O_2 est assez obscur. Il est très probablement déterminé, du moins en partie, par les modifications de la cavitation qui

([13]) M. HAÏSSINSKY et M. LEFORT : *Journ. Chim. Phys.*, **48**, 429 (1951).

surviennent par la présence de sels: diminution de solubilité, augmentation d'absorption des ultrasons. D'après les mesures de TAMM, citées par BERGMANN ([1a]), cette dernière est très sensible à la valence des ions. Elle est cependant indépendante de la concentration dans le cas des sulfates de cations bivalents, tandis que d'après nos expériences, la formation de H_2O_2 varie nettement avec la concentration de $MgSO_4$. On ne voit pas clairement non plus les raisons du comportement différent des solutions ultrasonnées sous l'argon et sous l'oxygène. La recherche de l'ozone dans le cas des solutions de $MgSO_4$ ultrasonnées sous oxygène montre que ce gaz ne se forme pas ou se forme tout au plus à l'état de traces difficilement détectables et qui ne pourraient expliquer la forte augmentation du rendement en solution 1.65 *M*. Ces facteurs physiques ne sont probablement pas les seuls qui entrent en jeu et nous rappelerons à ce propos que la formation de H_2O_2 dans l'eau irradiée aux réacteurs nucléaires est également affectée par la présence d'électrolytes neutres ([11]).

A l'état actuel de nos recherches, nous croyons qu'il est encore prématuré d'en tirer des conclusions plus générales. Tout au plus nous pouvons dire que les analogies frappantes avec les actions des rayons α sont compatibles avec la théorie déjà mentionnée de Frenkel. Il faudrait alors penser que les électrons de faible énergie formés par des décharges électriques à travers les cavités sont fortement localisés et produisent des densités d'ionisation élevées. On aurait ainsi une distribution de produits radicalaires et moléculaires issus du solvant, analogue à celle des rayons α. On doit cependant noter que la théorie attribuant les effets ultrasoniques à la rupture des cavités prévoit également des concentrations locales élevées des espèces actives.

([14]) M. HAÏSSINSKY et J. PUCHEAULT: *Journ. Chim. Phys.*, **49**, 294 (1952).

RIASSUNTO

È stata studiata la formazione ultrasonica di H_2O_2 e l'ossidazione di vari composti inorganici in una atmosfera di ossigeno e di argon. Si introduce una unità *U* che permette di esprimere in grandezze relative le trasformazioni suono-chimiche e di compararne i rendimenti in varie condizioni. La presenza di ossigeno non è indispensabile alle azioni ossidanti degli ultrasuoni e alla formazione di H_2O_2. Questa è notevolmente affrettata della presenza di elettroliti neutri. Si mettono in rilievo nuove analogie fra le azioni degli ultrasuoni e quelle dei raggi α.

On the Mean Life Time of K-Mesons Produced by the Cosmic Radiation (*).

L. Mezzetti

Palmer Physical Laboratory, Princeton University - Princeton, N. J.
Istituto di Fisica dell'Università - Roma

J. W. Keuffel (+)

Palmer Physical Laboratory, Princeton University - Princeton, N. J.

(ricevuto il 2 Agosto 1956)

Summary. — An experiment performed at Echo Lake (Colorado) in order to measure the mean lifetime of charged heavy mesons produced by the cosmic radiation is described. The experimental procedure consists in the electronic measurement (by means of a « chronotron ») of the time lag between the occurrence of a nuclear interaction and the delayed emission of a fast charged secondary in the decay (at rest) of an unstable particle produced in the interaction. The nuclear event is detected through its penetrating secondaries by means of a large scintillation counter and a Geiger counters hodoscope, whereas the decay secondary is detected by means of a large directional water Čerenkov counter. The experimental arrangement is described in Sect. **2**; the timing errors and the criteria used to select and classify the events are discussed in Sect. **3**. The delay distributions obtained are analyzed in Sect. **4**: they can be resolved into a short life component (lifetime $(9.6 \pm 0.8 \cdot 10^{-9})$ s) and a long life component (lifetime (2.2 ± 0.2) μs); the latter is interpreted as due to the electrons of the composite $\pi \to \mu \to e$ decay of π^+-mesons produced locally by the incident nucleons. The possibility that the short life component is due to spurious effects of some kind is discussed and ruled out in Sect. **5** on the basis of the results of auxiliary measurements: the conclusion is that the lifetime obtained should be associated essentially with the $K_{\mu 2}$ decay mode, with a possible small admixture of $K_{\pi 2}(\theta^+)$. A rough

(*) Sponsored by the joint program of the U.S. Office of Naval Research and the U.S. Atomic Energy Commission.

(+) Now at the University of Utah, Salt Lake City, Utah.

estimate of the production ratio of such particles to positive π-mesons is made, taking into account the corresponding detection efficiencies; the value found is rather higher than those (1:30 - 1:70) obtained from previous cosmic ray experiments. The lifetime obtained is compared with the recent results of other Authors and the assumptions of a purely exponential decay curve with an unique lifetime is discussed.

1. – Introduction.

Experimental knowledge of the properties of K-particles has increased rapidly during the past year, to the point where one may almost venture to state that all the important modes of decay have by now been identified. Each decay mode implies a parent particle of integral spin, and measurements at Berkeley show that the masses of the particles are closely the same. On the other hand, there is good evidence that at least two of the K-particles —the τ and the θ—cannot have both the same parity and the same spin.

The situation, the so-called τ-θ puzzle, lends special interest to mean life measurements on the K-particles, over and above the normal interest in such measurements per se. It is natural to inquire if all the decay modes have the same mean life. Unfortunately, in the present experiment it is possible to sort out the various types of decay only to the extent of stating with certainty that we do *not* detect the τ-decay. Other experiments, particularly those of FITCH and MOTLEY [1] at the Brookhaven Cosmotron, have been more successful in this regard.

On the other hand, the present work affords an independent check on the FITCH and MOTLEY measurements. It also provides a comparison between K-particles produced in the cosmic radiation and those artificially produced at lower energies.

A preliminary report of the experiment appeared in 1954 [2]. Since that time, additional film has been analyzed and an improved evaluation of the background carried out. A complete discussion of the experiment is presented here.

It is gratifying to note that our original interpretation of the decay curve as due to K-particles has been confirmed by the work of BARKER, BINNIE, HYAMS, ROUT and SHEPHERD [3]. These authors used a cloud chamber to

[1] V. FITCH, R. MOTLEY: *Phys. Rev.*, **101**, 496 (1956).

[2] L. MEZZETTI and J. W. KEUFFEL: *Phys. Rev.*, **95**, 858 (1954).

[3] P. R. BARKER, D. M. BINNIE, B. D. HYAMS, R. J. ROUT and J. SHEPHERD: *Phil. Mag.*, **46**, 307 (1955).

make a positive identification of their events (at the expense of a much lower rate than ours) and found a mean life in agreement with ours within the rather large statistical errors.

2. – Experimental Arrangement.

2·1. *General description.* – During the course of the experiment, several different arrangements were used, in order to gather all the information necessary to interpret the results and to correct for the existence of suspected spurious effects of various kinds.

The main arrangement (referred to as « Disposition A » in the following) is shown in Fig. 1. It consists essentially of the scintillation counter S and the two *directional* Čerenkov counters C (water), heavily shielded from all four sides by a 10 cm lead wall, and from above by a « generating thickness » of 20 cm Pb.

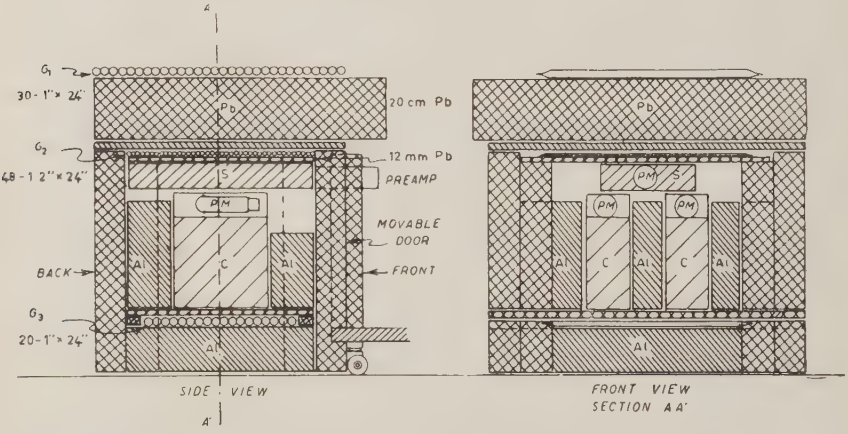

Fig. 1. – Arrangement of counters and absorbers (disposition A); for a top view see Fig. 3.

The lead house is lined almost completely with aluminium bricks, so that the Čerenkov counters are embedded in Al, 10 cm to 15 cm thick, according to the internal geometry of the lead house. It was thought that less back-scattering would occur in aluminium than in lead. G_1, G_2 and G_3 are Geiger counter trays; each counter in tray G_2 (48 counters $\frac{1}{2}'' \times 24''$) and in tray G_3 (20 counters $1'' \times 24''$) and each group of three adjacent counters in tray G_1 (30 counters $1'' \times 24''$) are connected to a neon bulb through an 80 channel hodoscope. A thin layer of Pb (~ 12 mm) is inserted below counter tray G_2, in order to prevent the latter from being triggered by delayed electrons from

$\mu \to e$ or $\pi \to \mu \to e$ decays happening inside the C-counters. This layer also prevents a knock-on electron from a fast μ-meson from *both* triggering a G_2 counter and contributing to a large S-pulse.

The outputs of the two C counters are suitably mixed; the C-pulse and the S-pulse are then fed, through fast amplifier chains, into a 17 channel, chronotron type timing device ([4]). The width of each delay channel is 3.1 ns (*); by means of auxiliary electronics we also measure delays in the μs range, from about 0.1 μs to ~ 8 μs.

The triggering requirements are very loose: at least two counters discharged in tray G_2, and a pulse in both S and C, satisfying certain pulse height and rise time requirements.

In addition to the counters shown in Fig. 1 there were two large « extension (E) trays » connected to two additional neon bulbs in the hodoscope panel. On the basis of the hodoscope information we were thus able to single out the events in which either one of the E-trays and/or more than one group of counters in tray G_1 appeared to have been discharged (see Sect. 4·1).

This arrangement was designed to select events of the following type (Fig. 2). A high energy nucleon of the cosmic radiation produces in the generating layer of Pb a nuclear interaction in which π-mesons and possibly K-mesons are produced. Some of the shower particles traverse the scintillation counter S, giving a pulse at time zero; some of them will also cross the Čerenkov counter in the *downward direction*, but as the counter is (ideally) sensitive only to particles traveling *upwards*, they will not give rise to a C-pulse. A slow charged unstable particle produced in the same interaction may come to rest near or inside one of the C-counters, and there decay into an *upward-going* fast secondary, which *is* detected in C. The time lag between the S-pulse and the C-pulse can then be measured, and the delay distribution obtained analyzed in terms of one or more exponentials.

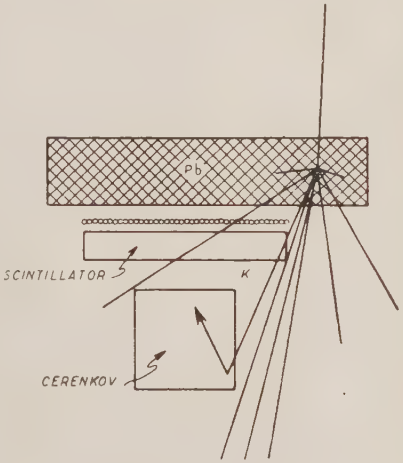

Fig. 2. - Sketch of a typical event selected by the counter arrangement of Fig. 1. The decay of the K-particle can happen also in the material surrounding the Čerenkov counter.

(*) Following the international system of symbols and abbreviations recommended by the IUPAP we use the name and notation 1 nanosecond = 1 ns for 1 mμs = 10^{-9} s.

Both the directional and velocity threshold properties of the Čerenkov radiation are eploited in order to reduce the chance of the C-counter being triggered at time zero, either by the shower particles or possibly by the slow products of secondary nuclear interactions taking place inside or near the counter itself. This zero time pulse would make the detection and timing of the following, often much smaller pulse exceedingly difficult, and the measurement would probably be open to sources of error that would be very hard to assess. The energy threshold property is also useful in order to bias against the $\pi \to \mu$ decay, whose mean lifetime is of the same order of magnitude as the lifetime of the K-particles. The $\pi \to \mu$ decay energy is in fact well below the Čerenkov threshold for water (corresponding to a kinetic energy $E - 0.52\ mc^2$).

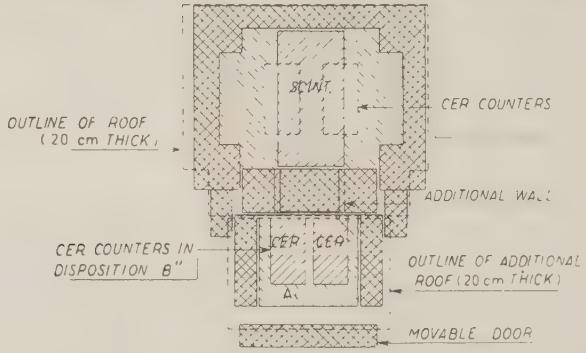

Fig. 3. – Top view of the arrangement of counters used to test the existence of spurious delays (disposition *B*). With respect to disposition *A*, the Čerenkov counters are displaced horizontally by ~ 80 cm. Al=aluminium stuffing (20 cm thick) on which the Čerenkov counters rest.

A group of measurements were carried out with the arrangement shown in Fig. 3 (« Disposition B »). In this arrangement the C-counters are displaced laterally by about 80 cm and enclosed in a separate lead house, separated from the main house by a 20 cm Pb wall and covered with a 20 cm Pb roof. This arrangement was designed to test the existence of spurious delays of some kinds (see later, Sect. 5·2).

Short runs were also carried out with two arrangements similar to A but for the nature of the absorbers surrounding the Čerenkov counters. Disposition C was designed to increase the detection efficiency of decay processes in which a high energy π^0 or γ-ray is emitted (e.g. $\theta^+ \to \pi^+ + \pi^0$): a 12 mm Pb converter was interposed between the Al stuffing and the C-counter box. In disposition D the Al surrounding the Čerenkov counters was replaced by Pb.

An auxiliary arrangement, which was used to test the properties of the Čerenkov counters and to study the timing errors, will be described later.

All the measurements were carried out in the Interuniversity High Altitude Laboratory at Echo Lake, Colorado (altitude 3260 m).

2·2. *Čerenkov and Scintillation counters.*

2·2.1. Čerenkov counters. – The Čerenkov counters are $15 \times 30 \times 30$ cm³ polished lucite boxes (wall thickness 1 mm) completely filled with distilled water. The bottom is painted with an opaque, black paint. Each counter is viewed through the center of one of the smaller faces by a RCA 6372 (lateral window) photomultiplier. Optical contact is ensured by a small, carefully machined lucite adapter, sealed to the box and to the PM by means of a thin film of vaseline. The PM type was chosen because of the large photocathode area (~ 100 cm², equivalent to ~ 6 times that of the 5819). Two small mirrors are placed at the sides of the PM, to increase (by about 20%) the light collection efficiency. Counter and PM are enclosed in a light tight metal box; a fast preamplifier stage is mounted directly onto the box.

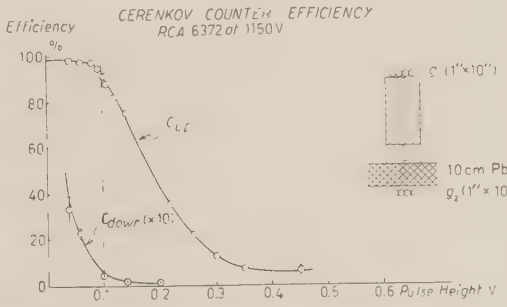

Fig. 4. Čerenkov counter efficiency vs pulse height curve, as measured with the counter arrangement drawn on the right. The subscripts « up » and « down » refer to the field of view of the photomultiplier. The operating conditions used in the experiment are indicated with the dotted line.

The properties of the counters have been studied, in order to choose the correct working conditions. The efficiency for detection of relativistic particles crossing the counter both in the « right » and « wrong » direction has been measured as a function of output pulse height, using a fast μ-meson beam as defined by a Geiger counter (and Pb absorber) telescope. The results are shown in Fig. 4. The subscripts « up » and « down » refer to the field of view of the PM.

The choice of the PM operating voltage was the result of a compromise between the opposite requirements of smallest possible spread in the electron transit times through the PM structure and low noise. The threshold for acceptance of a pulse to trigger the coincidence system was then fixed according to criteria which will be discussed in Sect. 2·3: the equivalent integrated pulse height at the PM output corresponds approximately to the dotted line in Fig. 4.

The single C_{down} rate (which was mostly due to PM noise) was measured

at the beginning and end of every run; its average over the whole running time amounted to about $10\ s^{-1}$, with individual determinations fluctuating between the extreme value of $\sim 3\ s^{-1}$ and $\sim 20\ s^{-1}$.

The « antidirectionality factor » [4] (ratio of « up » and « down » detection efficiencies) was also frequently checked by measuring the rates of twofold coincidences between the Čerenkov counters (at the standard bias level) and any one of the Geiger counters G_2 ($G_2^1C_{up}$ and $G_2^1C_{down}$ in our notations). Although the rates themselves were not very stable, their ratio was always greater than 50:1. Note that in this test the particles had a broad angular spread.

In another set of test measurements, slow μ-mesons of a few different energy intervals were selected and the corresponding C-efficiencies were measured. The results are in qualitative agreement with those obtained by others [5], and particularly with the theoretical prediction of zero efficiency for kinetic energies $< 0.52\ mc^2$.

All the above mentioned efficiencies are, of course, averages over beams of trajectories with cross-section comparable with that of the counter and with rather large angular spread. To measure the dependence of the efficiency on the position in space of individual trajectories is very difficult in practice if the cosmic ray beam has to be used; and to calculate it from the theoretical formulas and the geometry of the counter would be exceedingly laborious. As a very rough indication, we have found that the efficiency for detection of fast μ-mesons decreased from about 100% to about 15% when the counter was tilted at 60° to the axis of a narrow Geiger counter test telescope (the nominal path length of the particle in the counter was $\sim 15\ cm/\cos 60°$).

2·2.2. Scintillation counter. – The scintillation counter S is a $28 \times 61 \times 7.5\ cm^3$ brass box (wall thickness 1.5 mm) lined internally with thin polished Alzac sheets and filled to about 9/10 of the volume with the standard p-terphenyl in toluene solution (5 mg/l). The scintillating liquid is viewed from one end of the box by a single RCA 5819 PM, held in place by means of a neoprene O-ring seal [6], with the front face in direct contact with the solution. A fast preamplifier stage is mounted directly onto the brass box, as in the C-counter.

Due to the very small (cathode area)/(total area) ratio, relatively poor reflection coefficient of the walls and asymmetrical position of the PM, the light collection efficiency is far from uniform over the sensitive volume. With

[4] M. MANDÒ: *Nuovo Cimento*, **12**, 5 (1954).

[5] J. V. JELLEY, in O. FRISCH: *Progress in Nuclear Physics*, **3**, (London, 1953), p. 84.

[6] J. W. KEUFFEL, F. B. HARRISON, T. N. K. GODFREY and G. T. REYNOLDS: *Phys. Rev.*, **87**, 942 (1952).

the operating voltage and pulse height threshold used during the runs, the average efficiency is about only 50% for minimum ionizing particles crossing the counter vertically but is nearly 100% over the whole horizontal section for a pulse equivalent to two minimum ionizing normally incident particles. The effects of pulse height and photon collection time on delay measurements will be discussed later (Sect. 3·1 and 3·2).

2·3. *Electronic circuits.* – A block diagram of the circuits used is shown in Fig. 5. They maybe divided into three groups: timing, selection and auxiliary circuits.

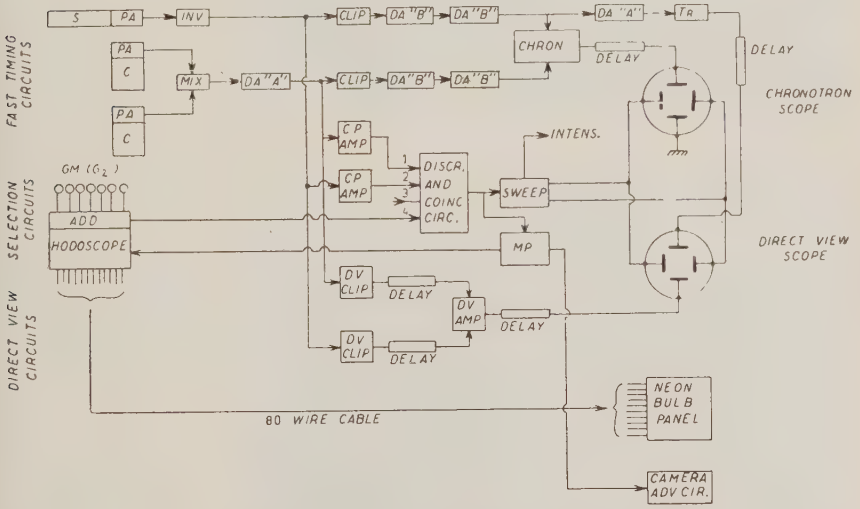

Fig. 5. – Simplified block diagram of the electronic circuits used. S = scintillation counter; C = Čerenkov counter; *GM* = Geiger Müller counters; *ADD* = adding circuit; *INV* = inverter; *MIX* = mixing; *D.1* = distributed amplifier (Hewlett-Packard model 460 A or B); *CLIP* = clipping circuit; *CP* = control pulse circuits; *DV* = « direct view » circuits; *MP* = master pulse generator; *TR* = rise time indicator. Other abbreviations are self-explanatory.

The fast timing circuits consist of the Chronotron timing device, including its C.R.T. presentation system, and the two fast amplifying and pulse shaping chains to feed it with the proper pulses: preamplifiers, mixers, distributed amplifiers and clippers. The chronotron circuit is of the same type as that described by KEUFFEL and coworkers ([6,7]); some additional circuitry was found neces-

([7]) J. W. KEUFFEL: *Rev. Sci. Instr.*, **20**, 197 (1949). For a detailed discussion of the techniques and problems connected with the use of a chronotron timing system, see ref. ([8]).

sary to provide the appropriate acceptance criteria of the input pulses ([8]), and will be briefly described in the following. The delay channel width used throughout the experiment was 3.1 ns.

The basic function of the clipper is to standardize the pulse from the photomultiplier both as to amplitude and width, because uniform pulses are necessary for correct operation of a chronotron with very small channel widths. The method used is, as usual, to cut-off the standing current in a pentode whose plate load consists of a shorted coaxial cable and a terminating resistor. Secondary emission tubes (Philips EFP60) have been used for the clippers (as well as for the preamplifiers and mixers) because of their high transconductance and large plate current. With appropriate choice of the operating point, a plate current of about 10 mA can be cut-off with about 0.7 V grid signal. The long range stability of these tubes is, however, not very good, and appreciable loss of transconductance is observed after a few hundred hours of operation.

To measure delays in the range $\sim 0.1 - \sim 10\ \mu s$, the counter pulses are also presented, after suitable amplification, on a second C.R.T. (called « Direct View (D.V.) scope ») triggered by the same sweep and intensifier circuit as the « chronotron scope ». This system should also allow us, in principle, to measure the corresponding pulse heights; unfortunately, saturation in the preamplifier and mixing stages, which had not been originally designed for this purpose, made meaningful pulse height measurements impossible, and the study of the timing-pulse height correlation was therefore carried out with an indirect method, using the information provided by the hodoscope (see Sect. 3·2.).

The output of the clipper on the Čerenkov counter side is fed not only to the chronotron line but also to a separate detector (« T_R indicator ») whose operation will be described in Sect. 3·1.

The function of the selection circuits is to determine which events are worth photographing. Control pulses (C.P.) derived from the PM pulses are split off from the outputs of the two fast amplification chains, amplified further (risetime $\sim 0.2\ \mu s$) and fed to discriminators in a coincidence circuit. An adding circuit is fed directly from the Geiger counters of tray G_2 and its output brought to a third input of the coincidence circuit. The discrimination threshold for the control pulses was fixed (feeding pulses from a mercury switch pulser ([9]) to the preamplifier inputs) at a level corresponding to about twice the pulse height necessary to cut-off the clippers. The discrimination threshold for

([8]) J. W. KEUFFEL: *Techniques of Cosmic Ray Timing Experiments*, Palmer Physical Laboratory, Princeton University, Cosmic Ray Laboratory, Technical Report no. 15, 1954.

([9]) R. L. GARWIN: *Rev. Sci. Instr.*, **21**, 903 (1950).

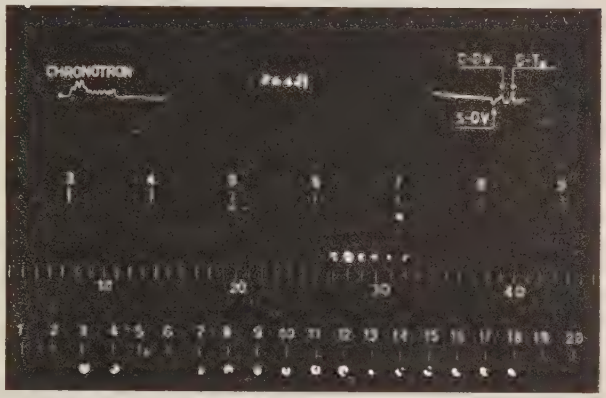

a)

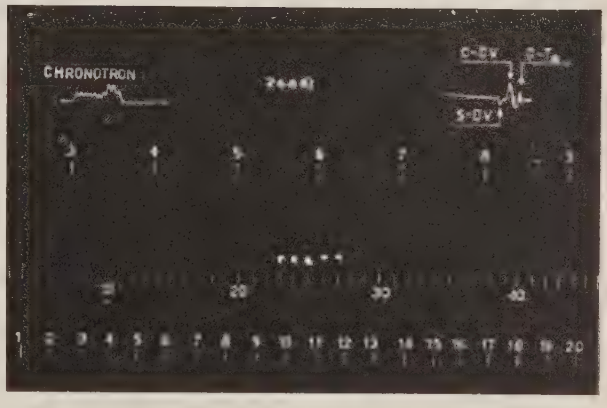

b)

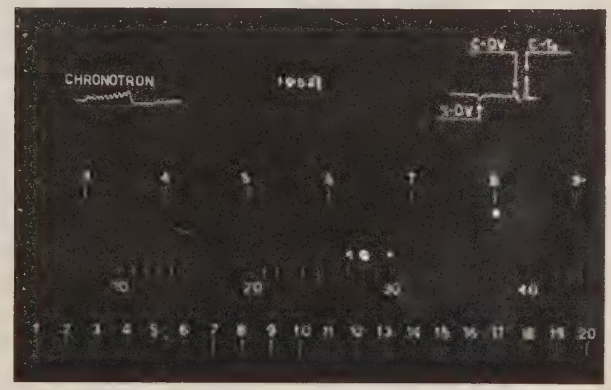

c)

Fig. 6. – Typical pictures of C.R.T. traces and hodoscope neon bulb panel. The Chronotron scope is on the left, the « Direct View » scope is on the right. The position of the 78 hodoscope neon bulbs has been indicated with short vertical lines drawn on the photograph. In (*a*) a rather large shower, initiated by a ionizing particle which discharges one counter in tray G_1, spreads out through the apparatus, crossing the C-counter and producing in it a « zero delay » pulse, as is shown by the chronotron pattern at the left: the meeting point on the chronotron line is between detectors no. 2 and 3. In (*b*) a small shower which hits only a few counters in tray G_2 is associated with a delayed C-pulse: the meeting point on the chronotron line is shifted towards the left, between detectors no. 8 and 9. The shift amounts to about ten delay channels, corresponding to a delay of about 31 ns. (*c*) represents a typical « long delay », probably due to the two step decay of a π-meson belonging to the small shower indicated by the hodoscope. No peak appears on the chronotron pattern, and the spacing of the two DV pulses on the right scope is much larger than in (*b*) or in (*a*).

the G_2 pulses was fixed at the level corresponding to the discharge of at least two counters. Appropriate delays are inserted to obtain the correct time relationships of the pulses at the various points. The output of the coincidence circuit triggers a sweep circuit, whose output waveform ($\sim 12\ \mu s$ long) and intensifier pulse are applied to the two cathode ray tubes.

The auxiliary circuits consist of the camera advancing circuit and the hodoscope, both triggered by the output of the coincidence circuit. The hodoscope was developed from a basic circuit designed by the Cornell University Cosmic Ray Group (*), and its operation is discussed in detail in reference (8). It includes the above mentioned adding circuit which is part of the selection system, and a master pulse generator, triggered by the coincidence output, to gate the firing of the neon bulbes. The 80 neon bulbs (type NE-2) are mounted on a 16 cm × 46 cm panel, in three rows corresponding to the three Geiger counter trays, and are photographed along with the C.R.T. screens and a mechanical register.

The camera is provided with a f:2.5, 50 mm objective, and is driven by a small electrical motor, actuated, via relay, by the camera advancing circuit. This circuit also operates, after each sweep, the mechanical register and a small lamp for the illumination of the latter.

Pictures of the two C.R.T. traces and hodoscope neon bulbs corresponding to a typical « zero delay event », a « chronotron delay event » and a « long delay » are reproduced in Fig. 6.

2·4. *Operation tests and calibration.* – As already mentioned, the single rates of all counters were measured at the beginning and end of each run. The performance of the fast amplification chains was checked at least once every day, and the gain adjusted, together with the discrimination threshold on the control pulses, in order to compensate for the drift of tube characteristics and to ensure proper cut-off conditions of the clipper circuits. An overall test of the fast timing, including chronotron, was, of course, offered by the results of the timing runs, which were read off the film and analyzed « in the field ». Another overall performance test consisted in feeding artificial pulses of appropriate height from the mercury switch pulser to the inputs of the preamplifiers, and locating the meeting point on the chronotron line by visual observation of the chronotron superposition locus on the C.R.T. This gave us what we call the « electronic zero delay ».

The position of the zero delay meeting point on the chronotron line was frequently shifted by inserting additional cable lengths in one of the two input

(*) We are indebted to Prof. K. GREISEN of Cornell University for sending us this unpublished diagram.

lines, and/or inverting the two inputs. This was done in order to minimize the effect of fluctuations in channel width from one delay channel to the other. A similar procedure was used to calibrate the time scale, that is to measure the delay channel widths, using cables of accurately known electrical lengths. The reading accuracy, using mercury switch pulses, is better than 0.1 ns, and the measured differences in channel widths were less than 0.5 ns.

The time base of the D.V. scope was calibrated by means of a crystal oscillator, in the conventional way.

3. – Timing Errors.

3·1. *General.* – The measurement of the delay between the S-pulse and the C-pulse is affected by errors of various kinds (timing errors), part of which are of a systematic nature and can therefore be corrected for to some extent.

The principal sources of timing errors in any experiment using scintillation or Čerenkov counters are ([8]):

1) Decay time of the phosphor (in scintillation counters).
2) Time of flight of the fluorescence or Čerenkov photons to reach the PM cathode.
3) Dispersion of transit times of the electrons through the PM structure.
4) Rise time of the electronics.

In the present experiment effect no. 3 was predominant, as we shall see, but the other effects were certainly not negligible.

Under certain conditions, the effect of the dispersion of transit times of the electrons through the PM structure can be described by means of an effective risetime at the PM collecting electrode. This description holds for statistically uniform pulses. In the case of the scintillator S, about 50 photoelectrons at least were required for acceptance of a pulse by the selection circuits. The shape of such pulses was therefore reasonably uniform, and timing errors due to statistical fluctuations in the pulse *shape* were not important. However, the finite rise-time due to all four of the above effects, coupled with the wide spread of pulse heights occurring in S, turned out to be a serious source of timing errors. These errors arise simply because the larger pulses reach a level sufficient to cut-off the clipper sooner than do the smaller pulses.

An obvious consequence of the above considerations is that the experimental determination of the overall instrumental timing errors which affect a delay distribution should be made on a sample of « prompt » events whose pulse height distributions are identical with that of the delaye events under study. Alternatively, one may try to determine the correction to be applied to each

measured delay according to the measured pulse heights of the pair of counter pulses considered ([10,11]).

The analysis of timing errors for the Čerenkov counters differs from the above analysis for the scintillator. Effect (1) is now absent, while effect (2) is small due to the optical design of the counters. The range of pulse heights expected is not large, since the vast majority of pulses in the inverted Čerenkov counters are bunched near the acceptance threshold, but statistical fluctuations in pulse shape are now to be expected.

A problem peculiar to the RCA 6372 photomultipliers was the following. Visual observation of the C-pulses with a fast oscilloscope, and examination of the chronotron patterns produced by them showed that a considerable fraction of the total charge collected at the anode may arrive with a delay (up to several times 10^{-8} s) much greater than the clipping time used. Thus the voltage waveform at the P.M. output and at the clipper grid appears often composed of a fast rise followed by a much slower slope, and the integrated pulse height as read by the slow D.V. pulses does not offer a good criterion to reject events in which the clipper has not been properly cut-off. In order to meet this requirement, the Čerenkov clipper output pulse was fed, after convenient amplification, to a « risetime (T_R) indicator », identical to a single chronotron detector. The output of this (T_R pulse) was presented on the trace of the « D.V. scope » (see preceeding section) and if its height was less than a certain empirically determined value, indicating that the clipper had not been properly cut-off, the event was rejected.

3·2. *Experimental zero-delay distributions.* – Two types of « timing errors runs » were carried out: in the first one (referred to in the following simply as timing run and indicated with the symbol TA), the two Čerenkov counters were simply turned upside down, so that they became sensitive to downwards traveling fast particles, everything else being unchanged in the experimental arrangement and in the triggering requirements. Under these conditions the great majority of the events recorded were fast atmospheric μ-mesons accompanied by one or more knock-on electrons when emerging from the lead roof (the coincidence circuit was then gated with a time window of about 600 μs every 1/60 s, in order to reduce the triggering rate to a value compatible with the long dead time of the camera advancing system).

([10]) A pulse height selection method to improve the performance of a fast coincidence circuit has been used by G. R. J. McLusky and N. F. Moody: *Electronic Engineering*, **24**, 330 (1952). See also I. A. D. Lewis and F. H. Wells: *Millimicrosecond Pulse Techniques* (London, 1954), p. 252.

([11]) J. W. Keuffel, W. H. Sandmann and R. K. Stitt: *Rev. Sci. Instr.*, **26**, 1191 (1955).

A corrected and convenient average (*) of all timing runs of this type is reproduced in Fig. 7. The distribution is approximately gaussian, with a standard deviation of about 2.5 ns. As already mentioned, however, this distribution cannot be taken as representative of the true timing errors affecting

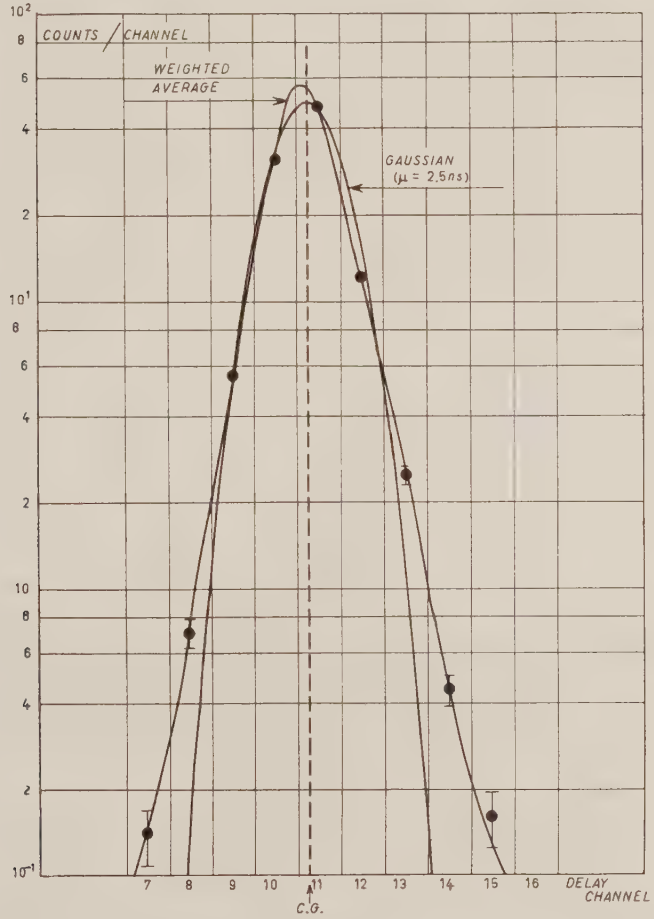

Fig. 7. - Average delay distribution of all timing errors runs. A smooth curve is drawn through the experimental points and compared with a gaussian distribution having a standard deviation $\mu = 2.5 \cdot 10^{-9}$ s. Channel width $= 3 \ .1 \cdot 10^{-9}$ s.

(*) In fact, it turns out that the method of averaging has very little influence on the shape of the average distribution.

the delay distributions obtained with the other experimental arrangements used, because of the pulse heights effects discussed in Sect. 3·1 and below.

In a typical K-event, the C-counter is supposed to be excited by a single fast particle traveling upwards, while the amount of light collected by the photocathode in the S-counter can vary within very wide limits, according to the number, nature and position of particles which emerge from the lead and cross its sensitive volume. In order to study the influence of pulse heights on the timing we used the arrangement shown in Fig. 8 and indicated in the

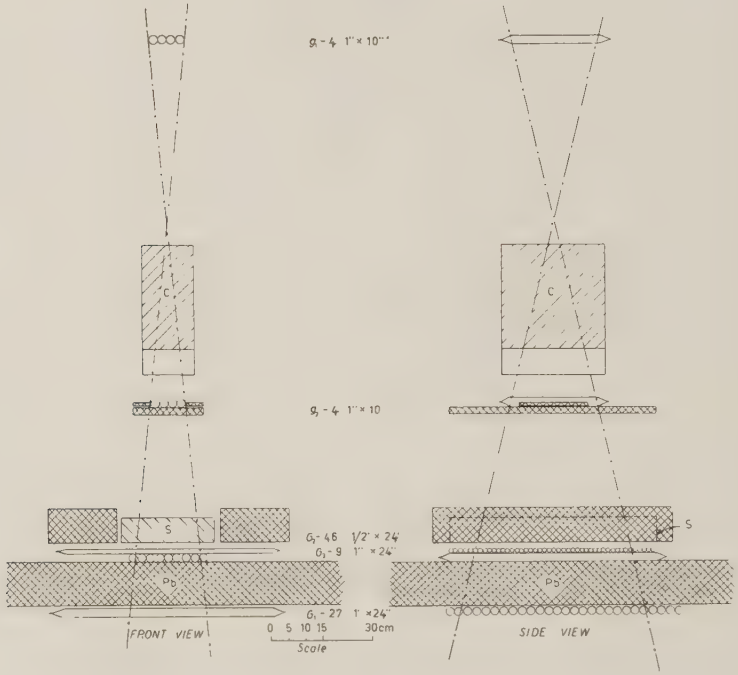

Fig. 8. – Arrangement of counters to test the correlation between timing and hodoscope multiplicity. The multiplicity gives a measure of the pulse size in the S counter. (Disposition TM).

following with the symbol TM. Soft showers produced by fast electrons in the thin Pb absorber below counter tray g_2 cross the S-counter and the Geiger counters G_2, each connected to a neon bulb through the hodoscope. The delay between the S-pulse and the pulse produced in the C-counter by the primary electron is measured in the usual way. Unfortunately we could not measure pulse heights directly, because of amplifier saturation; a rough approximation

to the pulse height is given by the number of G_2-counters discharged. The delay distributions obtained for five different multiplicity groups are shown in Fig. 9: the gradual broadening of the distributions and the shift towards the right of their centers of gravity with increasing multiplicity are clearly apparent (a bigger S-pulse, which cuts off the clipper sooner, appears as a *delay of the* C-*pulse*). The observed effect is actually a combination of the effects of particle multiplicity, non uniformity of light collection and photon times of flight. A more detailed analysis would be possible in the case of the TM runs (by using all the hodoscope information), but of no use for our purposes. In the K-runs, in fact, due to the great variety and complexity of the events, the correlation between the hodoscope information and the physical situation inside the scintillation tank is much looser and no quantitative method of correction could be worked out on that basis.

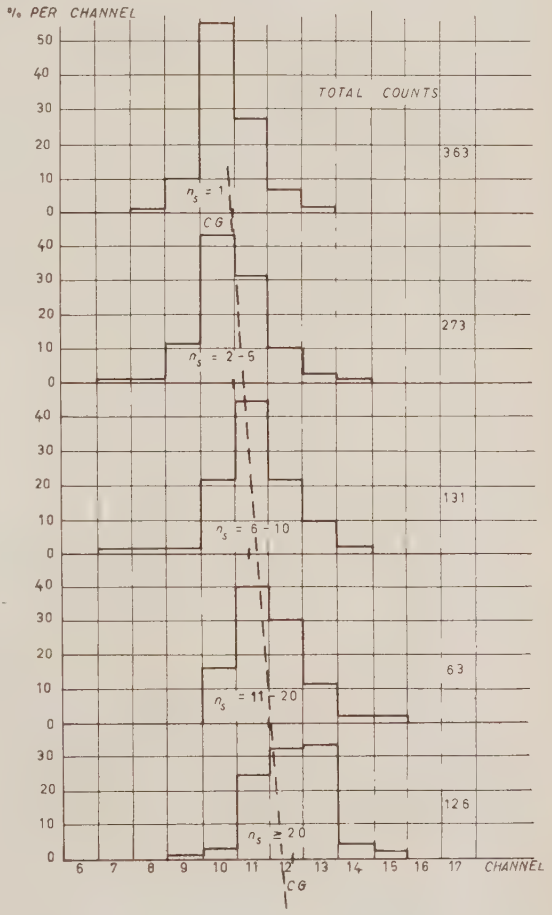

Fig. 9. – Timing error delay distributions for different multiplicity groups, obtained with the arrangement of Fig. 8. Channel width $= 3.1 \cdot 10^{-9}$ s.

It is however important to note that the delay distributions obtained in this way for small multiplicities ($\leqslant 6$) are almost identical with those obtained in the TA timing runs.

4. – Experimental Results.

4·1. *Classification of events.* – The apparatus has been run for about four months with several different geometrical arrangements of the counters and absorbers, and different triggering requirements. A summary of the various types of runs is given in Table I.

TABLE I. *Summary of Runs.*

Run type	Geometry	Material surrounding C-counters	Triggering requirements	Running time (h)	Approximate no. of pictures
KA_5	Fig. 1	Aluminium	G_2^2SC (down)	36.9	3 300
KA_{20}	» 1	Aluminium	»	310.7	20 000
KB_{20}	» 3	Aluminium	»	180.8	2 000
KC_{20}	» 1	Al+$\frac{1}{2}$" Pb	»	34.3	2 100
KD_{20}	» 1	Lead	»	57.7	3 200
μA_{20}	» 1	Aluminium	G_2^1SC (down)	11.8	1 300
TA_{20}	» 1	Al or Pb	G_2^2SC (up)	145.4 (*)	5 900
TM	» 9	—	g_1g_2SC (up)	10.5	1 300

In the symbol of the run type, the first letter K, μ, or T) refers to the triggering requirements, specified in column 4, the second letter to the geometry of the counters and to the disposition and nature of the absorbers around the C-counters, and the subfix indicates (in cm) the thickness of the « generating layer » of Pb. In the triggering requirements, the superscript indicates the number of GM tubes required in a tray; the subscript denotes the tray.

(*) Corresponding to an effective time of about 5.4 h because of the time window factor (see Sect. 3·2).

The pictures have been scanned with the help of a Recordak (Kodak) film reader, which reprojected them at about life size. On the basis of the information contained in each picture, all events have been selected and classified according to the following criteria:

(1) The events in which either one of the two extension trays and or more than one group of counters in tray G_1 appeared to have been discharged were grouped together and defined (rather arbitrarily) as « Air Showers » (AS). This group was rejected in order to eliminate possible delays due to differences in the time of arrival of two particles belonging to the same air shower ([12,13]) About 15% of the events recorded belonged to the AS group. Their multiplicity distribution is markedly different from that of the other events (see

([12]) P. BASSI, G. CLARK and B. ROSSI: *Phys. Rev.*, **92**, 441 (1953).
([13]) G. CLARK: *Phys. Rev.*, **99**, 609 (1955) (A).

below), the great majority of them belonging to the higher multiplicity groups ((*b*) and (*c*)), for which the timing errors are known to be large. The number of lower multiplicity AS events is too small for a useful study of the delay distributions. A contamination from AS lags in the K runs is anyhow ruled out by the results of the « KB » run (see Sect. 5·2).

(2) In a number of cases the appearence of the chronotron pattern on the C.R.T. showed that the delay between the S-pulse and the C-pulse fell outside of the chronotron range. In such (or dubious) cases the spacing of the two D.V. pulses was measured, and the event was classified as a « long delay » (LD).

(3) The remaining events (as well as the LD events) have been subdivided into two classes, according to the measured height of the T_R pulse (see Sect. 3·1), above a certain minimum value (corresponding approximately to the readability limit of the chronotron pattern).

A typical example of classification referring to a sample of about 6000 events of type KA_{20} is shown in the following table.

TABLE II. – *Classification of events.*

	AS (1)	LD (2)	Chronotron unreadable	Chronotron delays (3)		Total
				T_R pulse (4) small	T_R pulse (4) large	
Percent	14	5	16	9	56	100

(1) « Air Showers ». (2) « Long Delays » i.e. delays $\gtrsim 0.1$ μs (including most of the chance coincidences). (3) Short delays readable on chronotron ($\lesssim 50$ ns). (4) Output of the « rise-time indicator (see Sect. 3·1, p. 1108).

(4) The events have been also classified according to the numbers N_2, N_3 of counters discharged in trays G_2 and G_3; calling N the greater of the two, three hodoscope multiplicity groups were defined as follows:

groups (*a*): $2 \leqslant N \leqslant 6$ (the lower limit of 2 is fixed by the triggering requirement)

group (*b*): $7 \leqslant N \leqslant 10$

group (*c*): $N \geqslant 11$

The group limits were fixed keeping in mind the discussion on the effects of multiplicity on timing (Sect. 3·2).

4·2. *Chronotron delay distribution of* KA-*runs.* – The delay distributions obtained from all the runs of the type KA (*) are reproduced in the semi-logarithmic plots of Fig. 10. The ordinates give the actual number of counts per 3.1 ns delay channel and per 347.5 hours of running time. The errors indicated are square root errors.

Fig. 10 refers to the class of events (excluding AS and LD) for which the T_R pulse was sufficiently large. The three curves refer respectively to the

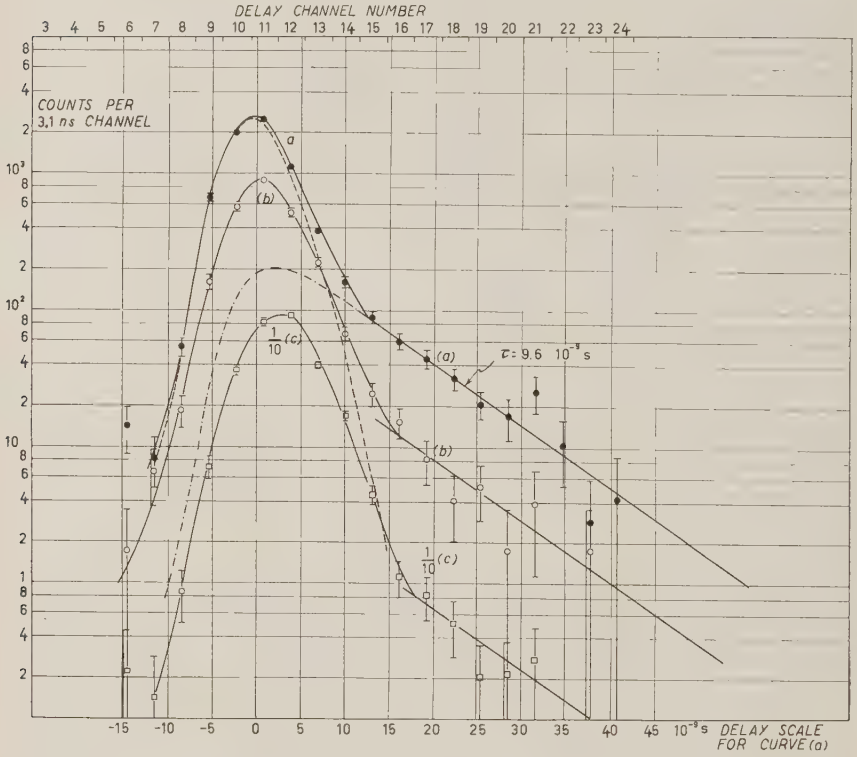

Fig. 10. – Chronotron delay distributions of all KA runs. The three curves refer to events of different multiplicities, increasing from (*a*) to (*c*). The ordinates of curve (*c*) should be multiplied by 10 in order to be compared with the other curves and with the scale indicated on the left. The position of the zero of the time scale at the bottom of the figure is that calculated from the timing error distribution referring to multiplicity group (*a*). The dotted lines represent the result of an analysis of the experimental distribution (*a*) into a « zero delay » component and a pure exponential component, both smeared out by timing errors.

(*) This includes KA_5 as well as KA_{20} runs.

multiplicity groups (*a*), (*b*) and (*c*), as defined in the preceeding section, with the following distribution: 57% to group (*a*), 20% to (*b*), 23% to (*c*). The general appearence of the three distributions gives strong support to the assumption that each one of them is brought about by the superposition of two components: a « zero delay » component, smeared out by the timing errors, and an exponentially decaying component, extending well outside the first one, particularly in the first multiplicity group (*a*).

The presence of an abundant zero delay component, in spite of the directional discrimination of the Čerenkov counters is not surprising. The efficiency of the C-counter for downwards going particles, although small, is known to be different from zero (Sect. 2·2.1). Thus, although quantitative estimates are difficult because of the complicated geometry, one can easily convince oneself that the rate of penetrating showers and of knock-on showers from fast μ-mesons is sufficient to account for the observed number of zero delays. The increasing spread of the delay distribution of the zero delay component with increasing multiplicity and the shift towards the right of its center of gravity are well in agreement with the discussion of Sect. 3·2.

The average probability for a shower hitting the C-counters to give rise to a prompt C-pulse is a rapidly increasing function of its multiplicity. This explains the greater proportion of zero delay component in the (*b*) and (*c*) delay distributions (Fig. 10). Considering the small number of useful events in groups (*b*) and (*c*), we will base our considerations mainly on multiplicity group (*a*).

In the delay distributions obtained from events with a small T_R pulse, the spread of the zero delay distribution appears to be larger, and the separation into two components is less evident. The slope of the exponential « tail » is, however, the same as in Fig. 10, and the general appearance increases our confidence in the adequacy of the criteria used to select the « good » events.

4·3. *Analysis of delays in the microsecond range.* – As already mentioned, our apparatus is not sensitive to $\pi \to \mu$ decays, because the Čerenkov threshold energy is well above the energy of the π-meson. Such decay processes can, however, be detected through the subsequent $\mu \to e$ decay, if the electron happens to cross the Čerenkov counter in a favorable direction and through a sufficiently great distance. It is readily shown that a slow μ-meson of the cosmic ray beam, which is about to stop within or in the vicinity of the Čerenkov counters, has a very small probability of emerging from the Pb roof accompanied by a knock-on electron capable of discharging another G_2 counter. The contribution of atmospheric μ-mesons to the LD rate in the KA runs is therefore negligible.

About 70% of the LD's found in the KA runs belong to the hodoscope multiplicity group (*a*) and exhibit a large T_R pulse. This group is the ap-

propriate one to be used in estimating backgrounds for curve (*a*) in Fig. 11. A typical delay distribution is shown in Fig. 11. The measured timing precision is about 0.025 μs. The curve has been corrected to allow for a small

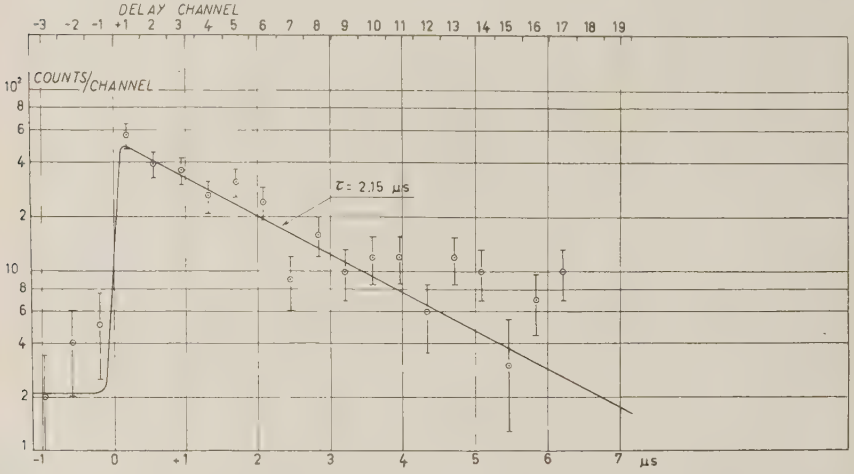

Fig. 11. – Delay distribution of « long delays » associated with events of multiplicity group (*a*) (not corrected for chance coincidence background).

contribution of K-mesons. Application of PEIERLS analysis ([14]) and least squares method to the delays > 0.12 μs yeld, with a successive approximation procedure, a mean life time $\tau = (2.17 \pm 0.24)$ μs and a flat background of about 12 counts per μs for the total running time of the KΛ runs (347.5 h), in rough agreement with the counting rate of the negative delay channels and in good agreement with the chance coincidence rate calculated from the counters' rates. The total extrapolated number of μ-e decays in the same runs is 461 28 (for group (*a*) only), corresponding ot an *average* background of 0.49 counts per 3.1 ns channel to be subtracted from the distribution (*a*) in Fig. 11.

To test the overall detection efficiency for $\mu \to e$ decay processes, a similar analysis has been carried out on the results of a short run (called μΛ run) in which the triggering requirement was changed as to favour atmospheric μ-mesons (just one counter in tray G_2, instead of two). A total of 60 μ-e decays satisfying the standard pulse height requirements have been found (in 11.8 h), corresponding to a rate about 4 times greater then in the KΛ runs. Considering only the μ-mesons stopping in the water of the C counters (~ 30 kg),

([14]) R. PEIERLS: *Proc. Roy. Soc.*, A **149**, 467 (1935).

their total number in the above running time, as calculated from the known μ-meson flux at mountain altitude ([15]), taking into account the average efficiency of the S counter, turns out to be about 120 times greater than the observed one.

The detection efficiency for the secondary electron thus appears to be very low, but not surprisingly so if one assumes that the cone of favorable decay directions is about $4\pi/15$ and that a minimum path length of 15 cm water is necessary to produce enough Čerenkov light (see Sect. 5·3), and one considers that the *average* range of a $\mu \to e$ decay electron in water is only about 13 cm ([16,17]).

4·4. *Mean lifetime and rate of chronotron delays.* – Assuming that the «tail» of the delay distribution represented in Fig. 10 (*a*) is due to a single exponential, Peierl's method ([16]) can be applied to calculate the mean lifetime. The background in this case is essentially that due to the composite $\pi \to \mu \to e$ decay distribution; for this the results of the preceding section have been used. A successive approximation procedure has been applied, assuming at start that the timing errors are correctly represented (see Sect. 3·2) by the average timing distribution of Fig. 7, both for the zero delay component and for the true delays. In each step, only the data of delay channels 15 to 24 have been used in computing the mean life. In this way one gets for the mean lifetime the value

$$\tau_K = (9.6 \pm 0.8) \text{ ns} ;$$

for the number of delayed events (extrapolated to zero delay) the value

$$\mathcal{N}'_K = 1106 \pm 110 ,$$

and for the zero delay component the distribution shown with a dotted line in Fig. 10, which is almost identical with the timing distribution assumed at start.

The delay distributions of multiplicity groups (*b*) and (*c*) are well consistent with the above value of τ_K. Using this, extrapolated numbers of delayed events can be calculated for them on the basis of the few counts in the delay channels definitely outside of the broad zero delay distributions. In this way, a total number of delays from all events satisfying the standard pulse height condition is obtained

$$\mathcal{N}_K = 1390 \pm 140 \text{ (in 347.5 h)} .$$

([15]) K. Wirtz, in W. Heisenberg's: *Kosmische Strahlung* (Berlin, 1953), p. 303.
([16]) R. R. Wilson: *Phys. Rev.*, **84**, 100 (1951).
([17]) J. Steinberger: *Phys. Rev.*, **75**, 1142 (1949).

5. Discussion.

5·1. *General.* – The results of the analysis of the previous sections can most reasonably be interpreted if one identifies the delayed component (with mean life (9.6 ± 0.8) ns) as the decay curve of the long-lived K-mesons appearing as S- and V-particles in cloud chamber experiments ([18-20]).

This conclusion was already reached in a preliminary analysis of part of our experimental results ([2]) (*), in which we tentatively identified our delayed events as decays of the $K_{\mu 2}$ type discovered by the group of the Ecole Polytechnique of Paris ([20]).

A series of measurements carried out, with essentially the same arrangement, by ROBINSON ([21]) yelded a similar result. The identification was shown directly by the elegant experiment of BARKER *et al.* ([3]), who obtained $11.0^{+4.1}_{-2.4}$ ns for the mean life time, in good agreement with our own value.

Recently, measurements of the lifetimes of artificially produced K-mesons have been performed by various groups in the U.S.A. using both the emulsion technique (attenuation in air of a collimated K-meson beam, due to decay in flight) ([22,23]), and electronic timing of decays at rest ([1,24]). In these experiments the identity of the decaying K-particle was established directly by statistical mass measurement of the primary and/or from the range and type of the secondaries. The mean lifetimes obtained for the three most abundant kinds of K-mesons ($K_{\mu 2}$, θ^+, τ) are, within statistics, all the same, and not much different from the values obtained in cosmic ray experiments.

The purpose of this section is to discuss the arguments which substantiate our conclusion that the exponential delay distributions obtained from our measurements actually represent the decay curve of $K_{\mu 2}$ mesons, with a possible admixture of θ^-'s.

([18]) H. S. BRIDGE, C. PEYROU, B. ROSSI and R. SAFFORD: *Phys. Rev.*, **90**, 921 (1953).

([19]) J. P. ASTBURY, J. S. BUCHANAN, P. CHIPPINDALE, D. D. MILLAR, J. A. NEWTH, D. PAGE, A. RYTZ and A. B. SAHIAR: *Phil. Mag.*, **44**, 242 (1953).

([20]) B. GREGORY, A. LAGARRIGUE, L. LEPRINCE-RINGUET, F. MULLER and CH. PEYROU: *Nuovo Cimento*, **11**, 292 (1954).

(*) The present value of the mean life is somewhat different from that given in the previous paper, as a result of an increased statistics and better evaluation of the background.

([21]) K. W. ROBINSON: *Phys. Rev.*, **99**, 1606 (1955).

([22]) G. HARRIS, J. OREAR, and S. TAYLOR: *Phys. Rev.*, **100**, 932 (1955).

([23]) E. L. ILOFF, W. W. CHUPP, G. GOLDHABER, S. GOLDHABER, J. E. LANNUTTI, A. PEVSNER and D. RITSON: *Phys, Rev.*, **99**, 1617 (1955).

([24]) L. W. ALVAREZ, F. S. CRAWFORD, M. L. GOOD, and M. L. STEVENSON: *URCL-3165* (1955); *Phys. Rev.*, **100**, 1264 (1955) (A).

5·2. *Spurious Delays.* – Spurious delays might arise in our measurements from:

1) Instrumental effects.

2) Times of flight of two associated high-energy particles coming from a distant origin (or of a single particle crossing the S-counter and being scattered back into the Čerenkov counter at some distance in the ground below the apparatus).

3) Times of flight, within the apparatus itself, of neutrons in the MeV range, which are known ([23]) to emerge in great numbers from energetic nuclear interactions in lead; the neutrons are not detected directly by the Čerenkov counters, but may eventually give rise to a nuclear reaction whose products can be detected.

4) Nuclear or fundamental particle decay processes.

Instrumental timing errors have been discussed in Sect. 3·2. Instrumental resolution can account quantitatively for the width of the central peak or « zero delay » component of the distribution, but the exponential tail appears to be a real effect. No delays greater than 12 ns were found in any of the timing runs.

Time-of-flight delays were studied by shifting the Čerenkov counters 80 cm to the side (disposition B, Fig. 3). The results of these runs (designated KB_{20}) are shown in Fig. 12, together with the corresponding KA curve: both graphs refer to hodoscope multiplicity group (a). For a correct comparison, the KB distribution has been shifted towards the left by half a delay channel (~ 1.5 ns) to account for the increased time of flight between the S-counter and the C-counters, and normalized to the same running time as the KA distribution.

The total rate of delays greater than 12 ns is about 17 times smaller than the corresponding KA rate. Such a sharp decoherence cannot possibly be attributed to associated particles from a distant origin. Of course, there is some bias in the KB triggering since the delayed particle which actuates the Čerenkov counter cannot help to trigger the pair of Geiger counters required in G_2. The KB data tend to underestimate the frequency of spurious delays for this reason, but this bias is probably offset by the presence of bona-fide K-particle events among the KB delays.

The KB test also provides an upper bound on instrumental timing errors with a Čerenkov pulse height distribution closer to actual running conditions than in the timing runs. Enormous numbers of fast μ-mesons traverse our apparatus, giving rise occasionally to a small pulse in the inverted Čerenkov counters. Peculiar photomultiplier transit-time effects may arise when a very

small number of photoelectrons are released from the large cathode of the RCA 6372 (*), but the KB run shows no spurious lags from this effect.

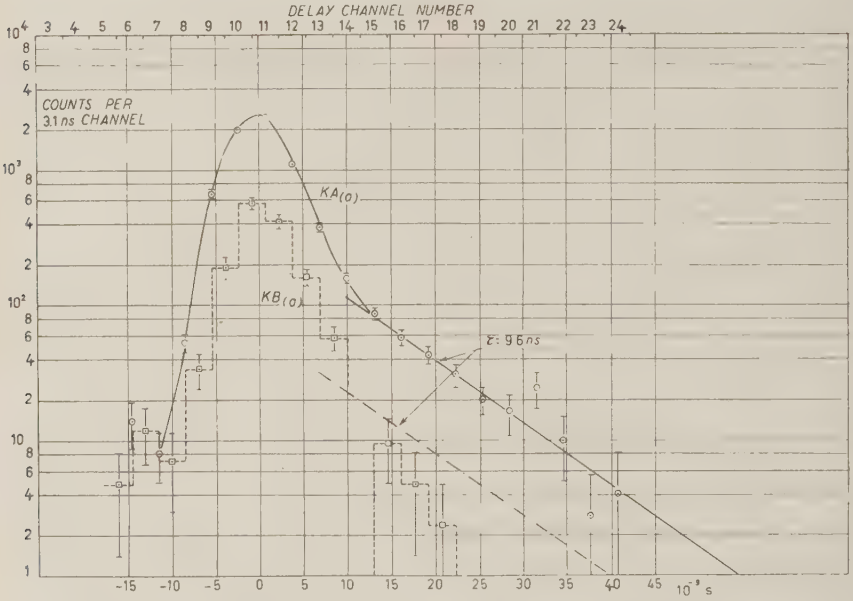

Fig. 12. – Comparison of delay distributions obtained (for multiplicity group (*a*)) with the two arrangements « A » (Fig. 1) and « B » (fig. 3). The KB distribution is normalized to the same running time as the KA distribution.

To test for spurious lags from (3), a 2 mg Ra-Be neutron source was embedded in the lead roof of disposition A at about 5 cm from its bottom surface, near the center. The increase of the C_{down} single counting rate was 0.1 counts/s. Even if one assumes that all this increase is due to a neutron capture effect similar to that mentioned above, and that each penetrating shower produced in the lead roof and detected by our apparatus is accompanied by 50 neutrons, a detection efficiency of at most 3.10^{-4} per penetrating shower is calculated. This is about 30 times too small to account for the observed number of delays greater than 12 ns.

Effect (4) is not easily subjected to experimental check. One should bear in mind, however, the bias of the Čerenkov counters not only against non-relativistic particles, but also against relativistic particles of short range. This

(*) We are indebted to Mr. K. Robinson for helpful discussion on this point.

bias should completely eliminate all effects with energies in the range of nuclear binding energies, as well as many elementary particle transformations (see Sect. 5·4).

5·3. *Absolute flux of stopping* K-*mesons and* K/π *ratio.* – The total extrapolated rate of K-meson decays (4.0 h^{-1}) deduced from our measurements appears very high, if compared with the rates obtained in experiments using cloud chambers or nuclear emulsions. The great amount of stopping power surrounding the C-counters in our experiment has, of course, to be considered in such comparisons. An exact calculation of the absolute rate of K-mesons stopped per unit time and unit mass is very difficult because of the complicated geometry and the insufficient knowledge of the detailed properties of our C-counters, but a crude estimate can be made in the following way.

In order to calculate the contribution of the material outside the C-counters, we idealize the situation assuming that:

a) Each counter is a cylinder of horizontal cross-section equal to that of the actual lucite and water block, resting on an infinite horizontal layer of Aluminium of sufficiently large thickness. The radius of the cylinder is $R = 12$ cm (Fig. 13).

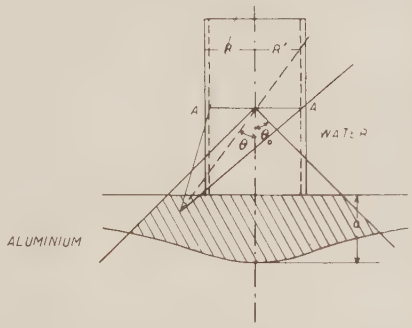

Fig. 13. – Cylindrical model of Čerenkov counter for the evaluation of the absolute rate of stopping K-mesons.

b) All K-mesons are of the $K_{\mu 2}$ type (energy of the secondary 155 MeV ([25]) corresponding to a range of ~ 70 g/cm² Al). Actually, the $K_{\mu 2}$ mode is the most abundant ($\sim 56\%$ of the total ([24])); one makes probably no great error in assuming the detection efficiency to be the same for a $K_{\pi 2}$ meson as for a $K_{\mu 2}$, due to the presence of the two γ-rays from the secondary π^0; and the abundance of the other K_L decay modes is very small.

c) For each point of decay the cone of favourable directions of flight of the secondary μ-meson is that subtended by a horizontal disc of radius $R' = 11$ cm placed at the center of the counter (AA in Fig. 13), provided that the angle θ formed with the vertical by the line joining the point of decay to the center of the disc is less than 45°. The radius R' (which is slightly smaller than the radius of the counter) is chosen in such a way that all permitted lines

([25]) G-STACK COLLABORATION: *Nuovo Cimento*, **2**, 1063 (1955).

of flight go through at least 15 cm within the cylinder. The choice of the limiting angle $\theta = 45°$ results from a rough measurement of the efficiency vs. zenithal angle (see Sect. 2°2.1).

d) In order to be detected (with efficiency 1) the secondary particle must traverse at least 15 cm of water with a velocity greater than the Čerenkov threshold (corresponding to a kinetic energy $E = 0.52\ mc^2$).

It is then easily shown that the effective mass $\times$ solid angle factor is approximately given by

$$2\pi \cdot \pi R'^2 \left[\int_0^{h_0} (1 - \cos\theta_0)\, dh + \int_{h_0}^{a} \left(1 - \frac{h}{a}\right) dh \right],$$

where $h_0 = a \cos\theta_0$ and $a = 38\ g/cm^2$. The shape of the volume contributing to the counting rate is indicated in Fig. 13 (shaded region).

For the material inside the Čerenkov counters the same factor is estimated to be given by half the mass of the counter (~ 7.5 kg of water) times an average solid angle of $2\pi \times 0.133$, corresponding to a cone of half aperture 30°. With the numerical values indicated above one gets a total (for both counters) of $\sim 2\pi \times 9.1$ kg steradians. This value represents almost certainly a lower limit for the true $M\Omega$ factor (note in particular that the Aluminium actually surrounded the C-counters from all sides), and we believe that a better estimate is given by

$$M\Omega = 1.5 \cdot (2\pi \cdot 9.1) \sim 2\pi \cdot 14 \text{ kg steradians}.$$

The rate J_K of stopping and decaying K-particles per unit mass is then given by the equation

$$J_K T_K \left\langle \frac{M\Omega}{4\pi} \right\rangle = n_K,$$

where T_K is the « triggering efficiency », that is, the probability that the stopping K-particle is associated with a nuclear event capable of triggering the G and S counters, and n_K is the (extrapolated) rate of observed decays. Using for n_K the values indicated in the preceding section, one gets finally

$$J_K = \frac{0.6}{T_K} \text{ kg}^{-1}\text{ h}^{-1} = \frac{14}{T_K} \text{ kg}^{-1}\text{ day}^{-1}$$

for all K-mesons, and

$$J'_K = \frac{0.5}{T_K} \text{ kg}^{-1}\text{ h}^{-1} = \frac{12}{T_K} \text{ kg}^{-1}\text{ day}^{-1}$$

for the K-mesons associated with low multiplicity events.

As regards the triggering efficiency T_K, it is probably not very different from unity, due to the very loose requirements set by our apparatus. The above value of J_K appears rather higher than the approximate rate quoted by MENON [26] for nuclear emulsions exposed at the Jungfraujoch under 30 cm of lead (4 kg^{-1} day^{-1} if the relative stopping power of light and heavy materials is taken into account), but the uncertainties involved in both estimates are very large.

To calculate in a similar way the absolute rate of stopped π-mesons would be practically impossible, because of the difficulty of evaluating directly the correct average $M\Omega$ factor for the electron of the $\pi \to \mu \to e$ decay. This factor, however, is approximately the same as for the $\mu \to e$ decays from atmospheric μ-mesons and can therefore be deduced directly from the results of the μA runs (Sect. 4·3). If one denotes by R_μ and R_π the observed rates and with T_π the corresponding triggering efficiency, one gets (considering only the delays associated with low hodoscope multiplicity events)

$$J'_{\pi^+} \cdot T_\pi / J_\mu = \frac{R'_\pi}{R_\mu} \sim \frac{1}{4} .$$

Now, the rate of (positive and negative) atmospheric μ-mesons accepted by our apparatus within the solid angle subtended at the center of the C-counters by the S and G counters (~ 1 steradian) and decaying at rest per unit time and unit mass of water is

$$J_\mu \sim 650 \text{ kg}^{-1} \text{ day}^{-1} .$$

(This figure has been corrected for the average efficiency ($\sim \frac{1}{2}$) of the S-counter for single particles). In this way one obtains

$$J'_{\pi^+} \sim 160 \text{ kg}^{-1} \text{ day}^{-1} / T_\pi$$

and finally, taking $T_\pi \sim T_K$

$$J'_K / J'_{\pi^+} \sim \frac{1}{16} .$$

Also this value appears to be larger than the values obtained for the same ratio from Cosmic Ray experiments [18,27,29] which range from 1/30 to 1/70.

---

[26] P. H. MENON: *Report on Heavy Meson Conference*, Bristol, Dec. 1951, p. 13.

[27] A K/π^+ ratio of about 1/35 can be calculated from the data of C. CASTAGNOLI, G. CORTINI and A. MANFREDINI: *Nuovo Cimento*, **2**, 565 (1955), the rate of π^+ stoppings estimated (for the same stack of emulsion) by E. AMALDI, G. BARONI, G. CORTINI,

The uncertainties involved in the calculations and the differences of experimental conditions are, however, too large to speak of a discrepancy. The influence of the experimental conditions appears evident from a consideration of the experiments on artificially produced and magnetically analyzed beams of K particles, where K^-/π^- ratios as high as 1/10 and 1/15 *per equal momentum interval* can be computed (taking into account the attenuation due to the decays in flight) from the measured rates ([22,24,29]), thus favoring our high value for the absolute flux J_K of stopping K-mesons in comparison with the other cosmic ray estimates.

It should be noted that our very large mass of Al may enrich the K/π ratio deep in the apparatus, since low energy K^+ mesons are known to interact weakly with nuclei, while the π-mesons are strongly absorbed. Also, many K's (perhaps most of them) may be produced by secondary π-nucleon collisions.

5·1. *Nature of* K*-mesons detected.* – As already mentioned, a definite identification of the unstable particles which triggered our apparatus is not possible. However, the requirement of a Čerenkov pulse excludes the three-charged-π mode of decay of the τ-meson (because the maximum velocity of the decay particles is well below the Čerenkov threshold) and favors strongly the $K_{\mu 2}$ mode.

A series of runs (KC) were carried out with a 12 mm Pb converter inserted between the C-counters and the Aluminium surrounding them, to increase the detection efficiency of the 0^+ mode through the two-gamma decay process of the neutral pion. Another series of runs (KD) were carried out with Pb instead of Al all around the counters, as a bias against soft secondaries. The data have been analyzed with the same procedure as previously described, and the relevant results are summarized in Table III.

In spite of the very limited statistics, there is an indication that the rate of decays is actually greater for the KC runs and smaller for the KD runs, as compared with the KA rate. The mean lives, however, are consistent with the KA value, within the rather large statistical errors. An increased detection efficiency through the use of a Pb γ-ray converter has been observed also by Robinson ([21]), in rough agreement with the relative abundance of the $K_{\mu 2}$ and θ^- modes known from nuclear emulsion work ([26]).

C. Franzinetti and A. Manfredini (*Suppl. Nuovo Cimento*, **12**, 181 (1954)) and an estimate of the relative observation efficiency (C. Castagnoli and A. Manfredini: private communication).

([28]) The Paris nuclear emulsion group quotes a ratio $K/\pi^{\pm} \sim 1/60$ (uncorrected for scanning efficiencies; see T. F. Hoang, L. Jauneau, G. Kayas, A. Orkin-Lecourtois, L. Leprince-Ringuet, D. Morellet, G, Tariel and J. Trembley: *Suppl. Nuovo Cimento*, **12**, 242 (1954).

([29]) G. Harris, J. Orear and S. Taylor: *Phys. Rev.*, **101**, 1214 (1956).

TABLE III. – *Summary of results of* K *runs.*

Run Type	T (h)	$\mathcal{N}_K$	$(\mathcal{N}_K/T)$ (h^{-1})	$\mathcal{N}_K/n_0$	τ_K (ns)
KA	347.5	1106 ± 110	3.2 ± 0.3	0.155 ± 0.015	9.6 ± 0.8
KC	34.3	145 ± 37	4.2 ± 1.1	0.21 ± 0.05	$16.5\ ^{+8.2}_{-4.2}$
KD	57.7	135 ± 36	2.3 ± 0.6	0.13 ± 0.04	$17.0\ ^{+9.2}_{-4.6}$

T = effective running time; $\mathcal{N}_K$ = Total number of K-decays, extrapolated from delay zero to infinity (using the mean life time $\tau_K = (9.6 \pm 0.8)$ ns); n_0 = total number of events. All data refer to multiplicity group (a) (Sect. 4·1); all errors quoted are purely statistical.

We conclude therefore that the value of the mean life obtained in this experiment should be associated essentially with the $K_{\mu 2}$ particle, with a small admixture of 0^+ particles. Other decay modes with relativistic secondaries are known to have abundances of only a few percent.

One may notice a tendency of the Cosmic Ray experiments ([3,21]) (including the present one) to give values of the mean life somewhat smaller than those obtained from the electronic measurements on artificially produced K-mesons ([1,24]). The lowest value of the mean life, that of ROBINSON ([21]), is (8.05 ± 0.66) ns, but the $\pi \to \mu \to e$ background in Robinson's experiment was very high and could be the source of a large systematic error. The result of BARKER *et al.* ([3]) is clearly consistent with Fitch's $11.7^{+0.8}_{-0.7}$ ns ([1]). Our own result is a little low, but a systematic error of ~ 1 ns is certainly not excluded.

An independent value of τ_K can be deduced, in our experiment, from the delays observed in the first channel of the « long delays » distribution in excess over the $\pi \to \mu \to e$ distribution: $\tau_K = (14.0 \pm 1.5)$ ns. This value, which refers to the experimental delay range from about 10 ns to infinity, is in better agreement with the values obtained from artificial K-mesons beams than with our own other determination discussed above and is almost inconsistent with Robinson's value. This discrepancy, if true, would suggest that the assumption of a pure exponential for the decay curve of K-mesons is not correct; but the experimental uncertainties are still too large, and it will require a much better decay curve, with points taken over a wide range of *absolute* delays, to establish the real existence of such an effect.

* * *

The measurements described in this work were carried out while one of us (L.M.) was a Research Associate at the Cosmic Ray Laboratory of the Princeton University, on leave of absence from the University of Rome. He wishes to thank the U.S. Government Authorities (Fulbright and Smith-Mundt program) and the Princeton University for financial support, and the Princeton Cosmic Ray Group and Prof. GEORGE T. REYNOLDS for their hospitality.

RIASSUNTO

Si descrive un esperimento eseguito a Echo Lake (Colorado) per misurare la vita media dei mesoni pesanti carichi generati nelle interazioni nucleari della radiazione cosmica. La tecnica sperimentale consiste essenzialmente nel misurare elettronicamente (mediante un « chronotron ») il ritardo fra l'interazione nucleare e l'istante in cui il mesone K eventualmente generato decade (a riposo) in una particella carica di elevata velocità. L'interazione nucleare viene rivelata attraverso i suoi secondari penetranti con un grande contatore a scintillazione e un odoscopio di contatori di Geiger, mentre il secondario della disintegrazione viene rivelato con un grande contatore di Čerenkov direzionale ad acqua. Il dispositivo sperimentale è descritto nella Sez. 2; nella Sez. 3 vengono discussi gli errori nella determinazione dei ritardi ed i criteri di selezione e classificazione degli eventi. Le distribuzioni di ritardi ottenute, analizzate nella Sez. 4, permettono di separare una componente a vita media breve ($(9.6 \pm 0.8) \cdot 10^{-9}$ s) ed una a vita media lunga ((2.2 ± 0.2) μs) che viene interpretata come dovuta agli elettroni del decadimento $\pi \to \mu \to e$ dei mesoni π generati localmente dai nucleoni incidenti. Nella Sez. 5 viene esaminata ed esclusa, sulla base dei risultati di misure ausiliarie, la possibilità che la componente a vita media breve sia dovuta ad effetti spurii di varia natura: si conclude che la vita media stessa deve essere associata essenzialmente con il modo di decadimento $K_{\mu 2}$; con una eventuale piccola contaminazione di $K_{\pi 2}$ (θ^+). Il rapporto di produzione di queste particelle rispetto ai mesoni π viene grossolanamente stimato tenendo conto delle relative probabilità di rivelazione e risulta alquanto maggiore dei valori (1:30 - 1:70) precedentemente ottenuti da altri con emulsioni nucleari o camere a nebbia esposte ai raggi cosmici. Infine, il valore ricavato per la vita media viene confrontato con i valori ottenuti recentemente da altri Autori e viene discussa l'attendibilità della ipotesi di una curva di decadimento puramente esponenziale con una unica vita media.

Sulla teoria bilocale dell'elettrone.

E. Minardi

Società Nazionale Cogne - Aosta
Istituto Nazionale di Fisica Nucleare - Sezione di Torino

(ricevuto il 2 Agosto 1956)

Riassunto. — Si mostra che dalla teoria bilocale dell'interazione tra una particella con spin $\frac{1}{2}$ e il campo elettromagnetico quantizzato precetentemente proposta consegue, assumendo in approssimazione zero una particella di massa arbitrariamente piccola ma non nulla, l'esistenza di una particella la cui massa è praticamente di natura puramente elettromagnetica. Nell'approssimazione in cui non si considerino transizioni tra stati di massa differente la massa ottenuta per questa particella è dovuta interamente a processi di emissione e di assorbimento di fotoni virtuali che interagiscono esclusivamente con la parte interna del campo bilocale. Tali processi non hanno equivalente nel limite locale e la massa della particella è proporzionale a una quantità arbitrariamente piccola in questo limite.

Introduzione.

In questa nota si presentano ulteriori considerazioni sulla teoria di una particella con spin $\frac{1}{2}$ in interazione con il campo elettromagnetico quantizzato nell'ipotesi di lavoro che il campo descrivente la particella dipenda da due variabili spazio-temporali, una variabile x connessa con il suo moto osservabile, ed una variabile cosidetta interna η, connessa con la sua struttura.

Il modo più naturale per pervenire alle equazioni del campo bilocale consiste nel lasciarsi guidare dal principio della simmetria formale tra le variabili x ed η, cosicchè si ottiene una generalizzazione lineare della teoria locale. Tale simmetria vale sino al punto in cui si introducono nel formalismo le condizioni supplementari, che a loro volta introducono nella teoria un certo fatto fisico. Tali condizioni distruggono la simmetria tra gli spazi delle x e delle η.

attribuendo a tali spazi un differente significato fisico. Le equazioni proposte [1], rispettivamente nel caso senza interazione e con l'interazione con il campo elettromagnetico, sono:

$$\alpha_\nu \left(\frac{\partial}{\partial x_\nu} + \frac{\partial}{\partial \eta_\nu} \right) \psi(x, \eta) = 0 \,, \tag{1}$$

$$\alpha_\nu \left(\frac{\partial}{\partial x_\nu} - ieA_\nu(x + \eta) + \frac{\partial}{\partial \eta_\nu} \right) \psi(x, \eta, q) = 0 \qquad (\nu = 1, 2, 3, 4) \tag{2}$$

ove

$$A_\nu(x') = \exp[iH_0 t'] A_\nu(\boldsymbol{x}') \exp[-iH_0 t'] \qquad (x' = x + \eta); \tag{3}$$

H_0 è l'operatore hamiltoniano del campo elettromagnetico nel vuoto e q indica la coordinata del campo elettromagnetico.

Alle (1) e (2) deve aggiungersi la seguente condizione supplementare:

$$\frac{\partial^2}{\partial x_\nu \partial \eta_\nu} \psi = 0 \,, \tag{4}$$

la quale può denominarsi « condizione di disaccoppiamento » poichè esprime l'indipendenza del problema della determinazione della struttura di una particella neutra del problema del calcolo del suo moto osservabile.

La condizione supplementare (4) è ancora simmetrica nelle variabili x ed η. Non così invece per le altre condizioni supplementari che è necessario introdurre onde ulteriormente precisare il significato fisico del formalismo. È tra queste la condizione di seconda quantizzazione la quale, mentre introduce la natura corpuscolare del campo bilocale, è caratteristica dello spazio delle x, concernendo la possibilità di misure indipendenti in questo spazio. In questa nota non discutiamo la seconda quantizzazione del campo bilocale, ma essa, in conseguenza della linearità della teoria, non deve presentare difficoltà.

Un'ulteriore condizione supplementare è la condizione di quantizzazione della massa, una condizione che riguarda tipicamente la parte interna del campo bilocale, imponendo che esso sia nullo sulla superficie ed al di fuori di una sfera baricentrica nello $S_3^{(\eta)}$ di raggio l, ove l è una costante universale. Si introduce così nel formalismo, con la precedente condizione sul campo interno, una nuova costante universale cosicchè tale condizione gioca un ruolo in certo senso analogo alle condizioni di prima quantizzazione della meccanica quantistica, concernenti il moto osservabile, le quali introducono la costante di Planck.

[1] E. MINARDI: *Nuovo Cimento*, **11**, 694 (1954); **3**, 968 (1956). Tali lavori saranno indicati nel seguito con I e II rispettivamente.

Le ipotesi precedenti sembrano le più semplici che si possano introdurre per sviluppare l'idea bilocale. Il loro valore, per ora, risiede unicamente nel fatto che offrono un esempio delle possibilità della teoria e permettono di avere una chiara base per l'ulteriore sviluppo o per la critica.

1. - L'emissione e l'assorbimento dei fotoni nella teoria bilocale.

L'equazione (2) può risolversi perturbativamente esprimendo come serie di potenze della carica i coefficienti $a_{m_n,J}$ dello sviluppo in serie del campo bilocale perturbato nelle autofunzioni $\psi_{0,m_n}(x,\eta)$ del campo bilocale relativo alle differenti masse e negli autostati del puro campo di radiazione elettromagnetica:

$$\Psi(x,\eta,q)=\sum_n\sum_J a_{m_n,J}\psi_{0,m_n}(x,\eta)\Psi_{0,J}(q)\,. \tag{5}$$

Si ottengono così nel modo usuale i seguenti elementi di matrice che descrivono rispettivamente l'emissione e l'assorbimento di un fotone (cfr. II, form. (7)):

$$\begin{cases} H'_{\mathrm{II/I\,em.}}=-e\sqrt{\dfrac{2\pi}{k}}\exp[ik_0t]\,\delta(\boldsymbol{p}_{\mathrm{I}}^{(x)}-\boldsymbol{p}_{\mathrm{II}}^{(x)}-\boldsymbol{k})\displaystyle\int\varphi_{\mathrm{II}}^{+}\gamma_\alpha\varphi_{\mathrm{I}}\exp[-ik_\nu\eta_\nu]\,\mathrm{d}^4\eta\,, \\ H'_{\mathrm{II/I\,ass.}}=-e\sqrt{\dfrac{2\pi}{k}}\exp[-ik_0t]\,\delta(\boldsymbol{p}_{\mathrm{I}}^{(x)}-\boldsymbol{p}_{\mathrm{II}}^{(x)}+\boldsymbol{k})\displaystyle\int\varphi_{\mathrm{II}}^{+}\gamma_\alpha\varphi_{\mathrm{I}}\exp[ik_\nu\eta_\nu]\,\mathrm{d}^4\eta\,. \end{cases} \tag{6}$$

I precedenti elementi di matrice descrivono processi di emissione e di assorbimento di fotoni interagenti con quella parte del campo bilocale che descrive il moto osservabile: essi infatti non danno contributo nullo solo se è conservato l'impulso connesso con questo moto.

È tuttavia un'interessante proprietà della presente teoria la possibilità di processi di emissione e di assorbimento di fotoni virtuali i quali interagiscono esclusivamente con la parte interna del campo bilocale.

Onde ottenere gli elementi di matrice descriventi questi ultimi processi occorre separare la parte interna del campo bilocale, che dipende dalla variabile η, dalla parte dipendente dalla variabile x, connessa con il moto osservabile. Ciò è ottenuto ponendosi nel sistema del baricentro della particella, ove $\nabla_x\psi=0$, $\partial\psi/\partial\eta_4=0$. Allora la (2) diviene

$$\left(i\frac{\partial}{\partial x_4}-ie\alpha_\nu A_\nu(x+\eta)+\boldsymbol{\alpha}\nabla_\eta\right)\psi(x_4,\eta,q)=0\,, \tag{7}$$

e ponendo in questa $\psi(x_4,\eta,q)=\exp[(x_4+\eta_4)H_0]\exp[-x_4E_{0k}]\exp[\pm x_4m]\cdot\varphi(\boldsymbol{\eta},q)$, ove E_{0k} è un autovalore dell'hamiltoniana H_0 del campo elettromagnetico nel vuoto, si ottiene, ricordando la (3), l'equazione del campo interno in

interazione con il campo elettromagnetico:

$$(8) \qquad (E_{0k} \mp m)\varphi(\boldsymbol{\eta}, q) = (H_0 - e\alpha_\nu A_\nu(\boldsymbol{x}+\boldsymbol{\eta}) - i\boldsymbol{\alpha}\cdot\nabla_\eta)\varphi(\boldsymbol{\eta}, q) \quad (\boldsymbol{p}^{(x)} = 0,\ p_4^{(\eta)} = 0).$$

La quantità m rappresenta il contributo all'energia totale, calcolato nel sistema del baricentro, dovuto esclusivamente ai fotoni virtuali in interazione con il campo interno e si assume che la teoria sia simmetrica rispetto ai due segni di m. La quantità m può essere calcolata sviluppando nella (8) m e q in serie di potenze di e. Si ottengono i seguenti elementi di matrice che contrassegneremo con l'indice η per indicare che descrivono processi in cui i fotoni interagiscono solo con la parte interna del campo bilocale:

$$(9) \qquad \begin{cases} (H'_{\mathrm{II/I\,em.}})^\eta = -e\sqrt{\dfrac{2\pi}{k}}\exp[-i\boldsymbol{k}\cdot\boldsymbol{x}]\cdot\int\varphi^\dagger_{\mathrm{II}}\gamma_\alpha\varphi_{\mathrm{I}}\exp[\ \ i\boldsymbol{k}\cdot\boldsymbol{\eta}]\ \mathrm{d}^3\eta\,, \\ (H'_{\mathrm{II/I\,ass.}})^\eta = -e\sqrt{\dfrac{2\pi}{k}}\exp[i\boldsymbol{k}\cdot\boldsymbol{x}]\cdot\int\varphi^\dagger_{\mathrm{II}}\gamma_\alpha\varphi_{\mathrm{I}}\exp[i\boldsymbol{k}\boldsymbol{\eta}]\,\mathrm{d}^3\eta\,. \end{cases}$$

Il contributo m deve essere poi sommato al contributo all'energia totale ottenuto senza separare l'equazione (2) nelle variabili x ed η e dovuto ai fotoni descritti dagli elementi di matrice (6). L'espressione di m del secondo ordine della teoria delle perturbazioni è data dalla formula seguente avente l'aspetto usuale:

$$(10) \qquad \mp m'' = \sum_1^4{}_\alpha \sum_k \sum_n \frac{(H'_{0|nk\alpha})^\eta (H'_{nk\alpha|0})^\eta}{m_0 - m_n - k}\,.$$

La sommatoria sugli stati intermedi del campo interno implica la somma rispetto alle masse negative ed agli spin.

2. – La teoria bilocale dell'elettrone.

Vogliamo ora mostrare che dai processi di emissione e di assorbimento dei fotoni virtuali interagenti con la parte interna del campo bilocale, consegue l'esistenza di una particella di massa interamente elettromagnetica, cosicchè si ha per la prima volta un modello quantistico dell'elettrone come particella di origine elettromagnetica. Nel procedimento perturbativo assumeremo come approssimazione zero del campo bilocale $\psi_0(x, \eta)$ una funzione avente la forma $V_x^{-\frac{1}{2}}\exp[-ix_\nu p_\nu^{(x)}]\cdot\varphi_0(\eta)$ ove $\varphi_0(\eta) = u_\mu \exp[-i\eta_\nu p_\nu^{(\eta)}]f(\eta_\nu^2)$, $f(\eta_\nu^2)$ essendo una funzione normalizzata, costante e diversa da zero per $\eta_\nu^2 < l^2$ e nulla per $\eta_\nu^2 > l^2$ (2).

(2) Notiamo che se si assume la discontinuità del campo interno delle particelle con spin $\frac{1}{2}$ sulla superficie della sfera quadridimensionale (cfr. II, fine di Sez. **1**) la (1) deve essere scritta con la funzione singolare $\delta([\eta_\nu\eta_\nu]^{\frac{1}{2}} - l)$ nel secondo membro.

Una tale soluzione è esclusa nel caso delle particelle con spin zero se si mantiene la ipotesi implicita in I (cfr. altresì II, Sez. 1) che in questo caso l'autofunzione interna sia continua sulla superficie della sfera quadridimensionale di raggio ma con derivata prima discontinua. Una tale soluzione discontinua è quindi caratteristica di una particella con spin semi-intero.

Notiamo che la funzione $\varphi_0(\eta)$ non è ortogonale agli autostati $\varphi_n(\eta)$ del campo interno (cfr. I, II) corrispondenti allo spettro di masse.

La matrice a una colonna e a quattro righe u_p è l'ampiezza corrispondente ad un dato segno dell'energia e dalla direzione dello spin, la quale è ottenuta da una delle matrici definite in Appendice di I, formule (22) e (23) prendendo i $p_\nu^{(\eta)}$ $(\nu = 1, 2, 3)$ arbitrariamente piccoli ma non nulli [3] cosicchè la massa $p_\nu^{(\eta)} p_\nu^{(\eta)} = m_0^2$ è a sua volta arbitrariamente piccola ma non nulla (i $p_\nu^{(\eta)}$ $(\nu = 1, 2, 3)$ saranno tra loro uguali per ragioni di simmetria, mentre $p_4^{(\eta)} = 0$ nel sistema del baricentro).

Poichè lo stato interno di approssimazione zero così scelto non è ortogonale agli autostati $\varphi_n(\eta)$ del campo interno, le formule per le grandezze perturbate non hanno l'aspetto usuale. Tuttavia si può avanzare l'ipotesi che siano trascurabili le transizioni coinvolgenti stati di massa differente da quella iniziale; in questa ipotesi si ha per il campo bilocale perturbato l'espressione:

$$\psi(x, \eta, q) = \varphi_0(\eta) \sum_{p^{(\eta)}} \sum_J a_{p^{(\eta)}, J} \exp\left[-i x_\nu p_\nu^{(\eta)}\right] \Psi_{0,J}(q) \,. \tag{11}$$

Le formule hanno allora l'aspetto usuale, con lo stato $\varphi_0(\eta)$ come unico possibile stato intermedio del campo interno.

Se ora mediante trattazione perturbativa dell'equazione (2) si vuole calcolare la selfenergia nel secondo ordine dovuta a quei fotoni che interagiscono con la parte del campo bilocale descrivente il moto osservabile (facendo uso degli elementi di matrice (6)), si può seguire un procedimento identico a quello tradizionale [4], tranne che per la comparsa di un fattore di taglio di WATAGHIN [5] $G^2 = \int \mathrm{d}^4\eta_I f(\eta_I^2) \exp\left[i k_\nu \eta_{I\nu}\right]^2$ che, secondo il procedimento di II Sez. 2, è valutato nel sistema del baricentro, ove $\eta_4 = 0$, ponendo poi il risultato in forma invariante; ma indipendentemente dall'espressione del fattore di taglio, si ottiene per la selfenergia un valore arbitrariamente piccolo, poichè, com'è noto, essa è proporzionale alla massa della particella imperturbata che nel presente caso è appunto arbitrariamente piccola.

[3] Con ciò si considera $\varphi_0(\eta)$ come una funzione lentamente variabile della η entro la sfera.

[4] Cfr. per es. W. HEITLER: *Quantum Theory of Radiation* (Zürich, 1953), p. 293.

[5] G. WATAGHIN: *Nuovo Cimento*, **10**, 1602 (1953); *Suppl. Nuovo Cimento*, **1**, 103 (1954).

Vi è invece un contributo non nullo da parte di quei processi caratteristici della parte interna del campo bilocale descritti dalla equazione (8).

Come nel caso precedente, anche in questo calcolo si ottiene una grande semplificazione se si trascurano le transizioni in stati intermedi coinvolgenti masse diverse da quella iniziale.

Si ha allora:

$$(12) \qquad \mp m'' = \sum_{1}^{4}{}_{\alpha} \sum_{k} \frac{(H'_{0|0k\alpha})^{\eta}(H'_{0k\alpha|0})^{\eta}}{-k}$$

ove è sottointesa la sommatoria su tutti i possibili stati intermedi con massa m_0.

La (12) è facilmente valutata assumendo come asse z la direzione di propagazione del fotone. Allora la somma dei termini con $\alpha = 1$ e con $\alpha = 2$ è costituita da un unico termine con il prodotto $\boldsymbol{\gamma}\cdot\boldsymbol{e}$ al posto di γ_α nell'elemento di matrice, $\boldsymbol{e}$ essendo il versore di polarizzazione del campo magnetico, mentre il termine con $\alpha = 3$ è nullo. La somma sugli stati intermedi è effettuata con le regole solite. Si ottiene:

$$(13) \qquad m'' = \pm \frac{e^2}{\pi l} \int_0^\infty \mathrm{d}\varrho\, G^2(\varrho) = \pm \frac{3e^2}{5l} \qquad (\varrho = kl)$$

ove $G(\varrho)$ è il fattore di taglio di Wataghin [5]. La presente teoria bilocale, prevede quindi, nell'approssimazione assunta, che la massa dell'elettrone sia uguale a $3e^2/5l$, cioè all'energia mutua elettrostatica, secondo la teoria classica, di una distribuzione omogenea di carica totale e in una sfera spaziale di raggio l.

* * *

L'Autore ringrazia il prof. G. WATAGHIN per le numerose e chiarificatrici discussioni.

SUMMARY (*)

It is shown that from the previously proposed bilocal theory of interaction between a spin $\frac{1}{2}$ particle and the quantized electromagnetic field follows, assuming in zero approximation a particle of arbitrarily little but not zero mass, a particle the mass of which is practically of pure electromagnetic nature. In the approximation in which we do not consider transitions between states of different mass, the mass obtained for this particle is entirely due to emission and absorption processes of virtual photons which interact exclusively with the interior part of the bilocal field. These processes have no equivalent in the local limit and the mass of the particle is proportional to an arbitrary little quantity in this limit.

(*) *Editor's Translation.*

IL NUOVO CIMENTO Vol. IV, N. 5 1° Novembre 1956

Mouvement de tangage d'une suspension élémentaire sur lames élastiques.

J. E. Plainevaux

Université Libre de Bruxelles

(ricevuto l'8 Agosto 1956)

Résumé. — Le présent travail étudie le mouvement de tangage (beccheggio, pitching) d'une suspension élémentaire ainsi que la position optimum à donner à la bielle de poussée pour diminuer ce phénomène parasite. Si on traite comme un infiniment petit principal le déplacement horizontal de la platine, il est montré que le tangage dû à la dissymétrie de la charge est du second ordre; celui dû à la position de la force de poussée est en général du troisième ordre. Ce terme du troisième ordre est annulé par un choix convenable de la hauteur du point où on pousse la platine. Ce point est sensiblement à mi-distance de la platine et de l'encastrement dans le bâti. Si on préfère souvent pousser la platine dans son plan, c'est pour éviter des vibrations relatives parasites de la platine travaillant en sismographe.

Introduction.

Les suspensions sur lames élastiques destinées à réaliser un guidage rectiligne proviennent du désir des constructeurs de s'affranchir des difficultés inhérentes aux résistances passives rencontrées dans les dispositifs classiques de chariots à glissières ou à billes. Elles permettent d'éviter entre autres les ennuis causés par les poussières et la lubrification. L'emploi de ces suspensions est limité à des courses relativement faibles (50 mm) devant être réalisées avec de très grandes précisions atteignant et dépassant même celles que l'on peut espérer obtenir au moyen des meilleurs chariots; une seule réserve devant être faite: celle des chariots des rares machines à tracer les réseaux. Ceux-ci sont par contre très coûteux et très délicats d'emploi.

La suspension à lames tendant à remplacer un dispositif de guidage rectiligne mécanique, doit se développer normalement dans des applications de

haute précision ainsi que dans des laboratoires et ateliers dont le « potentiel industriel » ne permet pas la réalisation de pièces mécaniques de haute précision avec des prix de revient admissibles.

Malheureusement une étude approfondie des suspensions élastiques montre que celles-ci laissent entrevoir à la place de difficultés *matérielles* de réalisation, de graves difficultés de conception. Nous nous sommes attachés à étudier quelques problèmes soulevés par les suspensions élastiques symétriques et symétriquement chargées et avons été conduits à décrire une suspension asservie pour affaiblir la trajectoire parasite dans le plan vertical ainsi que des vibrations gênantes de la platine. Une étude plus poussée de la question nous a permis de montrer qu'il était possible de concevoir des suspensions asservies caractérisées par une absence de trajectoire parasite et une faible sensibilité au chargement de la platine ([1,2]). Une telle suspension asservie a été essayée avec de bons résultats entre autres par JONES et YOUNG ([3]). Les mêmes auteurs ont amorcé le problème du tangage de la platine auquel est dévolue la présente étude.

Les suspensions élastiques utilisées en pratique (à compensation et avec ou sans asservissement) sont analytiquement fort ardues à étudier; leur étude expérimentale est délicate sans support théorique sur leur comportement. Nous nous bornons dans ce travail à ne considérer que des suspensions élémentaires qui sont les parties constitutives d'une suspension élaborée.

Pour cette étude, nous utiliserons les résultats, publiés récemment, relatifs à la déformation plane d'une lame isolée ([4]).

1. – Recherche de la hauteur à laquelle il faut agir sur la platine pour éviter le tangage.

Nous considérons des lames élastiques identiques de longueur L (moment d'inertie I, module d'élasticité E). La longueur de la platine est A. La platine (Fig. 1) est sollicitée par une force verticale, peu importante et dissymétrique, V agissant à une distance v de l'extrémité A. Le déplacement horizontal de la platine est obtenu grâce à une force horizontale H agissant sur un appendice (non dessiné) de la platine et dont la ligne d'action est à une distance a de la platine mobile. Nous nous proposons d'essayer de déterminer la valeur de a pour qu'il n'y ait pas de tangage.

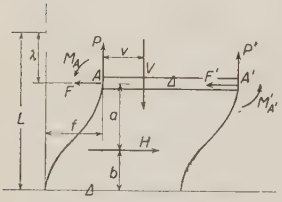

Fig. 1.

([1]) J. E. PLAINEVAUX: *Nuovo Cimento*, **10**, 1451 (1953).
([2]) J. E. PLAINEVAUX: *Nuovo Cimento*, **12**, 37 (1954).
([3]) R. V. JONES et I. R. YOUNG: *Journ. Scient. Instr.*, **33**, 11 (1956).
([4]) J. E. PLAINEVAUX: *Nuovo Cimento*, **4**, 922 (1956).

En l'absence de tangage, les déplacements horizontaux f et f' des extrémités A et A' des lames sont les mêmes ainsi que les « descentes » verticales λ et λ' des mêmes points. (Ces descentes sont mesurées à partir de la position non déformée de la platine). A la Fig. 1 on a dessiné les forces et couples agissant sur la platine.

Les équations d'équilibre de translation de la platine sont

$$P + P' = V \qquad \text{et} \qquad F + F' = H .$$

Quant à l'équation d'équilibre de rotation, elle est de la forme:

$$M_A + M'_{A'} + Ha - Vv + P'\Delta = 0$$

quand on l'écrit autour du point A.

Les tangentes aux extrémités des lames étant toutes verticales, on a en se limitant aux deux premiers termes du développement (voir [4]):

$$\frac{\lambda}{L} = \frac{3}{5}\left(\frac{f}{L}\right)^2\left[1 + \frac{1}{420}\,\frac{PL^2}{EI}\right].$$

De même pour la descente λ' de l'extrémité A'.

Ayant $L = L'$; $f = f'$; $\lambda = \lambda'$, il en résulte que $P = P'$, donc: $P = P' = V/2$.

On a aussi $M_A = M'_{A'}$, avec

$$\frac{M_A L}{EI} = -6\,\frac{f}{L}\left[1 - \frac{1}{60}\,\frac{PL^2}{EI}\right] = -6\,\frac{f}{L}\left[1 - \frac{1}{120}\,\frac{VL^2}{EI}\right]$$

et $F = F' = H/2$ avec:

$$\frac{FL^2}{EI} = 12\,\frac{f}{L}\left[1 - \frac{1}{20}\,\frac{VL^2}{EI}\right].$$

De l'équation d'équilibre de rotation on déduit:

$$Ha = 2Fa = V(v - \tfrac{1}{2}\Delta) - 2M_A ,$$

d'où:

$$a = -\frac{M_A}{F} + \frac{V(v - \frac{1}{2}\Delta)}{2F}$$

remplaçant M_A et F par les valeurs trouvées, on obtient en supposant $f \neq 0$:

$$a = \frac{L}{2}\,\frac{1 - \frac{1}{120}\,\frac{VL^2}{EI}}{1 - \frac{1}{20}\,\frac{VL^2}{EI}} + \frac{VL^2}{24EI}\,\frac{r - \frac{1}{2}\Delta}{\left(1 - \frac{1}{20}\,\frac{VL^2}{EI}\right)\frac{f}{L}} .$$

La distance de la ligne d'action de la force horizontale à la platine se compose de deux termes. Le premier est indépendant du déplacement horizontal f de la platine. Quant au second, son dénominateur tend vers zéro avec le déplacement horizontal, sauf si le numérateur est identiquement nul, c'est-à-dire si $c = \Delta/2$ ou encore, si le chargement de la platine est symétrique. Donc, seule une platine chargée symétriquement ne possède pas de mouvement de tangage.

En fait, la hauteur de la poussée a été repérée par rapport à la platine mobile qui elle-même descend lorsqu'elle se déplace horizontalement.

Cherchons maintenant à repérer la position de la ligne d'action de la force H par rapport à un repère fixe, en l'occurrence le bâti inférieur dans lequel les lames sont encastrées. Soit b cette distance, on a:

$$b = L - \lambda - a\,,$$

remplaçant λ et a par les valeurs trouvées précédemment, on obtient tous calculs effectués:

$$b = \frac{L}{2}\,\frac{1 - \frac{11}{120}\frac{VL^2}{EI} - \frac{3}{5}\left(\frac{f}{L}\right)^2\left[1 + \frac{1}{840}\frac{VL^2}{EI}\right] - \frac{VL^2}{24EI}\frac{v - \frac{1}{2}\Delta}{\frac{f}{L}\left(1 - \frac{1}{20}\frac{VL^2}{EI}\right)}}{1 - \frac{1}{20}\frac{VL^2}{EI}}.$$

La hauteur de la force au dessus du bâti se compose de trois termes:

1) un terme constant,

2) une correction parabolique due à la descente de la platine,

3) un terme hyperbolique qui s'annulle en cas de chargement symétrique.

Le deuxième terme, variable, est heureusement petit devant le premier qui vaut sensiblement $L/2$. En conclusion, pour qu'une platine ne présente rigoureusement pas de mouvement de tangage, il faut que son chargement soit symétrique, et que la ligne d'action de la force qui la pousse varie très légèrement en hauteur lors de la course (deuxième terme). Cette légère variation en hauteur de la ligne d'action ne peut être réalisée que moyennant d'importantes complications. En général, la ligne d'action reste fixe par rapport au bâti et il y a un léger tangage que nous calculerons plus loin.

On prend donc la ligne d'action à une hauteur au-dessus de l'encastrement inférieur égale à:

$$b_{opt} = \frac{L}{2}\,\frac{1 - \frac{11}{120}\frac{VL^2}{EI}}{1 - \frac{1}{20}\frac{VL^2}{EI}}$$

ou en dessous de la platine (en position non déformée) à une distance:

$$a_{opt} = \frac{L}{2}\,\frac{1-\dfrac{1}{120}\dfrac{VL^2}{EI}}{1-\dfrac{1}{20}\dfrac{VL^2}{EI}}\,.$$

Au cas où le chargement de la platine est négligeable, on trouve:

$$a_{opt} = b_{opt} = \frac{L}{2}\,,$$

c'est-à-dire que la platine doit être poussée à mi-distance entre le bâti et la platine. Ce résultat est en accord avec ce que trouvent JONES et YOUNG [3].

2. – Détermination du mouvement de tangage d'une platine montée sur suspension élémentaire.

Nous supposerons, Fig. 2, que la platine de longueur Δ a son centre de masse en G dont les coordonnées liées à la platine sont v et h à partir de l'encastrement A. Les lames de suspension sont identiques, $EI = E'I'$ et $L = L'$. Les encastrements des lames dans la platine sont perpendiculaires à la droite AA' joignant les encastrements ($\theta = \theta'$). Enfin la distance entre les encastrements parallèles dans le bâti est égale à Δ. Les forces et couples dessinés à la figure sont ceux agissant sur la platine.

Les équations d'équilibre de translation s'écrivent:

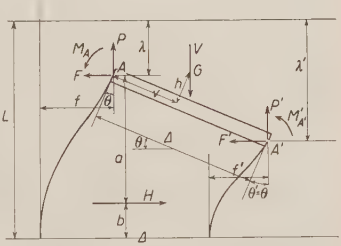

Fig. 2.

$$P + P' = V\,, \tag{1}$$

$$F + F' = H\,, \tag{2}$$

Quant à l'équation d'équilibre de rotation écrite autour de A, elle est:

$$M_A + M'_{A'} + Ha - V(v\cos\theta + h\sin\theta) + P'\Delta\cos\theta - F'\Delta\sin\theta = 0\,. \tag{3}$$

De plus, on possède les deux relations géométriques suivantes:

$$\lambda' = \lambda + \Delta\sin\theta\,, \tag{4}$$

$$f' = f - \Delta(1-\cos\theta)\,, \tag{5}$$

ainsi que les équations de déformation des lames (¹), où nous admettons que les charges verticales sont faibles de manière à pouvoir limiter les développements en série aux deux premiers termes:

$$\frac{\lambda}{L} = \frac{3}{5}\left(\frac{f}{L}\right)^2\left[1 + \frac{1}{420}\,\frac{PL^2}{EI}\right] - \tag{6}$$

$$- \frac{1}{10}\,\frac{f}{L}\,\mathrm{tg}\,\theta\left[1 + \frac{1}{70}\,\frac{PL^2}{EI}\right] + \frac{1}{15}\,\mathrm{tg}^2\,\theta\left[1 + \frac{11}{420}\,\frac{PL^2}{EI}\right],$$

$$\frac{M_A L}{EI} = -\,6\,\frac{f}{L}\left[1 - \frac{1}{60}\,\frac{PL^2}{EI}\right] + 4\,\mathrm{tg}\,\theta\left[1 - \frac{1}{30}\,\frac{PL^2}{EI}\right], \tag{7}$$

$$\frac{FL^2}{EI} = 12\,\frac{f}{L}\left[1 - \frac{1}{10}\,\frac{PL^2}{EI}\right] - 6\,\mathrm{tg}\,\theta\left[1 - \frac{1}{60}\,\frac{PL^2}{EI}\right], \tag{8}$$

les trois équations ci-dessus sont relatives à l'encastrement A. Pour l'encastrement A' les formules sont analogues.

La résolution du système des 11 équations précédentes est un problème fort complexe. Nous pouvons simplifier la résolution en faisant des approximations que nous allons d'abord justifier.

Supposons les déplacements horizontaux petits, et considérons f/L ainsi que f'/L comme des grandeurs infiniment petites du premier ordre. Nous supposons le mouvement de tangage faible. On sait que les raccourcissements réduits λ/L et λ'/L sont du second ordre par rapport à f/L tout en étant influencés par l'angle de tangage θ. Ayant

$$\sin\theta = \frac{\lambda' - \lambda}{l},$$

on en déduit que θ est *au moins* un infiniment petit du second ordre, puisqu'obtenu par différence de λ' et λ, à condition de supposer que la longueur l de la platine n'est pas petite, ce qui est tout à fait admissible pour les suspensions que nous avons en vue (*).

Pour résoudre le système commençons par rechercher P' entre les équations (1), (4), (5), (6), et son analogue (6′) non écrite. Tous calculs effectués, négligeons les quantités d'ordre supérieur à trois; on trouve alors pour P'

(*) Le problème serait différent pour un mécanisme amplificateur à lames jumelles où l est alors *très* petit (ex.: Reed gauge de The Sheffield Corporation, U.S.A.).

l'expression:

$$\frac{P'L^2}{EI} = \frac{1}{2}\frac{VL^2}{EI} + \frac{350\dfrac{\Delta}{L}\sin\theta}{\left(\dfrac{f}{L}\right)^2 - \dfrac{f}{L}\operatorname{tg}\theta}$$

qu'on peut encore écrire sous la forme simplifiée suivante:

$$\frac{P'L^2}{EI} = \frac{1}{2}\frac{VL^2}{EI} + \frac{350(\Delta/L)\theta}{(f/L)^2}$$

en négligeant $(f/L)\operatorname{tg}\theta$ devant $(f/L)^2$ et en confondant le sinus de l'angle de tangage avec cet angle.

Avec les mêmes approximations calculons H entre (2), (5), (8) et son analogue (8'); ainsi que les quantités F', M_A et $M'_{A'}$, et portant toutes ces valeurs dans l'équation d'équilibre de rotation (3) on trouve, après de trop longs calculs pour être détaillés ici, qu'on a sensiblement:

$$\theta = \frac{\dfrac{v-\Delta/2}{L}\dfrac{VL^2}{EI}}{350\left(\dfrac{\Delta}{L}\right)^2}\left(\frac{f}{L}\right)^2 + \frac{12\left(1-\dfrac{1}{120}\dfrac{VL^2}{EI}\right) - 24\dfrac{a}{L}\left(1-\dfrac{1}{20}\dfrac{VL^2}{EI}\right)}{350\left(\dfrac{\Delta}{L}\right)^2}\left(\frac{f}{L}\right)^3 + \cdots$$

Cette relation va nous permettre d'énoncer quelques conclusions intéressantes.

L'angle de tangage en cas de charge dissymétrique est du second ordre par rapport au déplacement horizontal de la platine, et proportionnel à la charge vertical V.

En cas de charge symétrique, le premier terme étant identiquement nul, il reste un tangage du troisième ordre qu'on peut affaiblir en choisissant judicieusement la hauteur à laquelle on va attaquer la platine par la force horizontale H.

En cas de poussée restant à une distance fixe de la platine égale à la valeur a_{opt} trouvée précédemment, le tangage disparait.

Etudions le cas plus courant où la hauteur de la ligne d'action de la poussée reste fixe par rapport au bâti. Dans ce cas, on utilise la valeur b_{opt} trouvée précédemment. Introduisant dans la formule donnant l'angle de tangage la quantité

$$u = L - b_{opt} - \lambda,$$

on trouve qu'aux approximations effectuées il reste, en cas de charge symétrique, un tangage du cinquième ordre, donc de peu d'importance.

Le phénomène du tangage d'une platine suspendue élastiquement est donc d'importance assez faible. L'angle de tangage est du second ordre en cas de charge dissymétrique. Il tombe au troisième ordre en cas de charge symétrique et peut même être rendu d'un ordre supérieur au troisième par le choix de la position de la bielle de poussée agissant sur la platine.

Il y a toujours intérêt à utiliser une platine longue par rapport à la hauteur de la suspension.

Dans cet espace éthéré, cher aux auteurs de projets, où les poids sont nuls, le tangage est quasi totalement supprimé par le choix de la ligne d'action de la force à mi-hauteur de platine.

En conclusion le phénomène le plus désagréable est dû à la dissymétrie de la charge, c'est une des sujétions de la suspension à lames.

Quand on recense les platines construites ayant donné satisfaction, on est frappé par le fait que la plupart de ces platines sont poussées dans le plan de la platine en désaccord avec ce qui précède. Cela provient de ce qu'on n'introduit ainsi que des erreurs d'ordre trois, donc faibles par rapport aux erreurs laissées par une dissymétrie accidentelle de la charge à laquelle il faut toujours penser.

D'autre part, sauf cas exceptionnels, le centre de masse de la platine est toujours voisin du plan de celle-ci. Or, une platine montée sur lames est aussi, hélas, qu'on le veuille ou non, un sismographe doué d'un amortissement très faible. Au cas où l'axe de poussée ne passe pas par le centre de masse, toute force d'inertie horizontale va introduire un couple donnant lieu à une vibration horizontale relative de la platine fort pernicieuse. Dans le cas d'un microscope, cette vibration donnera une image floue, ce qui est un défaut fort grave.

C'est là la raison pour laquelle il y a souvent lieu d'abandonner la poussée à la hauteur optimum pour la remplacer par une vis de poussée agissant dans le plan horizontal de la platine. Ce qu'on perd en tangage (du troisième ordre!) est regagné par une moins grande sensibilité aux vibrations.

Nos résultats confirment bien ceux annoncés par Jones ([3]) qui écrit: « ... the effect of changing the height of drive is not very great, and it is apt to be masked by other effects... ». « It should be noted, however, that this effect is often not large compared with some of the effects due to other causes mentionned in this paper and, depending on the magnitude of these effects, it may sometimes be better to drive the movement at other than the ideally correct height. »

Dans un autre ordre d'idées, ce sont ces phénomènes relevant de la technique des vibrations qui ont fait abandonner les suspensions compensées simples pour les suspensions compensées asservies.

Toutes ces considérations illustrent bien l'adage du mécanicien suivant lequel le dessin d'une pièce de machine, aussi simple soit-elle, ne peut jamais

être entièrement effectué à partir des résultats donnés par la résolution mathématique d'une équation, aussi compliquée soit-elle.

* * *

L'auteur tient à exprimer sa gratitude au professeur G. P. S. Occhialini pour l'amical intérêt qu'il n'a cessé de prendre à son travail.

RIASSUNTO (*)

Il presente lavoro studia i movimenti di beccheggio (tangage, pitching) di una sospensione elementare, come pure la posizione ottima da dare alla biella di spinta per diminuire tale fenomeno parassita. Se si tratta lo spostamento orizzontale della platina come un infinitesimo di primo ordine si dimostra che il beccheggio dovuto alla posizione della forza di spinta è generalmente del terzo ordine. Questo termine del terzo ordine è annullato da una scelta opportuna dell'altezza del punto in cui si applica la spinta alla platina. Tale punto è sensibilmente a metà distanza tra la platina e l'incastro nel supporto. Se spesso si preferisce applicare la spinta nel piano della platina è per evitare le vibrazioni parassite della platina che in tal caso lavora come un sismografo.

(*) *Traduzione a cura della Redazione.*

A High Energy Nuclear Interaction.

A. Debenedetti, C. M. Garelli, L. Tallone and M. Vigone

Istituto di Fisica dell'Università - Torino
Istituto Nazionale di Fisica Nucleare - Sezione di Torino

(ricevuto l'11 Agosto 1956)

Summary. — We determined the $p\beta$ of the secondaries of a high energy jet from scattering measurements. We calculated the angular and momentum distribution in the centre of mass system and we found a good agreement with Heisenberg's and Wataghin's theories. We give also the value of the percentage of K-mesons emitted in the nuclear interaction and an estimate of the mean free path for nuclear interactions of the charged π-mesons.

Introduction.

During a search for high energy events we have observed a nuclear jet of high multiplicity, produced by a particle of charge 1, at plateau ionization, travelling almost parallel to the emulsion plane. The star consists of 42 tracks, of which 39 are due to relativistic particles; the narrow cone of the jet lies in one plate for 16.8 cm.

The 39 relativistic tracks are contained within a cone of half opening 0.17 rad. The remaining 3 tracks have ionization higher than the plateau value. The first one makes an angle greater than 90° with the direction of the primary, and is due to a particle of mass greater or equal to the proton mass. The other two tracks lie on opposite sides of the core of the jet; one is too steeply inclined to be identified, the other is probably a π-meson of a hundred MeV.

In a careful search within a cone of half-opening 10^{-2} rad around the direction of the primary particle, 12 independent pairs were found in the first 4 cm from the origin of the jet. The study of the cascades generated by these pairs is reported in reference [1].

---

[1] A. Debenedetti, C. M. Garelli, L. Tallone and M. Vigone: *Nuovo Cimento*, **4**, 1151 (1956).

On account of the favourable geometrical conditions, it has been possible to carry out scattering measurements on almost every track of the jet. The description of the method applied and the results obtained from scattering measurements are reported in Sect. **1**.

In Sect. **2**, with the help of the usual formulae of relativistic kinematics, we derive the distribution of angles and momenta of the secondary mesons in the centre of mass system.

In Sect. **3** we report the comparison with the theoretical previsions of HEISENBERG [2], WATAGHIN [3] and FERMI [4].

Adding to the data of the present jet those concerning other events having energies of the same order [1], we calculate in Sect. **4** the ratio $R = n_{\pi^0}/(n_{\pi^\pm} + n_K)$ between the number of π^0-mesons and the number of charged mesons ($\pi^\pm$ and K) which are produced in the nuclear interactions; in Sect. **5** we report our estimated value of the mean free path for nuclear interactions for the charged π-mesons.

1. – Scattering Measurements.

The reliability of scattering measurements on tracks of high energy has been discussed recently be several authors [5-8]. Scattering on individual tracks has been shown to be greatly affected by « spurious scattering », besides grain noise, reading noise and stage noise. The spurious scattering increases with the cell length and thus covers the effect of the true Coulomb scattering.

We therefore first tried to evaluate the magnitude of the spurious scattering and its dependence on cell size in our stack. For this purpose we carried out two types of measurements:

1) Measurements on the track of the primary of the jet. The basic cell used was of 500 μm. Following the methods suggested by the quoted authors, the contour of the track was determined by reading the position of the individual grains over a distance of 30 μm; a repeated measurement was taken at points displaced of 50 μm along the track. The stage noise had already been determined for our microscope. We make use of a formula, whose validity

---

[2] W. HEISENBERG: *Zeits. f. Phys.*, **126**, 569 (1949).

[3] G. WATAGHIN: *An. Ac. Bras. de Ciências* (Symposium 1941); *Phys. Rev.*, **74**, 975 (1948); *Nuovo Cimento*, **10**, 1602 (1953).

[4] E. FERMI: *Progr. Theor. Phys.*, **5**, 570 (1950); *Phys. Rev.*, **81**, 683 (1951).

[5] S. BISWAS, B. PETERS and RAMA: *Proc. Ind. Acad.*, A **41**, 154 (1955).

[6] H. FAY: *Zeits. f. Naturfor.*, **10** A, 572 (1955).

[7] E. LOHRMANN and M. TEUCHER: *Nuovo Cimento*, **3**, 59 (1956).

[8] F. A. BRISBOUT, C. DAHANAYAKE, A. ENGLER, P. H. FOWLER and P. B. JONES: *Nuovo Cimento*, **3**, 1400 (1956).

was shown by LOHRMANN (7), relating the quantities D_{total}, measured sagitta; D_{Coulomb}, sagitta due to the Coulomb scattering; D_{noise}, due to the various kinds of noises; D_{ss}, sagitta due to the spurious scattering:

$$D^2_{\text{total}} = D^2_{\text{Coulomb}} + D^2_{\text{noise}} + D^2_{\text{ss}} .$$

Since the energy of the primary of the jet is certainly greater than 10^{12} eV, the contribution of the Coulomb scattering to the measured sagitta is negligible; we can therefore obtain the value of the spurious scattering, for a given cell size, from the relation:

$$D^2_{\text{ss}} = D^2_{\text{total}} - D^2_{\text{noise}} .$$

By calculating D_{ss} for different cell lengths we obtained the dependence of the spurious scattering on the cell size. We found that D_{noise} varies only slowly with varying cell size; therefore we assumed for it a constant value of 0.135 μm.

2) Measurements on tracks of the central core of the jet. The signal obtained from relative scattering measurements on a pair of tracks, D_{d}, is independent of spurious scattering; the same tracks, when measured individually, give a signal, D_{sing}, which is affected by spurious scattering. The value of the spurious scattering can be deduced from the formula:

$$D^2_{\text{ss}} = D^2_{\text{sing}} - \tfrac{1}{2} D^2_{\text{d}} ,$$

where both D_{sing} and D_{d} have been corrected for noise.

The values for the spurious scattering sagitta found with the two methods were in good agreement within the statistical errors. The dependence on cell size is of the form t^n, with $n = 0.84$.

It appears therefore that theoretically energies up to 10 GeV can be determined from scattering measurements with cell size of 1 mm, and energies up to about 40 GeV can be obtained with cells of 1 cm, because in this way the signal observed is more than twice the signal due to spurious scattering. In practice, the reliability of the values thus obtained depends of course on the number of measured cells.

Having evaluated the spurious scattering in our stack, it was possible to determine the $p\beta c$ of the secondary particles of the jet through one of the following methods:

a) tracks of the inner cone: from relative scattering measurements we obtain the average value of the $p\beta c$ of the two measured tracks. This kind of measurement is reliable as long as the two tracks are contained in the optimum zone of the optical system: in our cases, their projected distance did not exceed 50 μm, and the difference in depth was smaller than 20 μm;

b) tracks of the outer cone: scattering measurements on individual tracks, after elimination of noise and spurious scattering, give the $p\beta c$ of the particles. For these tracks the measured length is limited by the fact that the emulsion sheet has been cut at a distance of 4 cm from the origin of the jet, and that the identification of the tracks after the cut is of remarkable difficulty.

In both cases the basic cell size was 500 μm; to calculate the $p\beta c$ of the tracks we choose the cell, multiple of the basic one, for which the obtained signal was at least double of the signal due to the spurious scattering. The results are collected in Table I.

2. – Angular Distribution in the Centre of Mass System.

We deduce the angular distribution in the centre of mass system from the formula:

$$\gamma_c \operatorname{tg} \theta^* = \pm \frac{\sin \theta}{\cos \theta - (\beta_c/\beta)}, \tag{1}$$

where θ, β refer to the secondary particles and represent respectively the angle with the primary direction and the velocity (in c units) in the laboratory system (L.S.). The corresponding quantities in the centre of mass system (G.S.) are marked with a star. β_c is the velocity of the G.S., and $\gamma_c = 1/\sqrt{1-\beta_c^2}$.

We measure experimentally the quantities θ and $p\beta c$. In order to calculate the β which appears in formula (1), we need to know the mass of the secondaries. Our measurements do not allow the determination of the mass of each single particle; we therefore assumed that all the secondary particles are π-mesons, and consequently that the number of unseen neutral particles is one half of the number of the charged particles. In our case this approximation is not as rough as it could appear: in fact, even for the lowest measured energies, the error due to the uncertainty in the mass is smaller than the experimental error.

Another quantity that we need in order to apply the Lorentz transformation and that we cannot determine experimentally is γ_c. A criterion for the choice of γ_c is given by the hypothesis of nucleon-nucleon collision, without any further restrictive assumption of isotropic emission and equipartition of energy in the G.S. This hypothesis is supported by the fact that only 3 non-relativistic tracks are visible in the interaction.

In the case of nucleon-nucleon collision, γ_c represents also the total energy (in rest mass units) of each colliding nucleon in the G.S., and is related to the

TABLE I.

Track No.	Angle with the primary direction (10^{-3} rad)	$p\beta c$ (GeV)	Remarks
1	0	—	
2	0.5	220 ± 180 *	
3	0.9	220 ± 180 *	
4	3.2	110 ± 50	
5	3.3	110 ± 50	
6	3.6	> 50	relative scattering measurements
7	4.6	> 50	
8	5.4	65 ± 26	
9	6.0	57 ± 26	
10	7.0	12 ± 4	
11	7.1	—	
12	9.0	128 ± 40	
13	10.0	128 ± 40	
14	10.6	42 ± 13	scattering on individual track
15	12.0	19 ± 5	relative scattering
16	12.7	19 ± 5	
17	15	3.5 ± 0.4	
18	16	16 ± 4	
19	17	41 ± 16	
20	27	4.8 ± 1.0	
21	30	3.5 ± 1.3	
22	32	5.8 ± 1.4	
23	33	1.0 ± 0.5	
24	36	5.6 ± 0.7	
25	37	23 ± 13	
26	40	2.0 ± 0.7	
27	41	1.1 ± 0.3	scattering on individual tracks
28	45	1.1 ± 0.1	
29	46	0.6 ± 0.3	
30	47	3.3 ± 0.4	
31	63	—	
32	92	2.2 ± 0.7	
33	128	3.7 ± 1.3	
34	131	1.9 ± 1.1	
35	133	5.5 ± 2.5	
36	138	2.9 ± 0.3	
37	143	3.1 ± 1.0	
38	148	0.8 ± 0.3	
39	168	6.4 ± 2.9	

(*) The value reported in the table has been obtained with cells of 10 mm, in agreement with the value 180 ± 60 GeV obtained with cells of 6 mm.

total energy of the primary nucleon (in rest mass units), γ_L, in the L.S., by the formula $\gamma_L = 2\gamma_c^2 - 1$. A lower limit for the sum of the energies of the secondaries in the L.S. was determined experimentally (sum of the secondary energies 2 100 GeV, of which about 1 400 GeV measured for the charged secondaries and 700 GeV attributed to the neutral secondaries); consequently the energy of the primary in the L.S. must be at least of 2 100 GeV, and the corresponding lower limit for γ_c is 34. If we assume that the distribution of the momenta of the neutral mesons is similar to the distribution of the charged ones, we can deduce the velocity of the centre of mass system from the momentum balance of the charged mesons in the G.S. The value of γ_c thus obtained is 45. We remark that for $\gamma_c = 45$ the angular distribution in the G.S. is nearly symmetrical with respect to the equatorial plane (18 tracks in the forward direction and 21 in the backward direction) and that this symmetry remains unaltered until γ_c reaches the value 55. For $\gamma_c > 55$ the number of tracks emitted in the backward cone increases (for $\gamma_c = 100$ only a quarter of the tracks are in the forward cone). Consequently the interval where a reasonable value of γ_c can be found is $35 \div 55$.

In Fig. 1 we give the angular distribution in the G.S.

This distribution has been calculated both for $\gamma_c = 40$ and $\gamma_c = 50$, and the results do not differ appreciably.

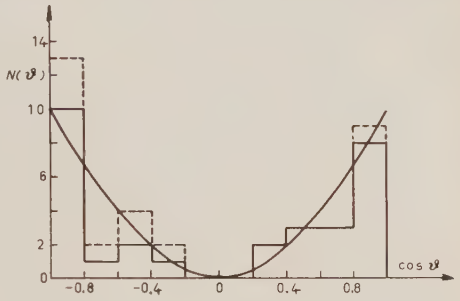

Fig. 1. – The dotted part refers to tracks whose $p\beta c$ was only roughly determined. The hystogram is well fitted by a function $\cos^2\theta$.

The comparison between the experimental angular distribution and the distribution obtained with the methods suggested by DILWORTH *et al.* [9] and by CASTAGNOLI *et al.* [10] is shown in Figs. 2 and 3.

It appears that both the mentioned approximate calculations give a fairly good agreement with the experimental data.

We wish to point out that both the calculations of C. C. DILWORTH *et al.* and of C. CASTAGNOLI *et al.* give a value of γ_c which is in good agreement with our estimate. As in these methods γ_c is deduced from the angular distribution in the L.S., with the hypothesis of the equipartition of the momentum

---

[9] C. C. DILWORTH, S. J. GOLDSACK, T. F. HOANG and L. SCARSI: *Nuovo Cimento*, **10**, 1261 (1953); T. F. HOANG: *Journ. de Phys.*, **14**, 395 (1953).

[10] C. CASTAGNOLI, G. CORTINI, C. FRANZINETTI, A. MANFREDINI and D. MORENO: *Nuovo Cimento*, **10**, 1539 (1953).

among the mesons in the G.S., one should conclude that the angular distribution in the L.S. depends only weakly on the spectrum of momenta in the G.S.

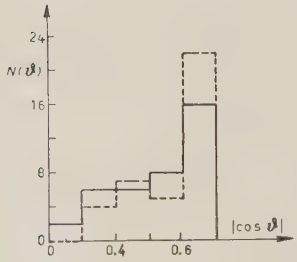

Fig. 2. – The full line hystogram refers to the distribution given by DILWORTH *et al.*; the dotted part gives the experimental distribution.

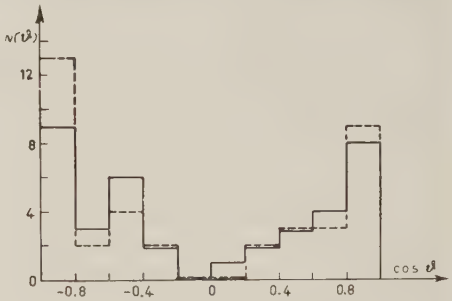

Fig. 3. – The full line hystogram refers to the distribution given by CASTAGNOLI *et al.*; the dotted part gives the experimental distribution.

3. Momentum Distribution in the Centre of Mass System.

In Sect. 2 we deduced the angular distribution in the G.S.; we can now obtain the momentum distribution from the preceding result and from the formula of transverse momentum conservation:

$$p^* \sin \theta^* = p \sin \theta \,, \tag{2}$$

where p is the momentum of a secondary particle in the L.S., and p^* is the corresponding quantity in the G.S.

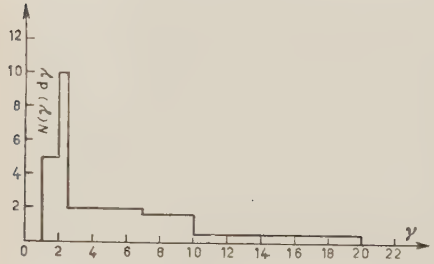

Fig. 4.

In Fig. 4 we show the momentum distribution obtained by using the angular distribution of Fig. 1.

The average value of the total energy of the π-mesons emitted in the collision is of about 1 GeV in the G.S.

The anelasticity factor K varies from 0.66 to 0.78 when $\gamma_{\text{c.m.}}$ decreases from 50 to 40.

We have now deduced three elements on which we can base a comparison with the results of the theories of multiple meson production: the spectrum of the momenta in the G.S., the average value of the momentum of the mesons in the G.S. and the multiplicity. It is well known that Heisenberg's [2] and Wataghin's [3] theories greatly differ from Fermi's [4] theory in the evaluation of the quantities listed above.

In Fig. 5 we show the comparison between the experimental spectrum of momenta in the G.S. and the one predicted by Fermi. For the parameter ϱ of Fermi's theory the value $\varrho = 0.9$ was deduced from the experimental angular distribution.

According to Fermi's theory, the probability that mesons of high momentum are emitted in the G.S. is much higher than the probability deduced from our results. Consequently the value of the multiplicity given by Fermi is considerably lower than the observed one.

The agreement seems to be better with the spectrum of Heisenberg's theory, of the type $\mathrm{d}p/p^2$. In Table II we compare the values of some quantities deduced from our experimental data with the results of Heisenberg's and Wataghin's theories, calculated for the same energy of the incoming nucleon and the same anelasticity factor.

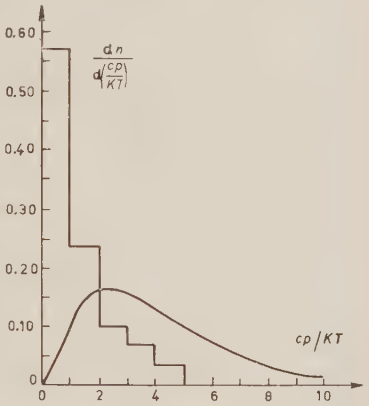

Fig. 5. – The hystogram shows the experimental distribution; the curve gives the predictions of Fermi's theory, for $\varrho = 0.9$.

TABLE II.

	Experimental	Theoretical (Heisenberg)	Theoretical (Wataghin)
Average momentum of the mesons in the G.S.	1 GeV	0.8 GeV	0,85 GeV
Multiplicity	59 particles	71 particles	66 particles

If we take into account the uncertainty of our experimental data and the approximations needed in our calculations, we can conclude that the event is in sufficiently good agreement with the theories of Heisenberg and Wataghin.

4. – Ratio of Neutral π-Mesons to Shower Particles.

Following the method suggested by BRISBOUT *et al.* [11], we have calculated the ratio of the number of neutral mesons to the number of charged mesons

[11] F. A. BRISBOUT, C. DAHANAYAKE, A. ENGLER, Y. FUJIMOTO and D. H. PERKINS: private communication.

(π- and K-mesons) emitted in the collision. The results concerning jets 1, 2, 3 reported in reference [1] have been included in the calculations in addition to the data of the present event. The value obtained is:

$$R = \frac{n_{\pi^0}}{n_{\pi^\pm} + n_K} = 0{,}426 \pm 0{,}060 .$$

5. - Mean Free Path for Nuclear Interactions of High Energy Charged π-Mesons.

From the total length of π-mesons track followed (335 cm), and from the number of interactions observed (9), we can calculate the mean free path for nuclear interactions of high energy charged π-mesons. A correction has been made on the total length of π-mesons track, by taking into account the percentage of K-mesons among the shower particles, deduced from the estimated value of R (see Sect. **4**). We find for the mean free path for production of stars the value 37 ± 6 cm.

* * *

We are greatly indebted to Prof. R. DEAGLIO for his constant interest in our work and to Prof. G. WATAGHIN for many stimulating discussions.

We wish to thank the organizers of the Texas flights and the organizers of the Po-Valley expedition of 1955, for the exposure of the plates, the Bern and Milan Universities for leaving at our disposal their part of the stack.

Our thanks are also due to our group of scanners, and especially to Mr. M. GRECO and Mr. CHIAUDANO for their useful cooperation.

RIASSUNTO

Abbiamo determinato il $p\beta$ dei secondari di un getto di alta energia mediante misure di scattering. Abbiamo calcolato la distribuzione degli angoli e dei momenti nel sistema del baricentro trovando un buon accordo con le teorie di Heisenberg e di Wataghin. Diamo anche il valore della percentuale di mesoni K emessi nell'interazione e quello del cammino libero medio per interazioni nucleari dei carichi.

A Study on Electromagnetic Showers in Nuclear Emulsions.

A. Debenedetti, C. M. Garelli, L. Tallone and M. Vigone

Istituto di Fisica dell'Università - Torino
Istituto Nazionale di Fisica Nucleare - Sezione di Torino

(ricevuto l'11 Agosto 1956)

Summary. — A considerable number of electromagnetic cascades have been analyzed to determine the increase of the multiplicity with the primary energy, the spectrum of the energies of the secondaries and the trident production. No appreciable discrepancy from the theory has been remarked.

Introduction.

In the last few years, some authors (1) have observed in nuclear emulsions showers of electron pairs that are not immediately comprehensible because of the high multiplicity and the production of a too large fraction of energetic secondaries.

Excluding the introduction of unknown particles, two types of assumptions are suitable to interpret these events:

a) the electrodynamical theory does not describe exactly the development of a cascade in the first radiation length;

b) these events are produced by photons of very high energy (10^{13}—10^{14} eV) or by more than one photon.

(1) M. Schein, D. M. Haskin, and M. G. Glasser: *Phys. Rev.*, **95**, 855 (1954); A. Debenedetti, C. M. Garelli, L. Tallone and M. Vigone: *Nuovo Cimento*, **2**, 220 (1955); A. Jurak, M. Mięsowicz, O. Stanisz and W. Wolter: *Bull. Acad. Pol. Sci., Cl. III*, **3**, 369 (1955); M. Koshiba and M. F. Kaplon: *Phys. Rev.*, **100**, 327 (1955); A. Debenedetti, C. M. Garelli, L. Tallone, M. Vigone and G. Wataghin: *Nuovo Cimento*, **3**, 226 (1956); L. Barbanti-Silva, C. Bonacini, C. De Pietri, I. Iori, G. Lovera, R. Perilli-Fedeli and A. Roveri: *Nuovo Cimento*, **3**, 1465 (1956).

Our purpose is to say something more on the assumption *a*) investigating:

1) the increase of the multiplicity with the energy of the primary photon;

2) the energy spectrum of the secondary electrons;

3) the mean free path for trident production.

The reliability of the results of an investigation on these phenomena is weakened by the indetermination of the energy of the primary photon and the difficulty in calculating the fluctuations of the cascade development. We think that the only way to overcome these difficulties is to compare with the theory a considerable number of cascades of which we can independently determine the order of magnitude of the energy of the primary photon. We made a systematic scanning for high energy events in a stack of nuclear emulsions exposed to the cosmic radiation at about 30 km of altitude with the balloons technique. We found 112 electromagnetic cascades and 4 nuclear jets with associated electromagnetic cascades.

1. – Increase of the Multiplicity with the Energy of the Primary Photon.

To study this problem, we can use only the electromagnetic cascades associated with nuclear jets, because these only allow us to evaluate their energy independently from the development of the cascade.

In this connection we observe that:

— the photons that give rise to these cascades are produced in the disintegration of π^0-mesons, secondaries of the jet;

— it is probable that in a collision with multiple meson production the available energy is equally distributed between neutral and charged mesons;

— we can calculate the momenta distribution of the secondary charged mesons in the laboratory system (L.S.), from the knowledge of their angles with the direction of the primary particle, if we assume that all the secondaries have the same mass, that, in the centre of mass system (G.S.), they have all the same energy and their velocity is equal to the velocity of the colliding nucleon, and that they are produced in a nucleon-nucleon collision;

— these assumptions are rather restrictive, and we have no reason to think that they are valid in our cases, but the results of the calculations made under these assumptions are susceptible of a control if we can measure in a completely independent way the momentum of some secondary mesons.

Consequently our proceeding was the following: for each jet we determined the γ_c (energy of the colliding nucleon in mass rest units in the G.S.) from

the angular distribution of the secondary particles in the L.S. ([2,3]) and then we deduced the energy of the mesons in the L.S. attributing to each meson

TABLE I.

Jet No.	Primary	Number of shower particles	γ_c of the primary	Secondary particles: angle with the primary (10^{-3} rad)	pc from scattering measurements (GeV)	pc from secondary interaction (GeV)	pc from the γ_c of the primary (GeV) *
1	p	46	93	1	$\geqslant 100$	—	182
				2	$\geqslant 100$	—	178
				2.4	$\geqslant 100$	—	176
				2.5		$3 \div 4$	175
				3.4	—	~ 2	168
				7.1	—	$100 \div 200$	129
2	p	15	29	2	$\geqslant 50$	—	57
				3	$\geqslant 50$	—	57
				4	$\geqslant 50$	—	57
3**	α	25	140 per nucleon	0.6	—	2 800	—
				3	—	1 600	—
				10	—	$30 \div 40$	—
4	p	39	45 ± 10	$p\beta c$ of all the secondary particles have been determined from scattering measurements. Details on the event are reported in the paper: *A High Energy Nuclear Interaction*, in *Nuovo Cimento*, **4**, 1142 (1956).			

(*) The figures of the last column represent the momenta, in the L.S., of the mesons ejected in the forward direction in the G.S. The mesons emitted in the backward direction have in the L.S. momenta of some GeV. Therefore, the first and the second secondary star of jet no. 1 are probably produced by a meson emitted in the backward direction in the G.S.

(**) In the case of jet no. 3, since it is produced by an α-particle and the centre of the jet is in the cut of the emulsion sheet, the γ_c of the primary has not been calculated from the angular distribution of the secondaries in the L.S. The γ_c that we report in the table has been deduced from the angular distribution of the secondaries of a jet with a neutral primary associated with jet no. 3. The jet with neutral primary has 5 relativistic tracks in a cone of $1.7 \cdot 10^{-2}$ rad, and has neither evaporation tracks nor recoil. It seems logical to think that this jet has been produced by a neutron of the α-particle and that therefore the energy of this neutron can be assumed as the energy of each nucleon of the α-particle and in particular of the nucleon producing the jet no. 3. From the interactions of the secondaries of jet no. 3 in the cone of half opening angle of 10^{-2} rad, we deduce that these secondary mesons can have an energy between 2 800 and 30 GeV. We compare the energy of the cascades associated with the jet no. 3 with this interval of energy (comparison shown in Table II).

([2]) C. C. DILWORTH, S. J. GOLDSACK, T. F. HOANG and L. SCARSI: *Nuovo Cimento*, **10**, 1261 (1953); T. F. HOANG: *Journ. de Phys.*, **14**, 395 (1953).

([3]) C. CASTAGNOLI, G. CORTINI, C. FRANZINETTI, A. MANFREDINI and D. MORENO: *Nuovo Cimento*, **10**, 1539 (1953).

a mean energy of 1 GeV in the G.S. We choose this mean energy according to Heisenberg's theory (1), because our events are high multiplicity events. Every time it has been possible, we determined the secondary energies either from the study of their interactions with the nuclei of the emulsion, or from relative scattering measurements.

Table I shows the comparison between the values of the momenta in the L.S. which we deduced in the described way and the experimental data which we could obtain.

We think that the agreement is sufficiently good to justify our deduction of the energy of the secondary mesons.

We made a scanning in a cone of half opening angle $\sim 10^{-2}$ rad along the axis of each jet, to look for electron pairs created by photons coming from the disintegration of π^0-mesons. We choose the independent pairs (i.e. the pairs that are not produced through bremsstrahlung), checking the distance of each pair with respect to those already materialized with the help of a target diagram. Each independent pair has been followed for a radiation length, and its secondary production has been analyzed. From the number of secondary pairs we deduced the energy of the primary photon using Arley's curves (5).

In Table II we collected the energies of the π^0-mesons which make an angle $\leqslant 10^{-2}$ rad with the primary direction, calculated in the way explained before, and the energies of photons found in the same cone, calculated from the development of the cascades that they produce.

TABLE II.

Jet No.	Energy of π^0-mesons (GeV)	No. of photons of energy				Remarks
		< 1 GeV	1–10 GeV	10–100 GeV	100–1000 GeV	
1	186–100	3	3	9	1	—
2	58–53	1	1	4	—	—
3	2800 30	—	7	4	2	—
4	200–60	1	5	4	2	The last two photons have energy $E < 200$ GeV

The two figures of the second column, refer respectively to the energy of a π^0-meson that makes on angle of 0 rad and 10^{-2} rad with the direction of the primary.

The slow pairs are partly due to the disintegration of π^0-mesons emitted in a backward direction in the G.S., and partly to the non-equipartition of energy between the two γ-rays arising from π^0 emitted in a forward direction in the G.S.

(1) W. HEISENBERG: *Zeits. f. Phys.*, **126**. 569 (1949).
(5) N. ARLEY: *Proc. Roy. Soc.*, A **168**. 519 (1938).

It results that these energies, deduced in completely independent ways, (the π^0 energy from the study of the nuclear jet, the photon energy from the study of an electromagnetic cascade) are compatible.

In conclusion, it seems possible to say that, at least up to energies of the order of 1 000 GeV, the energy deduced from the longitudinal development of a cascade, with Arley's calculations, is acceptable as order of magnitude.

2. – Energy Spectrum of Secondary Electrons.

When the energy of the primary photon is known, the cascade theory foresees an energy spectrum for the secondary pairs ([5]). To attempt a comparison of this spectrum with experimental data, it is necessary to know the energies of the primary photon, of each bremsstrahlung pair, and to reduce as much as possible the error due to fluctuations by extending the analysis to a remarkable number of cases. In Sect. 1 we demonstrated that it is possible to deduce the energy of the primary photon from the development of its cascade up to an energy of the order of 1 000 GeV. This allows us not to

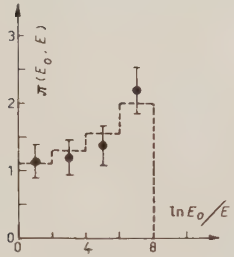

Fig. 1. – Cascades initiated by a photon of energy of the order of 100 GeV $\pi(E_0, E)$: number of electrons of energy $> E$ produced in one radiation length by an electron of energy E_0.

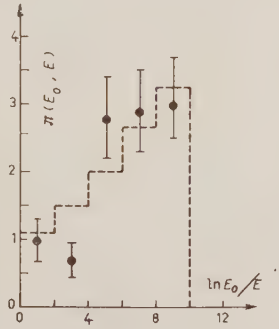

Fig. 2. - Cascades initiated by a photon of energy of the order of 1 000 GeV $\pi(E_0, E)$: number of electrons of energy $> E$ produced in one radiation length by an electron of energy E_0.

limit ourselves to the study of cascades associated with jets. Besides these cascades we analyzed 12 independent ones chosen between the 112 found in systematic scanning with the following criterion: cascades initiated by a photon that materialized inside the emulsion and whose angle with the plane of the emulsion is not $> 20°$.

We divided the cascades (associated with jets or not) in two groups: 19 cascades produced by a photon of energy E_0 of the order of 100 GeV, and

9 cascades produced by a photon of the order of 1 000 GeV. To calculate the energy of the bremsstrahlung pairs, we do not have at our disposal any data but the opening angle. LOHRMANN (6) demonstrated that it is right to calculate the energy of a pair from its opening angle as long as the measurement of the opening angle can be made at a distance $\leqslant 100$ μm from the origin of the pair. For pairs with smaller opening angle, we used Stearn's formula (7) which gives the mean square angle corresponding to a certain energy; we think that this method is justified because we do not apply the formula to a single pair, but to groups of pairs with the same opening angle.

In the Figs. 1 and 2, we show the comparison between the theoretically foreseen distribution and that experimentally obtained.

In conclusion, the experimental data agree with the energy spectrum foreseen by the cascade theory, at least for energies of the primary photons up to 100 GeV.

3. – Mean Free Path for Trident Production.

The cascade theory does not take into account the direct production of pairs by the electrons (trident production) and is therefore suitable till the mean free path for trident production is large compared to the radiation length. Some experiments (8) seem to indicate that the mean free path for trident production is shorter than that calculated following the theory of Bhabha (9).

Let us call « apparent trident » either the true tridents (i.e. electron pairs directly produced by electrons) or the pseudo-tridents (i.e. the bremsstrahlung pairs that materialized at a distance $\leqslant 0.2$ μm from an electron track). KAPLON and KOSHIBA (8) calculated as a function of the energy of the parent electron the percentage of bremsstrahlung pair that are pseudo-tridents. From their work it results that 20% of the pairs created in one radiation length by an electron of energy 10 GeV materialize at a distance $\leqslant 0.2$ μm from the parent track and that this percentage increases very rapidly with the energy of the primary electron (it is 60% at 100 GeV). Theoretically it would be possible to apply this correction to the experimental data and therefore give an experimental value of the mean free path for trident production. Unfortunately, the correction to be applied is so large that the results have statistical significance only if the calculation is made on the total production observed, while it would be desirable to compare the theoretical mean free

(6) E. LOHRMANN: *Nuovo Cimento*, **2**, 1029 (1955).
(7) M. STEARNS: *Phys. Rev.*, **76**, 836 (1949).
(8) M. KOSHIBA and M. F. KAPLON: *Phys. Rev.*, **97**, 193 (1955); **100**, 327 (1955).
(9) H. J. BHABHA: *Proc. Roy. Soc.*, A **152**, 559 (1935).

path to the experimental one in each energy interval. Therefore, for each interval of energy, we determined the number of true tridents foreseen by the theory ([9]); we evaluated the number of bremsstrahlung pairs produced by the followed electron tracks, and hence the number of apparent tridents applying Kaplon's method. The total number of apparent tridents thus obtained is the only figure that we can compare with the experimental datum.

The results are given in Table III.

TABLE III.

Order of magnitude of the parent electron energy (GeV)	Mean free path for trident from Bhabha's theory (mm)	Total track length observed (mm)	Theoretical number of true tridents	Mean track (radiation units)	Evaluated number of bremsstrahlung pairs	Calculated number of apparent tridents
1	480	2370	4.9	0.6	28	6.2
10	250	1300	4.8	0.7	30	10.8
100	140	1320	9.4	1.1	48	35.2

Total calculated number of apparent tridents: 52.3
Total experimental number of apparent tridents: 55

From this comparison, no anomalous trident production is visible.

We wish to point out that, as it is shown in Table III, the number of pseudotridents is of the same order as the theoretical number of true tridents. Consequently our result depends in a very critical way on the evaluation of the number of pseudotridents. Such an evaluation requires the knowledge of the energy of the primary electron and a choice of the minimum energy of the secondaries: these factors introduce a very large uncertainty that might be responsible for the divergence between our result and that of KAPLON ([8]).

4. – Unusual Events.

During the scanning made for the present work, we observed two cases of cascades that look different from those analyzed in the preceding sections because of the high multiplicity and the very strong collimation and that, for these features, can be associated with the cases already published ([1]). Unfortunately, also these two events are not in good geometrical conditions, so that direct measurements giving elements to allow an interpretation are not possible.

TABLE IV. *Event A - initiated by an electron.*

Distance from entrance point (radiation lengths)	Number of electrons	Opening angle of the secondary pairs (10^{-4} rad)	Radius of the section of the shower (μm)
0.36	3	< 0.4	
0.62	5	< 5	
0.75	7	< 10	
0.82	9	< 10	
0.96	11		8
1.02	13		15
1.8	40		100
3.2	177		200
4.3	240		600

In the last column is reported the radius of the section of the shower that contains the number of electron tracks given in the second column.

TABLE V. - *Event B - initiated by a photon.*

Distance from the origin of the first pairs (rad. lengths)	Number of electrons	Opening angle of the secondary pairs (10^{-3} rad)	Radius of the section of the shower (μm)
0	2	0.1	
0.14	4	5	
0.36	6	< 1	
0.45	8	< 1	
0.51	10	< 1	
0.57	12	< 1	
0.63	14	50	
0.67	16	25	
0.74	18	< 1	
0.77	20	< 1	
0.78	22	60	
0.81	24	50	
0.81	26	50	
0.98	28	< 1	
1.01	30	20	
1.07	32	< 1	
1.30	26		20
1.50	36		25
1.75	72		50
2.00	100		60
2.20	117		65
2.40	154		70

In the last column is reported the radius of the section of the shower that contains the number of electron tracks given in the second column.

Thinking that only the study of a big number of such cases can give some reliable results, and because of the rarity of these events, we believe that it is useful to give all the data that it has been possible to collect.

In a completely tentative way, we can make some considerations about these events, following the two types of assumptions that we pointed out in the introduction of this work.

From the results of the preceding sections and according to the work of PINKAU ([10]), we concluded that a statistics on a rather remarkable number of events with energy ~ 1000 GeV, did not show any sensible deviation from the electromagnetic theory. We can therefore exclude that the unusual events can be explained under assumption *a*).

With regard to the hypothesis *b*), unlike the two cases that we studied before ([1]), these last two cases do not show any geometrical feature that indicates the presence of more than one photon. The longitudinal development of these showers of electron pairs, is explainable as produced by one photon (one electron in case A) if we attribute to the primary an energy of 10^{13}-10^{14} eV.

* * *

We are greatly indebted to Prof. R. DEAGLIO for his constant interest in our work and to Prof. G. WATAGHIN for many stimulating discussions.

We wish to thank the organizers of the Texas flights and the organizers of the Po-Valley expedition of 1955, for the exposure of the plates, the Bern and Milan Universities for leaving at our disposal their part of the stack.

Our thanks are also due to our group of scanners, and especially to Mr. M. GRECO and Mr. CHIAUDANO for their useful cooperation.

([10]) K. PINKAU: *Nuovo Cimento*, **3**, 1285 (1956).

RIASSUNTO

Studiando un notevole numero di cascate elettromagnetiche, abbiamo determinato l'andamento della moltiplicazione in funzione dell'energia del primario, lo spettro di energia delle coppie secondarie e la produzione di tridenti. Non abbiamo rilevato nessuna apprezzabile differenza dalle previsioni teoriche.

Magnetic and Scintillation Spectrometers; the case of the γ-Rays of $^{228}_{90}$Th and its Decay Products.

B. Chinaglia and F. Demichelis

Istituto di Fisica Sperimentale del Politecnico - Torino

(ricevuto il 28 Agosto 1956)

Summary. — We have investigated the γ spectrum of $^{228}_{90}$Th in equilibrium with its decay products by means of a scintillation spectrometer, and particularly the γ spectrum of $^{212}_{84}$Po. The results are in agreement with those of some Authors. We then discuss the reliability of our results. These are compared with those obtained by means of the magnetic spectrometer.

The spectroscopy of radiations emitted by radioactive nuclides can be performed either with the classical magnetic or with the scintillation spectrometer.

The γ-ray scintillation spectroscopy seems to be able to give us more and more good results owing to the reliability of NaI(Tl) crystals.

We have pursued the researches on scintillation γ-spectroscopy referred in [1] and this paper contains a study of the γ-spectrum of $^{228}_{90}$Th in equilibrium with its decay products. This study follows the program of the researches developed by one of us (F. D.), who in this work had a useful collaboration (B. C).

Among these decay products the following nuclides are emitting γ-rays (see Table I).

The results on $^{212}_{84}$Po obtained by means of the magnetic spectrometer don't agree very well among themselves; on the contrary the data on the other nuclides are not discordant.

[1] B. Chinaglia and F. Demichelis: *Nuovo Cimento*, **3**, 51 (1956).

TABLE I.

Nuclide	Energy in MeV
$^{224}_{88}$Ra	0.083
$^{220}_{86}$Em	0.241
$^{212}_{83}$Bi	0.2386 0.115; 0.164; 0.176 } weak intensity 0.250; 0.300 }
$^{208}_{81}$Tl	0.040 0.124; 0.164; 0.288 } 0.328; 0.432; 0.452 } weak intensity 0.472; 0.616. }
$^{202}_{82}$Pb	0.233; 0.277; 0.510; 0.582; 0.859; 2.62 .
$^{212}_{84}$Po	various γ-rays with energy between 0.73 and 2.20 MeV.

TABLE II.

Authors	Energy in MeV								
ELLIS (1934)	0.726						1.62	1.80	
ALICHANOW and DZELEPOV (1938)					1.35	1.50	1.60	1.80	2.20
CURRAN, DEE and STROTHERS (1940)				1.10			1.68		
LATYSHEV and KULCHITSKY (1941)					1.35	1.50	1.60	1.80	2.20
ITOH and WATASE (1941)			0.96					1.77	
MANDEVILLE (1942)	0.73						1.58	1.77	
JOHANSSON (1947)	0.72	0.83	1.03		1.34		1.61	1.81	
MARTIN and RICHARDSON (1950)	0.726								
MULLER, HOYT, KLEIN and DUMOND (1952)	0.729								
MARTIN and PARRY (1955)							1.60		

In Table II are reported the results on $^{214}_{84}$Po [2].

Owing to the lack of agreement between the above data an investigation of the $^{212}_{84}$Po γ-spectrum with the scintillation method seemed us to be useful.

Experimental Apparatus and Results.

The detector is a NaI(Tl) crystal coupled with a DuMont 6292 photomultiplier. The pulses from the photomultiplier are sent, through a linear amplifier, to a pulse height analyzer.

We have used several crystals of various sizes: $\frac{3}{4}'' \times \frac{3}{4}''$, $1'' \times \frac{1}{2}''$, $2'' \times 2''$.

The spectrometer, calibrated with $^{137}_{55}$Cs (0.661 MeV), $^{60}_{27}$Co (1.17 and 1.33 MeV) and the same $^{208}_{82}$Pb (2.62 MeV), has a linear response till 2.62 MeV.

In Fig. 1. the experimental results obtained by means of the $2'' \times 2''$ crystal are represented. In this case the resolution (full width of peak at 1/2 counting rate) for 2.62 MeV is 9%.

Using crystals of smaller sizes we obtained spectra of slightly different shape, owing to the greater Compton continuum and to the lower detection efficiency. Actually the useful range of energy for the $\frac{3}{4}'' \times \frac{3}{4}''$ crystal is limited to about 2 MeV.

However, except for the 2.62 MeV γ-ray, which can be hardly detected with the smaller crystals, the same peaks are easily recognized in all the spectra obtained with the various crystals.

From Fig. 1 we can deduce the existence of the following γ-rays:

0.08 MeV of $^{224}_{86}$Ra;

0.236 MeV of $^{212}_{83}$Bi (the 0.241 MeV γ-ray of $^{220}_{84}$Em and the 0.233 MeV γ-ray of $^{208}_{82}$Pb give rise to the same peak);

0.51; 0.58; 2.62 MeV of $^{208}_{82}$Pb;

0.83 MeV peak can be ascribed either to $^{212}_{84}$Po or to $^{208}_{82}$Pb;

0.73; 1.04; 1.34; 1.50 (Compton edge at 1.28 MeV); 1.80;

2.20 (Compton edge at 1.97 MeV) of $^{212}_{84}$Po.

[2] C. D. Ellis: *Proc. Roy. Soc.*, A **143**, 350 (1934); A. I. Alichanow and V. P. Dzelepov: *Compt. Rend. Acad. Sci. URSS*, **20**, 113 (1938); S. C. Curran, P. I. Dee, J. E. Strothers: *Proc. Roy. Soc.*, A **174**, 546 (1940); G. D. Latyshev and L. A. Kulchitsky: *Journ. Phys. USSR*, **4**, 515 (1941); J. Itoh and Y. Watase: *Proc. Phys. Math. Soc. Japan*, **23**, 142 (1941); C. E. Mandeville: *Phys. Rev.*, **62**, 309 (1942); G. D. Latishev: *Rev. Mod. Phys.*, **19**, 132 (1947); A. Johansson: *Ark. Mat. Astr. Fys.*, A **34**, 9, 1 (1947); D. G. E. Martin and H. O. W. Richardson: *Proc. Phys. Soc.*, A **63**, 223 (1950); D. E. Muller, H. C. Hoyt, D. J. Klein and J. W. DuMond: *Phys. Rev.*, **88**, 775 (1952); D. G. E. Martin and G. Parry: *Proc. Phys. Soc.*, A **28**, 1177 (1955).

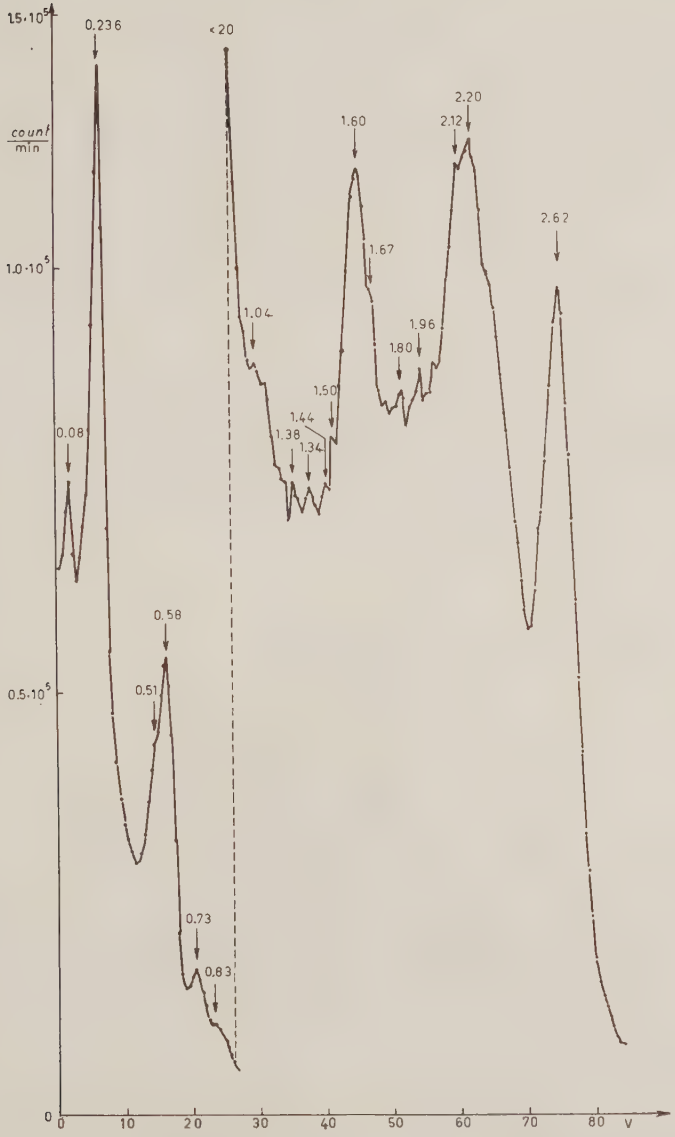

Fig. 1. – γ-rays spectrum of $^{228}_{90}$Th in equilibrium with its decay products. Energy is indicated through arrows and is in MeV. Statistical errors are not reported; they are evaluated < 1 %.

The broad peak at 2 MeV is composed of the 2.62 MeV pair peak representing escape of one annihilation photon with complete absorption of the other (2.11 MeV), and the photoelectric line of 2.20 MeV.

Some uncertainty arises in the region near 1.60 MeV. Indeed, the 2.62 MeV pair peak representing escape of both annihilation photons (1.60 MeV) conceals the 1.60 MeV photoelectric line of $^{212}_{84}$Po; the 1.38 MeV Compton edge of this latter γ-ray is disguised by the 1.34 MeV photoelectric line. On the other hand the existence of this 1.34 MeV γ-ray is confirmed by the Compton edge at 1.12 MeV.

Moreover from Fig. 1 and from the other experimental results obtained with the various crystals, we cannot exclude the existence of a 1.67 MeV γ-ray whose Compton edge is at 1.43 MeV.

Therefore more detailed studies on these spectra are in progress.

From Table II and from Fig. 1 we can see that our results are in agreement with those of LATYSHEV and KULCHITSKY and with those of JOHANSSON: a similar agreement lacks for the other Authors.

In conclusion we think that scintillation spectroscopy can be considered as a good source of information.

* * *

We thank Prof. E. PERUCCA for his kind interest and Dott. Ing. G. TRIVERO for his collaboration in the measurements.

RIASSUNTO

Mediante uno spettromero a scintillazione è stato esaminato lo spettro γ del $^{228}_{90}$Th in equilibrio con i suoi prodotti di decadimento. È stato studiato in modo particolare lo spettro del nuclide $^{212}_{84}$Po. I risultati relativi sono in accordo con quelli recenti di taluni Autori. Si discute quindi l'attendibilità dei nuovi risultati e il valore che la spettroscopia γ a scintillazione ha raggiunto rispetto a quella dello spettrometro magnetico.

NOTE TECNICHE

An Electronic Scanner for Nuclear Emulsions.

E. Amaldi, C. Castagnoli and C. Franzinetti

Istituto di Fisica dell'Università - Roma
Istituto Nazionale di Fisica Nucleare - Sezione di Roma

(ricevuto il 9 Giugno 1956)

Summary. — The preliminary results obtained by means of an electronic scanner for nuclear emulsions, are given. This instrument makes it possible to count and record tracks produced by almost parallel particles such as those obtainable from an accelerator. The general principles of the method upon which a technique of electronic scanners can be developed, are discussed. A description of the main features of the apparatus, built at the University of Rome, is given and some preliminary results are reported.

1. – Introduction.

The use of emulsions as a tool for research in nuclear physics as well as in other branches of science, is often limited by the amount of work and time which is required for scanning them after they have been exposed and processed. This is a particularly important factor either when the observation of a very large number of events is required, or when the search is concentrated on rare events which are dispersed over a large volume often crowded by other unwanted tracks.

In either case any automatic device which could increase the velocity of scanning by a large factor, would be of great importance. Having this in mind, about a year ago the present authors started the construction of an electronic scanner. As a first step we considered the problem of counting the number of nearly parallel tracks produced by a homogeneous beam of particles generated by an accelerator.

A similar idea has been followed by Goldsack and Van der Raay [1] who have recently published the description of an automatic scanner working on the same principles as ours although differing in some aspects.

[1] S. J. Goldsack, H. B. Van der Raay: *Journ. Scient. Instr.*, **33**, 135 (1956).

The present article is a first report on our work giving details of our apparatus and of the results which we have obtained, although we consider them as preliminary.

2. – General Principle of the Method.

The following ideas have been the basis of our work: considering, that by means of electronic devices, it is much easier to detect transient inputs rather than continuous ones, it will be convenient to move the image of the events being scanned as given by the microscope with respect to the sensitive photocathodes used for their detection. Such a movement, indicated in the following as vision-movement, will be in general independent of and different from the scanning movement necessary to explore the emulsion in all its area and depth.

The second very obvious remark is that all the events in which we are interested, are constituted by a certain number of tracks and that each one of these is a succession of black grains placed along a line which is interrupted at intervals and is almost a straight line. Many of the more complicated events can be decomposed in elementary events of this type.

The third remark is that in the experiments with counters the arrival of one particular type of particle in a given direction is recognized in a background of other types of events by means of time coincidences between two or more counters. In order to obtain a high efficiency for each counter, it is necessary that its dimensions and gas pressure are such that the probability that a particle crossing the counter does not produce any pair of ions inside the counter, may be neglected. Furthermore the geometry of the counters defines the angular opening and the mean direction of the detected particles. A good resolving power of the coincidence circuit eliminates, or at least reduces, the number of pulses due to particles moving in different directions and in chance coincidence.

One of the simplest operations that we can expect to be performed by an electronic scanner, is analogous to that of the detection of a beam of particles by means of a two counters telescope.

This is obtained by placing in the image plane F_2 of a projection microscope two little holes or slits which define a direction x parallel to the mean direction of the tracks to be detected. In this simple case the vision movement may be identical with the scanning movement and will simply consist in a displacement with constant velocity v of the object (nuclear plate) in the y direction. Two lenses give images of the two slits lying in the plane F_2 on the photocathodes of two photomultipliers whose outputs are connected to a conventional coincidence circuit.

In the following pages we shall describe an electronic scanner which is essentially of this type. We wish to point out that, at least in principle, by placing in the plane F_2, a suitable number of slits according to a convenient design, and by recording electronically the outputs of the corresponding photomultipliers, it may be possible in the future, to construct electronic scanners able to recognize and select rather complicated events, or possibly, capable of delicate measurements such as for instance, gap counting and gap length or scattering determinations.

The above general considerations and the problem of designing electronic

scanners capable of increasingly elaborated operations may have also some interest in connection with the problem of vision: the analysis of the more complicated vision operations in a convenient number of elementary steps may be clarified by the planning and construction of electronic models.

3. – Details of the Experimental Apparatus. Optical and Mechanical System.

We have used a type M 10 Wild microscope with its standard camera attachment and we have placed in its image plane a slit 35 mm long of adjustable width parallel to the x direction (Fig. 1). The slit was divided in three parts by two screens and three lenses L_1, L_2, L_3 threw images of these three parts on the photocathodes of three 1P21.

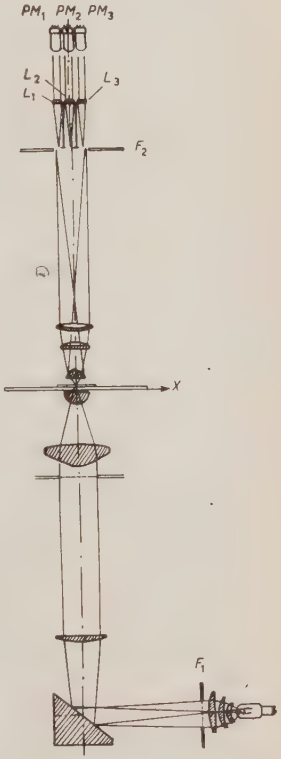

Fig. 1. – Schematic diagram of the optical system.

A system of 2 or 3 aligned slits can be compared to a two or three counter telescope and therefore in the following we shall call it a microtelescope. One can define the corresponding angular aperture both in the emulsion plane and in dip.

From the beginning we had proposed to build a system whose angular aperture was not too small and possibly adjustable at will inside rather wide limits in order that our instrument could also record tracks which are appreciably scattered.

With this in mind one could think at first of using slits larger than the width of the track image. In practice however we have found more convenient to work with slits narrower than the image of the track formed in the plane of the slits themselves. On the other hand, in order to obtain not too small an angular aperture in the horizontal plane, we placed next to the amplifier connected to the output of each one of the three phototubes, a univibrator providing a square pulse of adjustable time length T which performs a function comparable to what is called the persistency of the image in the case of animal eyes.

If V is the velocity of the image (vision movement) in the plane of the slits, in the calculation of the angular opening in the horizontal plane, each narrow slit can be treated as a slit of effective width

$$A = VT = MvT\,, \tag{1}$$

which can be adjusted by changing T. M is the total linear magnification of the microscope. As an example, let us consider a microtelescope composed of 2 slits each of length B short with respect to their distance L (measured from their centres).

We define the corresponding angular aperture in an horizontal plane as the probability that a track due to a particle of momentum p, can be counted when its angle of incidence with respect to the axis of the microtelescope is α: one gets immediately

$$P_2(\alpha, p) = \frac{1}{2}\left\{ \Phi\left(\frac{\alpha_0 + \alpha}{\sqrt{\pi}\theta_l}\right) \pm \Phi\left(\frac{\alpha_0 - \alpha}{\sqrt{\pi}\theta_l}\right)\right\}, \tag{2}$$

where

$$\Phi(x) = \frac{2}{\sqrt{\pi}}\int_0^x \exp\left[-x^2\right] \mathrm{d}x\,, \tag{3}$$

$$\alpha_0 \simeq \operatorname{tg} \alpha_0 = \frac{A}{L} = \frac{VT}{L}\,, \tag{4}$$

and the (+) is to be used for $\alpha \leqslant \alpha_0$, the (—) for $\alpha \geqslant \alpha_0$; θ_l is the mean angle of scattering for a cell of length $l = L/M$.

The fact that the angular aperture is a function of the momentum p is obviously a feature of the method of which one can try to make use in the future.

The angular aperture in dip corresponding to the depth of focus of the microscope is fixed by the choice of the objective and in general it is small. As we will see later, the depth of focus is, with the magnification and objective (Koristka X100) used, about 11 μm which, with a length l of about 70 μm, corresponds for straight tracks to an angle of $\pm\varphi = \pm \operatorname{arctg} 0.2 = \pm 12°$.

In order to increase this angle we have made use of the field curvature of the microscope: as a consequence of this field aberration, the two lateral slits correspond to images in the plane F_2 of objects placed at a different depth in the emulsion (by about 5 μm) with respect to the central one. For the same distance l one obtains $\pm\varphi = \pm 19°$. By means of a conventional circuit we may record the double coincidences of the three photomultipliers in all three combinations: 1-3 counts tracks almost horizontal, while 1-2 and 2-3 counts tracks with opposite inclination.

An effect of this type may obviously be enhanced by placing the 3 slits in different horizontal planes.

The use of microtelescopes of rather wide angular aperture in both directions is very useful in order to scan thick emulsions. But with thick emulsions one has to face the problem of the effect of the light scattered by the emulsion itself which produces a decrease in the contrast of the image of the track with respect to the background and therefore a reduction of the pulse amplitude.

In order to reduce the scattered light we have placed in front of the lamp (30 W supplied by a 6 V battery) a slit F_1 whose width was reduced so that not all the microscope field was illuminated but only a rather narrow band parallel to the x direction: the image of the slit F_1 was focussed by the condenser roughly in the plane where the tracks to be counted were located.

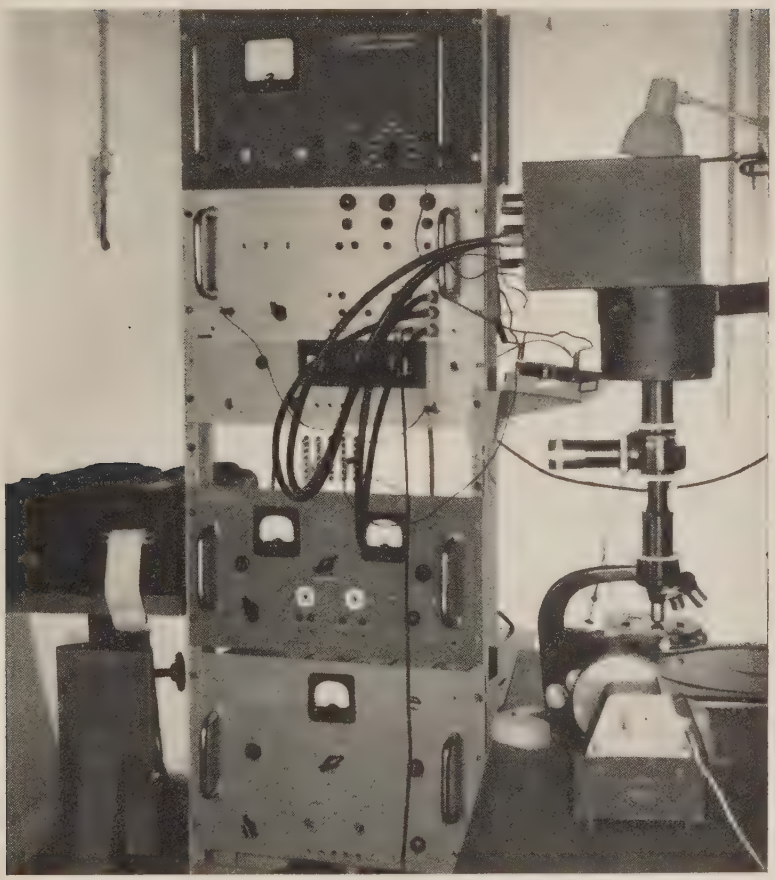

Fig. 2. – Photograph of the apparatus.

4. – Electronic Circuits.

The electronic circuits are schematically described in Fig. 3. Pulses from any one of the photomultipliers are amplified about 50 times and fed into univibrators which respond with pulses of a duration T adjustable at will. Threefold coincidences N_3 are recorded by means of a new-Rossi type circuit as well as twofold coincidences N_2 taken in all possible combinations among the three channels.

The amplifiers A of the feedback type have an adjustable bias which can be set to cut away the background or pulses smaller than a given amount.

When the number of tracks in which we are interested is large, the output of the coincidences is connected to a scaler which may allow a counting of the

order of $10^3 \div 10^4$ tracks in a few seconds, corresponding, under typical working conditions, to the time necessary to cross a plate 1 inch wide.

In other cases, when we are interested in finding a few tracks of rather large ionization dispersed in a very large number of other tracks due to faster particles, we adjust the biases of the amplifiers and we connect the output of the coincidences to a Brush BL201 recording oscillograph which marks on a moving paper the coordinate y of the interesting tracks.

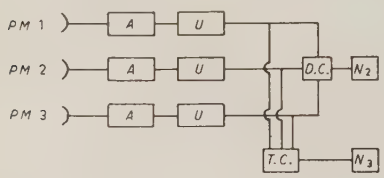

Fig. 3. – Circuit block diagram. PM = photomultiplier; A = amplifier; V = univibrator; T.C. = Threefold coincidences; D.C. = Twofold coincidences among any pair of channels [i.e., (1-2) + (2-3) + (1-3);; N_2, N_3 = mechanical counters, or scalar, or recorder used to mark coordinate y of track satisfying certain assigned conditions (direction and ionization).

5. – Preliminary Results.

5·1. *Optimum operational conditions for individual channels.* – In order to find the best conditions with regard to the optical system and to the voltage across the dynods of the photomultipliers, we have at first examined separately the behaviour of individual channels on selected tracks of various specific grain densities at different depths, in emulsions of different thickness.

For this purpose a selected track was moved back and forward by an oscillatory movement and the pulse given by the photomultiplier was observed in a fixed position on the screen of a syncroscope.

In Fig. 4 the height of a pulse obtained from a track of $g \sim 5g_0$ is given as a function of the focal depth. This track was approximately in the middle of a 400 μm Ilford G-5 emulsion. The track was exactly focussed at the apex of the peak in the region « seen » by the photomultiplier. In a region of 14 μm its pulse was definitely above the background of pulses chiefly due to slow electrons and also to other tracks coming from different directions or single grains. The graph reported here is typical of tracks in thick emulsions: it must be pointed out that in thinner emulsions or for tracks closer to the surface of thick emulsions the height of the pulses due to tracks of comparable ionization is much higher in comparison with the background pulses. For 50 μm thick emulsions, for instance, a ratio 15 : 1 between pulse and background is easily obtainable.

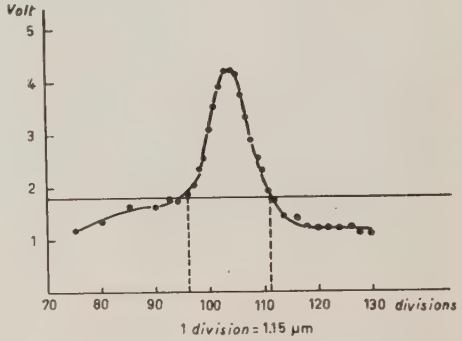

Fig. 4. – Pulse amplitude at the output of a single photomultiplier as a functin of the focal depth. Used track: $g/g_0 \sim 5$. Objective ×100; total magnification 320; slit width 250 μm. Emulsion: G5 400 μm thick.

The effect of the depth in the emulsion on the background is indicated on Fig. 5. Here the height of the background pulses is shown as a function of the depth in the emulsion. It appears to be a slowly varying function of the latter decreasing with increasing depth. In general the pulse due to a thick track decreases more rapidly so that the contrast between a thick track and the background usually decreases.

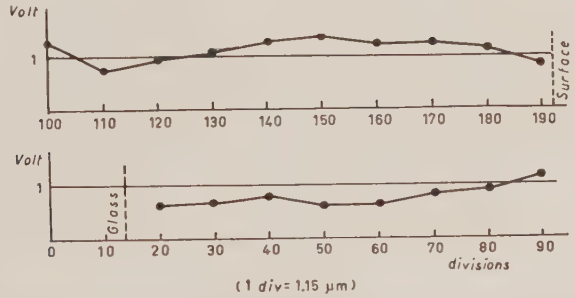

Fig. 5. – Background as a function of depth under the same conditions and in the same units of the data of Fig. 4.

The graph of Fig. 4 was obtained on a track giving an image parallel to the slit which was adjusted to be 250 μm wide. We operated in identical condition to study the influence of the angle α between the image of the track and the slit. The full line in Fig. 6 shows the dependence of the pulse height on the angle α when the track was in focus. An idea of the influence of the width of the slit is given by the comparison between the full curve and the dotted curve which refers to a 560 μm wide slit. As should be expected the distribution is somewhat broader.

Particular attention was given to the behaviour of the photomultipliers operated with an anodic resistence of 10 Ω under different conditions of illumination.

In Fig. 7 the photomultiplier current is plotted against the diameter d of the field diaphragm which is proportional to the square root of the light flux going through the emulsion. Three curves are reported here, referring to 250 μm, 150 μm, 76 μm, slit width respectively. Correspondingly the pulse amplitude – versus – light has been measured. The amplitude is seen to increase almost linearly up to a value of d close to that corresponding to the knee in the current-versus-light diagram, and then to decrease down to negligible values.

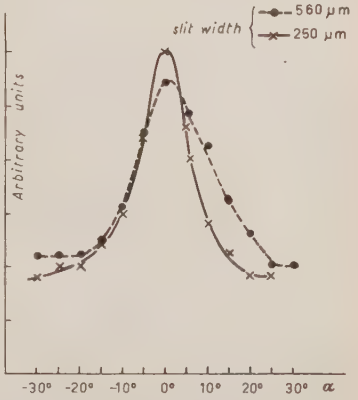

Fig. 6. Pulse amplitude as a function of the angle α between the mean direction of the track and the axis of the slit.

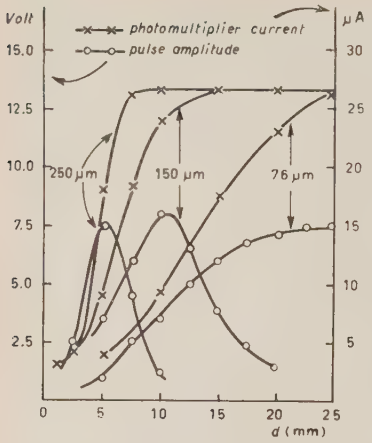

Fig. 7. – Pulse amplitude and photomultiplier current as a function of the flux of the light: d = diameter of the field diaphragm in millimeter.

The decrease of the width of the slit only stretches the curves towards higher values of the abscissae.

An inspection of these graphs indicates that the best operating conditions are close to the knee in the current-light curve. These can be found simply by measuring the light current on the photomultiplier.

5·2. *2-fold and 3-fold coincidence counting. Angular distribution of a beam of protons having* $g = 3.5g_0$. – Once the best operational conditions have been found for each individual channel, one has to set the bias of the discriminator amplifiers above the background pulses in order to reduce spurious coincidences to a tolerable value. This sets also a limit on the maximum angle (with respect to the slit) which a track can have in order to be recorded (see Fig. 6) as well as on the maximum interval of focal depth at which a track can be seen (see Fig. 4).

The setting of the input bias was obtained by feeding in the recording circuits a sinusoidal wave of approximately the same period corresponding to the width and minimum height of a pulse given by the tracks when moving at a given speed under the microscope. In this way a good precision could be obtained in the calibration of the discriminators.

Subsequently the « persistency » of the image was brought to the wanted value by adjusting the time constants of the univibrators.

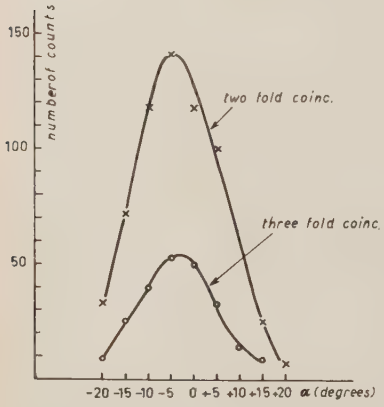

Fig. 8. – Threefold and twofold coincidences as a function of α obtained with a beam of protons ($g/g_0 = 3.5$): $T = 5 \cdot 10^{-3}$ s; $v = 3.3$ mm/s.

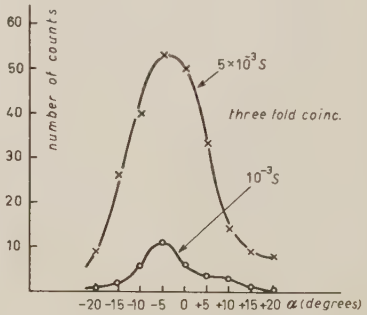

Fig. 9. – Threefold coincidences as a function of α obtained with a beam of protons ($g/g = 3.5$) for $T = 5 \cdot 10^{-3}$ s and $T = 1 \cdot 10^{-3}$ s, $v = 3.3$ mm/s.

In Fig. 8, the angular sensitivity of 3-fold and 2-fold coincidences for a persistency of $2 \cdot 10^{-3}$ s is shown. The two curves have been obtained scanning a plate irradiated with a parallel beam of protons which entered the emulsion lying very close to the plane of the emulsion.

The scanning took place where the protons had an energy of ~ 80 MeV. The plate was scanned several times, each time being at a different angle α with respect to the direction of the slits. The number of tracks counted by the automatic scanner at several values of α is reported. Two fold coincidences are more numerous as it should be expected since they are triggered by more stipping tracks than those recorded by 3-fold ones.

For a given persistency, only tracks forming an angle of less than the corresponding $\Delta\alpha$ with respect to the slits are recorded. Increasing the persistency, $\Delta\alpha$ increases and so does the number of tracks recorded at each run. Three fold coincidences obtained with two different values of the persistency (10^{-3} s and $5 \cdot 10^{-3}$ s respectively) are shown in Fig. 9. The corresponding values of $\Delta\alpha$ are $\pm 3.7°$ and $\pm 16°$.

* * *

It is our pleasant duty to acknowledgement the kindness of Prof. H. W. B. Skinner who allowed us to expose to the Liverpool synchrocyclotron some of the plates used in this research.

RIASSUNTO

Vengono presentati i primi risultati ottenuti mediante un osservatore elettronico per emulsioni nucleari che permette di contare e registrare tracce pressocchè parallele come quelle di particelle ottenibili con macchine acceleratrici. Dopo aver esposto i principi generali su cui sembra possibile sviluppare una tecnica degli osservatori elettronici, vengono descritte le caratteristiche dell'apparecchio costruito all'Università di Roma e vengono dati i primi risultati.

Spettrografo a microonde con modulazione ausiliaria.

P. Favero
Istituto di Chimica Fisica dell'Università - Padova

G. Grifone
Micro Italiana - Milano

(ricevuto il 3 Agosto 1956)

Riassunto. — Si descrive uno spettrografo a microonde con modulazione ausiliaria applicata alla sorgente e le apparecchiature ad esso connesse per la misura delle grandezze relative alle righe spettrali. Vengono discussi i criteri di dimensionamento in rapporto a determinate prestazioni di sensibilità e potere risolutivo nella banda d'impiego da 18000 a 36000 MHz.

1. – Criteri per la scelta del tipo di modulazione.

La sensibilità, intesa come l'ampiezza del minimo coefficiente di assorbimento rivelabile quando il rapporto segnale-disturbo è uguale a uno, e il potere risolutivo, inteso come la minima larghezza di riga a metà intensità che è possibile osservare, caratterizzano sempre le prestazioni di uno spettrografo a microonde (1). Una valutazione della sensibilità e del potere risolutivo, previsti per determinate ricerche, permette di dimensionare i vari componenti dell'apparecchiatura.

Il potere risolutivo di uno spettrografo a microonde risulta sempre elevato per l'impiego di sorgenti praticamente monocromatiche quali sono i Klystron e di rivelatori seguiti da amplificatori a banda molto stretta e con una convenientemente bassa frequenza di scansione. La sensibilità richiesta ad uno spettrografo a microonde dipende dalla gamma di frequenze interessata. Infatti, per esempio, per le righe spettrali di rotazione di molecole lineari la distri-

(1) M. W. P. Strandberg, H. R. Johnson e J. R. Eshbach: *Rev. Sci. Instr.*, **25**, 776 (1954).

(2) W. Gordy, W. V. Smith e R. F. Trambarulo: *Microwave Spectroscopy* (New York, 1953), p. 95.

buzione della intensità varia con il cubo della frequenza assorbita, essendo [2]:

$$(1) \qquad \alpha_{max} = 4.94 \cdot 10^{-12} \left[\frac{\mu^3 \nu^3}{T^2 (\Delta\nu)_1} \right] F_v \exp \left[- 4.8 \cdot 10^{-5} \frac{BJ(J+1)}{T} \right],$$

dove: α_{max} = Coefficiente di assorbimento in cm^{-1} al picco di risonanza.

F_v = Frazione di molecole nello stato particolare di vibrazione sotto osservazione.

B = Costante di rotazione in MHz.

μ = Momento dipolare in unità Debye.

T = Temperatura assoluta.

$(\Delta\nu)_1$ = Larghezza della riga in MHz per $T = 300°$ K e $p = 1$ torr.

J = Numero quantico per lo stato di rotazione più basso della transizione.

Dalla grande quantità dei dati raccolti dalla letteratura è possibile dedurre che nella gamma di frequenza da 20 000 MHz a 30 000 MHz l'intensità media delle righe spettrali è dell'ordine di 10^{-6} cm $^{-1}$. Per questa gamma di frequenze, ad uno spettroscopio adatto a ricerche di strutture si richiede una sensibilità di 10^{-8} cm^{-1}, valore questo necessario per l'analisi delle strutture fini. Nella gamma di frequenze da 40 000 a 60 000 MHz sarebbe sufficiente una sensibilità di 10^{-7} cm^{-1}, essendo l'intensità media delle righe spettrali dell'ordine di 10^{-5} cm^{-1} in base alla (1).

Sensibilità anche maggiori di 10^{-8} cm^{-1} possono essere ottenute nella gamma di frequenze sino a 30 000 MHz con spettroscopi a modulazione Stark.

Tuttavia la modulazione Stark, che deve essere applicata direttamente al gas in esame a mezzo di uno speciale elettrodo contenuto nella cella, non si presta ad essere impiegata agevolmente alle frequenze maggiori di 30 000 MHz e cioè quando si deve ricorrere a celle in guida d'onda di sezione trasversale molto ridotta.

Per le ricerche interessanti la forma delle righe non è necessario disporre di una sensibilità estremamente elevata, ma occorre un buon potere risolutivo e, soprattutto, una elevata fedeltà di riproduzione.

Potendo disporre di una sensibilità dell'ordine di 10^{-7} cm^{-1} sino a 30 000 MHz e di 10^{-6} cm $^{-1}$ sino a 60 000 MHz, gli spettroscopi del tipo superterodina [3] o del tipo a modulazione ausiliaria [4] si prestano meglio per questo genere di ricerche.

Gli spettroscopi a conversione di frequenza consentono un elevato potere risolutivo, ma risultano molto complessi e la rivelazione per comparazione di fase riesce meno efficiente. Invece uno spettroscopio a modulazione ausiliaria

---

[3] S. Geschwind: *Ann. New York Acad. Sci.*, **55**, 751 (1952).

[4] N. Carrara, P. Lombardini, R. Cini e L. Sacconi: *Nuovo Cimento*, **6**, 552 (1949); W. Gordy e M. Kessler: *Phys. Rev.*, **72**, 644 (1947).

ha un potere risolutivo minore, ma permette una rivelazione per comparazione di fase molto efficiente da cui consegue una maggiore purezza del segnale rivelato.

La sensibilità di questi tipi di spettroscopi risulta limitata dalla presenza delle piccole risonanze delle strutture a microonde, non più discriminabili dalle righe spettrali di piccola intensità. Tuttavia per le righe di notevole intensità, 10^{-5} cm^{-1} ed anche 10^{-6} cm^{-1}, il rapporto segnale-disturbo è molto elevato, tanto che, per queste sensibilità, il sistema con modulazione ausiliaria, può essere più efficiente del sistema con modulazione Stark. Infatti il primo sistema consente l'amplificazione delle derivate delle funzioni che rappresentano le righe e questa amplificazione può essere esaltata quando la riga è ben risolta dalle risonanze delle strutture.

Curando opportunamente la costruzione e la messa a punto dei circuiti a microonde e la cifra di rumore degli amplificatori selettivi è possibile ottenere sensibilità dell'ordine di 10^{-7} cm^{-1} nella gamma da 20 000 a 30 000 MHz con un rapporto segnale-disturbo molto elevato.

Le considerazioni sino ad ora svolte, unitamente alla possibilità di esplorare una gamma più estesa di frequenze con un solo sistema di modulazione e con una sola cella, hanno consigliato la realizzazione di uno spettrografo con modulazione ausiliaria.

2. – Descrizione della apparecchiatura.

Lo schema a blocchi dello spettrografo è riportato in Fig. 1.

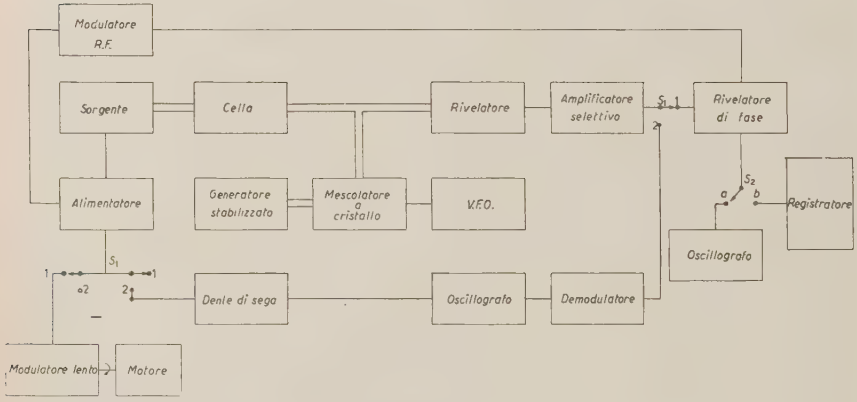

Fig. 1.

Come può vedersi dallo schema, la sorgente a microonde alimenta tramite opportune strutture la cella che è terminata su di un rivelatore. Il rivelatore è seguito da un amplificatore selettivo accordato alla frequenza di modulazione, 100 kHz o 6 kHz, generata da un modulatore accoppiato alla sorgente.

Per la registrazione, la demodulazione viene effettuata per comparazione di fase con riferimento diretto dal modulatore e il segnale demodulato viene applicato ad un registratore. In questo caso l'esplorazione di frequenza viene ottenuta variando lentamente e in sincronismo con la rotazione del rullo registratore la tensione di repulsore del Klystron sorgente a microonde. Tale variazione viene ottenuta sovrapponendo alla tensione base di repulsore una tensione prelevata da un potenziometro servito da un motorino elettrico opportunamente sincronizzato. È prevista e in corso di realizzazione la variazione della tensione di repulsore passando attraverso il circuito di stabilizzazione di frequenza a cavità duale di cui si varia la sintonia con asservimento meccanico.

Quando l'osservazione delle righe spettrali viene effettuata sull'oscillografo, allora è necessaria una scansione di frequenza che si ottiene applicando una tensione a denti di sega direttamente al repulsore del Klystron. Si produce così uno spazzolamento di frequenza di qualche MHz e la cadenza di ripetizione viene fatta la più bassa possibile rispetto alla persistenza dell'immagine sullo schermo oscillografico. Con un tubo R.C. del tipo 5ADP7 si può usare una frequenza minima di scansione dell'ordine di 0.1 Hz.

Per la misura della larghezza delle righe spettrali e per le misure delle distanze in frequenza delle strutture iperfini, l'apparecchiatura è stata dotata di un generatore di marche a microonde a distanza variabile con continuità. La lettura di queste grandezze viene direttamente effettuata sulla scala del generatore a frequenza variabile, indicato in Fig. 1 con V.F.O.

Per le misure delle frequenze centrali delle righe viene impiegato un campione di frequenza a microonde pilotato da un quarzo controllato sulle frequenze campioni irradiate dalla Radio Televisione Italiana e dall'Istituto Galileo Ferraris.

3. – Sorgenti a microonde.

Come sorgenti a microonde sono stati impiegati Klystron del tipo 2K50 della Bendix e del tipo X13 della Varian.

I Klystron 2K50 coprono la gamma da 23 000 MHz sino a 25 000 MHz, richiedono tensioni di alimentazione basse e dispongono di sintonia termica molto sensibile e precisa. Questo tipo di Klystron viene impiegato in quelle ricerche dove si richiede l'esplorazione di una limitata gamma di frequenze. Invece per le ricerche dove si richiede l'esplorazione di una vasta gamma di frequenze si fa uso di Klystron X13 seguiti da moltiplicatori di frequenza a cristallo. Con questi Klystron e con una serie di tre moltiplicatori a cristallo è possibile coprire la gamma di frequenze da 18 500 MHz sino ad oltre 36 000 MHz senza soluzioni di continuità e con potenze largamente sufficienti per spettroscopia. Infatti i Klystron X13 erogano una potenza media maggiore di 100 mW mentre il rendimento di un cristallo distorcitore del tipo 1N26 per la terza armonica è dell'ordine di qualche per cento. Pertanto a 30000 MHz si riesce ad avere ancora una potenza di qualche mW pilotando il moltiplicatore con un Klystron X13 alla frequenza fondamentale di 10000 MHz. Per la seconda armonica si ottengono potenze anche maggiori e in ogni caso la potenza a microonde erogata dal moltiplicatore deve essere ridotta a valori dell'ordine del centinaio di μW a mezzo di un attenuatore per evitare gli effetti di saturazione che conducono ad un allargamento delle righe.

La possibilità di disporre di una potenza sufficientemente elevata per pilotare il cristallo distorcitore rappresenta un notevole vantaggio. Infatti noi abbiamo sperimentalmente constatato che quando la potenza del Klystron è contenuta in limiti relativamente elevati, nel caso per es. dei cristalli 1N26 per correnti comprese fra 0.4 e 0.7 mA, il rapporto fra la potenza dell'armonica prelevata dal moltiplicatore e la potenza di rumore presenta una zona di massimo.

Potendo disporre di potenze maggiori di 100 mA all'ingresso del moltiplicatore in definitiva si realizza una sorgente a microonde comparabile come purezza ai Klystron per la gamma dei 30000 MHz. Una maggiore purezza della sorgente a microonde migliora sia la sensibilità, sia il potere risolutivo dello spettrografo.

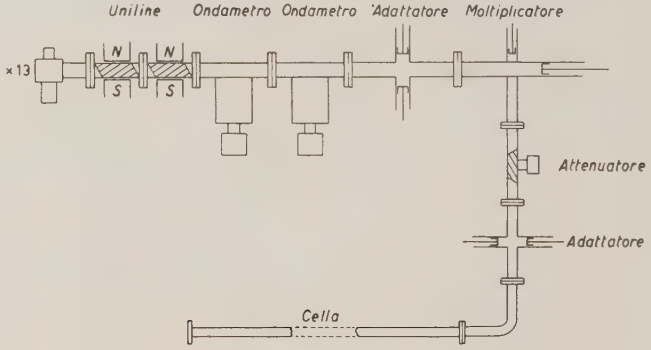

Fig. 2.

La testa a microonde dello spettrografo è rappresentata nello schema di Fig. 2. Come può vedersi dalla figura, il Klystron X13 è seguito da due isolatori a ferrite del tipo « uniline » che consentono una attenuazione inversa dell'ordine di 40 dB contro una attenuazione diretta dell'ordine del dB. Due soli ondametri di precisione, indispensabili per l'individuazione delle righe spettrali, sono sufficienti per coprire tutta la gamma da 18500 a 36000 MHz. I due ondametri coprono rispettivamente le gamme $8200 \div 9800$ MHz e $9800 \div 12400$ MHz che poi vengono trasposte con la moltiplicazione nella gamma d'impiego dello spettrografo. Gli ondametri funzionano per assorbimento e sono accoppiati direttamente in serie alla cella.

Dopo gli ondametri segue un adattatore d'impedenza a doppio stub, nel piano E e nel piano H della guida d'onda, e quindi il moltiplicatore a cristallo. All'uscita del moltiplicatore di frequenza è posto un attenuatore per dosare il livello di energia all'ingresso della cella e quindi un nuovo adattatore E-H.

Il carico visto dalla parte del Klystron, dopo gli isolatori a ferrite, presenta sempre un buon adattamento (vedi più avanti) e tutta la potenza erogata viene riversata sul cristallo distorcitore.

Eliminate le instabilità di oscillazione del Klystron per effetto della reazione del carico a mezzo degli isolatori a ferrite, rimangono le instabilità dovute al residuo di tensione alternata sovrapposto alle tensioni continue di alimentazione e alle derive termiche della cavità del Klystron.

Le instabilità a carattere periodico della sorgente a microonde si traducono in un disturbo che non solo abbassa la sensibilità della apparecchiatura, ma soprattutto produce un allargamento delle righe spettrali.

Disponendo di uno stabilizzatore di frequenza con cavità di riferimento, le piccole derive delle tensioni continue di alimentazione e le derive termiche del Klystron possono essere compensate, mentre più difficile rimane l'eliminazione dei residui di alternata. A tale scopo l'alimentatore è stato studiato per fornire una attenuazione dell'ordine di 120 dB alla tensione alternata sovrapposta alla tensione di risonatore, mentre la tensione al repulsore è stata fornita a mezzo di una batteria di pile a secco accuratamente schermate.

Gli isolatori a ferrite sono stati realizzati con lamine di ferrite IV E della Philips secondo gli schemi proposti da J. H. Rowen [5]. I circuiti magnetici sono registrabili da un minimo di 2900 G ad un massimo di 4400 G, in modo da poter variare la risonanza ferromagnetica da 8200 MHz a 12400 MHz circa. L'attenuazione inversa è dell'ordine dei 40 dB e la diretta è dell'ordine di 1 dB.

I moltiplicatori di frequenza, già descritti in altro lavoro [6], impiegano un cristallo del tipo 1N26 e sono stati modificati per permettere l'accoppiamento di un oscillografo di controllo e del generatore V.F.O. quando vengono usati per il circuito di marche. Una sezione schematica del moltiplicatore è riportata in Fig. 3.

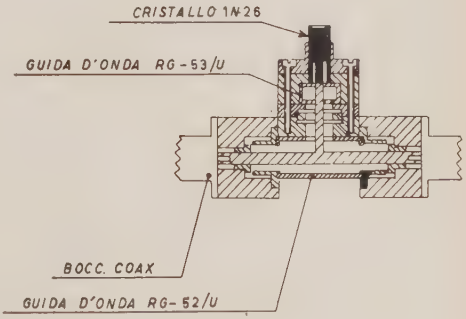

Fig. 3.

Come può vedersi dalla figura, gli estremi della barra orizzontale della transizione « cross-bar » costituiscono i conduttori interni di due bocchettoni coassiali, preceduti da due trappole che assicurano il cortocircuito per la componente a microonde.

Un ulteriore vantaggio dovuto all'impiego di un Klystron per la banda di 3 cm seguito da moltiplicatore come sorgente a microonde è rappresentato dalla maggiore semplicità del sistema stabilizzatore di frequenza che può essere realizzato con una cavità duale anzichè con il ben noto circuito di Pound che è più complesso e permette una banda di impiego più ridotta.

La stabilizzazione di frequenza a microonde è necessaria per una buona registrazione degli spettri e comunque indispensabile nelle misure della larghezza delle righe spettrali.

4. – Modulazione ausiliaria.

La modulazione ausiliaria si rende necessaria per poter impiegare dopo i rivelatori amplificatori selettivi a banda stretta che non solo migliorano il po-

---

(5) J. H. Rowen: *Ferrites in Microwave Applications B.S.T.L*, **32**, 1333 (1953).
(6) L. Grifone: *Ric. Scient.*, **24**, 1870 (1954).

tere risolutivo, ma aumentano fortemente la sensibilità rispetto alla amplificazione diretta del segnale video. Infatti (7) la potenza di rumore presente ai capi del rivelatore è esprimibile con la relazione:

$$P_n = (G \cdot s + F + t - 1)kTB \,, \tag{2}$$

dove: G = Fattore di perdita di conversione del cristallo rivelatore.

s = Cifra di rumore della sorgente.

F = Cifra di rumore dell'amplificatore.

t = Temperatura di rumore del cristallo rivelatore.

B = Larghezza di banda dell'amplificatore.

La temperatura t, che rappresenta il deterioramento del rapporto segnale-disturbo provocato dal rumore proprio del cristallo rivelatore, è espressa dalla relazione:

$$t = R\frac{P_0^2 \exp[-2\alpha_c l]}{f} + 1 \,, \tag{3}$$

dove: R = Costante di rumore del cristallo usato.

α_c = Coefficiente di assorbimento della cella.

l = Lunghezza della cella.

P_0 = Potenza immessa nella cella.

f = Frequenza di modulazione.

La temperatura t, come si può constatare dalla (3), tende a 1 quando f tende a ∞. Comunque passando da uno spettrografo video, con la sola modulazione a denti di sega a frequenza dell'ordine dei 50 Hz, ad uno spettrografo con modulazione ausiliaria a frequenza dell'ordine dei 100 kHz, si ottiene un sensibile abbassamento per la temperatura t e quindi un aumento della sensibilità dello spettrografo per la diminuzione della potenza di rumore P_n.

Tuttavia non è conveniente aumentare oltre i 100 kHz la frequenza di modulazione, poichè in tal caso si fornirebbe un nuovo contributo alle cause di allargamento delle righe spettrali. Infatti come è già stato mostrato (8), la componente fondamentale della riga spettrale (demodulata dalla frequenza di modulazione f) ha una semilarghezza $\Delta\omega_f$ dipendente dal quadrato della frequenza di modulazione:

$$\frac{\Delta\omega_f}{\Delta\omega_0} = 1 + \tfrac{1}{4}f^2 \cdot \tau^2 \,, \tag{4}$$

---

(7) Vedi nota (1), loc. cit., pag. 776.

(8) D. J. E. Ingram: *Spectroscopy at Radio and Microwave Frequencies* (London, 1956), pag. 75-76.

essendo τ il tempo di collisione che corrisponde ad una frequenza dell'ordine dei 50 kHz alle pressioni normalmente usate. Pertanto, una frequenza di modulazione di 100 kHz aumenta di circa il 100% la semilarghezza della riga esaminata.

La scelta della frequenza di modulazione deve risultare un compromesso tra sensibilità e potere risolutivo. Per l'apparecchiatura qui descritta sono state previste le frequenze di 100 kHz e 6 kHz.

La modulazione ausiliaria, applicata direttamente al repulsore del Klystron, provoca una piccola modulazione di frequenza nell'intorno di una frequenza che varia lentamente per effetto della scansione a denti di sega.

La modulazione di frequenza interessa una banda strettissima, una decina di kHz, e dipende linearmente dall'ampiezza della tensione di modulazione ausiliaria. In definitiva si ha una portante a microonde e una sottoportante alla frequenza di modulazione modulata in ampiezza dalle righe con la frequenza della scansione. La discriminazione della sottoportante avviene proprio in corrispondenza di una risonanza a fronti sufficientemente ripidi quale può essere una risonanza molecolare. Le risonanze delle strutture a microonde, che hanno i bordi meno ripidi, non discriminano la sottoportante qualora le costanti di tempo del circuito di accoppiamento del rivelatore all'amplificatore siano sufficientemente piccole. Tuttavia rimangono sempre alcune risonanze non separabili dalle righe spettrali ed in particolare quelle dovute alle riflessioni nelle varie strutture a microonde che mascherano le righe di piccolissima ampiezza.

Per l'eliminazione di queste risonanze è stata necessaria una accurata costruzione delle strutture a microonde ed in particolare delle flange di accoppiamento. Inoltre, sulle pareti interne di tutti i componenti a microonde eccettuata la cella, è stato depositato un leggero strato di grafite colloidale che contribuisce a smorzare le risonanze.

Una migliore riproduzione della forma derivata della riga è stata ottenuta, in accordo con i risultati di HARTZ e VAN DER ZIEL [9], applicando la modulazione ausiliaria sotto forma di onda quadra.

Per lo spettrografo qui descritto la frequenza di scansione per la presentazione oscillografica viene mantenuta tra 0.1 Hz e un massimo di 10 Hz.

La tensione di modulazione ausiliaria viene generata da un oscillatore a quarzo che è seguito da un amplificatore squadratore con tempo di salita di circa 0.5 μs a 100 kHz. L'accoppiamento al repulsore del Klystron che presenta impedenza praticamente infinita, viene effettuato direttamente a mezzo di una capacità che preleva il segnale a bassa impedenza da un trasferitore catodico che segue l'amplificatore d'onda quadra. Questa disposizione si rende necessaria per evitare la deformazione della forma d'onda e per rendere possibile una regolazione continua della tensione di modulazione.

5. – Amplificatori e demodulatori.

La maggiore difficoltà nella realizzazione degli amplificatori selettivi si incontra nella messa a punto degli stadi di ingresso. Infatti i cristalli rivelatori

---

[9] T. R. HARTZ e A. VAN DER ZIEL: *Phys. Rev.*, **78**, 473 (1950).

per microonde presentano una impedenza variabile con l'ampiezza del segnale applicato, approssimativamente da 300 Ω sino a 10000 Ω e lo stadio d'ingresso deve potersi adattare entro questo campo di variazione e presentare la più bassa cifra di rumore possibile.

La soluzione migliore è risultata dall'impiego di un circuito cascode con uno speciale trasformatore d'ingresso che ha lo scopo di rialzare l'impedenza e quindi l'ampiezza del segnale all'ingresso del primo tubo, senza peggiorare il rapporto segnale-disturbo. Il primario è un circuito aperiodico con impedenza dell'ordine di 2000 Ω per la frequenza di modulazione, collegato direttamente al cristallo rivelatore, e permette anche la chiusura verso massa per la componente continua. Anche il secondario è un circuito aperiodico direttamente collegato alla griglia del primo triodo dello stadio cascode. Il rapporto di trasformazione è di 5. Il trasformatore è avvolto su un nucleo toroidale di Hyperm 800 della Widia-Krupp con permeabilità iniziale di 60000 e ha due schermature interne in rame tra gli avvolgimenti e tre schermature esterne in mumetal. Tra queste schermature e il trasformatore è disposto uno strato di gomma piuma per evitare gli effetti di microfonicità.

La scelta del tubo per lo stadio d'ingresso deve essere fatta per la minima cifra di rumore e i tubi 12AY7 si prestano bene allo scopo poichè il rumore proprio è dovuto praticamente solo ad effetto shot, mentre il contributo di rumore per effetto granulare è trascurabile. Invece, tubi realizzati espressamente per circuiti cascode in alta frequenza come i tipi 6BQ7-A ed EC88, possono presentare forti componenti di rumore per effetto granulare alle basse frequenze. Il tubo 12AY7 ha una pendenza di 1600 mho e quindi la resistenza equivalente di rumore

$$R_e \cong \frac{2.5}{g_m} = 1560\ \Omega\,,$$

risulta piuttosto elevata. Però anche il coefficiente di amplificazione è molto elevato e il contributo alla cifra di rumore del secondo triodo griglia a massa dello stadio cascode è praticamente trascurabile essendo elevato il guadagno del primo triodo. Si raggiunge così un buon compromesso per la minima cifra di rumore.

L'impiego di bolometri come rivelatori a microonde semplifica il problema della realizzazione degli stadi di ingresso dell'amplificatore. Infatti il bolometro è un rivelatore a impedenza costante e quindi può essere adattato più facilmente allo stadio d'ingresso a mezzo di un trasformatore in salita. Per la frequenza di 6 kHz è stato realizzato un trasformatore analogo a quello precedentemente descritto con impedenza primaria di 200 Ω e impedenza secondaria di 50000 Ω. Questo trasformatore consente di rialzare di circa 25 dB il segnale di ingresso senza peggiorare il rapporto segnale-disturbo.

Per la frequenza di 100 kHz è stato impiegato un amplificatore analogo a quello descritto da Gordy, Smith e Trambarulo ([10]), con preamplificatore cascode, mentre per la frequenza di 6 kHz è stato realizzato l'amplificatore il cui schema è riportato in Fig. 4. Questo amplificatore prevede l'impiego di rivelatori a cristallo e a bolometro assicurando un guadagno di 110 dB con

---

([10]) Vedi nota ([2]), loc. cit., pag. 61.

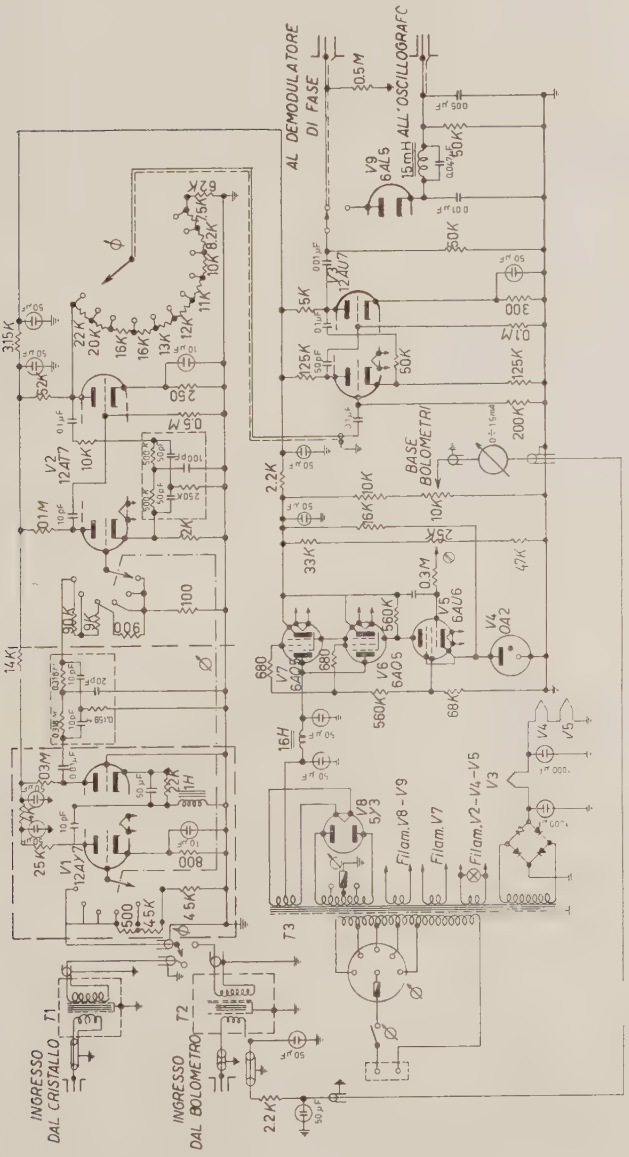
AL DEMODULATORE DI FASE
AL OSCILLOGRAFO
BASE BOLOMETRI
INGRESSO DAL CRISTALLO
INGRESSO DAL BOLOMETRO
Filam. V8 - V9
Filam. V7
Filam. V2 - V4 - V5
V3
T1
T2
T3

Fig. 4.

un rapporto segnale-disturbo di 20 dB su una banda di circa 300 Hz. La selettività è assicurata da una rete di controreazione tra il terzo e il quarto stadio. Gli attenuatori a scatti sono distribuiti tra i primi tre stadi per evitare il sovraccarico e consentono di introdurre una attenuazione complessiva di 100 dB. Un attenuatore a scatti di 1 dB, posto prima del quinto stadio, consente di introdurre una ulteriore attenuazione di 10 dB. Una rete selettiva *RC* subito dopo lo stadio d'ingresso filtra i residui di tensione alla frequenza della rete che potrebbero sovraccaricare gli ultimi stadi amplificatori. Per la demodulazione diretta del segnale di bassa frequenza si fa uso di un diodo del tipo 6AL5 seguito da un filtro *LC* per la frequenza di 6 kHz. Invece per la demodulazione per comparazione di fase è stato impiegato il circuito di sfasamento già realizzato da Erlandsson [11] e il circuito comparatore proposto dal Gordy [10].

La demodulazione per comparazione di fase consente una sensibile riduzione del livello di rumore all'uscita dell'amplificatore poichè permette la rivelazione delle sole componenti del segnale amplificato in fase con il segnale in ingresso, mentre non permette la rivelazione delle componenti dello spettro di rumore distribuite in modo casuale nell'intorno della frequenza di modulazione. Però la demodulazione per comparazione di fase diventa efficiente solo quando la frequenza di scansione è molto lenta poichè la larghezza di banda equivalente di tutto il sistema si riduce a qualche frazione di Hz. Perciò per l'apparecchiatura qui descritta è stata impiegata una frequenza di scansione di 0.1 Hz, ottenuta comandando a mezzo di un asservimento meccanico la tensione di repulsore del Klystron sorgente a microonde.

6. – Generatore di marche a microonde.

Per le misure della larghezza delle righe spettrali e delle distanze in frequenza delle componenti dello spettro relative a strutture iperfini è stato realizzato un generatore di marche a microonde. Il circuito, schematizzato in Fig. 5, fornisce uno spettro di marche la cui distanza può essere fatta variare con

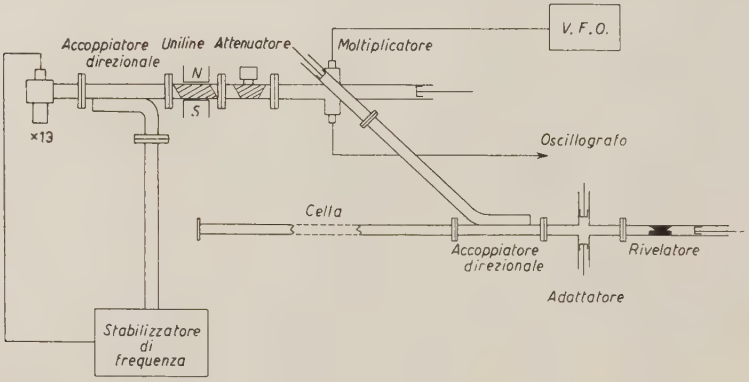

Fig. 5.

[11] G. Erlandsson: *Ark. f. Fysik*, **9**, 399 (1955).

continuità e tutto lo spettro può essere traslato lungo l'asse delle frequenze. Il generatore di marche è costituito da un Klystron X13, stabilizzato in frequenza, che alimenta tramite un disaccoppiatore a ferrite e un attenuatore variabile un moltiplicatore di frequenza a cristallo identico a quello già descritto in precedenza e dotato di due attacchi coassiali. Su uno di questi attacchi viene accoppiato un oscillatore, indicato con V.F.O., accordabile da 125 kHz e 4 MHz, mentre l'altro attacco coassiale viene usato per il controllo oscillografico. Il cristallo distorcitore funziona anche da mescolatore tra la frequenza del Klystron oscillatore locale e la frequenza del V.F.O. Lo spettro all'uscita del moltiplicatore sarà costituito dai prodotti di modulazione:

$$(5) \qquad nf_0 - f_1\,, \qquad nf_0\,, \qquad nf_0 + f_1\,,$$

avendo indicato con f_0 la frequenza emessa dal Klystron oscillatore locale e con f_1 la frequenza emessa dal V.F.O. Questo spettro di frequenze viene immesso, a mezzo di un accoppiatore direzionale, direttamente sul rivelatore a cristallo posto all'uscita della cella. Il cristallo provvede alla mescolazione dello spettro (5) con il segnale proveniente dalla sorgente a microonde attraverso la cella. Ogni volta che questo segnale, variabile per effetto della scansione a denti di sega, passerà per le frequenze dello spettro (5), si avrà un battimento. L'amplificatore selettivo a banda molto stretta filtra le componenti di Fourier di questo battimento separando quelle in prossimità della sua frequenza di accordo. Di conseguenza i battimenti appariranno sulla figura presentata sull'oscillografo e sul registratore come guizzi molto sottili e costituiranno un sistema di marche la cui distanza in frequenza può essere letta direttamente sulla scala dell'oscillatore V.F.O.

Questo dispositivo non solo permette la lettura rapida e diretta degli intervalli di frequenza, ma consente anche di seguire con continuità le variazioni di larghezza delle righe spettrali e può inoltre fornire una precisione di misura molto elevata.

La precisione di misura dipende soprattutto dalla stabilità percentuale in frequenza del Klystron oscillatore locale. Volendo apprezzare variazioni di forma delle righe interessanti alcune decine di kHz alla frequenza di 30 000 MHz e necessario effettuare le misure con la precisione di una parte su 10^6 e quindi è necessario che il Klystron oscillatore locale abbia una stabilità in frequenza dell'ordine di una parte su 10^7. Una stabilità così elevata ed anche maggiore può essere ottenuta con il ben noto sistema di stabilizzazione del Pound che però risulta alquanto complesso e di difficile messa a punto su tutta la banda di 4 000 MHz del Klystron X13. Per lo spettrografo qui descritto è stato realizzato un sistema di stabilizzazione della frequenza a cavità duale che è molto più elastico e consente di raggiungere una stabilità anche migliore di una parte su 10^7. Lo schema a blocchi del circuito di stabilizzazione è riportato in Fig. 6. Un ac-

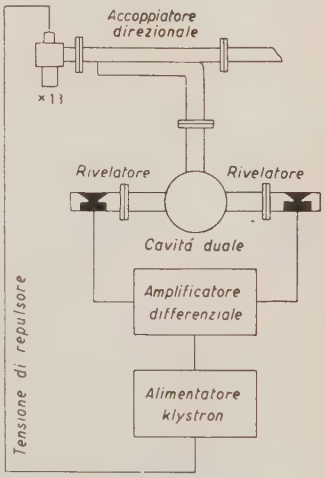

Fig. 6.

coppiatore direzionale preleva una parte dell'energia erogata dal Klystron oscillatore locale e la cede ad una cavità che lavora sul modo TE_{111} nella banda fra 8200 e 12400 MHz. Il discriminatore a microonde è la stessa cavità che ha due uscite che prelevano due componenti del campo magnetico in opposizione di fase. Il modo TE_{111} viene degenerato a mezzo di una opportuna discontinuità in corrispondenza di una delle due uscite sino a ottenere una separazione di frequenza dell'ordine di qualche MHz. Due rivelatori a cristallo, accoppiati rispettivamente a ciascuna delle uscite, alimentano un amplificatore differenziale seguito da due amplificatori in corrente continua e da un trasferitore catodico in serie alla tensione di repulsore del Klystron X13. Le variazioni di frequenza, trasformate in variazioni di tensione, riportano il Klystron ad oscillare sulla frequenza corrispondente al punto di zero del discriminatore a microonde. La ripidità di questo discriminatore è molto elevata poichè dipende dal Q di lavoro del modo fondamentale nella cavità che è dell'ordine di 1000. Il Q di lavoro del modo degenere è molto prossimo a questo valore poichè la perturbazione del modo è ottenuta senza elementi dissipativi.

Il complesso degli amplificatori in corrente continua fornisce un guadagno dell'ordine di 80 dB necessario per avere la tensione di errore sufficiente alla correzione del Klystron per derive dell'ordine di 1 kHz. Gli amplificatori differenziali impiegano tubi del tipo 12AY7 montati su circuiti cascode per mantenere una bassa cifra di rumore. Infatti la principale limitazione per valori di stabilizzazione maggiori di una parte su 10^7 è rappresentata dal rumore di fondo che si traduce in una tensione di errore caotica costantemente applicata al repulsore del Klystron.

7. – Registrazione delle righe spettrali.

Come è stato detto in precedenza, è in corso di messa a punto il sistema di scansione di frequenza passando attraverso il circuito di stabilizzazione. Infatti, l'impiego di un registratore a penna scrivente richiede una variazione molto lenta della frequenza della sorgente. Questa scansione lenta può essere ottenuta variando la tensione di repulsore del Klystron generatore a mezzo di un asservimento meccanico collegato ad un potenziometro dello stabilizzatore di tensione. Però in questo caso l'esperienza ha dimostrato che non è più sufficiente la stabilità propria del Klystron anche se alimentato con ottimi stabilizzatori di tensione.

Le derive di frequenza del Klystron non solo non consentono la riproduzione costante delle figure, ma introducono sensibili deformazioni e si rende quindi necessaria la stabilizzazione in frequenza della sorgente a microonde; il dispositivo è del tutto identico a quello descritto per il circuito di marche, solo che la sintonia della cavità di riferimento viene comandata da un motorino elettrico tramite un opportuno riduttore. L'energia per la cavità di riferimento viene prelevata a mezzo di un accoppiatore direzionale posto fra i due disaccoppiatori a ferrite in modo che eventuali riflessioni non siano sentite nè dal Klystron nè dalla cella.

Con la scansione lenta il potere risolutivo e la sensibilità risultano aumentati in modo notevole per l'impiego del demodulatore a comparazione di fase. La Fig. 7 riporta la riga J, $K = 13$, 11 del $^{14}NH_3$ ($\alpha = 6.0 \cdot 10^{-7}$ cm^{-1}); l'oscil-

logramma è stato ottenuto con una scansione di circa 0.1 Hz e con la rivelazione di fase. Durante lo sparpagliamento di frequenza non si nota alcuna instabilità apprezzabile del Klystron generatore e la forma della riga è del tutto soddisfacente. La disposizione usata in questo caso è quella di Fig. 1

Fig. 7.

Fig. 8.

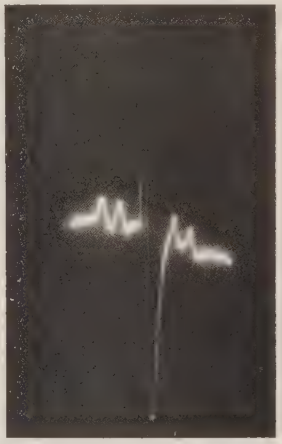

Fig. 9.

con S_1 e S_2 rispettivamente nelle posizioni 1 e a. La presentazione oscillografica con scansione più veloce e con rivelazione senza comparazione di fase si fà con S_1 in posizione 2. In questo caso la forma delle righe è quella riportata in Fig. 8 ($^{16}O^{12}C^{32}S$; $J = 1 \rightarrow 2$, $\alpha = 5.5 \cdot 10^{-5}$ cm^{-1}) e rappresenta con buona approssimazione il valore assoluto della prima derivata della riga. La tensione di scansione viene fornita dallo stesso oscillografo e si usa normalmente una frequenza non superiore ai 10 Hz, dato il basso valore della banda passante dell'amplificatore selettivo.

8. – Cella di assorbimento e impianto da vuoto.

La cella di assorbimento è costituita da una guida d'onda della banda K di circa 8 m di lunghezza, avvolta a spirale di un diametro di circa 40 cm e che porta in corrispondenza delle due estremità due prese per il collegamento all'apparecchiatura di vuoto e con la riserva di gas da studiare. Queste due prese sono state studiate in modo particolare per avere nello stesso tempo una buona portata di vuoto e una minima influenza sulla potenza microonde incidente. La cella termina con due flange dotate di un opportuno incavo intorno al foro centrale, profondo circa 0.3 mm, nel quale trova sede il foglietto di mica accuratamente scelto per la chiusura della cella ed ivi fissato mediante piceina da alto vuoto.

La cella completa è immersa in un termostato il quale permette di mantenere costante la temperatura fra — 70° e + 100 °C circa. Sulla conduttura

terminale verso il sistema di vuoto è inserita una valvola a comando magnetico immersa anch'essa nel bagno termostatico in modo che il gas in esame è da per tutto alla stessa temperatura. Un manometro differenziale a R.F. derivato da quello proposto da E. Rideal e A. J. B. Robertson [12] è inserito nello stesso ramo e permette di determinare la pressione del gas nella cella con una sensibilità dell'ordine di $1 \cdot 10^{-3}$ torr.

Al di sopra dei 40 °C, il fissaggio delle miche terminali viene realizzato con una delle normali tecniche per alta temperatura [13]. L'impianto del vuoto è del tipo convenzionale, ma è stato costruito in modo da presentare una certa flessibilità d'impiego e nello stesso tempo una buona portata di vuoto. Ad esso è collegato l'impianto per la produzione, purificazione e misura dei gas; inoltre, collegata direttamente alla cella di assorbimento, è stata disposta la sezione per le sostanze liquide e solide volatili. Allo stesso modo è stato collegato il pallone contenente il gas campione per i confronti di frequenza.

9. – Sensibilità e potere risolutivo.

Il maggior numero di esperienze eseguite per determinare le caratteristiche di sensibilità e potere risolutivo dello spettrografo sono state eseguite con l'ammoniaca.

La sensibilità di uno spettrografo a modulazione ausiliaria sulla sorgente è tra l'altro limitata dalle riflessioni delle strutture della cella; poichè queste si possono ridurre, come visto, ma non eliminare del tutto, la massima sensibilità ottenibile dipende dalla posizione di frequenza delle risonanze. D'altra parte è noto anche che la sensibilità è limitata dal rumore della sorgente e del cristallo rivelatore e questa limitazione è del pari funzione della frequenza. Una specificazione completa della sensibilità dello strumento richiederebbe pertanto la determinazione di una curva che desse l'andamento dell'assorbimento minimo rivelabile in funzione della frequenza in condizioni di optimum per la sorgente e per il rivelatore. Sfortunatamente una tale curva non è determinabile praticamente poichè occorrerebbe disporre di un gran numero di righe spettrali di intensità diverse e note, ciò che attualmente sembra impossibile.

Dalle misure eseguite con la scansione lenta e controllo di fase a presentazione oscillografica, risulta che l'assorbimento minimo determinabile è dell'ordine di $2\text{-}3 \cdot 10^{-7}$ cm^{-1}. Questa sensibilità è comparabile con quella ottenuta con altri strumenti dello stesso tipo [4].

Quanto al potere risolutivo, è noto che esso non dipende soltanto dalle proprietà dello strumento, ma anche dalla natura delle molecole studiate. In questo tipo di apparecchiatura l'allargamento delle righe è praticamente dovuto solo alla pressione, alle collisioni sulle pareti e all'effetto Doppler. A questo riguardo la modulazione ausiliaria sulla sorgente costituisce un punto in favore di questo metodo in confronto alla modulazione Stark. Il potere risolutivo dipende dalla

---

[12] E. Rideal e A. J. B. Robertson: *Journ. Sci. Instr.*, **32**, 349 (1955).

[13] Vedi, ad esempio, C. H. Townes: *Microwave Spectroscopy* (New York, 1955), pag. 443.

frequenza della modulazione ausiliaria nel senso che questa frequenza deve essere almeno metà della larghezza della riga in istudio: l'uso pertanto di 100 kHz limita l'osservazione a righe che abbiano larghezze non inferiori ai 200 kHz. Per migliorare da questo lato l'apparecchiatura è previsto e in corso di attuazione l'uso di una modulazione a 6 kHz.

Come esempio viene riportata in Fig. 9 la riga 4,4 del $^{14}NH_3$ le cui righe satelliti, completamente risolte, distano fra di loro di circa 0.5 MHz.

* * *

Desideriamo esprimere la nostra gratitudine al Prof. G. Semerano per il suo costante incoraggiamento e per i suoi preziosi consigli durante lo svolgimento delle ricerche. Ringraziamo ancora il Comitato per la Chimica del C.N.R. per il cui interessamento furono posti a nostra disposizione i fondi necessari all'attuazione del lavoro.

SUMMARY (*)

Description of a microwave spectrograph with auxiliary modulation applied to the source and the connected apparatuses for measurement of the quantities referring to spectral lines. Discussion of the dimensioning criteria for the obtention of given sensibility and resolution power in the working range from 18 000 to 36 000 MHz.

(*) *Editor's Translation.*

Phenomenological Theory of Conductivity.

G. Beck

Departamento de Física - São Paulo (Brasil)

(ricevuto il 6 Febbraio 1956)

The theory of conductivity has, so far, been based on a purely mechanical model, considering individual electrons interacting with an external field and with ions (lattice vibrations). We want to point out in the present letter, that any treatment of this type is necessarily incomplete and does not describe correctly the elementary processus involved.

We are used to describe a conductor consisting of N ions and N electrons by an eigenfunction

$$(1) \quad \Psi = \prod_{k=1}^{3N} H_{n_k}(\eta_k) \cdot \Phi(\zeta_1, \zeta_2, ..., \zeta_{3N}) ,$$

where $H_n(\eta)$ are oscillator eigenfunctions depending on the amplitudes η_1, η_2, ..., η_{3N} of Debye's normal vibrations of the solid, while ζ_1, ζ_2; ..., ζ_{3N} represent the remaining $3N$ degrees of freedom, which may be either the individual electron coordinates x_i or other collective variables, which, at ordinary temperatures, do not appreciably intervene.

If our system carries an electric current J the energy of this corrent is mainly given by the energy of its magnetic field

$$(2) \quad \frac{1}{8\pi} \int H^2 \, \mathrm{d}\tau = \tfrac{1}{2} \cdot L \cdot J^2$$

(L = selfinductance of the conductor). Expression (2) is due to the superposition of a great number, $N(N-1)$, relativistically small individual magnetic interactions between electrons and implies that the behaviour of electrons is no longer determined by ordinary mechanics, but rather by induction effects.

In the approximation of the theory of quasistationary currents we can account for these effects by including (2) into the energy expression of our system with

$$(3) \quad J = e/l \cdot \sum_i (\dot{x}_i - \dot{X}_i) = e/l \cdot \dot{\zeta}_1$$

(l = length of the conductor, X_i = ion coordinates, $\zeta_1 = \sum_i (x_i - X_i)$ reducing our general problem to an apparently mechanical one. The states of our system can, then, be described with good approximation by the eigenfunctions

$$(4) \quad \Psi_J = \prod_{k=1}^{3N} H_{n_k}(\eta_k) \cdot \varphi(\zeta_2; \zeta_3; ..., \zeta_{3N}) \cdot \cdot \exp\left[(i/\hbar)(e/l) L J \zeta\right] .$$

There remain, however, interaction terms, which couple the current to the internal vibrations of the system and which lead,

in time, to the decay of the initial current by successive elementary transitions and excitation of the thermal vibrations $H_n(\eta)$. This accounts in a direct way for what we know from experience: that the magnetic energy (2) of the current becomes transformed into Joule heat.

It remains to be seen, how our model can lead to a new approach to a quantitative theory of conductivity and whether a refinement of our description of the coupling between electrons and their magnetic field can account for the phenomenon of supraconductivity.

Über eine Approximation der Thomas-Fermi-Funktion.

T. Tietz

Physikalisches Institut der Universität - Łódź (Polen)

(ricevuto il 14 Agosto 1956)

Es ist bekannt, daß viele Probleme der Quantenmechanik sich mit Hilfe der Thomas [1]-Fermi [2]-methode lösen lassen. Dabei tritt eine charakteristische Funktion $y(x)$ auf. Die Funktion $y(x)$ genügt folgender D-Gl.

$$y'' = \left(\frac{y}{x}\right)^{\frac{1}{2}} y \,. \tag{1}$$

Mit der Randbedingung

$$y(0) = 1 \,, \tag{2}$$

hat die D-Gl. (1) eine einparametrige Lösungsschar. Wie bekannt, gibt es unter diesen Kurven eine, $y_0(x)$, die dem freien neutralen Atom entspricht ($y_0(\infty) = 0$). Mit Hilfe der Lösung $y_0(x)$ kann man alle anderen Lösungen der D-Gl. (1) mit der Fermi-Methode [2] finden. Bei der Behandlung einer Aufgabe mittels der Thoms-Fermi-Methode, stößt man meistens auf die Schwierigkeit, daß man die exakte Lösung der D-Gl. (1) in geschlossener Form nicht hat, oder daß die Näherungsfunktionen, die sich in geschlossener Form darstellen lassen, nicht einfach und handlich sind. Von diesen Näherungsfunktionen wird man verlangen, daß sie die D-Gl. (1) möglichst gut erfüllen, weiter einfach und handlich sind. Eine ausführliche Auskunft über fast alle bekannten Approximationen der D-Gl (1) für den Fall des freien neutralen Atoms findet man in der Arbeit von Umeda [3]. In zwei kürzlich erschienenen Arbeiten haben Latter [4] und Buchdahl [5] neue Approximationen für die Funktion y_0 vorgeschlagen. Die Lattersche Approximation ist sehr genau und darum sehr kompliziert. Die Lattersche Funktion eignet sich bloß für numerische Zwecke. Die Buchdalsche Funktionen sind einfacher und darum ungenauer. Die vorliegende Arbeit hat den Zweck, eine Approximation für y_0 anzugeben, welche noch für analytische Rechnungen für viele Probleme der statistischen Theorie zu gebrauchen wäre. Eine ein-

---

[1] L. H. Thomas: *Proc. Cambridge Phil. Soc.*, **23**, 542 (1926).

[2] E. Fermi: *Mem. Acc. Italia*, **1**, 1 (1930); *Zeits. f. Phys.*, **48**, 73 (1928); P. Gombas: *Die statistische Theorie des Atoms und ihre Anwendungen* (Wien, 1949).

[3] K. Umeda: *Journ. Phys. Soc. Japan*, **10**, 749 (1955).

[4] R. Latter: *Phys. Rev.*, **99**, 510 (1955).

[5] H. A. Buchdahl: *Ann. der Phys.*, **17**, 238 (1945).

fache elementare Funktion die den Randbedingungen

$$y(0) = 1\,; \qquad y(\infty) = 0\,, \tag{3}$$

genüge, ist wohl

$$\begin{cases} \bar{y} = (1 + ax + bx^2)^{-\frac{3}{2}} \\ a = 0.7105,\ b = 0.03919. \end{cases} \tag{4}$$

das nur für große x wesentliche Korrektionsglied bx^2 zugefügt ist, und demgemäß die Konstante $a = 0.80812$ durch die angemessenere, etwas kleinere, Konstante 0.7105 ersetzt ist. In der Tabelle I sind die Werte der Funktion $\bar{y}$ für verschiedene x zusammengestellt. Die erste Spalte (7) enthält die Funktionswerte y_0 nach Bush und Caldwell

Tabelle I.

x	y_0	$\bar{y}$	x	y_0	$\bar{y}$
0	1	1	20.0	0.0058	0.0058
0.01	0.985	0.989	22.85	0.0043	0.0043
0.03	0.959	0.969	24.0	0.0038	0.0039
0.06	0.924	0.939	26.67	0.0030	0.0029
0.1	0.882	0.902	28.24	0.0026	0.0026
0.3	0.721	0.745	30.0	0.0022	0.0023
0.6	0.562	0.578	32.0	0.0019	0.0020
0.8	0.485	0.497	34.0	0.0017	0.0017
1.0	0.425	0.432	40.0	0.0011	0.0011
1.2	0.375	0.379	50.0	0.00061	0.00064
1.5	0.315	0.316	55.0	0.00049	0.00050
1.7	0.283	0.283	60.0	0.00039	0.00040
2.0	0.244	0.242	70.0	0.000260	0.00026
2.5	0.193	0.190	80.0	0.00018	0.00018
3.0	0.157	0.154	95.0	0.00011	0.000115
4.0	0.108	0.106	100.0	0.00010	0.00010
4.792	0.0837	0.0819	200.0	$0.0^4\,15$	$0.0^4\,14$
5.0	0.0788	0.0796	300.0	$0.0^5\,46$	$0.0^5\,44$
5.209	0.0739	0.0723	500.0	$0.0^5\,10$	$0.0^6\,98$
8.75	0.0310	0.0306	800.0	$0.0^6\,26$	$0.0^6\,24$
10.0	0.0244	0.0240	900.0	$0.0^6\,18$	$0.0^6\,17$
12.01	0.0171	0.0169	1000.0	$0.0^6\,13$	$0.0^6\,125$
15.01	0.0109	0.0108			
17.78	0.0075	0.0075			

Est ist wohl von Interesse zu bemerken, daß man $\bar{y}$ als eine einfache Modifikation der Funktion (6)

$$\tilde{y} = (1 + ax)^{-\frac{3}{2}} \qquad a = 0.80812. \tag{5}$$

ansehen kann, bei welcher der letzteren ergänzt mit einigen Werten von Fermi und Miranda; in der zweiten Spalte finden sich die Werte unserer Approximation $\bar{y}$.

Die Tabelle I. zeigt, daß die Anschmiegung der Funktion $\bar{y}(x)$ an die numerisch berechnete Kurve $y_0(x)$ im

(6) Diese Approximation ist ein Sonderfall der Kerner-Tietz-Umeda Approximation. T. Tietz: *Journ. Chem. Phys.*, **23**, 1167 (1955); **23**, 1560 (1955).

(7) S. P. Gombás: (2) Seite 45, Tabelle 1.

Intervalle $0 \leqslant x \leqslant 1000$ gut ist. Die Approximation $\bar{y}(x)$ ist bedeutend einfacher, als die Lattersche Funktion. Unsere Funktion $\bar{y}(x)$ ist besser als die Buchdalsche Approximationen $\bar{y}_1$; $\bar{y}_2$ und im ganzen nicht schlechter als die Buchdahlsche Approximation [8] $\bar{y}_3$. Unsere Approximation $\bar{y}$ enthält bloß zwei Konstanten (Die lattersche Funktion hat sechs und die Buchdahlsche Funktion drei Konstanten). Die exakte Lösung der D-Gl. (1) für die Randbedingungen (3) verhält sich im Unendlichen wie $144/x^3$, und im unserem Falle für sehr große x hat man $\bar{y}(\infty) \sim 129/x^3$, so daß man für hinreichend große x einen von x unabhangigen relativen Fehler von etwa 10% begehen wird. In der Tat ist der Fehler selbst bei $x=1000$ nur ungefahr 4%. Die Funktion $I_0(P) = x^2 y_0$ von Coulson und March [9] hat bei $(P=(y_0/x)^{\frac{1}{2}} \approx 0.03)$ ein Maximum (≈ 2.5).

In unserem Falle hat $I_0(P)$ den befriedigenden Maximalwert 2.441 und zwar bei $x = 12.993$ d.h. bei $P=0.033$.

Bekanntlich läßt [10] sich die diamagnetische Suszeptibilität von Atomen und Ionen pro Grammatom in der statistischen Theorie mit Hilfe der Formel von Langevin und Pauli berechnen. In unserem Falle bekommen wir für die Suszeptibilität χ für den Fall des freien neutralen Atoms folgenden Wert $\chi = -32.5 \cdot 10^{-6} Z^{\frac{1}{3}}$. In der letzten Formel ist Z die Ordnungszahl. Dieser Wert von χ ist viel zu groß, wie man aus einem Vergleich der beobachteten Daten sieht; der Grund legt jedoch in der Natur des statistischen Modells. Wir sehen, daß für Probleme des inneren und äußeren Gebietes des Atoms unsere Approximation gut genug ist. Für Probleme des inneren Gebietes des Atoms braucht man nicht mit unserer Approximation $\bar{y}$ zu arbeiten: in diesem Falle, wie es gezeigt wurde, reicht schon die einfachere Approximation von Kerner-Tietz-Umeda aus [11].

[8] Die Bezeichnungen $\bar{y}_1$; $\bar{y}_2$; $\bar{y}_3$ sind dieselben wie in der Buchdahlscher Arbeit. S. (5).

[9] C. A. Coulson und N. H. March: *Proc. Phys. Soc.*, A **63**, 367 (1950).

[10] A. Sommerfeld: *Zeits. f. Phys.*, **78**, 283 (1932). Sommerfeld erhält mit Hilfe seiner Approximation fur χ den Wert $\chi = -31 \cdot 10^{-6} Z^{\frac{1}{3}}$.

[11] E. H. Kerner: *Phys. Rev.*, **83**, 71 (1951); K. Umeda: *Journ. Phys. Soc. Japan*, **10**, 749 (1955); T. Tietz: *Journ. Chem. Phys.*, **23**, 1565 (1955); *Nuovo Cimento*, **1**, 955 (1955).

Addendum

to « K-Mesons in Emulsions Exposed to a 6.2 GeV Proton Beam » (1).

J. Crussard, V. Fouché, J. Hennessy, G. Kayas, L. Leprince-Ringuet, D. Morellet et F. Renard

Laboratoire de Physique de l'Ecole Polytechnique - Paris

(ricevuto il 27 Agosto 1956)

Since January 1956, other flat secondaries of K^+-mesons have been measured and identified in the stack exposed to the 6.2 GeV proton beam of the Berkeley Bevatron.

The results of these measurements are quoted below: they should be added to those of Table II (p. 736-7-8 of (1)).

Table II-A.

No.	Type	Observed length	Scattering measurement $p\beta c$ MeV	Scattering measurement at (*) mm	Grain counts g/g_{pr}	Grain counts at (*) mm	Total range mm	Remarks
K_{513}	K_μ	163	180 ± 19	43	1.14 ± 0.04	40	212 ± 11	—
			—	—	1.39 ± 0.06	162	—	—
K_{103}	K_μ	158	—	—	1.13 ± 0.03	76	—	—
			98 ± 15	155	1.46 ± 0.05	155	210 ± 15	
K_{352}	K_μ	113	156 ± 14	38	1.08 ± 0.03	38	186 ± 14	—
			145 ± 16	103	—	—	—	—
K_{496}	K_μ	128	—	—	1.08 ± 0.04	65	198 ± 16	—
			116 ± 15	124	1.29 ± 0.06	126	—	—
K_{340}	K_μ	108	126 ± 14	106	1.12 ± 0.05	106	191 ± 14	—
K_{299}	K_μ	80	195 ± 23	6	1.00 ± 0.05	6	—	—
			—	—	1.05 ± 0.05	51	189 ± 15	—
			154 ± 12	64	$1.08 \pm .070$	61	—	—

(*) This is the distance from the decay point of the K to the middle point of the measurement interval.

(1) *Nuovo Cimento*, **3**, 731 (1956).

TABLE II (*Continued*).

No.	Type	Observed length	Scattering measnrement		Grain counts		Total range mm	Remarks
			$p\beta c$ MeV	at (*) mm	g/g_{pr}	at (*) mm		
K_{643}	K_μ	75.5	158±24	71	1.09±0.06	72	197±33	—
K_{410}	K_μ	73	149±25	69	1.12±0.05	69	186±26	—
K_{452}	K_μ	59	203±14	5	1.04±0.08	5	194±15	—
K_{328}	K_μ	57	174±30	55	1.00±0.05	5	205±32	—
K_{382}	K_μ	55	167±14	47	1.07±0.05	45	185±20	—
K_{717}	K_μ	52	163±19	49	1.06±0.045	49	186±26	—
K_{612}	K_μ	40	235±25	29	1.08±0.04	31	265±40	—
K_{453}	K_μ	20	202±23	6.5	1.06±0.03	6.5	197±25	—
K_{614}	K_μ	20	197±18	9	—	—	192±23	—
K_{373}	χ	114.8	—	—	—	—	114.8	$\pi\mu e$
K_{468}	χ	32.2	—	—	—	—	—	$4 + 0\pi$
K_{117}	χ	7.9	—	—	—	—	—	$3 + 0\pi$
K_{353}	χ	6.6	—	—	—	—	—	$4 + 0\pi$
K_{383}	χ	6.7	104±10	66	1.44±0.06	66	115± 7	—
K_{426}	χ	6	155±15	3	1.15±0.05	6	103±20	—
K_{431}	K_β	18.4	117±15	2.2	—	—	—	Becomes impossible to follow after 18.4 mm
			60± 7	7.3	1.10±0.03	8.9	—	
K_{229}	K_β	2.0	96±16	1.0	1.11±0.06	2.0	—	» » 2.0 mm
K_{618}	$\varkappa$	68.7	111	—	—	—	68.7	μ
K_{300}	$\varkappa$	17	106±30	2	1.33±0.05	2	—	out of stack

(*) This is the distance from the decay point of the K to the middle point of the measured interval.

Table III (p. 740 of [1]) compares the proportions of the various types of K-mesons found in different experiments. The results given for the G-stack were based on Table II (p. 1070) of the G-stack report [2]. However, we learn that these results cannot be used in this connection, as some of the geometrical standards used by the various contributing laboratories were not identical. For comparison purposes, only Table IV of the G-stack report (p. 1095) should be used. Furthermore, our Table III should be amended to take into account the new results enumerated above. With these two corrections, Table III now reads:

[2] G-STACK COLLABORATION: *Nuovo Cimento*, **2**, 1063 (1955).

TABLE III.

Type of K_L	Present experiment		G-stack		RITSON *et al.*	
	Number	%	Number	%	Number	%
K_μ	49	60	27	52	13	60
χ	22	27	17	33	7	32
K_β	7	9	5	10	1	5
$\varkappa$ with fast μ	3	4	2-4	5	—	3 (*)
Total	81		51-53		21	

(*) Two out of 60 K_L's have been identified by grain count.

It will be noticed that the new percentages of the various types of K-mesons identified in the present experiment are practically identical with those given in (1) although the statistics are increased by nearly 50 %.

A Probable Example of the Reaction $K^- - {}^{12}_{6}C \rightarrow K^+ + 3\,{}^{4}_{2}He$.

F. Anderson, D. Keefe, A. Kernan and J. Losty

Physics Department, University College, Dublin

(ricevuto il 3 Settembre 1956)

In the course of a systematic investigation of the interactions produced by positive heavy mesons with the nuclei of the constituents of the photographic emulsion, an event has been found which can be interpreted as the disruption of a ^{12}C nucleus into three α-particles by a positive K-particle, which later emerges from the collision. The event, a diagram of which is shown in Plate 1, was found in an emulsion stack (K_2) exposed to the K^+-meson beam at the Berkeley Bevatron and later shared among several European laboratories, and is the only event of its kind found during the scanning of 57 m of K^+-meson track at this laboratory.

The identity of the incoming particle responsible for track 1—see Plate 1—was established by grain density and scattering measurements, which gave a mass value of $m_k = (810 \pm 130)\, m_e$. The energy of the K-meson at the point of impact was determined to be 71 ± 3 MeV from an estimate of its ionization based on measurements of mean gap length in 3.5 mm of the track close to the star. Upon emerging from the interaction, the K-particle travelled 8.3 mm before leaving the Dublin section of the stack; ionization measurements near the point of exit show that its residual range was then 7 mm. The combination of ionization measurements at different points along this segment of track yielded a mass value of $(1\,000 \pm 350)\, m_e$ for the emerging K-particle. The momentum transferred by the K-particle in the collision was 370 MeV/c.

The three prongs (2, 3 and 4 of Plate 1) are too short to admit identification and have been assumed, for reasons given below, to be due to α-particles. The details of the event are summarized in the following Table.

The Q-value of the reaction $^{12}C \rightarrow 3\alpha + Q$ is 7.3 MeV, whereas experimentally the missing energy which does not appear as kinetic energy is (8 ± 4) MeV, in good agreement with our interpretation. Furthermore, the sum of the momenta of the outgoing particles is closely equal to the momentum of the incoming K-particle, the discrepancies in the longitudinal and transverse components being (24 ± 21) MeV/c and (23 ± 24) MeV/c respectively. The rather large errors arise mainly from the difficulty of accurately measuring the dip angles of the short tracks.

While both the momentum and energy balance agree very well with the inter-

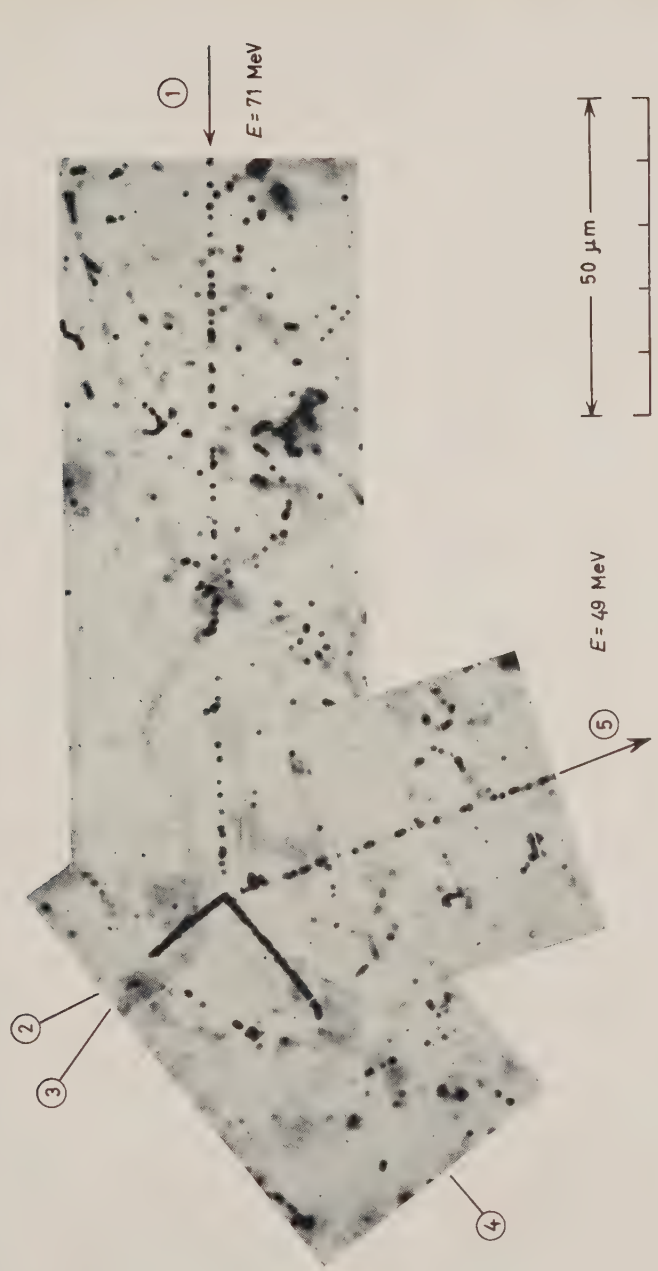

Fig. 1. – A microphotograph of the disruption of a Carbon nucleus into three α-particles (tracks 2, 3 and 4) by a positive heavy meson.

TABLE I.

Track	Range	Energy (MeV)	Momentum (MeV/c)
1	—	71 ± 3	273
2	15 μm	4.1 (*)	177
3	14.2 μm	4.0 (*)	172
4	28 μm	6.4 (*)	218
5	(8.3 + 7.0) mm	49 ± 2	225

(*) Assumed α-particles.

pretation of the event as the complete disruption of a carbon nucleus, it is necessary to examine whether it might not equally probably be explicable in terms of the ejection of three charged particles from a heavier nucleus, in an evaporation process. The extraction of three α-particles of the observed energies from a heavy nucleus such as Silver or Bromine, would require an energy of about 27 MeV, making the minimal assumption that no neutrons are emitted and that the residual nucleus is in its ground state. On the basis of current evaporation theory the emission of three α-particles without the ejection of any other particles seems unlikely. Moreover, α-particles from the heavy nuclei rarely have an energy less than ~ 9 MeV corresponding to escape over the potential barrier. Since the observed excitation of the nucleus is known to be (22 ± 4) MeV from measurements on the tracks of the ingoing and outgoing heavy mesons, this interpretation in terms of evaporation from a heavy nucleus appears improbable. (If the three prongs are assumed to have been produced by singly charged particles, the situation is worsened from an energy balance point of view, since about 4 MeV more is required to remove a nucleon than an α-particle from a nucleus of Silver or Bromine). Again, from a consideration of the measured amount of energy available and the observation of only three charged nuclear fragments it seems improbable that the target nucleus was that of either nitrogen or oxygen. We have therefore assumed that the event indeed represents an example of the reaction:

$$K^+ + {}^{12}C \to K^+ + 3{}^{4}He\ .$$

The disruption of a Carbon nucleus of the emulsion in the same manner by a negative π-meson of 82 MeV has been noted by BERNARDINI *et al.* [1]. They have pointed out the difficulty of reconciling such a mode of disintegration with the probably naive model of the incoming meson engaged in a collision with just one of the target nucleons, both particles being considered to be approximately independent of the surrounding nuclear matter. It may be therefore, that events such as the present suggest that the inelastic scattering of at least some types of K^+-meson by a nucleus is a many-body process, and that the interpretation of every inelastic event on the basis of a collision with a single nucleon may be unsound. Such conclusions obviously require a greater body of evidence since the event here reported may be a very rare one. It has been pointed out to us by Dr. R. H. DALITZ that the event may be compared with the well-known $^{12}C(p, p')^{12}C^*$,

[1] G. BERNARDINI, E. T. BOOTH and L. LEDERMAN: *Phys. Rev.*, **83**, 1277 (1951).

Note in proof: Several other such events have been analized by M. DELLA CORTE, T. FAZZINI and A. SONA: *Nuovo Cimento* **2**, 1345 (1955).

$^{12}C^* \rightarrow 3^4He$ reaction ([2]), in which it is established that the break-up generally proceeds through compound nucleus states of ^{12}C. Indeed the excitation energy of the intermediate ^{12}C nucleus required to explain the present event, viz. 15.6 MeV in the centre of mass system, is very close to a known level of ^{12}C at 16.1 MeV which has been observed to decay to three α-particles ([2]). The 3 α-particles travel in such directions that no two can be reconciled as arising from the break-up of an excited state of ^8_4Be; thus, if the disintegration of the Carbon nucleus did initially lead to a two-body state, the ground state of ^8Be must have been involved, the subsequent decay to two α-particles giving rise to tracks 2 and 3.

([2]) J. L. NEED: *Phys. Rev.*, **99**, 1356 (1955).

* * *

We are indebted to the members of the Berkeley group who kindly exposed the stack at the Bevatron, and in particular to Drs. E. J. LOFGREN, R. W. BIRGE and D. H. STORK. Our thanks are due to Professor C. F. POWELL, F.R.S., and the Bristol group who were responsible for the processing and cutting of the stack, to Mr. W. HARBOR for the photomicrograph, and to Miss MARY SMITH who found the event. We are grateful to Professor T. E. NEVIN for his interest and encouragement.

IL NUOVO CIMENTO Vol. IV, N. 5 1° Novembre 1956

Further Evidence of ^{12}C Tripartition induced by K^+-mesons.

N. N. Biswas, L. Ceccarelli-Fabbrichesi, M. Ceccarelli (*), K. Gottstein (+), N. C. Varshneya and P. Waloschek (−)

Max-Planck-Institut für Physik - Göttingen

(ricevuto il 3 Settembre 1956)

During the course of scanning of two emulsion stacks for nuclear interactions of K^+-mesons (1) two events have been found which can be interpreted as examples of the reaction:

$$(a) \quad K^+ + {}^{12}C \rightarrow K^+ + 3\,{}^4He - 7.3 \text{ MeV},$$

similar to an event reported by Anderson *et al.* (2) in the same issue of this journal. The data of these events are presented in the first two rows of Table I.

In both the cases the scattered K-meson as well as the three α-particles come to rest within the emulsion, thus permitting a precise determination of their energies. The energy of the primary particle has been computed from those of the secondaries assuming a Q-value of 7.3 MeV, corresponding to the reaction (a). The value obtained in this way agrees well with that derived from the distribution of the momenta of the K-mesons.

In order to see whether the events are consistent with the reaction (a), in addition to the test of energy balance the sum of the momenta of the three α-particles and the difference between the momenta of the incoming and the outgoing K-meson have been calculated. If the supposed reaction has taken place, these two vectors should be equal. As can be seen from Table I the angle between these two resultant vectors and the difference between their magnitudes are indeed very small.

In order to estimate both the background of spurious events which may be considered as ^{12}C tripartition and the possible biases, a number of events have been examined in which the scattering of a K-meson is accompanied by the emission of three prongs, even of extremely short range.

In this way four more possible cases of reactions have been found, in which the energy and momentum seem to be approximately conserved by the charged

(*) On leave from Padua University.

(+) At present at the University of California, Berkeley.

(−) On leave from the Argentine Comisión Nacional de la Energia Atómica.

(1) For a description of the plates used and of the scanning procedure see N. N. Biswas, L. Ceccarelli-Fabbrichesi, M. Ceccarelli, K. Gottstein, N. C. Varshneya and P. Waloschek: *Nuovo Cimento*, **3**, 825 (1956).

(2) F. Anderson, D. Keefe, A. Kernan and J. Losty: *Nuovo Cimento* **4**, 1198 (1956).

TABLE I.

Event	K-meson scattering angle (degrees)	Secondary meson and fragments		Primary meson Energy (MeV)		Angle between Δp_K and $\sum p_f$ (degrees)	Δp_K (MeV/c)	$\sum p_f$ (MeV/c)	Assumed reaction
		Identity	Energy (MeV)	from momentum dispersion	$T_K + \sum T_f - Q$				
4187	100	prob. $K_{\mu 2}$	23.0	35 ± 11	42.6 ± 1.0	6 ± 5	282 ± 5	307 ± 20	$K^+ + {}^{12}C \rightarrow K^+ + 3{}^4He - 7.3$ MeV
		(^{4}He)	6.4						
		(^{4}He)	4.1						
		(^{4}He)	1.8						
4388	92	τ	33.3	64 ± 7	63.4 ± 1.5	2 ± 3	325 ± 5	310 ± 15	$K^+ + {}^{12}C \rightarrow K^+ + 3{}^4He - 7.3$ MeV
		(^{4}He)	11.3						
		(^{4}He)	9.0						
		(^{4}He)	2.5						
4586	78	τ	53.9	102 ± 4	106.7 ± 2.0	11 ± 8	375 ± 6	374 ± 15	$K^+ + {}^{12}C \rightarrow K^+ + {}^7Li + {}^4He + {}^1H - 26.5$ MeV
		(^{4}He)	22.3						
		(^{7}Li) (^{6}Li)	1.4 1.3		105.4 ± 2.0	14 ± 8	373 ± 6	335 ± 14	$K^+ + {}^{12}C \rightarrow K^+ + {}^6Li + {}^4He + {}^2H - 24.6$ MeV
		(^{1}H) (^{2}H)	2.6 3.3						

particles. Subsequent analysis revealed that one of these events, described in the third row of Table I, is consistent with the two reactions:

(*b*) $K^+ + {}^{12}C \rightarrow$

$\rightarrow K^+ + {}^{7}Li + {}^{4}He + {}^{1}H - 26.5$ MeV

(*c*) $K^+ + {}^{12}C \rightarrow$

$\rightarrow K^+ + {}^{6}Li + {}^{4}He + {}^{2}H - 24.6$ MeV

and particularly with the first. The other three events do not satisfy completely the kinematical conditions for any of the tripartition reactions (3), but the association of a very low energy neutron or the assumption that one of the secondaries has suffered a scattering just after its emission would easily lead to the energy and momentum balance. For these last three events the K-mesons scattering angles are 27°, 135° and 148°.

The events described have been found by following a total K-meson track length of about 200 m. Combining our data with those of Dublin the mean free path for tripartition reaction can be estimated to be of the order of 50 m (*).

It may be noticed that in most of our events as well as in the Dublin event the K-meson is scattered in the backward hemisphere. If, as pointed out by ANDERSON *et al.* (2), the ^{12}C tripartition reactions have to be considered as examples of many body collisions, it would follow that for these collisions large angle scatterings make a significant contribution. This preferentially backward scattering may be helpful in reducing to some extent the difficulties which arise if one tries to derive the behaviour of K-nuclei collisions from the elementary K-proton cross-section with the assumption of an independent particle model for the nucleus. The rather frequent occurrance of large angle scatterings with small energy losses among the collisions of K-mesons with complex nuclei (4) may, indeed, be attributed to the many body collision processes with nucleon clusters inside the nucleus.

* * *

We are very grateful to Dr. KEEFE and his colleagues for calling our attention to this problem.

Two of the events listed in Table I were observed by Miss V. HEIDEBRECK and the remaining one by Miss ARNDT.

(3) A list of possible reactions of π-mesons interacting with light nuclei is given in the paper by M. DELLA CORTE, T. F. FAZZINI and A. M. SONA: *Nuovo Cimento*, **2**, 1345 (1955).

(*) This may be compared with the inelastic mean free path of K^+-mesons in nuclear emulsion which is known to be about 1 meter. J. E. LANNUTTI, W. CHUPP, G. GOLDHABER, S. GOLDHABER, E. HELMY, E. L. ILOFF, A. PEVSNER and D. RITSON: *Phys. Rev.*, **101**, 1617 (1956).

(4) See the results of the Göttingen group presented at the VI Turin Conference 1956 and forthcoming paper in the *Nuovo Cimento*.

Pion Theory of Nuclear Forces and n-p Polarization.

J. Iwadare, S. Otsuki (*), R. Tamagaki (*) and W. Watari (+)

Research Institute for Fundamental Physics, Kyoto University - Kyoto, Japan
(*) *Department of Physics, Kyoto University - Kyoto, Japan*
(+) *Department of Physics, Hiroshima University - Hiroshima, Japan*

(ricevuto il 3 Settembre 1956)

An experiment at Harwell on n-p polarization at an effective neutron energy 98 ± 3 MeV [1] has recently been reported in the present journal. The best fit to the experimental data of the polarization cross-section is given as

$$P(\theta)\,\mathrm{d}\sigma(\theta)/\mathrm{d}\Omega = \sin\theta[(0.8 \pm 0.3)\cdot P_0(\cos\theta) + (2.0 \pm 0.7)P_1(\cos 0) - (0.4 \pm 0.8)P_2(\cos\theta)]\ \mathrm{mb/sr}\,.$$

The purpose of the present letter is to point out that the experiment of n-p polarization at energies lower than 100 MeV may give valuable information on the pion theory of nuclear forces. It was found that all low energy phenomena below 20 MeV are explained quantitatively well by assuming the potential derived from the pion theory in the static limit [2]. However, it is not known at all to what extent the potential is modified at high energies. The static potential might describe the nuclear interaction correctly up to the pion threshold energy, or on the contrary the concept « potential » itself might lose its validity. Although there are several experiments on angular distribution of nucleon-nucleon scattering around 100 MeV, it is not sensitive to the detailed features of the nuclear interaction.

Here the n-p polarization cross-section was calculated assuming the g^2+g^4 potential in the perturbation approximation (the TMO potential [3]) that gives a fit to the n-p angular distribution as well as the total cross-section at 90 MeV [4]. (On the generality that the TMO potential has in the pion theory of nuclear forces, see the reference [2]). The result is that

$$P(\theta)\,\mathrm{d}\sigma(\theta)/\mathrm{d}\Omega = \sin\theta[-0.199P_0+1.790P_1 - 0.053P_2+0.051\sin^2\theta\cos\theta]\ \mathrm{mb/sr}\,.$$

(1) P. Hillman and G. H. Stafford: *Nuovo Cimento*, **3**, 633 (1956).

(2) J. Iwadare, S. Otsuki, R. Tamagaki and W. Watari: *Supplement to Progr. Theor. Phys.*, **3** (1956), to be published.

(3) M. Taketani, S. Machida and S. Onuma: *Progr. Theor. Phys.*, **7**, 45 (1952).

(4) S. Fujii, J. Iwadare, S. Otsuki, M. Taketani, S. Tani and W. Watari: *Progr. Theor. Phys.*, **11**, 11 (1954); M. Matsumoto and W. Watari: *Progr. Theor. Phys.*, **12**, 503 (1954).

With respect to the second coefficient, the main term, the theoretical result is in good agreement with the experimental one. This agreement is due to the fact that the sign of the α- wave phase shift of $({}^3S_1+{}^3D_1)$-state and that of the γ-wave

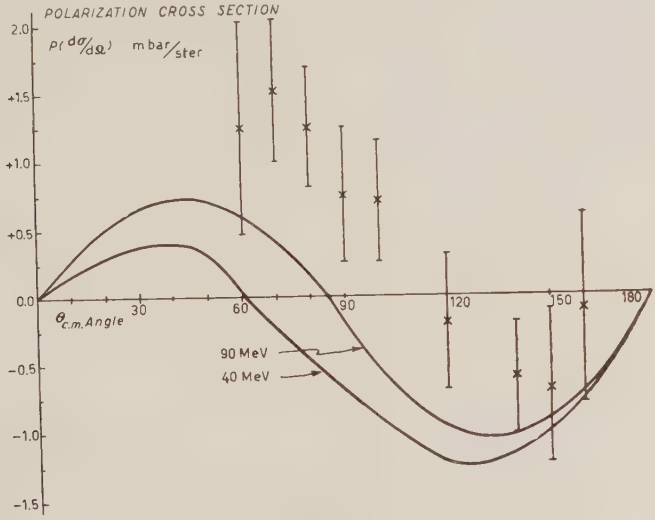

Fig. 1.

one are opposite, which is the consequence of the strong negative tensor force due to the one-pion-exchange process in the triplet even state.

However, the theoretical sign of the first coefficient is negative and is in disagreement with the experimental one. This disagreement is significant for the following reasons. The value of the first coefficient is sensitive to a possible small correction to one or both of the central and the tensor potentials in the triplet odd state, since several large terms due to the interference between the ${}^3P_{0,1,2}$-waves and the $({}^3S_1+{}^3D_1)$-wave, some ones being positive and the other negative, contribute to the coefficient. On the other hand, from the point of view of the pion theory; (i) It may not be true that the interaction due to the one-pion-exchange process is correctly described by the potential in the static approximation at such high energies. (ii) The P-waves are under strong influence of the interaction due to the two-pion-exchange processes, since the impact parameter of the waves is nearly equal to the pion Compton wave lenght. However, the two-pion-exchange potential has not yet been established quantitatively even at low energies. (iii) In the triplet odd state, the sign of the one-pion-exchange potential and that of the two-pion-exchange potential are opposite. Therefore even a small correction to either of them may give a large change in the P-wave phase shifts and in consequence in the first coefficient.

Thus the first coefficient of the n-p polarization cross-section is expected to give valuable information on the nuclear interaction and from the information we could infer how the pion theory of nuclear forces should be applied to high energy phenomena. Since the TMO potential without any modification can not reproduce the negative sign of the first coefficient, we

must examine: (1) To what extent the potential in the outer region or the one-pion-exchange potential is modified pion theoretically at high energies of about 100 MeV? (2) What correction is required at high energies to the potential that reproduces the low energy data correctly, in order to fit the experimental data on n-p polarization?

More experiments with higher accuracy are recommended, in particular at lower energies, for example, at about 40 MeV where the n-p angular distribution has been measured. A rough estimate shows that the theoretical result assuming the TMO potential at 40 MeV [4] is given as

$$P(\mathrm{d}\sigma/\mathrm{d}\Omega) \cong \sin\theta[-0.7P_0(\cos\theta) + 1.5P_1(\cos\theta)]\ \mathrm{mb/sr}\,.$$

The first coefficient is also negative at this energy. The maximum polarization is about 10%. Therefore it is not impossible to detect the n-p polarization at 40 MeV.

More detailed argument will be published in *Progress of Theoretical Physics*.

On the Scattering of High Energy Electrons by Protons.

E. Clementel and C. Villi (*)

Istituto di Fisica dell'Università - Padova
Istituto di Fisica dell'Università - Trieste (*)
Istituto Nazionale di Fisica Nucleare - Sezione di Padova

(ricevuto il 10 Settembre 1956)

Recent experiments (1) on the scattering of high energy electrons by protons have given evidence that the measured differential cross-section is larger than that concerning a point proton with no magnetic moment and smaller than the theoretical cross-section for a point proton with anomalous magnetic moment. The two possible explanations of these experimental results are either that the proton is not a point but a structured object or that there is a breakdown of the Coulomb law at short distances (2).

Let us confine ourselves to the former alternative assuming that the proton charge is statistically spread out over a distance of the order of 10^{-13} cm. Because of the extended structure of the proton, a colliding electron feels an effective proton charge e' which is smaller than the natural charge e, as a consequence of the electron penetration into the meson cloud (3). The effective proton charge e' is a decreasing function of the momentum transfer and can be determined from the equation

$$e' = eF_1(q) , \tag{1}$$

where

$$F_1(q) = \int \varrho(\boldsymbol{r}) \exp\left[i\boldsymbol{q}\cdot\boldsymbol{r}\right] \mathrm{d}\boldsymbol{r} \tag{2}$$

is the form or penetration factor corresponding to the proton charge density $\varrho(\boldsymbol{r})$ (normalized to 1) and to the momentum q transferred to the recoiling proton. In a system of units where $\hbar = c = 1$, the momentum transfer is given by

$$q = \frac{2E \sin(\theta/2)}{\left[1 + (2E/M)\sin^2(\theta/2)\right]^{\frac{1}{2}}} , \tag{3}$$

where E is the energy of the incident electron, θ the scattering angle in the

(1) R. W. Mac Allister and R. Hofstadter: *Phys. Rev.*, **102**, 851 (1956).

(2) Proceedings of the Sixth Rochester Conference (1956).

(3) M. N. Rosenbluth: *Phys. Rev.*, **79**, 615 (1950).

laboratory system and M the rest mass of the proton.

For sufficiently low energies, i.e. for values of q^{-1} larger than the dimension of the meson cloud, fixed by the density function $\varrho(\boldsymbol{r})$, the exponential in Eq. (2) can be expanded in a rapidly converging series. Assuming $\varrho(\boldsymbol{r})$ as spherically symmetric and taking into account that $(\boldsymbol{q}\cdot\boldsymbol{r})$ is an odd function, the form factor (2), after angular average, can be written as

$$(4)\quad F_1(q) = 1 - \sum_{n=1}^{\infty} (-1)^{n+1} \frac{I_{2n}}{(2n+1)!} q^{2n} ,$$

where I_{2n} is the $2n$-th moment of $\varrho(r)$, i.e.

$$(5)\quad I_{2n} = \int r^{2n} \varrho(r)\, \mathrm{d}\boldsymbol{r} .$$

It is of interest to see whether the charge density following from the Chew and Low theory ([4]) is in agreement with the electron-proton scattering experiments. To ascertain this point, we have used the proton charge density calculated in one-meson approximation by ZACHARIASEN ([5]) as expectation value $\varrho(r) = \langle\psi\,|\,\varrho_{[\mathrm{op}]}\,|\,\psi\rangle$ of the meson field charge density operator $\varrho_{[\mathrm{op}]}$ for a static proton in the physical state $|\,\psi\rangle$. From this distribution ($k_m = 6\mu$) it is found $I_2 = 0.198/\mu^2$ and $I_4 = 0.136/\mu^4$, where $\mu^{-1} = 1.4\cdot10^{-13}$ cm is the Compton wave length of the pion in natural units. The root-mean-square radius of the proton charge distribution is found to be $\langle r^{(2)}\rangle = (I_2)^{\frac{1}{2}} = 0.44/\mu$, a value which is smaller than that determined in ref. ([1]). The charge form factor (4) becomes

$$(6)\quad F_1(q) = 1 - 0.033(q/\mu)^2 + 0.001(q/\mu)^4 .$$

The data of MCALLISTER and HOFSTADTER ([1]) at 188 MeV have been compared with the theoretical cross-section

$$(7)\quad \sigma(\theta) = \sigma_{\mathrm{NS}}\{F_1^2 + (q/2M)^2\cdot \cdot[2(F_1 + \mu_{\mathrm{P}}F_2)^2 \operatorname{tg}^2(\theta/2) + \mu_{\mathrm{P}}^2 F_2^2]\} ,$$

assuming the static magnetic form factor F_2 equal to the charge form factor (6). In Eq. (7) $\mu_P = 1.79$ is the proton anomalous magnetic moment and the differential cross-section for a spinless point charge is given by

$$(8)\quad \sigma_{\mathrm{NS}} = \frac{(e^2/2E)^2 \operatorname{ctg}^2(\theta/2) \operatorname{csc}^2(\theta/2)}{1 + (2E/M)\sin^2(\theta/2)} .$$

The excellent agreement found over all angles between the calculated cross-section and the experimental one gives evidence that the charge density, predicted by the Chew and Low theory, fits the 188 MeV electron-proton scattering experiments with the same value of the coupling constant and the cut-off energy which is needed to fit also the meson-nucleon scattering data. However, since the form factor $F_1(q)$ is almost entirely dependent on the second moment of the charge density, such an evidence is unfortunately weaker than it may appear at first, because the fit obtained using Eq. (6) proves only that the asymptotic behavior of the Zachariasen distribution is in agreement with the data. In fact, inspection of Eq. (5) shows that the factor r^{2n+2} makes the detailed behavior of the charge density less important at short distances than at large ones, where it weights more heavily ([6]). Because of this mathematical circumstance, the influence on the electron-proton differential cross-section of the behavior

([4]) G. CHEW and F. LOW: *Phys. Rev.*, **101**, 1570 (1956).

([5]) F. ZACHARIASEN: *Phys. Rev.*, **102**, 295 (1956).

([6]) This arguments holds also for the electron-neutron interaction since the equivalent square well of depth V_0 and radius r_0 (conventionally) equal to the classical radius of the electron, is proportional to the second moment of the pion cloud charge density: $(-eV_0)_{\pi^-} = (mc^2/2r_0^2)I_2$, where m is the electron rest mass.

at short distances of the proton charge density, predicted by the Chew and Low theory, is practically suppressed in fitting the 188 MeV scattering data. As far as the check of the theory is concerned, it is more significant to examine scattering experiments for which the ratio q/k_m is larger than 1, because obviously in this case the fit cannot be independent of the short distance behavior of the charge distribution. Using in the form factor (2) the Zachariasen distribution, it is found that, at the highest available energy of 550 MeV [2], the agreement between the experimental data and the cross-section (7) ($F_1 = F_2$) is not as good as at 188 MeV. The discrepancy of about 35% for large momentum transfer points out that the experiments do not warrant the examined proton charge density, evaluated in one-meson approximation [7] assuming as negligible the contributions of all meson-nucleon states but the resonant one, and confirms that the successful result obtained at 188 MeV neither involves the physical content of the Chew and Low theory nor the reliability of the approximations used in deriving the charge density, but is largely independent of both.

In view of future more detailed investigations, the following attempt to interpret the high energy electron-proton scattering experiments along a different line, is believed to be of some interest.

Since the conjectured failure of the electrodynamics at short distances or the insufficiency of the assumption that the interacting particles are structureless can be accounted for by properly modifying the photon propagation function, we summarize these two alternatives assuming, in the spirit od STUECKELBERG's idea of compensation [8], that the Coulomb potential, experienced by the electron colliding with a proton, is given by

$$(9) \qquad V(r) = (e/r)\{1 - \eta \exp[-k_m r]\},$$

where η and k_m are two unknown parameters [9]. For $\eta = 1$, the cut-off for the photon propagation function implied by the static potential (9) readily follows from the one suggested by FEYNMAN [10].

Let us indicate with e'' the effective electron charge, which accounts for radiative corrections to scattering [11], and assume $e''V(r)$ as the electron-proton interaction energy. The Born approximation cross-section, calculated with this interaction energy, identifies with the Mott-Rutherford formula, modified by ROSENBLUTH [3], provided we define the effective proton charge according to Eq. (1), where the form factor in this case turns out to be

$$(10) \qquad F_1(q) = \frac{k_m^2 + (1-\eta)q^2}{k_m^2 + q^2}.$$

The potential (9) does not necessarily imply a failure of the electrodynamics at distances $r < k_m^{-1}$ if one assumes that the extended structure of the proton is ruled by the unknown parameter k_m according to the following relation

$$(11) \qquad \varrho(\boldsymbol{r}) = (\eta k_m^2/4\pi r)\cdot \exp[-k_m r] - (\eta - 1)\,\delta(\boldsymbol{r}).$$

Let us consider the case $\eta = 1$. Then, from Eq. (10), or substituting into Eq. (4) the $2n$-th moment $I_{2n} = (2n+1)!\cdot(\eta/k_m^{2n})$ of the proton charge density (11),

[7] The reliability of this approximation is discussed by M. CINI and S. FUBINI: *Nuovo Cimento*, **3**, 764 (1956).

[8] B. STUECKELBERG: *Helv. Phys. Acta*, **14**, 51 (1941); A. PAIS: *Phys. Rev.*, **69**, 125 (1946); S. SAKATA and H. UMEZAWA: *Progr. Theor. Phys.*, **5**, 682 (1950).

[9] This potential has been used also by VACHASPASTI in connection with the scattering of electrons by nuclei (*Phys. Rev.*, **93**, 502 (1954)).

[10] R. P. FEYNMAN: *Phys. Rev.*, **76**, 769 (1949).

[11] J. SCHWINGER: *Phys. Rev.*, **76**, 813 (1949).

it is found for $q/k_m < 1$

$$(12) \qquad F_1(q) = 1 - \sum_{n=1}^{\infty} (-1)^{n+1} (q/k_m)^{2n} ,$$

which identifies with the form factor (6) assuming $k_m \cong 5.6\ \mu$; i.e. using the charge density (11) with $\eta = 1$, it is not only possible to fit the electron-proton scattering data at 188 MeV equally well as with the Zachariasen distribution, although the considered charge density diverges at the origin, but the fit itself can be obtained provided the unknown parameter k_m assumes a cut-off value very close to that required by the Chew and Low theory. However, the charge density (11) with $\eta = 1$ is in disagreement over all angles with the 550 MeV data, because of the too slow decrease of the form factor (10) with increasing momentum transfer [12].

A consistent picture of the experimental data both at 188 MeV and at 550 MeV can be obtained assuming $\eta \neq 1$. The 188 MeV data are fairly well reproduced with $k_m = 6\ \mu$ and $\eta = 1.5$. The root-mean-square radius of the proton charge density (11) turns out to be $\langle r^{(2)} \rangle = (I_2)^{\frac{1}{2}} = 0.7 \cdot 10^{-13}$ cm, in close agreement with the value given by MACALLISTER and HOFSTADTER [1]. Using the same value of k_m and η, the 550 MeV data are also very well reproduced. The Stanford scattering experiments seem therefore to suggest that the electron-proton potential changes sign at the interparticle separation $r^* \cong 0.07/\mu$ and that the spatial extension of the proton charge is ruled by the parameter k_m^{-1}, which is closer to the Compton wave length of the nucleon rather than of the pion.

Whether the electron-proton interaction can be realistically described in terms of the potential (9), could be tested experimentally when higher electron energies will become available. In fact, from the form factor (10) it appears clearly that for momentum transfer $q = q_c = k_m/(\eta - 1)^{\frac{1}{2}}$ a very peculiar situation is to be expected, namely, the electron-proton differential cross-section will appear as a monotonically decreasing function of the angle θ for $q < q_c$, reaching the value zero for $q = q_c$, and then *increasing* slowly afterwards. For electron energies higher than a critical energy E_c, the condition $q = q_c$ fixes a critical angle θ_c at which $\sigma(\theta_c) = 0$. This critical angle is a decreasing function of

[12] For $\eta = 1$, the potential (9) may formally be derived either from the Bopp generalized electrodynamics (V. F. BOPP: *Ann. der Phys.*, **38**, 345 (1940); P. PODOLSKY and R. SCHWED: *Rev. Mod. Phys.*, **20**, 40 (1948)) or from the de Broglie's theory of mixed fields (*Journ. de Phys. et Rad.*, **11**, 481 (1950)). The electron-proton data at 550 MeV give therefore evidence against these generalizations of electrodynamics. It is however interesting to point out that the fourth order Bopp equation for a point source is formally equivalent to the second order Poisson equation for a Yukawa density function (Eq. (11); $\eta = 1$). The important point is that a generalized electrodynamics leads to a charge form factor although the source is assumed to be a δ-function. This can be easily seen assuming that the potential $V(r)$ is spherically symmetric. In this case the form factor can be written in the following general form

$$F_1(q) = (1/4\pi e) \int \nabla^2 V(r) \exp\,[i\boldsymbol{q}\cdot\boldsymbol{r}]\,\mathrm{d}\boldsymbol{r} .$$

Eq. (2) is therefore a special case valid when $\nabla^2 V(r) = 4\pi e \varrho(r)$. For instance, in case of the Bopp equation the form factor is given by

$$F_1(q) = 1 + (k_m^{-2}/4\pi e) \int \nabla^2 \nabla^2 V(r) \exp\,[i\boldsymbol{q}\cdot\boldsymbol{r}]\,\mathrm{d}\boldsymbol{r} ,$$

from which Eq. (10) can be derived using the potential (9). Because of the equivalence between a point source field obeying a generalized (linear or non-linear) equation and an extended source field obeying a second order differential equation, the electron-proton scattering experiments will hardly discriminate the two possible alternatives: (*a*) point-like source and failure of the electrodynamics, (*b*) extended source and validity of electrodynamics.

the electron energy. For instance, assuming as above $k_m = 6\mu$ and $\eta = 1.5$, it is found $E_c \cong 1.05$ GeV; for $E = 1.1$ GeV and $E = 1.3$ GeV the electron-proton differential cross-section goes to zero at $\theta_c = 140^\circ$ and at $\theta_c = 90^\circ$ respectively. The critical condition implying the proton effective charge e' to be zero, is in this case $q_c = 1.4 k_m$. This result is in many ways interesting, mainly because this value of q_c is very close to the cut-off ($= 1.4M$) for the photon propagation function required to reproduce the proton-neutron mass difference ([13]).

Note added in proof: In a paper appeared recently in the *Rev. Mod. Phys.*, **28**, 214 (1956) ideas similar to those suggested in this note have been extensively discussed albo by prof. R. HOFSTADTER.

([13]) R. P. FEYNMAN and G. SPEISEMAN: *Phys. Rev.*, **94**, 500 (1954).

IL NUOVO CIMENTO Vol. IV, N. 5 1° Novembre 1956

A New Proof of the One-time Equation in the Theory of Bound States.

W. Królikowski

Institute of Physics of the Polish Academy of Sciences - Warsaw

J. Rzewuski

Institute of Physics of the Polish Academy of Sciences - Wrocław

(ricevuto il 16 Settembre 1956)

In two preceding papers [1] we have used an equivalence theorem for integro-differential equations [2] to replace the many-time equations of the many-body problem in quantum field theory by equivalent one-time equations possessing the form of a Schrödinger equation. The proof was carried out by the intermediary of integral equations and it was essential that these equations are *inhomogeneous*. For the case of *homogeneous* equations the proof as given in I and II breaks down.

Now in the theory of bound states one is obliged to consider the inhomogeneity in the corresponding integral equations as vanishing—at least when the time integrals are extended over infinite regions. Therefore, the proof of I and II cannot be applied in this case.

A way out of this difficulty is to consider finite time intervals, in which case one has to do with inhomogeneous integral equations. Finite time intervals are more satisfactory from the physical point of view. However, for practical purposes, to have the possibility to apply Fourier integrals, one has to go over at the end of the calculation to the limit of infinite time intervals. One may assume that in this limiting case the one-time equation (II.2.17) still holds, such a procedure, however, is mathematically not satisfactory.

For this reason we thought it worthwhile to report on another proof of equivalence which may be carried out without the intermediary of integral equations and which is, therefore, independent on whether these equations are homogeneous or not. The resulting one-time equation is thus valid as well in the homogeneous as in the inhomogeneous case, which confirms the validity of the results of papers I and II for infinite time intervals.

It was shown in II that the equation for the distinguished component $\Psi_{\|}(t)$

---

[1] W. Królikowski and J. Rzewuski: *Nuovo Cimento*, **2**, 203 (1955) (quoted henceforth as I) and **3**, 260 (1956) (quoted henceforth as II).

[2] J. Rzewuski: *Acta Physica Polonica*, **13**, 135 (1954); **14**, 121 (1922).

of the state vector $\Psi(t)$ has the form (we use units in which $\hbar = c = 1$)

$$\left(i\frac{\mathrm{d}}{\mathrm{d}t} - \overset{0}{H}\right)\Psi_{\parallel}(t) = -i\int_{-\infty}^{+\infty} K(t-t')\,\mathrm{d}t'\,\Psi_{\parallel}(t'), \tag{1}$$

if one assumes that initially all other components of the state vector vanished ($\Psi_{\perp}(-\infty) = 0$).

We shall prove now that the integro-differential equation (1) is equivalent with the purely differential equation

$$\left(i\frac{\mathrm{d}}{dt} - \overset{0}{H}\right)\Psi_{\parallel}(t) = V\Psi_{\perp}(t)\,, \tag{2}$$

where V is an operator determined by the equation

$$V = -i\int_{-\infty}^{+\infty} K(t)\exp\left[i(\overset{0}{H}+V)t\right]\mathrm{d}t\,. \tag{3}$$

The equivalence is understood in the following sense. If there exists a unique operator V satisfying (3), then each solution of (2) satisfies (1) and vice versa each solution of (1) satisfies (2).

The transition from (2) to (1) is immediate if one considers that the general solution of (2) may be written in the form (we drop now the irrelevant subscript « $\parallel$ »).

$$\Psi(t') = \exp\left[-i(\overset{0}{H}+V)(t'-t)\right]\Psi(t)\,. \tag{4}$$

In fact, introducing (3) into (2) we get, by virtue of (4), equation (1).

The transition from (1) to (2) is more involved and requires a certain kind of approximation procedure. We assume that in the lowest order of approximation the function $\Psi(t)$ satisfies the approximate equation

$$\left(i\frac{\mathrm{d}}{\mathrm{d}t} - \overset{0}{H}\right)\Psi(t) = 0\,, \tag{5}$$

with the general solution

$$\Psi(t') = \exp\left[-i\overset{0}{H}(t'-t)\right]\Psi(t). \tag{6}$$

Introducing this solution into (1) we get

$$\left(i\frac{\mathrm{d}}{\mathrm{d}t} - \overset{0}{H}\right)\Psi(t) = -i\int_{-\infty}^{+\infty} K(t-t')\exp\left[-i\overset{0}{H}(t'-t)\right]\mathrm{d}t'\,\Psi(t) = \overset{1}{V}\Psi(t)\,, \tag{7}$$

with

$$\overset{1}{V} = -i\int_{-\infty}^{+\infty} K(t)\exp\,[i\overset{0}{H}t]\,\mathrm{d}t\,. \tag{8}$$

Considering (7) as the next approximation of the equation for $\Psi(t)$ we may introduce its general solution

$$\Psi(t') = \exp\,[-i(\overset{0}{H}+\overset{1}{V})(t'-t)]\Psi(t) \tag{9}$$

again into (1) and get in this way

$$\left(i\frac{\mathrm{d}}{\mathrm{d}t}-\overset{0}{H}\right)\Psi(t) = \overset{2}{V}\Psi(t)\,, \tag{10}$$

with

$$\overset{2}{V} = -i\int_{-\infty}^{+\infty} K(t)\exp\,[i(\overset{0}{H}+\overset{1}{V})t]\,\mathrm{d}t\,. \tag{11}$$

Repeating this procedure infinitely many times and assuming that there exists the limes

$$\overset{n}{V} \xrightarrow[n\to\infty]{} V\,, \tag{12}$$

where

$$\overset{n}{V} = -i\int_{-\infty}^{+\infty} K(t)\exp\,[i(\overset{0}{H}+\overset{n-1}{V})t]\,\mathrm{d}t, \tag{13}$$

we get equation (2) with V given by (3).

In paper II we derived equation (2) by a different method, involving the purely integral equation corresponding to (1) (cf. II, equation (2.3)). The potential V was expressed by means of the resolving kernel of this equation (cf. II, equation (2.12)). To compare this old form of V with the new form (3) let us expand the right hand side of (3) in powers of V. For this purpose we use the well known formula

$$\exp\,[i(\overset{0}{H}+V)t] = \exp\,[i\overset{0}{H}t]\sum_{n=0}^{\infty}(i)^n\int_0^t \mathrm{d}t_1\int_0^{t_1}\mathrm{d}t_2\ldots\int_0^{t_{n-1}}\mathrm{d}t_n\,V(t_1)\,V(t_2)\ldots V(t_n), \tag{14}$$

in which

$$V(t) = \exp\,[-i\overset{0}{H}t]V\exp\,[i\overset{0}{H}t]\,. \tag{15}$$

Going over to a representation $|N\rangle$ in which $\overset{0}{H}$ is diagonal ($\overset{0}{H}|N\rangle = E|N\rangle$) and introducing (14) into (3) we get after some calculations

$$V|N\rangle = \sum_{n=0}^{\infty}\sum_{N_1,N_2,\ldots N_n}\sum_{i=1}^{n+1}U(E_i)\prod_{k=1}^{n+1}{}'(E_i-E_k)^{-1}|N_1\rangle\langle N_1|V|N_2\rangle\ldots\langle N_n|V|N\rangle\,. \tag{16}$$

Here

$$U(E) = -i \int_{-\infty}^{+\infty} K(t) \exp [iEt] \mathrm{d}t \tag{17}$$

cf. II, formula (1.15)); the dash on the product sign means that only factors with $i \neq k$ are taken into account; the eigenvalue E is denoted by E_{n+1}; in carrying out the integrations in the transition from (14) to (16) we have used the formula

$$\sum_{i=1}^{n} \prod_{k=1}^{n}{}' (E_i - E_k)^{-1} = 0 \; ; \tag{18}$$

for $n = 0$ the product in (16) has to be replaced by unity.

Expanding now in (16) U and V in powers of the coupling constant (cfr. II.2.13-14)

$$U(E) = \sum_{m=1}^{\infty} U^{(2m)}(E) \, , \qquad V = \sum_{m=1}^{\infty} V^{(2m)} \tag{19}$$

and equating terms of the same order, we get the following recurrent formulae

$$V^{(2m)} | N \rangle = \sum (n) \sum_{m_0 + m_1 + \ldots + m_n = m} (m_0) \sum (m_1) \ldots \sum (m_n) \sum_{N_1, N_2, \ldots N_n} \sum_{i=1}^{n+1} U^{(2m_0)}(E_i) \cdot \tag{20}$$

$$\cdot \prod_{k=1}^{n+1} (E_i - E_k)^{-1} | N_1 \rangle \langle N_1 | V^{(2m_1)} | N_2 \rangle \ldots \langle N_n | V^{(2m_n)} | N \rangle \, ,$$

where the index n runs from 0 to ∞ and the indices m_0; m_1; ..., m_n run from 1 to ∞ with the subsidiary condition $m_0 + m_1 + \ldots + m_n = m$.

For the first two approximations we get easily

$$V^{(2)} | N \rangle = U^{(2)}(E) | N \rangle \tag{21}$$

$$V^{(4)} | N \rangle = U^{(4)}(E) | N \rangle + \sum_{n_1} \{ U^{(2)}(E_1)(E_1 - E)^{-1} | N_1 \rangle \langle N_1 | U^{(2)}(E) | N \rangle + \tag{21'}$$

$$+ U^{(2)}(E)(E - E_1)^{-1} | N_1 \rangle \rangle N_1 | U^{(2)}(E) | N \rangle \} \, .$$

These are just the old results (II.2.16). In fact, writing (II.2.9) in the representation $| N \rangle$ one gets in the first approximation

$$A^{(2)} | N \rangle = -(E - \overset{0}{H})^{-1} U^{(2)}(E) | N \rangle \, . \tag{22}$$

Introducing this into (II.2.16) and making use of (17) we obtain just (21).

* * *

We are indebted to Mr. A. Pawlikowski for pointintg out to us the defects of the old proof and to Dr. J. Łopuszański for valuable discussions.

A Generalization of Reissner-Nordström Solution - I.

R. L. Brahmachary

Institut für theoretische Physik - Universität Hamburg

(ricevuto il 27 Settembre 1956)

Tolman [1] has pointed out the great difficulties in obtaining explicit solutions of Einstein's gravitational field equations because of their complicated and non linear character. These very facts lead to an almost insuperable difficulty in obtaining general solutions of the field equations when the Energy-tensor $\mathcal{T}_\mu^\nu$ is composed of two parts, namely T_μ^ν, the material Energy-tensor and t_μ^ν the electro-magnetic Energy-tensor, namely the set of equations:

$$8\pi T_1^1 - 8\pi t_1^1 = \exp[-\lambda]\left(\frac{\nu'}{r} + \frac{1}{r^2}\right) - \frac{1}{r^2} + \Lambda\,,$$

$$-8\pi T_2^2 - 8\pi t_2^2 = \exp[-\lambda]\left(\frac{\nu''}{2} - \frac{\lambda'\nu'}{4} + \frac{(\nu')^2}{4} + \frac{\nu' - \lambda'}{2r}\right) + \Lambda\,,$$

$$T_2^2 = T_3^3\,,$$

$$8\pi T_4^4 = -\exp[-\lambda]\left(\frac{\lambda'}{r} - \frac{1}{r^2}\right) - \frac{1}{r^2} + \Lambda\,.$$

A generalization of Nordström-Reissner solution namely, the interior solution of a charged sphere can be obtained if and only if we are able to solve the above equations simultaneously. While in general, this is a very difficult task, two special singularity-free solutions are very easy to obtain. In order to show this, we have to start from the problem of finding the expression for t_μ^ν inside an electron or a distribution of constant charge density without mass. Following Eddington [2] we can obtain the t_μ^ν and the line-element inside an electron. Instead of the equation [2]

$$\frac{\partial}{\partial x_1}(F^{41}\sqrt{-g}) = -\sin\frac{\partial}{\partial r}(\exp[-\tfrac{1}{2}(\lambda+\nu)]r^2K_4') = 0\,,$$

---

[1] R. C. Tolman: *Phys. Rev.*, **55**, 364 (1939).

[2] A. S. Eddington: *The mathematical theory of Relativity*, p. 185 (1924).

(the condition of no charge and current) we now start from the equation (applying the method of co-variant derivative of an antisymmetric tensor)

$$F^{\mu\nu}_{\ \ \nu} = \frac{1}{\sqrt{-g}} \frac{\partial}{\partial x_\nu} (F^{\mu\nu}\sqrt{-g}) = c_1 .$$

$F^{\mu\nu}_{\ \ \nu} \neq 0$, only when $\mu = 4$, $\nu = 1$.

With the metric $g_{11} = -\exp[\lambda]$, $g_{22} = -r^2$, $g_{33} = -r^2 \sin^2\theta$, $g_{44} = e^\nu$ and from the condition $\lambda = -\nu$, we obtain $F_{41} = K_4' = (c_1 r^3/3 + c^2)/r^2$. Putting $c_2 = 0$ in order to avoid a singularity at the origin, we deduce $t_1^1 = -t_2^2 = -t_3^3 = t_4^4 = \frac{1}{2}\varepsilon r^2$. Following EDDINGTON we may further easily obtain $e^\nu = \exp[-\lambda] = 1 - 4\pi\varepsilon r^4 - 2m/r$.

We are now going to solve the field equations

$$(1) \qquad -8\pi T_1^1 - 4\pi\varepsilon r^2 = \exp[-\lambda]\left(\frac{\nu'}{r} + \frac{1}{r^2}\right) - \frac{1}{r^2} + \Lambda ,$$

$$(2) \qquad -8\pi T_2^2 + 4\pi\varepsilon r^2 = \exp[-\lambda]\left(\frac{\nu''}{2} - \frac{\lambda'\nu'}{4} + \frac{(\nu')^2}{4} + \frac{\nu' - \lambda'}{2r}\right) + \Lambda ,$$

$$T_2^2 = T_3^3 ,$$

$$(3) \qquad -8\pi T_4^4 - 4\pi\varepsilon r^2 = \exp[-\lambda]\left(\frac{\lambda'}{r} - \frac{1}{r^2}\right) - \frac{1}{r^2} + \Lambda .$$

1. – We assume the simple solution $\nu' = 0$, $\nu'' = 0$. The equations (1) and (2) now reduce to the simple form

$$8\pi p = 4\pi\varepsilon r^2 + \frac{\exp[-\lambda]}{r^2} - \frac{1}{r^2} + \Lambda .$$

$$8\pi p = -4\pi\varepsilon r^2 + \exp[-\lambda]\left(-\frac{\lambda'}{2r}\right) + \Lambda .$$

The equality of these two expressions immediately leads to the solution

$$\exp[-\lambda] = 1 + \alpha r^2 + 8\pi\varepsilon r^4 ,$$

$$\alpha = \text{constant of integration.}$$

Substituting $\exp[-\lambda]$ in (3), we can find ϱ. Thus a possible solution is

$$e^\nu = B^2 = \text{const} ,$$

$$e^\lambda = 1/(1 + \alpha r^2 + 8\pi\varepsilon) ,$$

with

$$8\pi p = 12\pi\varepsilon r^2 + \alpha + \Lambda ,$$

$$8\pi\varrho = -44\pi\varepsilon r^2 - 3\alpha - \Lambda .$$

Discussion. – At the origin, we have the non-singular value for $8\pi p = \alpha + \Lambda$. The pressure is a cohesive force which holds the charged matter together and is

therefore negative. At the boundary $p = 0$ and we have the equation $12\pi\varepsilon r_b^2 = -(\alpha + \Lambda) = k =$ a positive quantity to determine the value of r_b, the radius. Again at $r = 0$, we find the non-singular value of $8\pi\varrho = -3\alpha - \Lambda$ which must be positive. Thus we impose the condition $(-3\alpha) = c > \Lambda$. Again at $r = r_b$, we find the finite value of $8\pi\varrho = -(44/12)k - 3\alpha - \Lambda$, which must be a positive quantity. As k is positive, we impose the condition $(-3\alpha - \Lambda) > (44/12)k$. Thus this solution may be of interest to physicists.

* * *

I take this opportunity of thanking Prof. P. JORDAN and J. EHLERS for certain discussions.

On the Resonance Nucleon-Nucleus Scattering.

E. Minardi

Società Nazionale Cogne - Aosta
Istituto Nazionale di Fisica Nucleare - Sezione di Torino

(ricevuto il 28 Settembre 1956)

In this letter the possibility of applying the solution S' of the equation for diagonalization of the hamiltonian, found in a previous paper [1], to the resonance nucleon-nucleus scattering is briefly discussed. It is shown that the procedure seems reliable when reaction processes in nuclear matter exist, as, for example, if one assumes in zero approximation the complex potential of the nuclear model of Feshbach, Porter and Weisskopf [2].

Let us briefly discuss the resonance formula obtained with the S' matrix. If one assumes that only the matrix elements of S' describing transitions between the continuum states and the resonance bound state and viceversa, are important, one obtains for the element $\langle p m l \beta | S' | p_0 m l \beta_0 \rangle$ describing the resonance scattering a geometrical series (using the definition of S' with the generalized resolvent [I, form. (12)] and the development of I, form. (7)) wich surely converges if the a priori arbitrary parameter $c_{lm}(E_0)$ (depending on the azimutal and magnentic quantum numbers l and m and on the energy of the initial state) meets the condition [3]

$$|c_{lm}| > \left| \frac{i}{\pi \hbar^3 c^2} \sum_{l'} \sum_{m'} \sum_{\beta'} |\langle s | H' | p_0 m' l' \beta' \rangle|^2 \right| . \tag{1}$$

The series is then immediately summed. As a consequence of the appearance of the a priori arbitrary parameter c_{lm} the wave function cannot be determined using only boundary conditions at infinity, as in the usual resonance theory, but further boundary conditions are needed. In the case of the nucleon-nucleus scattering the parameter c_{lm} can be determined from the continuity condition of the

---

[1] E. Minardi: *Nuovo Cimento*, **2**, 799 (1955); this paper will be indicated with I.

[2] H. Feshbach, C. E. Porter and V. F. Weisskopf: *Phys. Rev.*, **96**, 448 (1955); this paper will be indicated with FPW.

[3] The same notations as in FPW are used. These notations are slightly different from those used in I. For example the imaginary parts of the formulas of I have an opposite sign and f_l of I is equal to f_l in FPW divided by R (R is the nuclear radius indicated by r_0 in I). Moreower the phase shift used in I must be multiplied by $i/2$ to bring it in accordance to the conventional definition.

logarithmic derivative of the wave function on the nuclear surface, when the energy of the incident particles is equal to the resonance energy. Then

$$(2) \qquad c_{lm} = \frac{i}{\pi\hbar^3 c^2} \sum_{l'} \sum_{m'} \sum_{\beta'} |\langle s|H'|p_0 m' l' \beta'\rangle|^2 + \frac{ip_0 W_0(p_0)}{\pi c^2 \hbar^3} \cdot \frac{|\langle p_0 m l \beta|H'|s\rangle|^2}{1 - \eta_l^{(0)}} .$$

The previous formula (2) is consistent with condition (1). We note that the geometrical series converges more rapidly if $|1 - \eta_1| \ll 1$, i.e. if the elastic scattering is not strong and the reaction processes are dominant.

The following scattering amplitude is then obtained:

$$(3) \qquad \frac{ip_0 W(p_0)}{\pi\hbar^3 c^2} \cdot \frac{|\langle s|H'|p_0 m l\beta\rangle|^2}{E_{0s} - E_0 - a_{lm} - ib_{lm}} ,$$

where

$$(4) \qquad a_{lm} + ib_{lm} = \frac{ip_0 W(p_0)|\langle p_0 m l\beta|H'|s\rangle|^2}{\pi c^2\hbar^3(1 - \eta_l^{(0)})} -$$

$$= -\frac{p_0 W(p_0)}{\pi c^2 \hbar^3} |\langle p_0 m l\beta|H'|s\rangle|^2 (A_l - iB_l) . \qquad (\eta_l^{(0)} \neq 1).$$

In the previous formulas $W(p_0)$ is the relativistic total energy of the incident particle whith momentum $\boldsymbol{p}_0 = \hbar\boldsymbol{k}$; the matrix element is calculated between the normalized resonance bound state of the system scatterer-incident particle, and the state of this system in which the nucleus is in the state β and the particle in a state with azimutal and magnetic quantum numbers l and m:

$$(5) \qquad \langle p_0 m l\beta|\theta_r \varphi_r r\rangle = \frac{1}{\pi\sqrt{2}} Y_{lm}(\theta_r, \varphi_r) J_l(kr)\psi_\beta ;$$

ψ_β is the wave function of the nucleus in the state β. A_l and B_l are given by the expressions:

$$(6a) \qquad A_l = \frac{(\mathrm{Im}\, f_l)^2 w_l v_l + (Rw_l' - \mathrm{Re}\, f_l \cdot w_l)(Rv_l' - \mathrm{Re}\, f_l v_l)}{2[\mathrm{Im}\, f_l^2 \cdot v_l^2 + (Rv_l' - \mathrm{Re}\, f_l \cdot v_l)^2]} .$$

$$(6b) \qquad B_l = -\frac{\mathrm{Im}\, f_l \cdot R}{2k[\mathrm{Im}\, f_l^2 \cdot v_l^2 + (Rv_l' - \mathrm{Re}\, f_l \cdot v_l)^2]} + \frac{1}{2} ,$$

where v_l, w_l, v_l' and w_l' are the real and imaginary parts and the respective derivatives of $rh_l^{(1)}(kr)$ at the point $r = R$. If the energy E_{0s} of the bound state is complex, i.e. $E_{0s} = E_s - i\Gamma_s/2$, one obtains from (3) a line with a width $\Gamma_s/2 + b_{ml}$ and with its maximum in $E_0 = E_s - a_{ml}$. From (6b) it follows that if the imaginary part of the logaritmic derivative is zero, i.e. if every nuclear reaction is absent, the width of the line is given by the second term of the right-hand side of equation (6b) and is equal to the result obtained by the Dirac approximation [4] of resonance theory for the m, l component of the incident wave.

[4] P. A. M. Dirac: *The Principles of Quantum Mechanics* (Oxford, 1947), p. 199.

If $|A^{(l)}_{\text{pot}}| \ll 1$, one obtains

$$b_{ml} = \frac{p_0 W(p_0)}{2\pi c^2 \hbar^3} |\langle s | H' | p_0 m l \beta \rangle|^2 \left(\frac{\Gamma^s_\tau}{\Gamma^s_\alpha} + 1 \right), \tag{7}$$

where Γ^s_τ is the « reaction width » and Γ^s_α the « particle width » in the channel α ([5]).

The first term on the right-hand side of formula (7), wich might be called « reaction term », may be much greater than the Dirac term. For example in the case of heavy nuclei and of very low energy of the incident neutron we have $\Gamma^s_\tau \approx 10^2 \Gamma^s_\alpha$, thus the reaction term is about one hundred times greater than the Dirac term.

As a simple preliminary application of the above formulas the contribution was calculated for an interaction describing a spin-orbit coupling to the width and to the shift of the line of the resonance in the average cross-section wich is experimentally observed at about 450 keV and for $A \approx 95$; this resonance is explained in the FPW model as due to a P-state.

As a zero approximation the FPW potential ($V_0 = 42$ MeV, $\xi = 0.03$) has been assumed and as interaction describing the spin orbit coupling the term proposed by ADAIR and coworkers ([6]), was taken:

$$\begin{cases} H' = -\sqrt{\dfrac{40}{19}}\, 1.5 \text{ MeV } (\boldsymbol{l}\cdot\boldsymbol{\sigma}), & r < R, \\ H' = 0, & r > R \qquad (R = 1.45 \cdot 10^{-13} \sqrt[3]{A} \text{ cm}). \end{cases} \tag{8}$$

From (4) one obtains an increase of the width $b_{11} \approx 150$ keV and a shift $a_{11} \approx -90$ keV.

It is also suggested that the present method might be useful to calculate the resonance parameters when one modifies the square FPW potential (for example rounding off the edges) by including this modification in H'.

* * *

Thanks are due to prof. M. CINI for a useful conversation.

([5]) These quantities are defined in M. BLATT and V. F. WEISSKOPF: *Theoretical Nuclear Physics* (New York, 1952), p. 407.

([6]) R. ADAIR, S. E. DARDEN and R. E. FIELD: *Phys. Rev.*, **96**, 503 (1954).

The Angular Distributions in the Hyperon Decays - II.

G. Morpurgo

Scuola di Perfezionamento in Fisica Nucleare
Istituto di Fisica dell'Università - Roma

(ricevuto il 29 Settembre 1956)

In a previous paper (1) we have derived the expressions of the angular distributions in the hyperon decays, under the assumption of parity conservation. Recently the difficulty of giving an adequate solution to the τ-θ problem has posed the question of whether or not the parity is conserved in the weak interactions (2); a consequence of such non conservation of parity is to produce certain asymmetries in some of the angular distributions in question. The purpose of this note is to examine such asymmetries, both in the case of parity non conservation and in the alternative case of the parity doublet model (3).

We begin in Sect. **1** with a general introduction to the problem; in Sect. **2** the asymmetries in the angular distributions from the Λ^0 and Σ decay will be calculated under the assumption of parity non conservation in the weak interactions. In Sect. **3** the same thing will be done under the Yang and Lee parity doublet assumption. The results are presented explicitely for the case of spin $\frac{1}{2}$.

1. – The Expression of the Angular Distributions.

As in I we shall consider the process of production of an hyperon and a heavy boson from a pion proton collision, and the subsequent decay of the hyperon. The angles which we shall consider are the same as in I, namely φ and θ; φ is the dihedral angle between the production and the decay planes; it may vary between 0° and 360°:

(1) G. Morpurgo: *Nuovo Cimento*, **3**, 1069 (1956) (indicated in the following as I). The present paper was stimulated by a letter from dr. Walker to the author and by a subsequent letter of Lee and Yang to prof. Amaldi. Several conversations with prof. N. Kroll have been also particularly useful. The concepts contained in the present paper have been more completely developped by T. D. Lee and C. N. Yang in two papers, to be published, arrived when the present work was completed; it must be said that Lee and Yang first had the idea of the possible asymmetries in the parity doublet model; however the independent derivations presented here are a natural continuation of I and are given here on account of their simplicity.

(2) T. D. Lee and C. N. Yang: *Is parity conserved in the weak interactions?* (to be published).

(3) T. D. Lee and C. N. Yang: *Phys. Rev.*, **102**, 290 (1956) and *Possible interference phenomena between parity doublets* (to be published).

θ is the angle between the line of flight of the hyperon and the line of flight of the decay pion in the rest system of the hyperon: $0° < \theta < 180°$. The above angles are illustrated in the Fig. 5 of I. Our φ differs by $\pi/2$ from Steinberger's ([4]) Φ.

The distributions in φ and in $\cos\theta$ may be generally written:

$$I_S'(\varphi) = \frac{1}{2\pi}(1 + \sum_M A_M^{(S)} \cos M\varphi + \sum_M B_M^{(S)} \sin M\varphi) , \tag{1}$$

and

$$I_S(\theta) = \tfrac{1}{2} + \sum_M \mathscr{A}_M^{(S)} P_M'(\cos\theta) , \tag{2}$$

where S is the assumed spin of the hyperon.

In I we did assume 1) that the parity is always conserved; 2) that no parity doubling exists, such as that proposed in ref. ([3]).

Under these assumptions the coefficients $A_M^{(S)}$ in (1) vanish for M odd, and the coefficients $B_M^{(S)}$ vanish for any M: similarly the coefficients $\mathscr{A}_M^{(S)}$ vanish for odd M. As a consequence the distributions in φ, θ have simple symmetry properties and may be plotted in the interval $0° \leqslant \varphi < \pi/2$ and $0° < \theta < 90°$ respectively; it was indeed the purpose of I to study the possible anysotropies in any of the above intervals, which, if present, would be indications of polarization and of a spin larger than $\frac{1}{2}$ for the corresponding hyperon. We may add here that such anysotropies, though present in the data discussed by Walker and Shephard ([5]), are not confirmed by Steinberger's collection of events; the statistics are however as yet too poor to draw definite conclusions.

If the parity is not conserved in the weak interactions or if a parity doublet model is accepted, then certain coefficients $A_M^{(S)}$, $B_M^{(S)}$, $\mathscr{A}_M^{(S)}$ with M odd may not vanish any more; this introduces certain asymmetries in the distributions which may be present even for spin $\frac{1}{2}$. It may be clarifying to mention that by the term « asymmetries » we shall mean in the following just the new terms in the distributions, introduced by the possible non vanishing of the coefficients mentioned above.

2. - The Asymmetries Ensuing From the non Conservation of Parity in the Weak Interactions.

We begin by considering the assumption that parity is not conserved in the weak interactions producing the decay of the new particles; it is, instead, of course conserved in the strong interactions, responsible for the associated production.

Using the same notation as in I, the wave function ${}_\alpha\chi_S$ of the hyperon produced in the pion-proton collision, when the proton spin is up, may be written:

$${}_\alpha\chi_S = A^{-\frac{1}{2}} \sum_M \lambda_M \chi_S^M , \qquad A = \sum_M |\lambda_M|^2 , \tag{3}$$

where the χ_S^M are the spin functions of the hyperon (the z axis being in the direc-

---

([4]) R. Budde, M. Chretien, J. Leitner, N. P. Samios and J. Steinberger: to be published, CU-113-56-ONR-110-1.

([5]) W. Walker and W. Shephard: *Phys. Rev.*, **101**, 1810 (1955).

tion of the line of flight of the hyperon) and the λ_M are $2M+1$ complex coefficients, specifying the polarization state of the hyperon.

As shown in I the wave function ${}_\beta\chi_S$ of the hyperon produced when the proton spin is initially down is simply obtained from ${}_\alpha\chi_S$ by application of the operator PR (defined in I) and is:

$$(4) \qquad {}_\beta\chi_S = PR\ {}_\alpha\chi_S = A^{-\frac{1}{2}} \sum_M (-1)^{|M-\frac{1}{2}|} \lambda_M \chi_S^{-M}$$

The process of decay of the hyperon is now described by each function χ_S^M giving rise to an outgoing $\pi \mapsto$ p wave ψ_S^M; the non conservation of parity in the weak interactions is expressed by the fact that the outgoing $\pi \mapsto$ p wave ψ_S^M is now a superposition, with certain coefficients a and b of the two waves with opposite parities, $\underset{+}{\psi_S^M}$ and $\underset{-}{\psi_S^M}$;

$$(5) \qquad \underset{+}{\psi_S^M} = \left(\frac{S+M}{2S}\right)^{\frac{1}{2}} \alpha Y_{S-\frac{1}{2}}^{M-\frac{1}{2}} + \left(\frac{S-M}{2S}\right)^{\frac{1}{2}} \beta Y_{S-\frac{1}{2}}^{M+\frac{1}{2}},$$

$$(6)\ (*) \qquad \underset{-}{\psi_S^M} = -\left(\frac{S-M+1}{2S+2}\right)^{\frac{1}{2}} \alpha Y_{S+\frac{1}{2}}^{M-\frac{1}{2}} + \left(\frac{S+M+1}{2S+2}\right)^{\frac{1}{2}} \beta Y_{S+\frac{1}{2}}^{M+\frac{1}{2}},$$

where α and β are the spin functions of the decay proton.

The angular distribution $I_S(\varphi)$ is therefore given by:

$$(7) \qquad I_S(\varphi) = \tfrac{1}{2} A^{-1} N^{-1} \cdot$$

$$\cdot \left[\int \left| \sum_M \lambda_M (a \underset{+}{\psi_S^M} + b \underset{-}{\psi_S^M}) \right|^2 \mathrm{d}\cos\theta + \int \left| \sum_M (-1)^{|M-\frac{1}{2}|} \lambda_M (a \underset{+}{\psi_S^{-M}} + b \underset{-}{\psi_S^{-M}}) \right|^2 \mathrm{d}\cos\theta \right],$$

and the distribution $I_S(\theta)$ is given by:

$$(8) \qquad I_S(\theta) =$$

$$= \tfrac{1}{2} A^{-1} N^{-1} \left[\int \left| \sum_M \lambda_M (a \underset{+}{\psi_S^M} + b \underset{-}{\psi_S^M}) \right|^2 \mathrm{d}\varphi + \int \left| \sum_M (-1)^{|M-\frac{1}{2}|} \lambda_M (a \underset{+}{\psi_S^{-M}} + b \underset{-}{\psi_S^{-M}}) \right| \mathrm{d}\varphi \right],$$

where the integral implies also a sum over the spins of the final proton and N is a normalization factor due to the fact that $\underset{+}{\psi_S^M}$ and $\underset{-}{\psi_S^M}$ are separately normalized: $N = |a|^2 + |b|^2$.

In the two expressions (7) and (8) above the asymmetric terms are due to the interference between the two waves $\underset{+}{\psi_S^M}$ and $\underset{-}{\psi_S^M}$ with opposite parity; we may fix our attention just on these interference terms, since all the other terms are the same as in I. Considering first the θ distribution, it is easy to check, using (8), (5) and (6) that the interference term from the first addend in (8) cancels the interference term from the second addend, so that no asymmetric term remains: the non conservation of parity in the weak interactions does not modify the θ distributions which remains symmetrical with respect to $\theta = 90°$.

(*) An oversight appeared in this formula in I – We take this opportunity to correct two other oversights of I: 1) on page 1074 footnote (*) read « indistinguished » instead of « indistinguishable »; 2) on page 1089 – first line: omit « it has to be kept in mind that ».

We next consider the φ distribution; here the interference terms do not cancel in (7) so that there is the possibility of asymmetric terms; such terms have the form $\sin\varphi$, $\sin 3\varphi$, $\sin(2M+1)\varphi$ etc.; no new terms of the form $\cos(2M+1)\varphi$ nor of the form $\sin 2M\varphi$ are introduced.

It may be interesting to evaluate the coefficients $B^{(S)}_{2M-1}$ of these new terms expressed through the polarization parameters and the parity mixture parameters a, b. For spin $\frac{1}{2}$ only $B^{(\frac{1}{2})}_1$ is different from zero. Its expression is:

$$B^{(\frac{1}{2})}_1 = (\quad i)\,\frac{\pi}{4}\,\frac{ab^* + ba^*}{|a|^2 + |b|^2}\,\frac{\lambda_{\frac{1}{2}}\lambda^*_{-\frac{1}{2}} - \lambda^*_{\frac{1}{2}}\lambda_{-\frac{1}{2}}}{|\lambda_{\frac{1}{2}}|^2 + |\lambda_{-\frac{1}{2}}|^2}\,. \tag{9}$$

For a spin larger than $\frac{1}{2}$ the coefficients have more complicated expressions but they all share with $B^{(\frac{1}{2})}_1$ the two properties: 1) of being proportional to $ab^* + ba^*$; 2) to vanish if the hyperon is unpolarized.

We may finally notice that the maximum value of $B^{(\frac{1}{2})}_1$ is $\pi/4$; this correspond to a ratio $\int_0^{\pi} I_S(\varphi)\,\mathrm{d}\varphi \Big/ \int_{\pi}^{2\pi} I_S(\varphi)\,\mathrm{d}\varphi = 3$, a quite large asymmetry.

3. – The Asymmetries Ensuing From the Parity Doublet Model.

We now investigate the assumption that parity is conserved both in the strong and in the weak interactions, but two kinds of hyperons and heavy bosons exist with opposite parities; the strong interaction part of the Hamiltonian is assumed to be invariant under the exchange of the two kinds of particles. This is Yang and Lee's parity doublet model.

In this case the hyperon-boson wave produced in the pion proton collision is a combination of four waves; considering first the proton spin up we may write such combination as:

$$\sum_M [\lambda^{++}_M \underset{+}{\chi^M_S}\underset{+}{\theta^0} + \lambda^{+-}_M \underset{+}{\chi^M_S}\underset{-}{\theta^0} + \lambda^{-+}_M \underset{-}{\chi^M_S}\underset{+}{\theta^0} + \lambda^{--}_M \underset{-}{\chi^M_S}\underset{-}{\theta^0}]\,, \tag{10}$$

where $\underset{+}{\chi^M_S}$, $\underset{-}{\chi^M_S}$ are the spin functions of the two hyperons with opposite parity and $\underset{+}{\theta^0}$, $\underset{-}{\theta^0}$ are the functions of the two bosons (which are assumed to have spin zero); the λ^{++}_M, λ^{+-}_M, λ^{-+}_M, λ^{--}_M are the amplitudes of these waves; the fact that the state in question is an eigenstate of the parity conjugation belonging to the eigenvalue $+1$ is expressed by the equalities:

$$\lambda^{++}_M = \lambda^{--}_M\,, \qquad\qquad \lambda^{+-}_M = \lambda^{-+}_M\,. \tag{11}$$

The four waves included in (10) may interfere at the decay if the lifetimes and masses of the two kinds of hyperons do not appreciably differ; the equality of the lifetimes is, at the moment, an assumption, not easy to understand in the parity doublet scheme.

Making use of (11) the wave (10) may be rewritten (normalized):

$$\begin{cases} \Lambda'^{-\frac{1}{2}} \sum_M (\lambda^{++}_M \underset{+}{\chi^M_S} + \lambda^{-+}_M \underset{-}{\chi^M_S})\underset{+}{\theta^0} + (\lambda^{-+}_M \underset{+}{\chi^M_S} + \lambda^{++}_M \underset{-}{\chi^M_S})\underset{-}{\theta^0}]; \\ \Lambda' = 2\sum_M (|\lambda^{++}_M|^2 + |\lambda^{-+}_M|^2)\,. \end{cases} \tag{12}$$

The wave produced when the proton spin is initially down is again obtained by application to (12) of the operator PR. It is:

$$(13) \qquad A'^{-\frac{1}{2}} \sum_M (-1)^{|M-\frac{1}{2}|}[(\lambda_M^{++} \underset{+}{\chi_S^{-M}} - \lambda_M^{-+} \underset{+}{\chi_S^{-M}})\theta^0 - (\lambda_M^{-+} \underset{+}{\chi_S^{-M}} - \lambda_M^{++} \underset{-}{\chi_S^{-M}})\theta^0] ,$$

where the changes of signs with respect to (12) are due to the application of the parity operator P, contained in PR.

As already mentioned we now assume that the weak interactions producing the decay of the hyperon do not change the parity. Each $\underset{+}{\chi_S^M}$ therefore goes into $\underset{+}{\psi_S^M}$ and each χ_S^M into $\underset{-}{\psi_S^M}$. The φ distribution is then obtained on writing:

$$(14) \qquad I_S(\varphi) = \tfrac{1}{2} A'^{-\frac{1}{2}} \cdot$$

$$\cdot \left\{ \int |\sum_M (\lambda_M^{++} \underset{+}{\psi^M} + \lambda_M^{-+} \underset{-}{\psi^M})|^2 \, \mathrm{d} \cos\theta + \int |\sum_M (\quad 1)^{|M-\frac{1}{2}|} (\lambda_M^{--} \underset{+}{\psi^{-M}} - \lambda_M^{+-} \underset{-}{\psi^{-M}})|^2 \, \mathrm{d} \cos\theta \right\} +$$

$$+ \text{ same expression with } \lambda_M^{++} \rightleftarrows \lambda_M^{-+}.$$

The θ distribution has the same expression with the integration over φ instead of over $\cos\theta$.

We first consider the θ distribution; contrary to the case treated in Sect. 2 such distribution may contain now asymmetrical terms, that is terms with odd M. For $S = \frac{1}{2}$ only $\mathscr{A}_1^{(\frac{1}{2})}$ is different from zero; its expression is:

$$(15) \qquad \mathscr{A}_1^{(\frac{1}{2})} = A'^{-1}(\lambda_{\frac{1}{2}}^{++} \lambda_{\frac{1}{2}}^{*-+} - \lambda_{-\frac{1}{2}}^{++} \lambda_{-\frac{1}{2}}^{*-+} + \text{C.C.}) .$$

Its maximum value is $\frac{1}{2}$ and the corresponding maximum asymmetry is 3. Also the φ distribution, calculated from (14) has asymmetric terms; they have now the form $\cos(2M+1)\varphi$, no term in $\sin M\varphi$ being present. For $S = \frac{1}{2}$ the coefficient $A_1^{(\frac{1}{2})}$ is reported below:

$$A_1^{(\frac{1}{2})} = \frac{\pi}{2} A'^{-1}[\lambda_{\frac{1}{2}}^{++} \lambda_{-\frac{1}{2}}^{*-+} + \lambda_{-\frac{1}{2}}^{++} \lambda_{\frac{1}{2}}^{*-+} + \text{C.C.}] .$$

The maximum value of $A_1^{(\frac{1}{2})}$ is $\pi/4$ and the maximum asymmetry is 3. Both $\mathscr{A}_1^{(\frac{1}{2})}$ and $A_1^{(\frac{1}{2})}$ vanish for an unpolarized hyperon. It may be noticed that to the maximum asymmetry in the φ distribution no asymmetry corresponds in the θ distribution and viceversa.

The experimental data are, as yet, insufficient to make detailed comparisons; we just refer to the graphs given in Steinberger's paper.

LIBRI RICEVUTI E RECENSIONI

S. S. Schweber, H. A. Bethe, F. de Hoffman: *Fields*, Volume I; H. A. Bethe, F. de Hoffman: *Mesons*, Volume II. Row, Peterson and Company; Evanston, Illinois 1955.

Scrivere oggi un'opera sui campi e sui mesoni richiede da parte degli autori un ammirevole spirito di sacrificio. Per bella e perfetta che l'opera riesca tutte le fatiche impiegate nello scriverla non varranno ad erigere ai suoi autori alcun « monumentum aere perennius ». La sua vita è destinata ad essere breve ed effimera, legata al variare delle conoscenze sperimentali e alla sorte dei tentativi di interpretazione teorica. E se l'opera poi non sarà bella e perfetta? Non tocca al recensore fare profezie: il suo compito è al più quello di dare consigli ai probabili lettori. Il consiglio di chi recensisce quest'opera è in sintesi questo: se il lettore è un giovane studioso di fisica teorica desideroso di apprendere la teoria dei campi, egli farà bene a non rivolgersi al primo volume di quest'opera (dedicato appunto alla teoria dei campi e dovuto essenzialmente a Schweber); se poi egli è un ricercatore già abbastanza esperto e fornito di spirito critico, potrà trovare nel secondo volume (praticamente indipendente dal primo e dovuto a Bethe e de Hoffmann) molte cose interessanti ed utili sulla fisica dei mesoni π unite purtroppo ad altre già alquanto invecchiate.

Venendo ad un esame più circonstanziato ecco l'indice del primo volume: equazioni relativistiche di Klein-Gordon e di Dirac; teoria classica lagrangiana; dei campi; quantizzazione dei campi; teoria della rinormalizzazione. Le prime tre parti sono di argomento ormai classico, ma sfortunatamente anzichè rappresentare un perfezionamento delle trattazioni precedenti, sono assai più confuse e meno rigorose. Citeremo qualche esempio: all'inizio della teoria dei campi, pag. 89 si legge « è ben noto (cfr. per esempio Fermi, 1932) che con una analisi in serie di Fourier si può tradurre il comportamento dinamico di questo campo (cioè il campo elettromagnetico, N.d.R.) in quello di una (doppia) serie infinita di oscillatori... Inoltre sembra evidente che a questo problema si debbano imporre le regole quantiche poichè siamo abituati a pensare al campo elettromagnetico come a un campo *classico* ». Trattandosi di una questione di tanta importanza per l'intera teoria dei campi non ci sembra opportuno limitarsi all'« evidente » e « ben noto ». A chi inizia lo studio della teoria dei campi, e non v'è dubbio che a questo genere di lettori il libro sia rivolto, tutto ciò non è nè evidente nè ben noto: occorre spiegarlo e giustificarlo per non edificare tutta la teoria sul vuoto. A pag. 107 si afferma che un campo vettoriale è descritto da un quadrivettore di cui solo tre componenti sono indipendenti; dopo di ciò l'A. afferma: « La quantità *tre* è connessa al fatto che lo spin della particella è uno e perciò può avere $2S + 1 = 3$ possibili orientazioni ». Questa affermazione è priva di senso quando ancora non si è parlato di quantizzazione del campo e quindi di particelle. Chi scrive non è riuscito a trovare nel corso del libro alcuna dimostrazione del fatto che lo spin di una particella sia legato alle proprietà

di trasformazione secondo il gruppo di Lorentz dell'operatore di campo. Forse anche questo, secondo l'A., è ben noto. Egualmente confusa e formale riesce la parte più moderna: si veda per esempio l'introduzione della matrice S, la discussione sulla coniugazione di carica e quella sulla connessione fra spin e statistica. Vogliamo ancora citare un esempio che dimostra lo spirito formale di questo volume. A pag. 320 si dimostra per mezzo della valutazione di un elemento di matrice che un mesone pseudoscalare pesante non può disintegrare in due mesoni pseudoscalari più leggeri. Ci sembra che non fosse il caso di valutare alcun elemento di matrice per ottenere un risultato tanto semplice. Ragionando in termini di momenti angolari e parità, l'A. si sarebbe anche accorto che la parità dei mesoni finali non ha alcuna influenza sulla regola di selezione.

Veniamo ora al secondo volume che tratta gli argomenti seguenti: proprietà dei mesoni π; diffusione dei mesoni; fotoproduzione; teoria mesonica; produzione di mesoni da particelle; altri mesoni. Come si è detto sopra questo volume si rivolge ad un pubblico di ricercatori che hanno già con il soggetto una certa famigliarità. Per esempio si ammette che il lettore già conosca i risultati della teoria dell'accoppiamento debole, il che sembra un po' strano quando si afferma che il libro, o gran parte di esso, si rivolge anche a fisici sperimentali. Non vi è dubbio che questi ultimi per procedere nella lettura devono fare un buon numero di atti di fede: per esempio a pag. 16 devono credere « of course » (!) che anche i mesoni π^+ hanno parità negativa; a pag. 45 devono accettare che gli antineutroni hanno parità e spin isotopico (terza componente cioè) opposti a quelli dei neutroni; a pag. 76 sono invitati ad usare il « Teorema Ottico » senza che si dica loro da dove viene; ecc.

Comunque, un lettore dotato di una solida conoscenza della meccanica quantistica e della teoria delle reazioni nucleari troverà la lettura di questo volume assai utile. Particolarmente soddisfacente è la discussione della proprietà dei mesoni, la trattazione semifenomenologica della diffusione di mesoni da nucleoni e della fotoproduzione come pure la discussione della produzione di mesoni nell'urto di due nucleoni. Sono questi i capitoli migliori dell'opera che stanno alla pari dei famosi articoli di rassegna che Bethe ci ha dato nel campo della fisica atomica e nucleare.

Assai meno convincente riesce la parte dedicata alla teoria mesonica, tutta informata ancora dalla fede che tre o quattro anni fa la teoria pseudoscalare aveva destato. Questo fa si che venga dedicato uno spazio eccessivo a teorie che oggi hanno perso parecchio interesse, come quella di Lévy delle forze nucleari, ecc., mentre altre, come quella di Chew, ricevono assai più scarsa attenzione. Data l'epoca in cui il libro fu scritto, gli sviluppi più recenti della teoria, quali l'equazione di Low, le regole di dispersione, ecc. non possono essere trattati convenientemente. Insufficiente risulta anche la breve trattazione dedicata ai mesoni μ, e ormai invecchiata è quella delle particelle strane.

L. A. Radicati

K. Przibram – *Irradiation Colors an Luminiscence*, xiv+332 pagg., 73 figg.; Pergamon Press, London, 1956; 63 s.

È questa una nuova edizione in lingua inglese dell'opera di Przibram già presentata ai lettori del *Nuovo Cimento* dal prof. Giulotto [*Nuovo Cimento*, **11**, 334 (1954)].

Il volume è stato tradotto e riveduto in collaborazione con l'Autore da J. E. Caffyn dell'Università di Durham. I principali cambiamenti rispetto alla prece-

dente edizione tedesca riguardano i paragrafi sulla colorazione degli alogenuri alcalini contenenti impurità, la colorazione dei composti delle terre rare, la fotoconduttività degli alogenuri colorati, le proprietà dei vari tipi di centri, il contenuto in elio del salgemma, la colorazione della fluorite e di varie altre sostanze e le bande di assorbimento del fluoruro di litio. Anche la lista dei riferimenti bibliografici è stata arricchita di circa 500 voci.

Così aggiornato e reso più accessibile dalla traduzione in lingua inglese, il volume riuscirà utilissimo a chiunque voglia introdursi in questi importanti argomenti di fisica dei solidi.

M. AGENO

R. OLDENBURGER editor – *Frequency Response*; XII+372 pp. The Mac Millan Co., New York, 1956.

Un problema che la tecnica si è trovata a dover risolvere con sempre maggior frequenza è quello del controllo di una o più variabili di un sistema.

« Sistema » è una espressione generica che può indicare un forno elettrico di cui occorre controllare la temperatura oppure una turbina di cui occorre regolare il flusso di acqua per mantenere costante la velocità anche in condizioni variabili di carico, e così via.

La soluzione del problema è sempre attuata con il seguente schema: si preleva dalla variabile da controllare un segnale che sia proporzionale alla variabile stessa. Questo segnale viene confrontato con un valore di riferimento fisso. La differenza tra il riferimento e la porzione di variabile da controllare costituisce il segnale di errore. Quest'ultimo, opportunamente amplificato, agisce sul generatore della variabile. Se il segnale di errore è nullo, il generatore dà il valore esatto della variabile.

Naturalmente occorre poter progettare il sistema di regolazione in modo che esso abbia un certo numero di requisiti. Ad esempio, occorre che il sistema sia stabile e cioè la regolazione agisca in modo da non far compiere alla variabile oscillazioni persistenti. Inoltre occorre che il sistema di regolazione, anche se stabile ad un certo istante di tempo, non divenga instabile con ragionevoli variazioni dei componenti.

In questo volume è esposto, sia in teoria sia in pratica, uno dei metodi generali che si possono usare per il progetto dei dispositivi di regolazione: quello del tracciamento della curva di risposta alla frequenza dei componenti del sistema.

Secondo questo metodo, esposto in una breve ed esauriente introduzione, se si traccia la risposta di ciascuno dei componenti del sistema per una eccitazione sinusoidale, è possibile, considerando l'insieme delle risposte alla frequenza delle varie parti, progettare il sistema in modo che esso sia stabile e risponda ai requisiti richiesti.

Dopo aver tracciato una breve rassegna dei fondamenti matematici elementari del metodo, nel corso del libro vengono affrontati, in altri otto capitoli, i seguenti argomenti. Dapprima viene esposto il modo di semplificare, sul piano pratico, la soluzione dei problemi, con procedimenti abbreviati di calcolo. I due capitoli seguenti sono dedicati ad una analisi di questioni concernenti i servomeccanismi e il controllo dei processi industriali. Con il quinto capitolo si torna a discutere il metodo da un punto di vista teorico. Si esamina la connessione esistente tra la risposta di un sistema ad eccitazioni impulsive e sinusoidali, per concludere che è possibile, con sistemi di calcolo semplificati, risalire dal comportamento in regime sinusoidale al comportamento sotto eccitazioni impulsive.

Un sistema di controllo deve essere studiato in modo da correggere nel miglior modo possibile le variazioni della variabile da controllare. Questo è l'argo-

mento del capitolo sesto. Gli ultimi capitoli sono dedicati alla considerazione di problemi che solo da pochi anni vengono studiati. In particolare viene approfondito il comportamento dei sistemi non lineari, pur limitando l'analisi a quelli in cui la variabile da correggere contiene, per eccitazione sinusoidale, armoniche superiori con ampiezza piccola in confronto a quella dell'oscillazione fondamentale. Da ultimo non poteva mancare una analisi della connessione tra la teoria dei servomeccanismi e i metodi statistici della teoria delle informazioni.

Come si è visto, lo studio del problema del controllo, condotto in questo libro, è molto ampio. Il maggior pregio del libro consiste da un lato nel fatto che alla sua stesura hanno collaborato i maggiori esperti mondiali nei singoli campi, dall'altro nel modo in cui tutti gli articoli sono inquadrati entro uno schema generale e semplice, che consente anche al lettore che affronta per la prima volta questo campo, di rendersi pienamente conto della validità e utilità dei procedimenti.

G. CORTELLESSA

Direttore responsabile: G. POLVANI Tipografia Compositori - Bologna

Questo fascicolo è stato licenziato dai torchi il 27-10-1956